ACOUSTIC EMISSION AND YIELD IN SAND

Andrew Lloyd Jackson

A Thesis submitted for the Degree of

Doctor of Philosophy

at

The University of Aston in Birmingham

July 1986

THE UNIVERSITY OF ASTON IN BIRMINGHAM

ACOUSTIC EMISSION AND YIELD IN SAND

A thesis submitted for the Degree of Doctor of Philosophy, by
Andrew Lloyd Jackson, July 1986.

SUMMARY

An experimental investigation into the Acoustic Emission (AE)
response of sand has been undertaken, and the use of AE as a
method of yield point identification has been assessed.

Dense, saturated samples of sand were tested in conventional
triaxial apparatus. The measurements of stresses and strains were
carried out according to current research practice. The AE
monitoring system was integrated with the soil mechanics
equipment in such a way that sample disturbance was minimised.

During monotonically loaded, constant cell pressure tests the
total number of events recorded was found to increase at an
increasing rate in a manner which may be approximated by a power
law. The AE response of the sand was found to be both stress
level and stress path dependent. Undrained constant cell pressure
tests showed that, unlike drained tests, the AE event rate
increased at an increasing rate; this was shown to correlate with
the mean effective stress variation. The stress path dependence
was most noticeable in extension tests, where the number of
events recorded was an order of magnitude less than that recorded
in comparable compression tests. This stress path dependence was
shown to be due to the differences in the work done by the
external stresses.

In constant cell pressure tests containing unload/reload cycles
it was found that yield could be identified from a discontinuity
in the event rate/time curve which occurred during reloading.
Further tests involving complex stress paths showed that AE was a
useful method of yield point identification. Some tests involving
large stress reversals were carried out, and AE identified the
inverse yield points more distinctly than conventional methods of
yield point identification.

KEY WORDS: ACOUSTIC EMISSION
              SAND
              TRIAXIAL TESTS
              STRESS LEVEL DEPENDENCY
              YIELD POINT IDENTIFICATION

ACKNOWLEDGEMENTS

I would like to thank my research supervisor, Dr Colin Thornton, for his advice, patience, enthusiasm, and support throughout the research period, especially during the writing of this thesis.

I would also like to thank Mike Lyons for his help and advice in the laboratory.

Contents

List of tables

Chapter 6

List of Figures

Chapter 2

Chapter 3

Chapter 4

Chapter 5

Chapter 1.

Introduction

Acoustic Emission (AE) monitoring is a recognised non-destructive testing technique which has not been widely used in the laboratory testing of soil. The application of AE monitoring to the behaviour of dense, saturated sand samples under axisymmetric stress conditions is new. One of the objectives of the research reported in this thesis was to examine the AE response of sand under these conditions. The behaviour of sand under axisymmetric stress conditions has been the subject of many investigations, some of which have attempted to identify the onset of plastic deformation (yield point). However, the identification of a yield point from conventional stress/strain data is often ambiguous and subjective. Therefore, another objective of the research was to determine whether AE would be useful as a method of yield point identification.

The main text of the thesis is divided into a number of chapters which follow this introduction. Where relevant, each chapter has a conclusions section which examines the results found and discusses the implications of the results. There is, therefore, no conclusions chapter as such but Chapter 8 provides some concluding remarks and suggests some ideas for future work.

Chapter 2 describes Acoustic Emission and its development as a non-destructive testing technique in soil mechanics. A review of AE in the laboratory and insitu monitoring of soils is undertaken. The soil mechanics laboratory equipment, together with the AE monitoring equipment, are described in Chapter 3.

This chapter also covers the details of sample preparation and the testing techniques which were adopted during the research program.

Chapter 4 describes the tests which were conducted in order to describe the basic AE behaviour of sand. The influences of end conditions, sample size, and rate of testing are studied. Several different methods of characterising the acoustic emissions from sand are considered. The effects of mean stress and stress path on the AE response are examined in Chapter 5, both of which have implications for laboratory and insitu testing.

Chapter 6 briefly reviews the concepts of yield and plasticity, and investigates how the AE response is affected by unloading and reloading. Following this, the AE technique is used to identify the yielding of sand subjected to complex loading histories. Chapter 7 presents the results of large stress reversal tests and considers the use of AE as an aid to the interpretation of such tests.

As is usual in a thesis of this type, various terms are used fairly frequently and, therefore, it is necessary to define them. All stresses referred to are effective stresses unless specifically noted and therefore the customary prime has been omitted, except where some ambiguity might arise. The vertical stress is referred to as σ_a (axial) and the horizontal stress referred to as σ_r (radial). This is to avoid any ambiguity arising from the use of terms such as σ_1, σ_3 which are normally used to refer to major and minor principal stresses. The stress

2

ratio is defined as:

$$R = \sqrt{2} \ (\sigma_a - \sigma_r) \ / \ (\sigma_a + 2\sigma_r) \qquad (1.1)$$

All strains reported in this thesis are total strains: no attempt
has been made to deduct elastic strains. The deviatoric strain is
defined as:

$$e_d = e_a - (e_v \ / \ 3) \qquad (1.2)$$

where e_a is the axial (vertical) strain, and e_v is the volumetric
strain.

The work done by the applied stresses is defined as:

$$W = \int \sigma \ \dot{e} \ dt \qquad (1.3)$$

and is calculated as the sum of the incremental energy measured
over a small time period and hence

$$W = \sum \sigma_a \Delta e_a + 2\sigma_r \Delta e_r \qquad (1.4)$$

where e_r is the radial (horizontal) strain, which is calculated
from the measured axial and volumetric strains.

The terms event rate and events are defined as follows: event
rate is the number of acoustic emission events occurring in a
fixed interval (normally 1 minute), and events is the sum of the
event rate.

Chapter 2.

Review of Acoustic Emission

2.1 Introduction.

The phenomenon of Acoustic Emission (AE) is not well known, and before proceeding with a review of Acoustic Emission it is useful to describe an emission and its associated parameters. The review does not touch on the wider aspects of AE but concentrates on the soils related research which has been carried out to date.

When materials are stressed the stored energy is released in various forms including sound. The generation of sound by wood, rock, and tin ('tin cry') when deformed is well known. This audible generation of sound is known as Acoustic Emission. However, Acoustic Emission is not restricted to the audible range, indeed most emissions are not audible without considerable amplification and frequency shifting.

As acoustic emissions propagate through the material they are modified by the structure of the material. The emissions may be reflected, refracted, distorted, and attenuated because of the material anisotropy and inhomogeneity. This modification of the acoustic emissions makes it very difficult to study and describe the actual source mechanisms involved, however, it does not detract from the ability to use this phenomenon in non destructive testing and monitoring.

The emissions can be picked up by a sensor and converted to an equivalent electrical signal. The sensor may be an accelerometer or one of a number of different transducer types: optical,

capacitive or piezoelectric. However, the piezoelectric type is the most widely used. When an emission reaches a piezoelectric sensor it applies a force to the crystal which generates a small voltage. The efficiency of this sound-voltage conversion is partly governed by the coupling of the sensor to the material being monitored. An efficient coupling can be formed by applying grease to the active face of the sensor, and to the material. The grease effectively makes the two mating surfaces flat by filling the small naturally occurring surface voids.

The output from the sensor contains background noise mixed with the AE signal. This noise may be mains (50 Hz) or mechanically related and of almost the same magnitude as the emission signal. Depending on the application, much of the noise can be removed by using a band pass filter. However, filtering does imply a knowledge of the frequency spectrum of the AE signal. The removal of background noise early in the signal chain is advantageous because much of the commercially available AE equipment is computer based and processing 'noise' reduces the equipment's efficiency. The filtered output of the sensor is amplified to give better noise immunity, allowing the rest of the monitoring equipment to be located elsewhere.

An acoustic emission may be characterised by a number of parameters and these are indicated in the idealised waveform shown in Figure 2.1. The number of parameters measureable depends upon the particular equipment being used; different manufacturers regard different parameters as more important and define some of the parameters in a slightly different way. Before an incoming signal may be classified as an Acoustic Emission event it has to

5

cross a Threshold Voltage, this is set with the monitoring equipment and defines the minimum voltage which a signal must have before registering on the equipment. The main use of this parameter is to remove background noise which might otherwise be taken as an event, and one manufacturer offers the option of an 'Automatic Threshold Voltage' which attempts to follow the rise and fall of the background noise.

Whenever the signal crosses the threshold voltage a Ringdown Count (count) occurs, the first of which indicates the start time of the event. Many of the smaller Acoustic Emission systems offer ringdown counting as the sole measure of Acoustic Emission activity and for many situations, e.g. insitu monitoring, it is perfectly acceptable since an abundance of information would detract from the system's ease of use.

The time for an event to reach its Peak Amplitude is the Rise Time. Peak amplitude is usually measured in Decibels (dB), with respect to some fixed voltage, because of the high gains used in Acoustic Emission monitoring. Rise time is useful as an indication of the validity of an event since acoustic emissions are characterised by their short rise times whereas background noise tends to have long rise times. The Slope of an event is a derived parameter which is given by the ratio of the peak voltage (in millivolts) to the rise time (in microseconds). Slope is a useful indication of event validity since background noise tends to have low slope - following the argument given above for rise time.

The Event Duration is the time between the first threshold crossing and the last threshold crossing. The last threshold crossing need not be a ringdown count as the signal voltage level may be falling below the threshold voltage rather than rising above it (see Figure 2.2). The **Energy** of an event is a derived parameter given by:

$$\text{Energy} = \text{Peak Amplitude(dB)} + 10 \text{xlog(Event Duration)} \quad (2.1)$$

Here energy is not the actual event energy but the energy of the signal from the sensor, which is the area under the voltage level/time curve. This is only one possible definition of energy; different manufacturers calculate it in different ways.

The information available to describe an event may be one or more of the following: event start time, number of ringdown counts (counts), event duration, peak amplitude, rise time, slope, and energy.

The use of ringdown counts as a measure of AE activity is widespread. Indeed, a great deal of the early research was based solely on ringdown counts. However, it has been realised that there are a number of limitations with the use of ringdown counts, see e.g. Williams (1980) and Beattie (1976). The main limitation with the use of ringdown counts is that it is frequency dependent, i.e. the count is biased towards large amplitude events. The use of events, rather than counts, is a logical step as the latter is a subset of the former. Another alternative is to use the energy of the events and, according to Beattie (1976), this will produce the same or better results than counts. However, when using energy it should be remembered that the energy is that of the transducer signal, not the acoustic wave.

2.2 Origins of Acoustic Emission Research.

The phenomenon of Acoustic Emission has been known for centuries in an intuitive and qualitative sense, for example wood cracking under stress could be taken as a sign that it was near to failure. However it was not until the 1930s that attempts were made to define Acoustic Emission in a quantitative manner. Obert (1975) described the preliminary investigations in the 1930s when working with Duvall in lead mines in Oklahoma. They attempted to determine whether seismic velocity was dependent on pillar load. It was found that extra pulses were triggering the equipment but these pulses were not due to equipment defects. After experimentation at different sites over a period of years it was found that areas of high 'microseismic' activity could be related to areas of high stress. This research has formed the basis for the Acoustic Emission monitoring of rock mechanics which has continued to develop since then.

It was not until the 1950s that investigations into Acoustic Emission in areas other than mines and rock mechanics began. Kaiser (1953) working with metals is generally credited with the first serious work. One of the most interesting observations made by Kaiser was that events were emitted by samples on first loading but that events ceased on unloading. Furthermore when reloaded the event rate did not reach its former level until the stress level passed its previous maximum. This is known as the 'Kaiser effect'. Since then it has been found that some materials, notably fibre reinforced plastics, do not exhibit this effect (Wadin 1982) because of their viscoelasticity.

In fields other than soil and rock mechanics Acoustic Emission is well established as a non destructive testing technique. Arrington (1975, 1978) summarises the current applications of the technique and indicates possible areas for expansion which includes soil and rock mechanics. Common applications include nuclear pressure vessel testing, and weld integrity monitoring.

2.3 Experimental studies

Beard (1962) monitored rock and soil slopes using a crystal pickup, amplifier, and set of earphones. Data analysis was based entirely on operator experience and as such was subjective. However, Beard was able to demonstrate that for rocks at least, the technique of aural pulse counting was successful but that it was very sensitive to extraneous noise from traffic, conversations, and water.

Fischer and Yorke (1964) using a Rochelle salt crystal of resonant frequency 1kHz, amplifier, and tape recorder extended the concepts developed by Beard (1962). Data were stored on the tape recorder at fixed intervals and, later, the count rate was determined by counting aurally. The equipment suffered the same limitations as Beard's because of extraneous noise and operator judgement. However the conclusions were more encouraging than Beard and indicated that soil slope monitoring was a feasible proposition.

Cadman and Goodman (1967) went a stage further than Fischer and Yorke (1964) and attempted to locate the slip surface of moist sand slopes in the laboratory. Using an oscilloscope and tape

recorder the difference in arrival times of an event between four
sensors was calculated. Using these time differences and knowing
the speed of sound in the sand it was possible to estimate, using
an iterative solution, where the slip surface lay. Although the
results indicated that satisfactory solutions could be found, the
study had been confined to ideal laboratory conditions where
extraneous noise was minimised.

Hakuno et al (1968) demonstrated that sand produced acoustic
emissions when stressed using a modified California Bearing Ratio
(CBR) apparatus with an embedded geophone as a sensor. Hakuno was
also able to produce some simple frequency distributions although
these reflect the geophone's conversion capabilities rather than
the actual sound wave frequency content.

Koerner, Lord, and other workers at Drexel University have made
significant advances in the understanding of AE in Soil
Mechanics. Early work at Drexel concentrated on some of the more
fundamental aspects of AE in soil. However, the subsequent
emphasis has been on the more practical applications of AE,
particularly in the area of insitu monitoring of dams and
embankments. This work is reviewed in the following section,
Insitu monitoring.

Lord et al (1975) reported the first serious investigation into
the AE response of soil. The initial experiments attempted to
define the basic characteristics of elastic waves in soil. The
characteristics considered were velocity, frequency, and
attenuation the last of these being considered the most
important. The values of wave velocity obtained (400-800 ft/sec)

were consistent with published data but the values obtained for attenuation (40dB/ft) were an order of magnitude different. This difference was attributed to a frequency dependence since the original reference's attenuation figures were recorded at 200Hz whereas Lord et al were testing at several kilohertz. By duplicating the experimental apparatus of Nybord et al (1950) it was demonstrated that sand attenuates sound waves to a high degree, with attenuation figures of 500 dB/m being recorded for dry sand. It was also found that the emitted frequency spectrum was dependent on confining pressure, a higher confining pressure resulting in a higher range of recorded frequencies. The conclusions from the frequency analysis of the emissions indicated that the frequency of the majority of the emissions lay in the region below 16kHz. This conclusion is not strictly true since the equipment could not measure frequencies above 16kHz.

Once the basic characteristics for various soil types had been established Lord et al considered the AE response of 3mm glass beads under triaxial stress conditions. The equipment used in this part of the investigation was, effectively, that used by Beard (1962) although the ringdown counting had been automated. The results indicated a high degree of similarity between the stress/strain and the stress/AE curves. In comparison to tests on sand the reported stress ratios were low, although the shape of the stress ratio curve was similar to that of sand. Unfortunately nothing more significant than this was reported, although Lord et al indicated that creep testing the glass bead samples gave favourable results.

Koerner et al (1976) investigated the behaviour of four granular soils by incremental loading under triaxial and isostatic conditions using the same apparatus as Lord et al (1975). The emissions were recorded using a sensor embedded in the sample and another in the base platen of the pressure cell. The published results indicated that there was a basic relationship between stress and Acoustic Emission, and that more angular samples were more emittive. Koerner et al acknowledged that the experimental technique was crude and that considerable improvements could be made. The use of an embedded sensor, whilst reducing attenuation losses, degraded the information obtainable from the experiments since it disturbed the sample behaviour to an unknown degree, and also precluded the use of saturated samples unless special precautions were taken to waterproof the sensor.

Koerner et al (1975) investigated the AE response of large soil masses, both in the laboratory and in the field, using waveguides to conduct the emissions to the monitoring equipment on the ground surface. A short preliminary study of the effect of the waveguides was made, the results of which indicated that the waveguide's performance was not adversely affected by the surrounding soil mass. Both the laboratory and the field work were concerned with embankment and bearing failure. The conclusions were of a qualitative nature and were that earth masses that did not generate acoustic emissions were in equilibrium and those that were generating large amounts of AE were unstable. These conclusions are in accord with those of Obert (1975). The conclusions from this work provide the basis for much of Koerner's later work relating to insitu monitoring.

Koerner et al (1977) investigated the AE behaviour of cohesive materials, adopting the same testing technique as in the paper on cohesionless materials (Koerner et al (1976)). Four cohesive soils were studied: clayey silt, silty clay, kaolinite clay, and bentonite clay. It was found that the AE response was markedly different from cohesionless soils; the AE signal level was one or more orders of magnitude less than that of cohesionless soils, and as the sample approached its failure stress the signal level dropped. It was proposed that this was due to reorientation of particles as the plastic state became fully mobilised. Additionally, fewer acoustic emissions were recorded in samples with high water contents or high plasticity indices. An unsuccessful attempt to use the Kaiser effect in determining the preconsolidation stress was made but the AE results indicated a much higher preconsolidation stress (8.0 tsf compared with 3.8 tsf). However, in a discussion of this paper Nathan (1978) showed that the preconsolidation stress, determined using the Casagrande method, had not been calculated correctly and there was a closer agreement between the traditional and AE methods than had been thought originally.

Tanimoto and Noda (1977) used AE to try and establish a method of predicting time to failure in soils, and used a water loading system to try and eliminate background noise which might have been generated by a motor. Tanimoto and Noda demonstrated the dependence of count rate on strain rate, also that count rate was proportional to the cell pressure. It was found that the count rate, after rising steadily, fluctuated about a more or less constant value. None of the work by Koerner and co-workers demonstrates this behaviour. The 'steady' value of the count rate

was used in estimating the time to failure of the sample; the actual value used in prediction was calculated on the basis of similar triangles to give emission rate. The point at which one process turned into the other was found to be, by inspection, the point of zero volume change. Tanimoto and Noda conducted several tests in both stress and strain controlled conditions and found that for strain controlled tests, there was a linear relationship between failure time and ringdown count rate. It was argued that the same was true for stress controlled tests but inspection of the results reveals a distinct curve.

Tanimoto et al (1978) expanded on the results of Tanimoto and Noda (1977), using equipment with better specifications. The number of counts recorded was shown to be proportional to the threshold level; lower threshold voltages resulted in more counts. It was concluded that there were two processes involved when testing sandy soils: one prior to 'steady state', the other being 'steady state'. Tanimoto et al (1978) also found that the energy done by the external stresses and the count rate for the two different processes could be described by a linear relationship. Tanimoto and Nakamura (1981a) summarised the results of the two earlier papers. All the results presented indicate that only medium dense samples were tested and gave those results described above. There is no presentation of results from dense specimens in which little compressive volume change occurs.

Lord and Koerner (1979) presented a method of estimating the magnitude of acoustic emissions in terms of acceleration. Using simple theory they related the acceleration of the acoustic wave

(emission) to soil volume under stress (V), radiation efficiency (R), frequency (f), and distance from source (r). The equation was of the form:

$$a_{max} = pi.f^2.e^2.V.R.c/(2.dt.r^2)$$ (2.2)

where pi=3.142, e=elastic strain, c=wave velocity, dt=time interval. However, many of the parameters have to be estimated to reach a solution which reduces the applicability of the equation. Also, unless every emission is studied, the magnitude of an emission is of very little practical use.

Tanimoto et al (1981) used AE as a method of enhancing several standard soils tests. Cyclic loading tests on an air dried sample of decomposed granite were carried out in a triaxial cell. The results showed that the Kaiser effect was present: most emissions were recorded during virgin loading, and few were recorded during the unloading and reloading stages of the test. Oedometer samples of sand were overconsolidated and monitored using AE equipment. The preconsolidation stress was calculated using the Casagrande construction and compared to the AE-stress plot. This plot showed that the point of maximum curvature on the AE-stress plot corresponded with the preconsolidation stress. This, in effect, is equivalent to the Kaiser effect in metals. Once the stress level has passed its previous maximum the count rate increases quickly, and hence a point of high curvature is established.

Following Tanimoto, Koerner et al (1982) used AE to try and determine the stress history of soil and rock; i.e. whether or not the Kaiser effect is present in those materials. A sandy clayey silt was tested in a standard oedometer and a AE-pressure

curve as well as the strain-pressure curve was plotted. The few results given indicated that AE provided a better method of identifying the preconsolidation pressure than the more usual strain-pressure plots. Koerner also reported tests on rock where the presence of the Kaiser effect was clearly demonstrated.

Lord et al (1982) studied the behaviour of steel rods when used as waveguides, and concluded that up to thirty times more (volume) soil could be sensed. The study also showed that damping of the waveguide by the soil reduced the amplitude of the received emissions.

Following Koerner at al (1982), Koerner et al (1984a) and Koerner et al (1984b) used AE to determine the level of prestress in granular soils and preconsolidation stress in cohesive soils respectively. It was found that the original prestress in granular soils could be predicted to within approximately 5% using both AE and deformation techniques. However, it was found that at low prestress levels the error rate was greater (12% or more). In cohesive soils the preconsolidation stress could be predicted to within +/- 10% using AE. Different soils, both cohesionless and cohesive, produced different error rates with cohesive soils giving more consistent results.

Romeril (1979) studied a number of different soils using AE equipment similar to that of Fischer and Yorke (1964). The soils were placed in a tank (400 long x 200 wide x 300 deep) and a sensor (50 diameter x 100 long) was embedded in it. The sensor was connected through an amplifier and filter to a set of headphones and an oscillograph. The results were similar to that

of Koerner et al (1975) in which it was found that stable earth masses did not generate AE whereas unstable masses did. The accuracy of the measurements given in the paper was limited by the ringdown counting method which used the trace recorded by the oscillograph: at times of high AE activity it was possible for the trace to go off the paper and hence it was not possible to determine accurately the number of ringdown counts. Mitchell and Romeril (1984) used the same techniques as Romeril (1979) and investigated the AE behaviour of clay. The conclusions were similar to Romeril (1979).

2.4 Insitu Monitoring

McCauley (1975) used a technique similar to that of Fischer and Yorke (1964) to monitor the slope stability of decomposed granite, sand, silt, and clay. The equipment was supplemented by an oscillograph to provide a permanent trace of the acoustic emissions. It was found that AE could not be used as an absolute indicator of slope stability but that it could be used if the AE history of the site was known. Also, the probability of failure could be predicted but an experienced operator was required since the method was based on subjective interpretation of the results.

Koerner et al (1975) used AE to monitor the stability of dams and, additionally, performed laboratory experiments to simulate bearing and slope failure. Waveguides were used to improve the detection of acoustic emissions. It was found that stable earth masses did not generate AE whereas unstable masses did. Also the Kaiser effect was noted when monitoring one dam, but most of the findings were of a qualitative nature. Koerner et al (1978)

summarised earlier papers and made suggestions for equipment selection, and monitoring decisions when considering AE for use as a monitoring tool. Much of the work by Koerner and other co-workers at Drexel University was summarised in an US Environmental Protection Agency (EPA) report (1978) which gave guidelines for the use of AE when monitoring dams. The EPA report also gave several case studies in which AE had successfully given warning of impending failures.

Tanimoto et al (1981) adapted a single cell pressuremeter for AE to determine the insitu stresses. An initial laboratory experiment had shown that the preconsolidation pressure could be accurately determined using AE (c.f. Koerner et al (1982)). Based on their initial results Tanimoto et al adapted the pressuremeter so that there were two pressure cells, both equipped with AE transducers, one above the other. However, no guard cells were employed as are used in the Menard type of pressuremeter. It was found that there was good agreement with the insitu stress determined by traditional methods. Some disagreement between the two methods was noted near the start of the test, which may be due to the lack of guard cells. Tanimoto and Nakamura (1981b) supplemented the results given by Tanimoto at al (1981) by reporting on a modified cone penetrometer. It was found that AE could be used to identify different soil layers but that sandy clay and clayey sand were hard to distinguish.

Following Tanimoto et al (1981), Lord and Koerner (1983) used a Menard pressuremeter with external AE transducers to determine the feasibility of using an adapted pressuremeter to measure insitu stresses. The results were confined to simple laboratory

experiments and, unlike Tanimoto et al (1981), no attempt was made to combine the AE transducers with the pressuremeter although this was one of the final project aims.

Villet et al (1981) used a modification of the Dutch cone penetrometer to try to characterise soils. The results were preliminary, as the research program was incomplete, but it was shown that the technique was consistent and that peak amplitude might be useful in characterising different soil layers.

Koerner et al (1981a) presented a state of the art paper covering both laboratory and insitu testing. A number of different case histories were given which covered the following areas: dam and slope stability, settlement monitoring, seepage monitoring, and grout monitoring. In one case history a slope was brought to failure by successive cuts at the toe of the slope over a period of 21 days. After each cut AE activity increased but then decayed (approximately exponentially). After the final cut had been made the emission rate started to rise sharply (having started to fall) and five minutes later a section of the slope slipped. Another interesting point to emerge from this study was that after a period of heavy rain the emission rate rose above its previous maximum, indicating reduced slope stability. Other case studies presented for seepage monitoring and settlement monitoring showed a similar success rate. The case history of AE in grout monitoring showed that it might be possible to identify the pressure at which hydrofracture occurred, but that to identify the location of travel of the grout front would require much more sophisticated AE monitoring equipment.

Koerner et al (1981b) investigated the AE response of mine tailings. The emissions were generated by means of anchor pullout, direct shear, impact loading so that repeatable results could be obtained. A number of different waveguides were used: steel and PVC, in rod and pipe form. It was found that the AE amplitude decayed exponentially from the source and that signals below the water table had larger amplitudes. It was concluded that, where possible, AE sensors should be placed at the bottom of boreholes, on waveguides, as this maximised the strength of the received signal and minimised the amount of background noise.
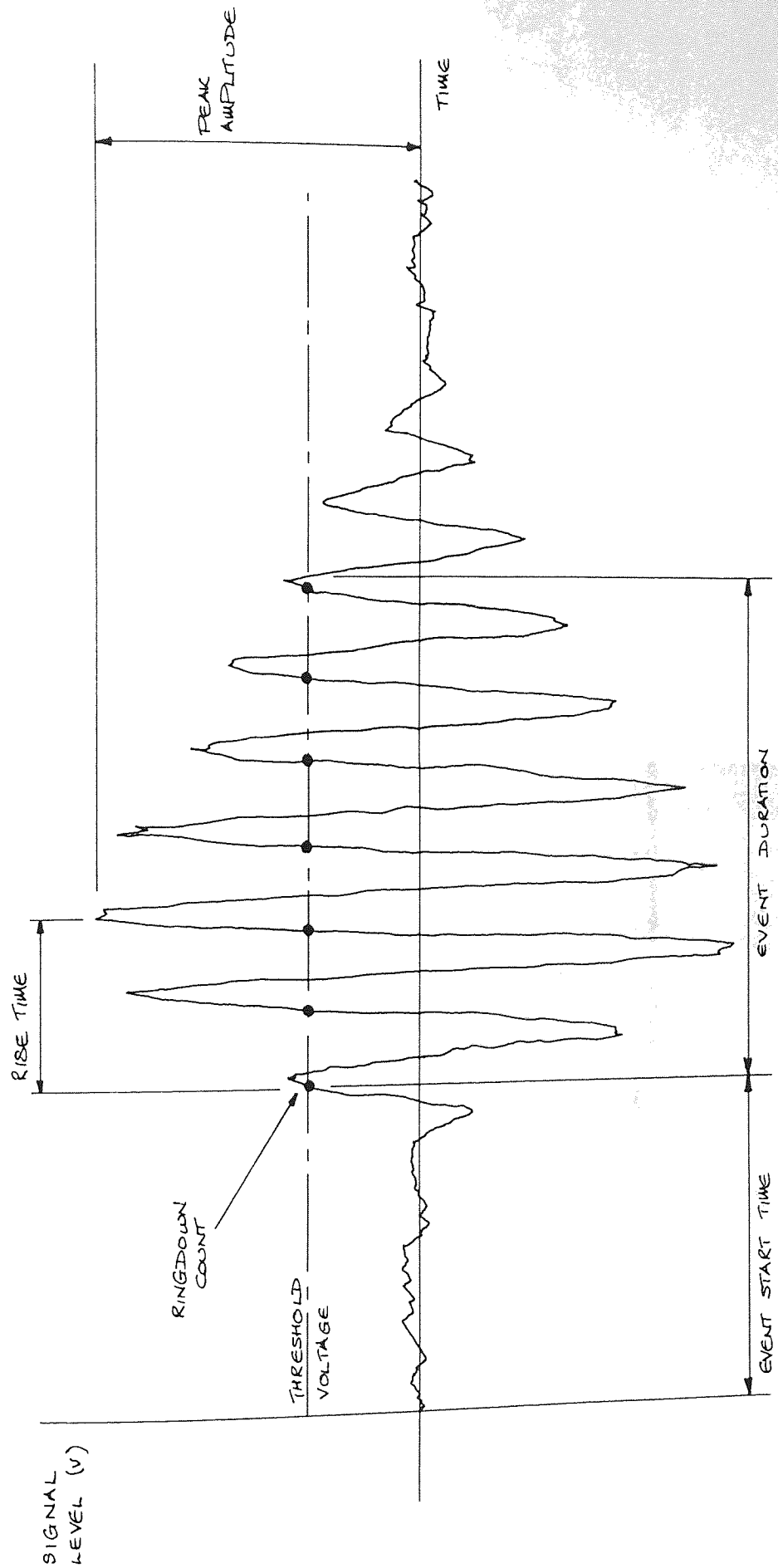
Figure 2.1 An idealised acoustic emission
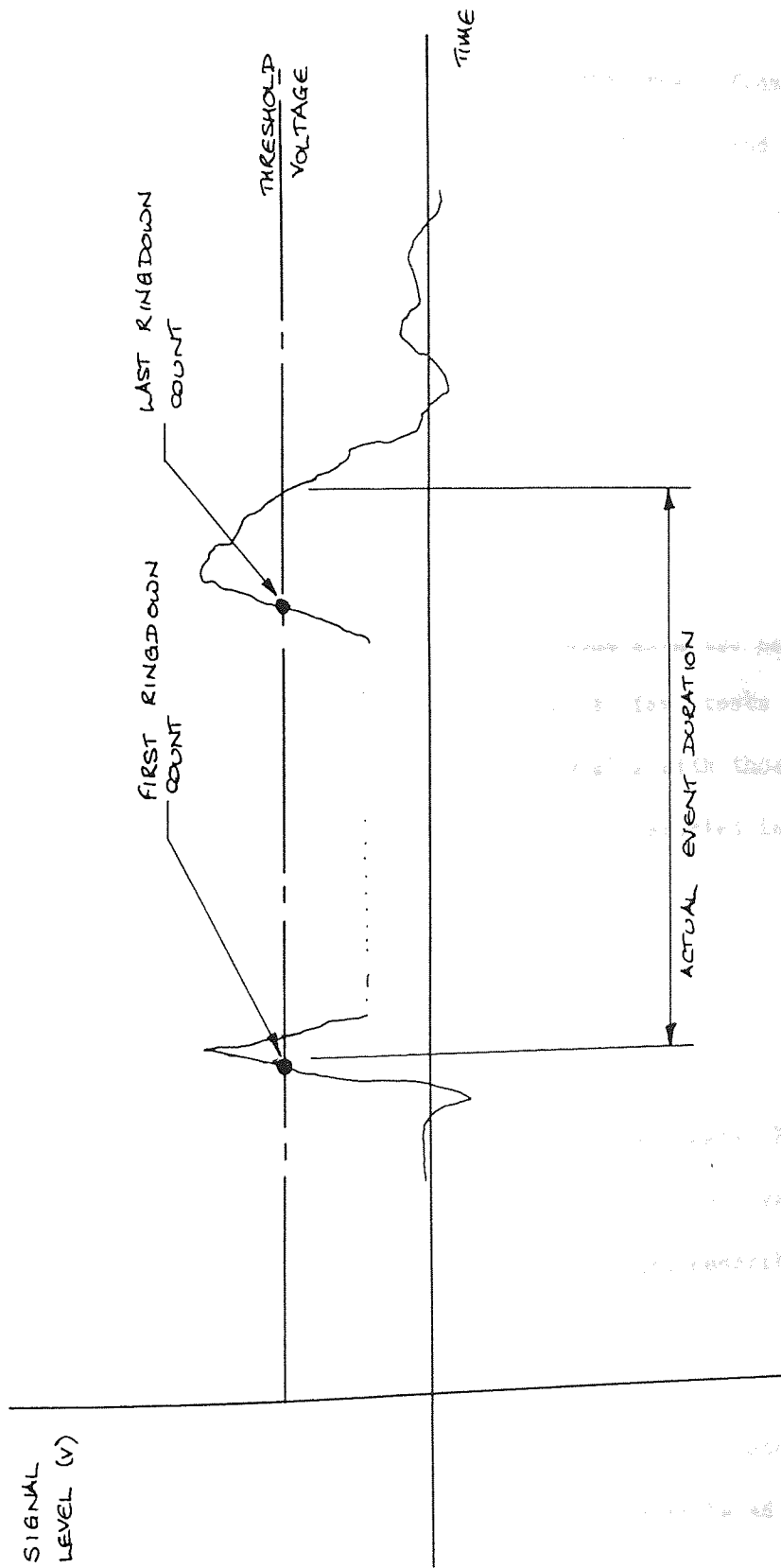
Figure 2.2 The duration of an event

Chapter 3.

Apparatus, Sample Preparation and Testing Technique.

3.1 Introduction.

The apparatus used in the research program was drawn from two distinct areas, that from conventional soils testing and that from electronic monitoring, and their successful combination was an important part of the program. Standard laboratory techniques were applied in the preparation and testing of the sand though in some instances adaptations had to be made because of the Acoustic Emission (AE) monitoring.

Normally samples were of a nominal 100mm diameter by 100mm high tested between enlarged, lubricated end platens with the samples being drained from the bottom platen only. A few tests were carried out on taller samples to compare results with those of other workers. Additional details of all tests reported in this thesis are given in Appendix A.

3.2 Standard Soils Equipment.

In general standard soils equipment was used in all tests (Figure 3.1). However, to accommodate the AE sensors various modifications were necessary; the modifications are described in more detail where appropriate.

The loading frame, a Wykeham-Farrance WF5000kg Stepless Compression Test Machine, allowed the strain rate to be adjusted with a set of thumbwheels and the strain direction to be changed

with push button switches. The design of the frame meant that there was no large gear train from which extraneous noises could be picked up by the AE equipment. Thus, when the strain rate was altered or when the strain direction was altered the effect on the AE measurements was negligible - given that suitable care was taken in setting up the parameters on the AE equipment.

The cell and cell base used were standard but for three drilled and tapped holes which were used in extension tests for bolting down the cell. To accommodate various extra items of equipment and to allow for the higher than normal base platen an extension ring, 50mm high, was provided. This incorporated the mounting point for the linear transducer, cable outlets for the same, and a second drainage outlet. The holding down rods of the cell screwed into the ring which in turn bolted to the cell base. In normal operation the ring was left bolted to the cell base.

For efficient AE monitoring it was necessary to have the sensor located as near as possible to the source of the acoustic emissions. Koerner et al (1976) used wave guides and even embedded sensors in the sample; both of these methods are unsatisfactory as the sample is disturbed. To avoid disturbance of the sample by the AE equipment an adapted base platen assembly was manufactured (Figure 3.2). The platen had a removable stainless steel top plate beneath which was a small void large enough to contain the AE sensor. The sensor lead passed out through the cell base, avoiding contact with the cell water. The sensor was held in position by packing with rubber membranes. The top plate was drilled so that the sample was drained centrally

24

through a porous stone although additional drainage was provided through four side drains. Both top and bottom platens were enlarged to 118mm diameter following Rowe and Barden (1964).

The load applied to the sample was measured internally using a Wykeham-Farrance 2700kg load cell, and by measuring the load internally any friction on the load cell shaft could be neglected in load calculations. Modifications to the load measuring equipment were necessary because of the planned extension tests (Figure 3.3). The load cell was fixed to the load frame by a short stainless steel pin, and was connected with the top platen by a bayonet fitting. The load cell shaft was inserted into a socket on the top platen and was twisted to engage lugs with appropriate slots in the the top platen. The cell base was bolted to the loading platen with three bolts to prevent uplift.

The change in the volume of the sample was measured using a Wykeham-Farrance WF17038 Automatic Volume Change Apparatus. The volume change device uses a plunger of fixed radius connected to a linear transducer and, by measuring the displacement of the plunger, the change in volume can be determined. Theoretically the device can accommodate an infinite change in volume as taps allow for reversal of the plunger direction; a change in volume of approximately 80ml can be measured before reversal is necessary.

The axial deformation of the sample was measured using a Linear Variable Differential Transducer (LVDT), RDP Electronics model D5-200AW, mounted inside the cell. The deformation was measured between the top platen and the cell base - allowing deformations

of the load cell to be neglected. The linear range of the LVDT was 12mm which was sufficient for many tests. For tests in which deformations greater than 12mm were to be recorded a double LVDT arrangement was used (Figures 3.4, and 3.5). The LVDTs were arranged in such a way that as one reached the end of its linear range the other was starting to record on its linear range. Adjustment was provided for different sample heights by means of threaded rods. By using this double LVDT arrangement deformations of 22mm could be recorded satisfactorily.

The cell and back pressures applied to the sample were measured using Bell and Howell 700KPa pressure transducers. These were connected into the drainage and cell water lines respectively and the actual pressures were controlled by a self compensating mercury pot system.

All the measuring instruments used except the AE equipment were connected to a datalogger which recorded the measured parameters at fixed intervals. Automatic logging allowed the AE behaviour to be monitored more closely as the test proceeded. The stresses and strains were calculated from the raw data using a small computer program.

All transducers and load cells were regularly calibrated over the research period. None showed any marked variation in their calibration except when a load cell started to leak oil and had to be repaired.

3.3 Acoustic Emission Equipment.

All AE monitoring was performed using an AET5000 system (Figure 3.6), supplied by Acoustic Emission Technology Corporation (AETC). The AET5000 is a computer based, general purpose acoustic emission monitoring system which can handle up to eight sensors and can output the AE data in numerical or graphical form. The basic AET5000 provides the minimum information necessary to describe an event (start time, event duration, and ringdown counts). Various options are available to enhance system performance and those fitted were: tape drives for data recording and an amplitude/rise time module for further information on the AE data. A simplified system diagram is given in Figure 3.7. The AET5000 is supplied as a complete system and access to the individual system components is difficult. However, it is useful to describe the function of each main component and its place in the signal chain so that its effect on the overall behaviour can be appreciated.

The sensor used was of the piezoelectric type model AC30L, manufactured by AETC with a nominal resonant frequency of 30kHz. The frequency response of the sensor is given in Figure 3.8. The sensor was mounted in the base platen directly below the sample and firm contact with the top plate was ensured by packing the sensor with rubber membranes. Koerner et al (1976) when testing sand claimed that the frequency of the majority of emissions lay in the region below 15kHz although Tanimoto et al (1978) successfully used a sensor with a frequency response to 40kHz. Also Koerner's tests were at a low cell pressure (35kPa) and it was demonstrated that as the cell pressure increased the

frequency distribution of the recorded emissions shifted towards the higher frequencies.

The sensor was connected to the preamplifier by a short (2 metre) cable. It was found that 'emissions' could be picked up by the cable unless it was prevented from moving. Koerner et al (1981a) found when monitoring a dam that unless the cables were shielded from wind extraneous 'emissions' were picked up. The high gains employed in the system (X100000) are undoubtedly the cause of this since cable movement induced a small voltage which was magnified to produce a false emission.

The preamplifier combined a fixed gain amplifier with a band pass filter. The fixed gain was factory set at 60dB (X1000). The filter attenuated any signal which had a frequency outside its prescribed range of 15kHz to 45kHz. By using a bandpass filter most of the mechanical noise was rejected as mechanical noise tends to be of low (<1kHz) frequency. The amplified and filtered signal then passed to the main amplifier of the AET5000.

The main amplifier has variable gain setting from -60dB (total attenuation) to 40dB (X100). Before the incoming signal was amplified it was compared to the previously set threshold voltage. If the signal crossed the threshold voltage it could be tentatively classed as an event by the AET5000. Once the start of an event had been recorded the various internal timers and counters were started. The end of an event was determined by the AET5000 when no further ringdown counts (threshold crossings) were recorded after a timeout period. The timeout period was described in terms of the number of 'ticks' of the event duration

clock, the time period of which was set at the start of the test. When the end of an event had been recorded the digital information representing the characteristics of the event were compared to preset limits. If any characteristics fell outside these limits the event was rejected.

The AET5000 was fitted with an optional tape drive which allowed the characteristics of each event to be recorded on tape and replayed at some later time. The data were recorded on digital tapes, the number used depending on what particular type of test was being carried out. Once recorded, the test could be replayed as many times as required. This particular option proved very useful because by replaying a test and outputting the information describing every event to the screen it was possible to transfer the information to a BBC microcomputer. Once the information was stored on the microcomputer the data could be combined with the stress and strain data to provide a complete test record.

The AET5000 has, at various points in the signal chain, outlets for connection to external equipment. These outlets comprise: preamplified and filtered signal, quasi RMS signal, and fully amplified signal. A storage oscilloscope could be connected to the first of these outlets to allow inspection of an event and comparison with the 'typical event'. By photographing the screen of the oscilloscope it was possible to obtain a permanent record of events occurring in a test.

Once a signal had been fully classified as an event the measured and derived information representing it was available for analysis. It was possible to output this in numerical form but

the AET5000 provides some powerful graphical facilities to aid analysis of the data. The graphical displays were set up at the start of the test and could consist of:

Events, Ringdown Counts, Rise Time, Event Duration, Energy, Peak Amplitude, Mean Slope and Voltage Level.

These could be plotted against time as a rate or as a total, and also to a logarithmic scale (rate or total). Distributions of events by a particular parameter (energy for example) could also be displayed.

For full details of system operation the AET5000 operating manual should be consulted. The manual also gives information on the optional equipment which may be supplied.

3.4 Sample Preparation and Testing Technique.

The sample preparation and testing techniques used were in accordance with current research practice. A detailed review of the triaxial testing of sand will not be undertaken here since others (e.g. Green (1969) and Thornton (1974)) have covered the relevant techniques very thoroughly.

The sand used was 'Leighton Buzzard' sand with a measured specific gravity of 2.68, the sand being that fraction which passed a 600um sieve and was retained on a 150um sieve. The minimum porosity was 34.8% using a vibrating table and the maximum porosity was 45.8% using Kolbuszewski's tilting method, Kolbuszewski (1948).

A measured quantity of sand was put on a tray in an oven overnight. Four end membranes were cut from a sample membrane, greased, placed on the platens and left under load overnight. The end membranes were laid such that no air was trapped in between them. The membranes on the bottom platen were separated from those on the top platen by a piece of paper to prevent sticking.

The sand was removed from the oven and weighed, it was then saturated by pouring deaired water onto it and was allowed to cool. The sample membrane was cut to length and its thickness determined at eight points to give an average thickness. The paper separating the end membranes was removed and the height of the assembly was measured using a vernier height gauge. The top platen was removed and the sample membrane was placed over the greased bottom platen and trapped in position by three 'O' rings. The 100mm high by 100mm diameter sample former was then positioned and the membrane stretched over the top of the former. The sample drainage tap was opened and the system was flushed with deaired water to remove any trapped air bubbles in the drainage system and sample membrane. The porous stone, which had been boiled to deair it, was placed in the bottom platen.

The sand was spooned into the former under water. The sample was constructed in three equal layers, after each layer had been formed it was tamped with a short steel rod (X50). The third and final layer was brought up to just above the top of the former but below water level (Figure 3.9). The top platen was then carefully placed on the top of the sample such that no air was trapped in the process. The membrane was turned up over the greased side of the top platen. Any excess length of membrane was

removed   and   two   'O'   rings were   positioned   to   complete   the
membrane seal.   The 'O' ring placement was achieved using a short
perspex tube to avoid sample disturbance.

A   small suction (0.6m of water approximately) was applied to the
sample   and   the   top   platen lightly tamped   to   ensure   a   good
contact.   The former was removed and the initial burette   suction
recorded   (Figure 3.10).   The height of the sample and top platen
was measured, the difference between this and the earlier reading
giving the sample height. The diameter of the sample was measured
using a 100-125mm vernier gauge,   a deduction being made for   the
thickness of the membrane.   After sample measurement, the burette
reading   was again noted.   The tray which contained the sand   was
returned   to   the oven to dry out any remaining sand so that   the
sample weight could be found.

The cell was placed over the sample and was bolted down. The load
cell was connected to the datalogger and the cell was filled with
deaired water.   When full,   the water supply was switched off and
the burette raised to the level of the mid height of the   sample.
The burette was isolated from the sample   after the final reading
had   been   taken.   The   load cell was then connected to   the   top
platen   using the bayonet fitting and the other end of   the   load
cell shaft was pinned to the load frame.

The   sample   was   ready   for   consolidation;   all   samples   were
consolidated   in   the   same manner.   All the   initial   transducer
readings   were noted.   The cell pressure was gradually raised   to
102   kPa   and   all transducer   readings   were   taken   again,   the
datalogger   being   set   to   record at   fixed   intervals.   A   back

pressure of 100 kPa was applied and the cell pressure raised to the desired level. The sample was then consolidated. After the sample had consolidated, indicated by no further volume change, the load train was engaged and the sample was ready for testing. Undrained tests required higher back pressures in order to avoid cavitation within the sample.

While the cell was filling with water the AET5000 was set up. This consisted of preparing data recording tapes, selecting any graphs to be displayed while the test was running, and setting the parameters which define an event.

All samples were tested at a constant strain rate, in general either 1%/hour or 3%/hour. These rates allowed time to examine the AE response of the sample and were slow enough to ensure accurate volume change readings.

Over the research period a number of different tests were performed which fell into three basic categories. The most straightforward was the 'constant cell pressure' test in which the cell pressure was kept constant over the test duration and where the sample was sheared at a fixed strain rate (i.e. a standard drained test). The next test category was the 'constant mean stress' test, in which the average of the principal stresses was maintained at some predetermined, fixed value over the test duration. The final test category was the 'constant axial stress' test; here, the value of the major principal stress was maintained at a fixed value over the test duration. The paths traced out by the test types on the $\sigma_a - \sqrt{2}\sigma_r$ plane in stress space are as follows: 'constant cell pressure' is a line parallel with

the σ_a axis, 'constant mean stress' is a line normal to the space diagonal ($\sigma_a = \sigma_r$), and 'constant axial stress' is a line normal to the σ_a axis. Later on in the research period several tests were performed in which a complex stress path was followed; here, a combination of the three test categories was used to achieve the desired stress path.

Associated with each test category was a sub-category: compression or extension. On the $\sigma_a - \sqrt{2}\sigma_r$ plane these sub-categories are represented by the direction of travel along the stress path line.

When testing at constant cell pressure all that was required was to set the required strain direction and start the motor. To perform an unload-reload cycle the motor was stopped, the strain direction reversed, and the motor restarted.

Tests involving a variable cell pressure required careful monitoring of the transducers, and at the end of every datalogger recording interval the currently required cell pressure was calculated using a programmable calculator. The mercury pot controlling the cell pressure was adjusted to the desired reading. At the start of a test it was necessary to overcorrect (using experience from previous tests) because the change in cell pressure was large. Consequently, there were minor deviations between the actual and the desired cell pressures during the initial stages of a test.

When the test finished the cell pressure was lowered to 102 kPa again, the drainage and cell taps being closed off. The cell was

drained, the bayonet undone and the cell removed. Usually it was not possible to take sample dimensions after the end of the test because the top platen had tilted very slightly and removing the bayonet disturbed the sample. The sand in the sample was collected, oven dried and weighed.

Data recording on the AET5000 was stopped and the test parameters, test statistics and numerical data representing the selected graphs were printed. The tapes containing the test event record were rewound and replayed at a slow rate to transfer the event information to the BBC microcomputer. It was not possible to transfer the data while the test was running because, when recording data, the AET5000 did not necessarily output all event information but, during post processing, it could be made to do so.
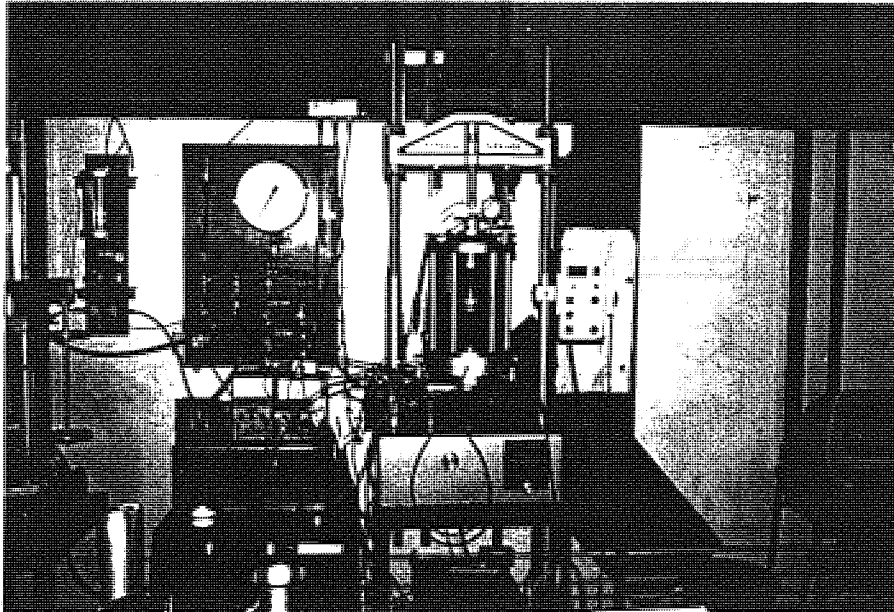
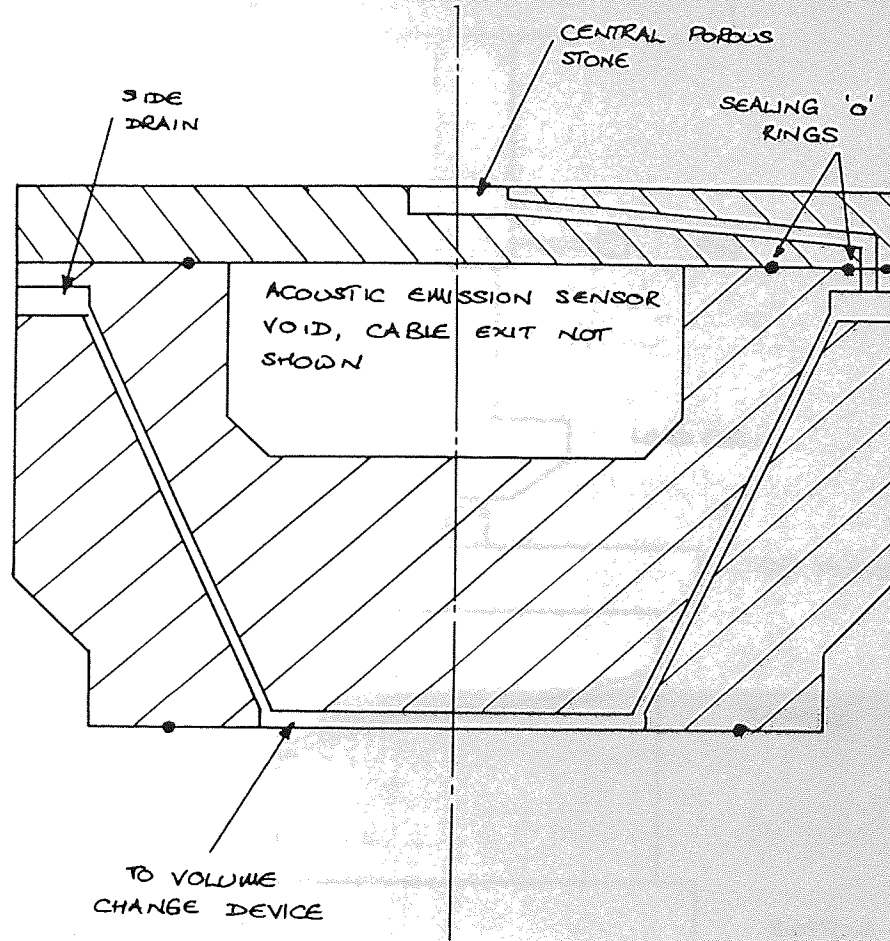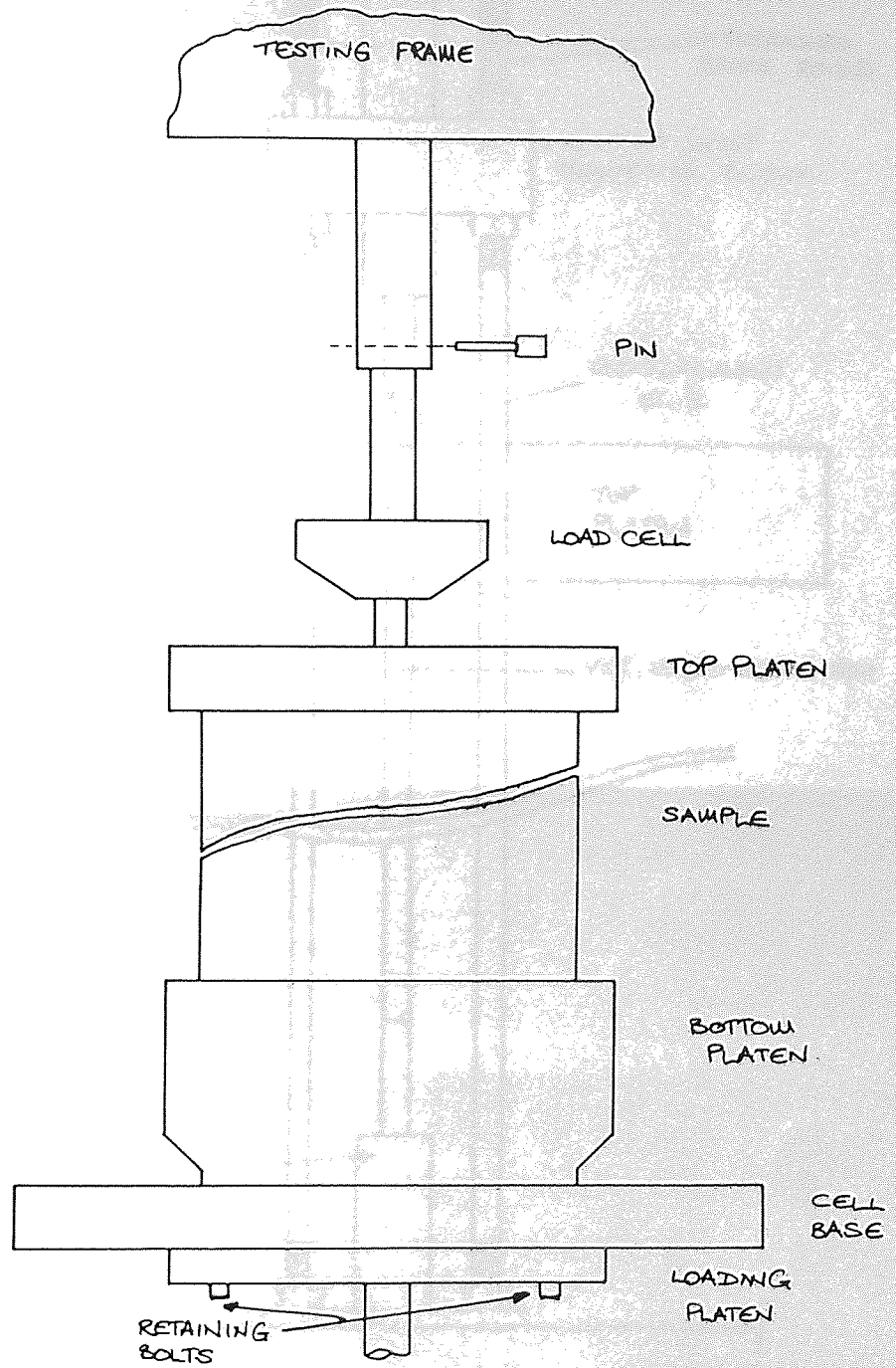Figure 3.1 General arrangement of soils equipment

Figure 3.2 Adapted base platen

Figure 3.3 Loading arrangement

The image shows a loading arrangement with the following labeled components (top to bottom):

- TESTING FRAME
- PIN
- LOAD CELL
- TOP PLATEN
- SAMPLE
- BOTTOM PLATEN
- CELL BASE
- LOADING PLATEN
- RETAINING BOLTS

CELL OMITTED FOR CLARITY.

TOP LVDT

THREADED BRASS RODS

TOP LVDT MOUNTING BLOCK

MEASUREMENT STUB

TOP PLATEN
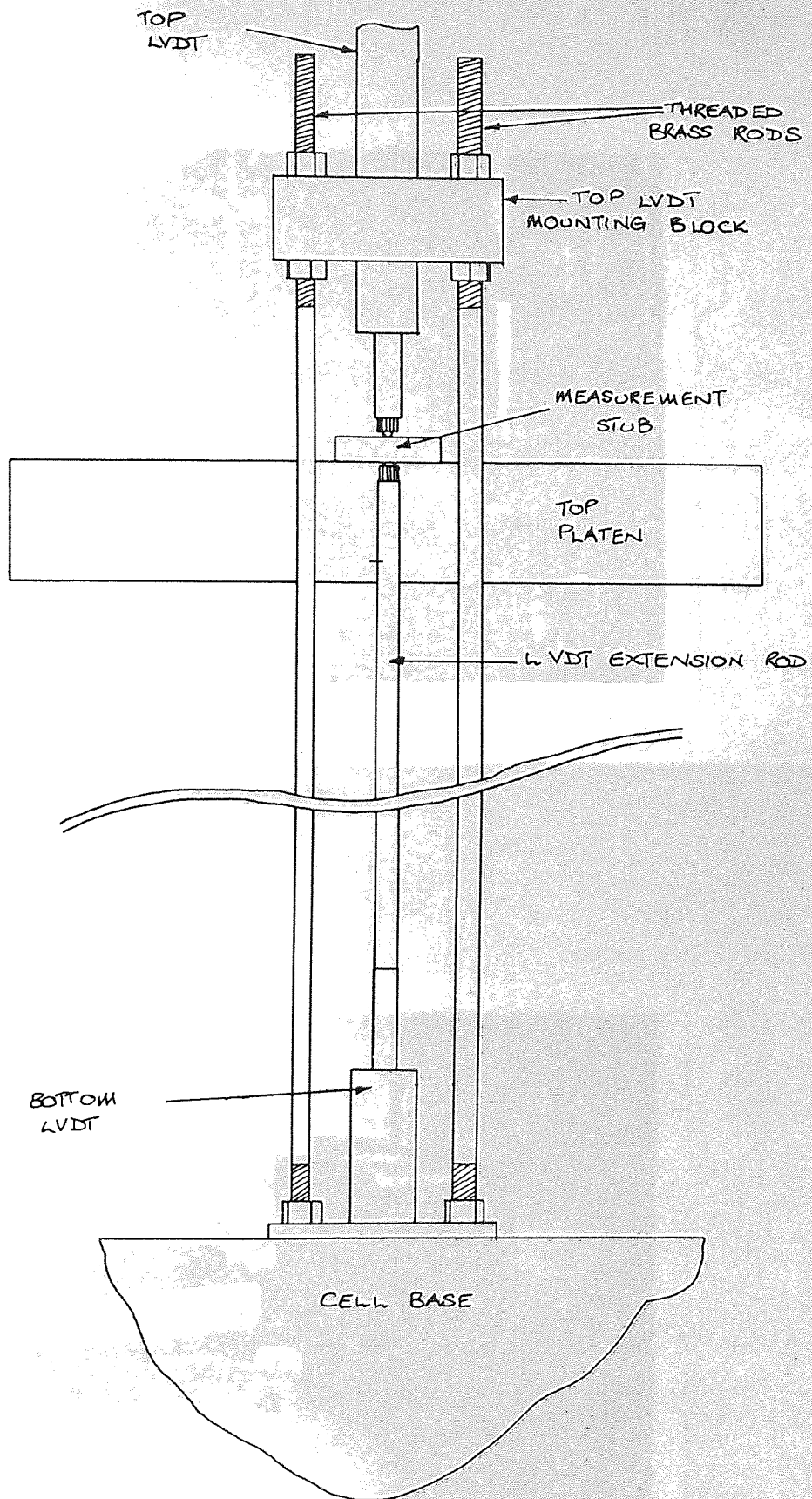
LVDT EXTENSION ROD

BOTTOM LVDT

CELL BASE

Figure 3.4 Linear transducer arrangement
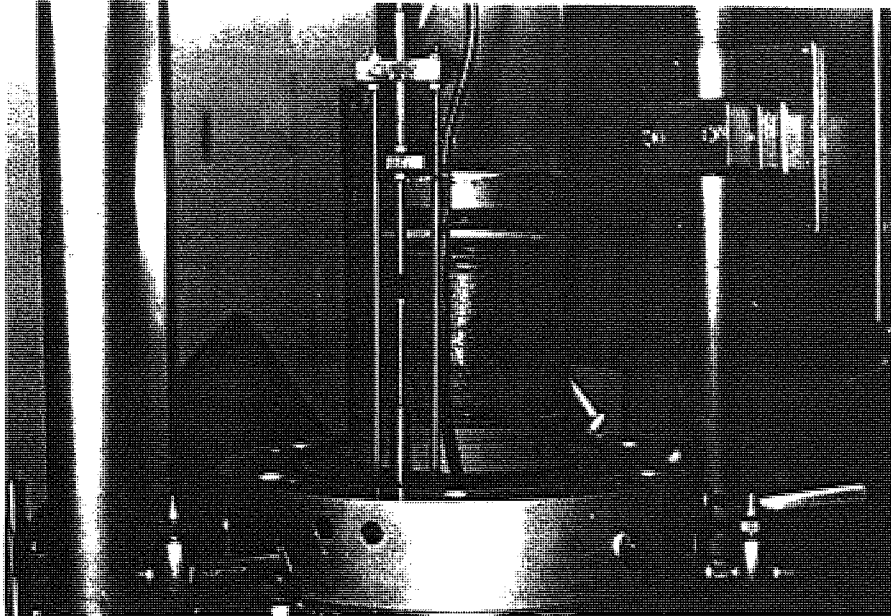
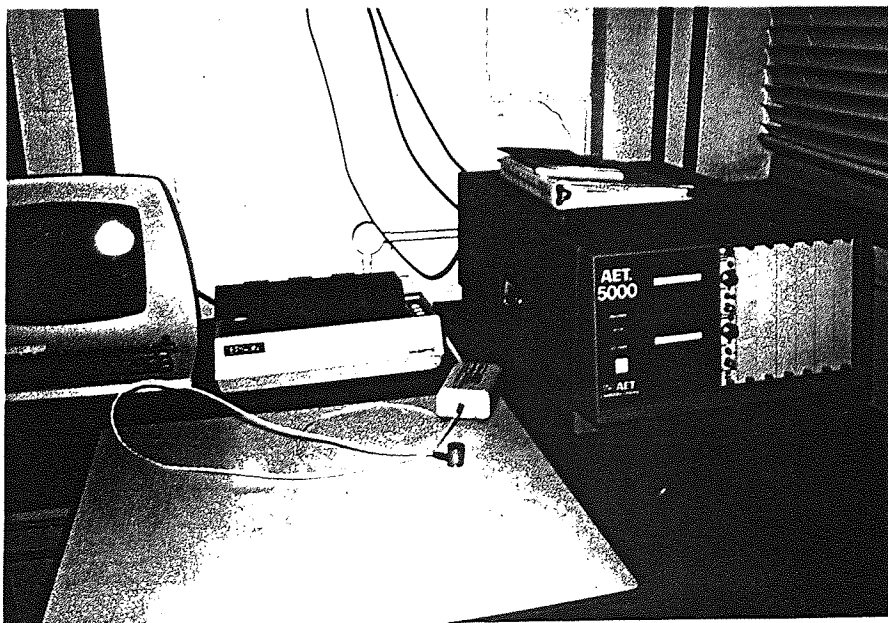Figure 3.5 Linear transducers

Figure 3.6 General arrangement of AE equipment
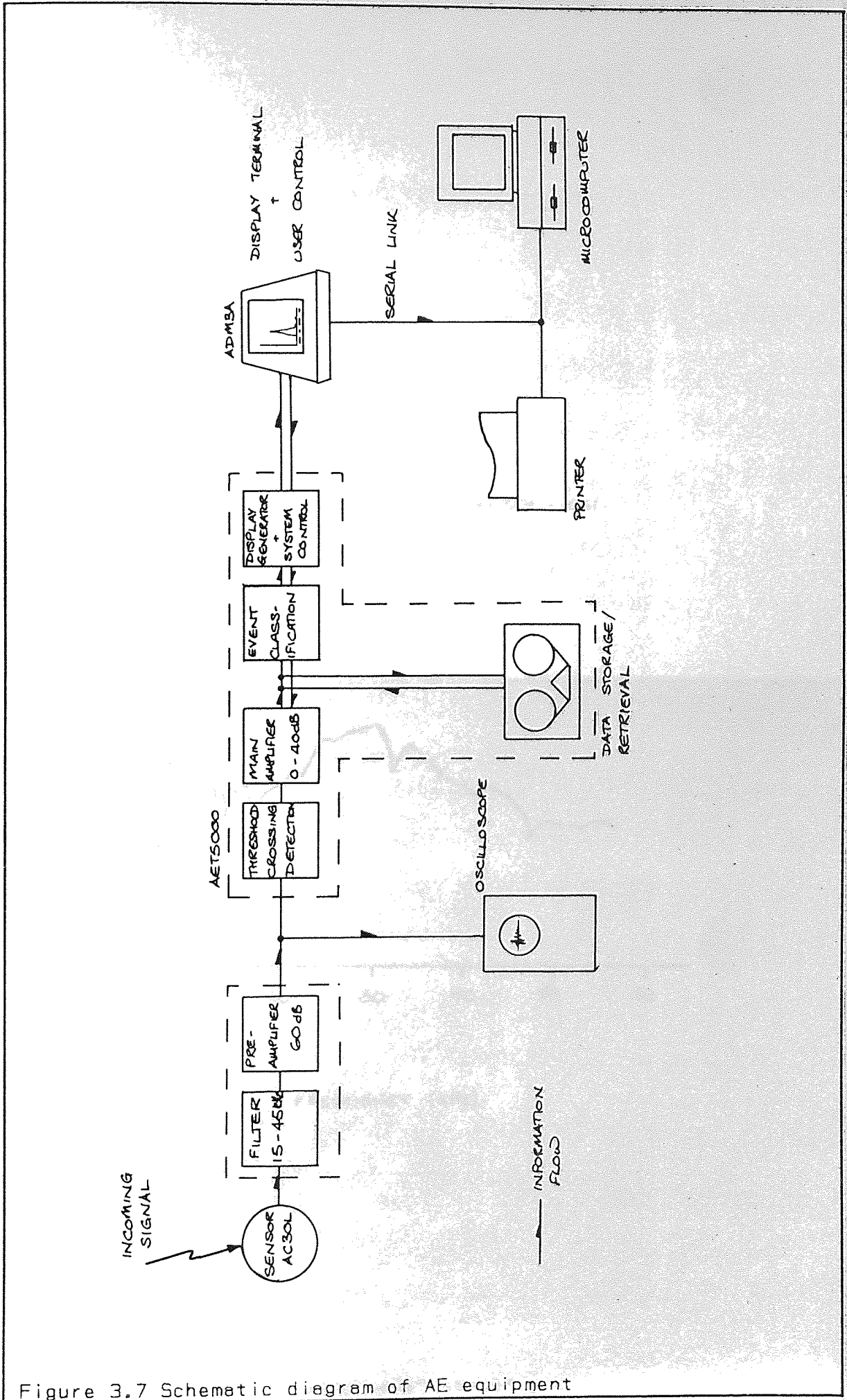
Figure 3.7 Schematic diagram of AE equipment

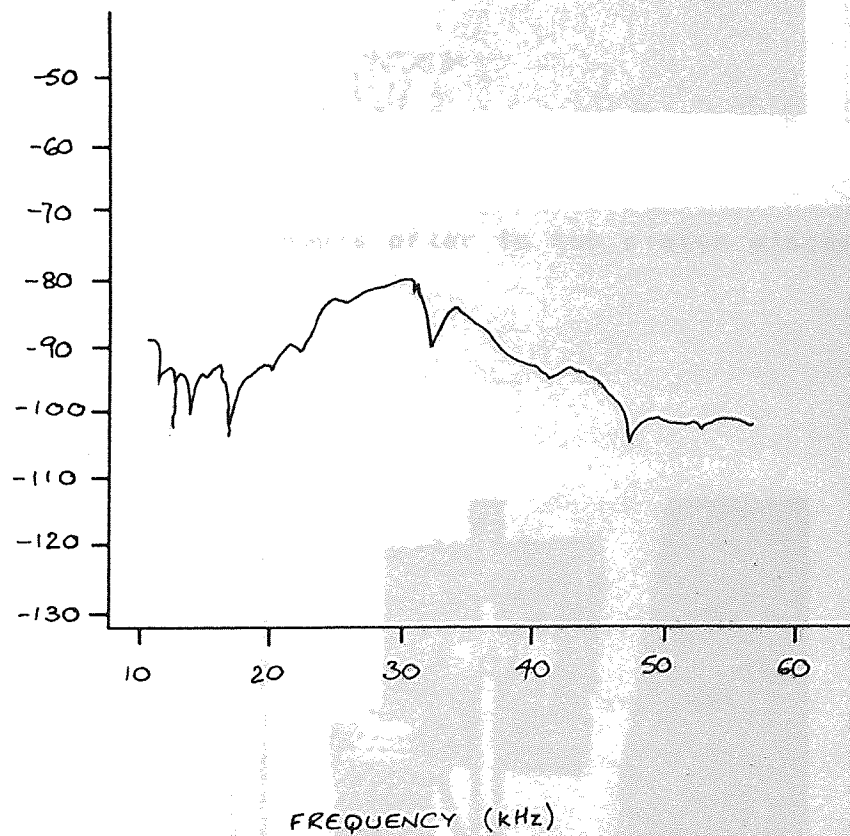SENSITIVITY (dB)   SENSOR   AC30L-1061

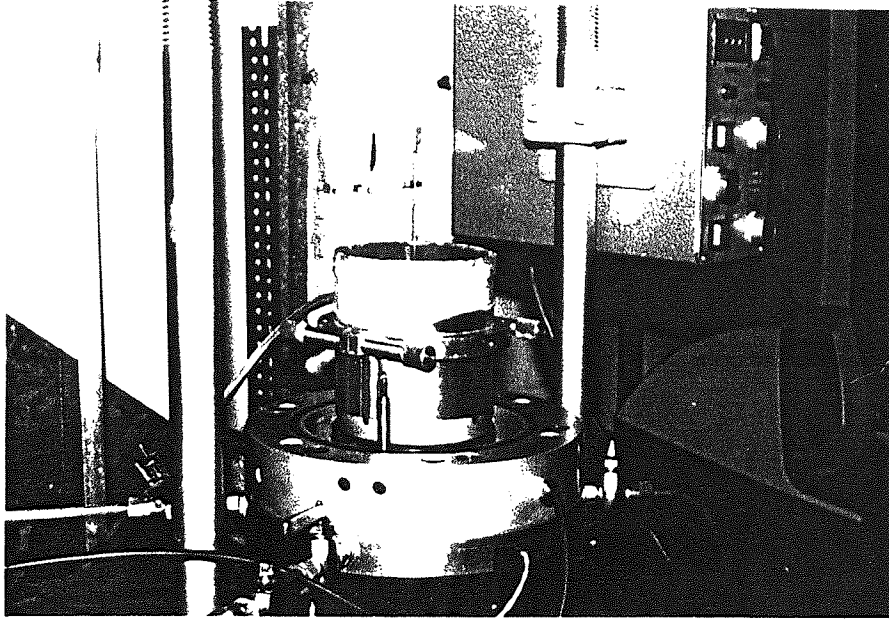Figure 3.8 Frequency response of sensor

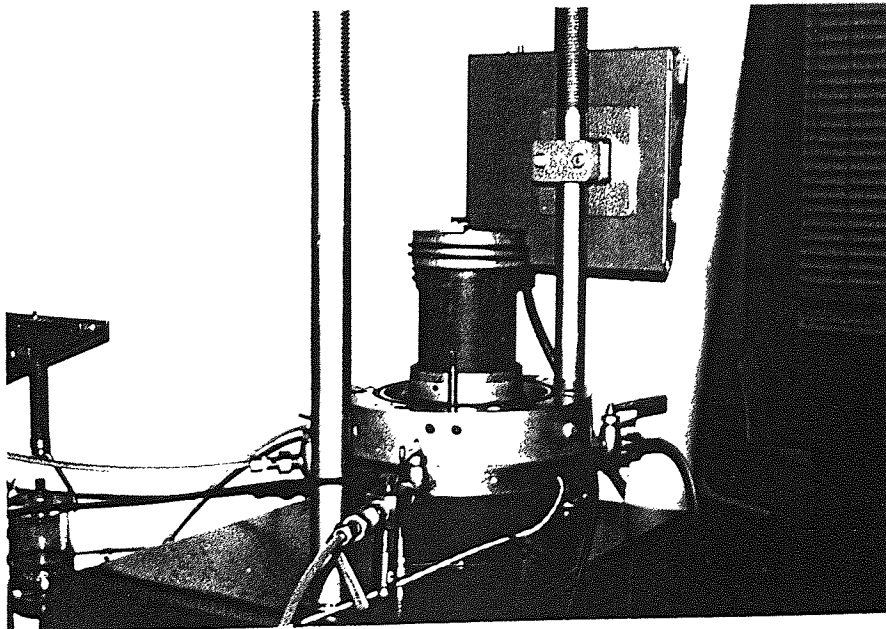Figure 3.9 Prepared sample prior to top platen placement

Figure 3.10 Fully prepared sample

Chapter 4.

Preliminary Tests.

4.1 Introduction.

The application of Acoustic Emission (AE) to soils testing is a
new technique and, as such, there is little literature on it.
When testing therefore it was important to minimise the effect of
the AE equipment on the sample. In standard soils testing many
conditions are taken for granted; this may not be possible for
tests using AE. The research program envisaged that complex tests
be performed on sand, and before proceeding, it was necessary to
establish the 'general AE characteristics' of sand in triaxial
testing. Information given in the literature (e.g. Koerner et al
(1976), Tanimoto and Noda (1977)) was conflicting and of
insufficient detail to be of any immediate use.

The results produced by the AET5000 are affected by a number of
constraints, some of which may be altered by control settings on
the AET5000. The most significant uncontrollable constraint is
attenuation: this is a function of the sand, platens, and AE
equipment. The nature of AE precludes any direct, exact
measurement of attenuation; but a reasonable estimate may be made
from simple tests. Experiments were carried out using two AE
sensors, one driven, the other receiving; the results of which
indicated that attenuation for dry sand is in the range 160-
1000dB/m. These compare well with those presented by Koerner et
al (1976) who found that attenuation in dry sand was in the range
300-1000dB/m. However, it was noted by Koerner that the
attenuation was dependent on the frequency of the acoustic
emissions.

The AET5000 system, as supplied, gives no indication as to the likely settings for its control parameters; however, it does assume default settings for most of these parameters. Initially the defaults for the bounds of event duration, number of ringdown counts, etc. were taken to be adequate so that the effect of gain and threshold voltage could be determined. Subsequent investigation of tests recorded on tape showed that the default settings were adequate and that no significant improvement in the number of events recorded was to be gained by varying them.

The number of events detected by the system is controlled by the gain and threshold settings on the AET5000. These are set at the start of a test and so it is important that they are adjusted for optimal performance. The AET5000, as supplied, provides no frame of reference to which these settings may be related. A series of tests was performed in which only the gain and the threshold voltage were altered, all other constraints remaining the same so far as was possible. The aim of this test series was to determine settings which would ensure that the AET5000 did not pick up an excessive amount of background noise, but provided enough information to be able to draw meaningful conclusions. It was found that a close link between gain and threshold voltage exists, and that increasing the gain is more useful than decreasing the threshold voltage since the latter allows more background noise to be detected. Also, it was found that satisfactory performance was obtained using a gain of 4.0 high (equivalent to 92dB overall) and a threshold voltage of 1.0V.

4.2 General Observations.

4.2.1 Soil Mechanics.

Once suitable parameters for the AET5000 had been found it was possible to describe the behaviour of a sample during monotonic loading with some confidence. Throughout the research period monotonic loading tests were carried out periodically as a check on the AET5000 system. Koerner et al (1976) plotted stress ratio/total counts graphs obtained from incrementally loaded triaxial tests and found that there was a correspondence between axial strain and the total counts. Figures 4.1 and 4.2 show the stress ratio/deviatoric strain and the volumetric strain/deviatoric strain graphs for a typical monotonic loading test (Test 110) in which the classic stress-strain response is clearly seen. The stress ratio increases at a decreasing rate until a maximum value is reached, after which the stress ratio decreases at a slow but steady rate. The volumetric strain curve shows a small initial contraction which is followed by a high rate of expansion, which is indicative of a dense specimen. The expansion continues at an approximately constant rate until peak, after which it decreases. The stress ratio/deviatoric strain and volumetric strain/deviatoric strain graphs for another monotonically loaded test, Test 88, are shown Figures 4.3 and 4.4; the same features may be noted as were found for Test 110.

4.2.2 Acoustic Emission.

Figure 4.5 shows the stress ratio plotted against events for Test 110. It is at once evident that stress ratio/events and stress ratio/deviatoric strain graphs are very similar but that the AE derived graph has a steeper gradient initially, when elastic strains are not insignificant. Figure 4.6 is the stress ratio/events graph for Test 88 and, here again, the same feature may be noted. Comparison of Figures 4.1 and 4.3 with 4.5 and 4.6 suggests that a relationship exists between deviatoric strain and events. Figure 4.7 plots deviatoric strain against events (Test 110). It is apparent that the relationship is non-linear and may be represented by a power law. Figures 4.8 (Test 110) shows the event rate/deviatoric strain graph; it is clear that the event rate is increasing with increasing strain but with considerable scatter. The scatter can be reduced by replotting the data using a moving average technique, Figure 4.9 (Test 110): it is not possible to remove all the scatter without compromising the validity of the data. Figure 4.9 shows two changes in gradient; one at a strain of approximately 2.0%, the other at a strain of approximately 10%. The second point corresponds to peak stress ratio. Post-peak the event rate becomes much more erratic but continues to rise.

4.2.3 The Work of Tanimoto and Co-workers.

Tanimoto and co-workers have carried out a large number of tests on sand in both a stress controlled and a strain controlled manner. The tests reported are on a partially saturated sand; the samples being, typically, 120mm high by 50mm diameter.

Unfortunately, in all the reported tests, few details of the apparatus are given. In particular no mention is made of end membranes although the height:diameter ratio might imply their absence. In reporting test results only ringdown counts, not events, are given; this is a limitation of the equipment used.

The results of a typical strain controlled test, Tanimoto and Nakamura (1981a), are reproduced in Figure 4.10. The deviator stress/axial strain curve is typical of that for dense sand specimens. However, the volume change curve shows that volumetric contraction occurs over a significant axial strain range; this feature is found in all the tests reported by Tanimoto. The ringdown counts/axial strain curve shows that the count rate rises rapidly until the constant volume point is reached, after which it oscillates about its previous maximum level. No significant change in the count rate is discernable at peak or post peak. This contrasts with the tests reported in this thesis, in which the event rate continues to rise throughout the test: although there is a distinction between events and ringdown counts it would not affect the results in this way. Koerner et al (1976) also showed that counts showed a steady rise throughout the test duration, again this is in contrast to the results of Tanimoto.

The change in count rate at the constant volume point was first reported by Tanimoto and Noda (1977), and was used as a method of determining the time to failure (actually, time to peak). The number of counts recorded during the initial pre-constant volume phase was divided into the number of events occuring in an (arbitrary) period afterwards. The results from a number of tests

48

were plotted against the time to failure on a semilog scale and showed a relatively good fit to a straight line. The exercise was repeated for stress controlled tests, with much the same results. However, in that type of test no levelling off of the count rate was observed: in fact the gradient increased after the constant volume point.

4.3 Preliminary Tests.

4.3.1 Sample Conditions.

It is now standard practice in laboratory soils testing to use lubricated end membranes. The case for the use of lubricated end membranes ('free ends') was presented by Rowe and Barden (1964) and their conclusions were that uniform deformation could be achieved using free ends. Previous practice had been to test fixed ended samples with a height/diameter ratio of 2:1 but a tendency for the samples to fail by buckling was noted. The influence of end restraint, and of sample dimensions on AE behaviour is not documented and, although experiments indicated little or no attenuation of signals by the membranes, several tests were performed in which no end membranes were present, and in some of which the height/diameter ratio was 2:1.

Test 89 was a standard test but for the absence of end membranes, the stress ratio/deviatoric strain curve for this test is given in Figure 4.11. The peak stress ratio is much higher than in other tests (c.f. Figure 4.1) and, post peak the stress ratio levels off at about 0.85. These results are consistent with this type of test and the levelling off of the stress ratio/deviatoric

strain curve is indicative of a developed shear plane. In fact, a shear plane was visible through the sample membrane during the later stages of post peak deformation. Barrelling of the sample, caused by end platen friction, was apparent at the end of the test.

A cursory inspection of the AE data showed that the event rate was much higher (15-25x) than that of tests using free ends. One effect of this is to make the event rate/deviatoric strain curve much smoother, although when the shear plane is present the event rate is more variable. Replotting the event rate/deviatoric strain curve (Figure 4.12), using the moving average technique to remove some of the variability, reveals that there are apparently two changes of gradient; one noticeable at peak, and a second more abrupt change during post peak deformation. The second, larger, change of gradient does not appear to correspond with any of the other stress/strain data; it is conceivable that this is the point at which a shear plane first develops.

Further tests involving double height samples with no end membranes were carried out, Tests 90 and 91. At the end of the tests both samples exhibited buckling and had well developed shear planes - indicative of non uniform deformation. The AE behaviour was similar to that of Test 89; an increased event rate, and a definite break of slope during post peak deformation, Figure 4.13 (Test 91). The large spike in the event rate/time graph was because undrained conditions developed when the volume change device ran out of travel before being readjusted. Figure 4.13 shows that the break of slope leads to a level phase rather

than a continuing positive gradient: in no other AE tests
performed during the research period was this constant event rate
observed.

4.3.2 Strain Rate.

The influence of strain rate on the AE behaviour of sand is not
well documented. Tanimoto and Noda (1977) showed that there was
a relationship between strain rate and ringdown count rate.
However, this related only to their 'second phase' of AE which
occurred after the constant volume point in their strain
controlled tests. Over the course of the research period the
axial strain rate used was either 1%/hour or 3%/hour; these rates
being deemed suitable for AE data capture. However, Tanimoto and
Noda (1977) used strain rates of between 25%/hour and 200%/hour
in their tests. In order to make a comparison with these results
it was necessary to examine the relationship between event rate
and strain rate. Additional tests on height:diameter 1:1 samples
with free ends were carried out at strain rates of 10%/hour (Test
92) and 15%/hour (Test 93); it was not feasible to test above
these rates.

Plotting the event rate/time graphs for the Tests 92 and 93
(Figures 4.14 and 4.15 respectively) shows that there is a steady
rise in the event rate/minute as the tests progress but there is
no evidence, as in Tanimoto's tests, of a levelling off of the
event rate. Therefore the levelling off is not a function of the
strain rate. Comparing the total number of events at particular
deviatoric strains for different tests (Figure 4.16) it may be
seen that more events are recorded at higher strain rates than
might be expected from a linear relationship.

4.4 Distribution of Events by Peak Amplitude.

Many workers in the field of AE use the distribution of events by peak amplitude as a method of characterisation of the material. For instance, glass reinforced plastic is known to exhibit a triple peaked distribution (Pollock (1978)), which is indicative of the different failure mechanisms at work within the material. Figures 4.17 and 4.18 show peak amplitude distributions for Tests 110 and 88 respectively; the single peak is, perhaps, an indication that only one mechanism is at work within the sand. The single right skewed peak was found in all tests carried out during the research program. This type of curve can be modelled using the beta-probability density function (beta p.d.f.). The beta p.d.f. is well suited to modelling distributions of data which are of limited range and positive in value. The general form of the beta p.d.f. is:

$$f(x) = k(x-a)^{alpha}(b-x)^{beta} \qquad\qquad (4.1)$$

where: a - lower bound of distribution.

b - upper bound of distribution.

k, alpha, beta - statistical parameters derived from the experimental range, mean, and standard deviation.

In an attempt to provide a unique AE description of sand, this curve fitting technique was applied to the peak amplitude distributions. The beta p.d.f.s corresponding to the peak amplitude distributions in Figures 4.17 and 4.18 are shown in Figures 4.19 and 4.20. It was found that the p.d.f. is extremely sensitive to the range of peak amplitudes recorded (especially if some extreme events are counted) and to the number of events in

the distribution; the calculated values of alpha and beta for Tests 110 and 88 were (0.3, 12.2) and (0.5, 11.0) respectively. Analysis of other tests indicated that the value of alpha was <1.0 and the value for beta was >7.0 which confirms the highly skewed nature of the distribution. However, the variation in the individual values of alpha and beta was too large to be able to provide a method of characterisation, except in the most general terms relating to the relative size of alpha and beta.

Mogi (1962) and Scholz (1968) identified a characteristic measure for rocks, the b value, which was calculated from the gradient of the amplitude distributions. Mogi proposed that the b value related to the heterogeneity of the material while Scholz supplemented this by accounting for variations in the stress field. To calculate the b value, the logarithm of the cumulative distribution of events by peak amplitude is plotted, the b value is then calculated as the slope of the line multiplied by -20 (Peak amplitude=20.log(Vout/Vmin (4.2)). The b value relates to the ductility of the material, and is a function of the deformation mechanism and the state of stress, Pollock (1978). Figure 4.21 shows the cumulative distribution obtained from Test 110 (n.b. the horizontal portion of the curve is not included in the calculation of b). The calculated value of b was 1.7: this is high in comparison to rocks for which values of less than 1.0 are commonly calculated. Pollock (1978) gives the values of b for a ductile and a brittle steel as 4.20 and 0.76 respectively. Sand however, behaves in a ductile manner, as is seen in the stress ratio/deviatoric strain curve (Figure 4.1). Analysis of a large number of tests gives an overall b value of 2.24 for the Leighton Buzzard sand which would seem to be of the right order. Note that

these b values refer to the final distribution of events by peak amplitude calculated at the end of the test.

The b value, as calculated, is not constant over the test duration. This can be seen if the test is divided into a number of periods and, for each period, the b value is calculated. Figures 4.22 and 4.23 show how the b value changes over the course of two tests (110 and 88): a steady rise in the value as the test proceeds. The suggestion, according to Pollock (1978) is that b increases with ductility and hence the increase observed indicates that the sand becomes more ductile as the test proceeds.

4.5 Frequency Distribution of Events.

The AET5000 does not provide the information relating to the frequency of the incoming events. However, as a means of validating the events, this information would be relevant. Hahnekamp (1981) shows that it is possible to provide a good approximation to frequency by dividing the number of ringdown counts in an event by its duration. It was demonstrated that the range of the frequency distribution derived from this method of analysis was typically 80% of the true frequency distribution. Figure 4.27 shows one such frequency distribution obtained and, on inspection, it is apparent that the range of the distribution is 75-80% of that prescribed by the band pass filter (15-45kHz). Events with a ringdown count of one have been discounted from the analysis because the measured event duration is an unknown proportion of the time period of the event; events with a ringdown count of two are subject to bias but to a lesser extent.

Events with a ringdown count of one make up 25-30% of all events recorded during a test; this was determined from an analysis of tests in which both event and ringdown count data were available. One reason for the shifted distribution is because the AET5000 calculates the event duration as the time above the threshold voltage and not the time above 0.0 volts.

Analysis of tests involving more complex stress paths indicate that the results for these psuedo-frequency distributions are consistent with each other (e.g. Figure 4.25) and all have a pronounced central frequency of '25kHz'. Adjusting this value to the 'true' value (multiplying by 1.25) gives a frequency of 31kHz which is close to the quoted resonant frequency of the sensor (30kHz). One deviation from the 'standard' pattern is provided by an undrained test (Figure 4.26) in which the spread of the frequency distribution was very small. Unfortunately it was not possible to analyse earlier undrained tests because the relevant information was not available.

4.6 Event Waveform and Distribution of Events by Energy.

The AET5000 provides an output representing the raw AE input signal and it is possible to attach auxilliary equipment such as oscilloscopes to it. In several tests the signal envelopes were displayed on a storage oscilloscope, and were photographed to provide a permanent record. It was found that the signal did not change over the test duration: a signal envelope was likely to be the same at the start of the test as at the end of the test. The oscilloscope provided visual confirmation that the acoustic emissions being received were distinct from the

background noise. Sample events are shown in Figure 4.27. It may be seen that they have short rise times and that the signal decay is exponential. Only the shape of the envelopes should be considered: the actual line traced is a consequence of the design of the oscilloscope.

Another interesting point to emerge from a study of the oscilloscope pictures may be seen in Figure 4.28. Three events have been recorded but they all occur close together, coalescing to form one larger 'event'. The AET5000 would interpret this series of events as one event (dependent on the gain and threshold settings) and it is clearly erroneous. This phenomenon was found to occur randomly throughout a test. Other examples of coalescence are shown in Figure 4.29 where two events are merging, the second being the larger of the two: the AET5000 would mis-record the rise time and hence slope and energy in these cases.

The AET5000 allows the energy of an incoming acoustic emission to be estimated, using the event duration and peak amplitude to calculate the area under the curve. Distributions of events by energy may then plotted in the same way as distributions of events by peak amplitude. A typical distribution is shown in Figure 4.30 (Test 110); the most striking aspect of this distribution is that there are two peaks which is in contrast to the single peak of the peak amplitude distributions. The double peak in the energy distribution was found in all tests performed. Initially it was thought that it might be because two mechanisms were at work during different parts of the test. However, subsequent investigation showed that the double peak occurred

throughout the test and that the peaks maintained the same ratio to each other during the test. It is therefore clear that two distinct types of events are present one of low amplitude and duration, the other of low amplitude but long duration (since the peak amplitude distribution is right skewed). A possible explanation is provided by the oscilloscope photographs - the second event type is in fact the coalescence of smaller events into a larger event.

4.7 Summary and Discussion of Results.

Initial experiments found that the AE response of sand was affected by the settings of the threshold voltage and the gain setting on the AET5000 system, but that there was a range of values for these settings which produced enough events for comparison with stress/strain data. The use of 'free' ends was found to be essential for uniform deformation of the sample. The AE event rate of samples tested without end membranes was significantly higher than those samples tested with end membranes. Taller specimens were also tested without end membranes, and the event rate became constant. This phenomenon was also found by Tanimoto and Noda (1977) who tested 2.4:1 specimens of sand. Results from tests disagreed with those reported by Tanimoto and Noda but a lack of experimental detail prevented exact test reproductions being made.

The relationship between event rate and the rate of strain was found to be non-linear. As the source mechanism of AE is not known it is difficult to account for this, but it may relate to

the rate at which acoustic emissions are generated within the sample. Each acoustic emission is subject to attenuation and, at 'slow' strain rates, the probability of another emission being generated close enough to it to reinforce the strength of the wave is low. However, as the rate of strain is increased, the probability that another event will occur in a given period of time is increased.

Simple monotonic loading tests show that a correspondence exists between strain and total events; this was first demonstrated by Koerner at al (1976). It was possible to identify peak using the event rate and deviatoric strain readings, this required some smoothing of the raw acoustic emission data by the use of moving averages.

It was possible to use the distribution of events by peak amplitude in two distinct ways. The first technique attempted to model the single peaked shape of the distribution using the beta probability density function. It was found that the parameters which describe this function could only be described in general terms because of the sensitivity of the function to the amount of data recorded, and to events which occurred at the extremes of amplitude. The second technique calculated the b value of the distribution; it was found that the average value was 2.24 which corresponds to data reported for ductile materials. Further, it was found the b value increased with increasing strain indicative of an increasing ductility.

The actual frequency distribution of the emissions was estimated and the resulting range of the distribution was found to be in

proportion with the one prescribed by the band pass filter in the AET5000 monitoring system.

The use of an oscilloscope allowed visual confirmation of the unprocessed AE signals and also showed that incoming events were often recorded simultaneously. This was confirmed by plotting the distribution of events by energy which showed a double peaked distribution.

Stress Ratio

Test 110

0.9

0

0   25
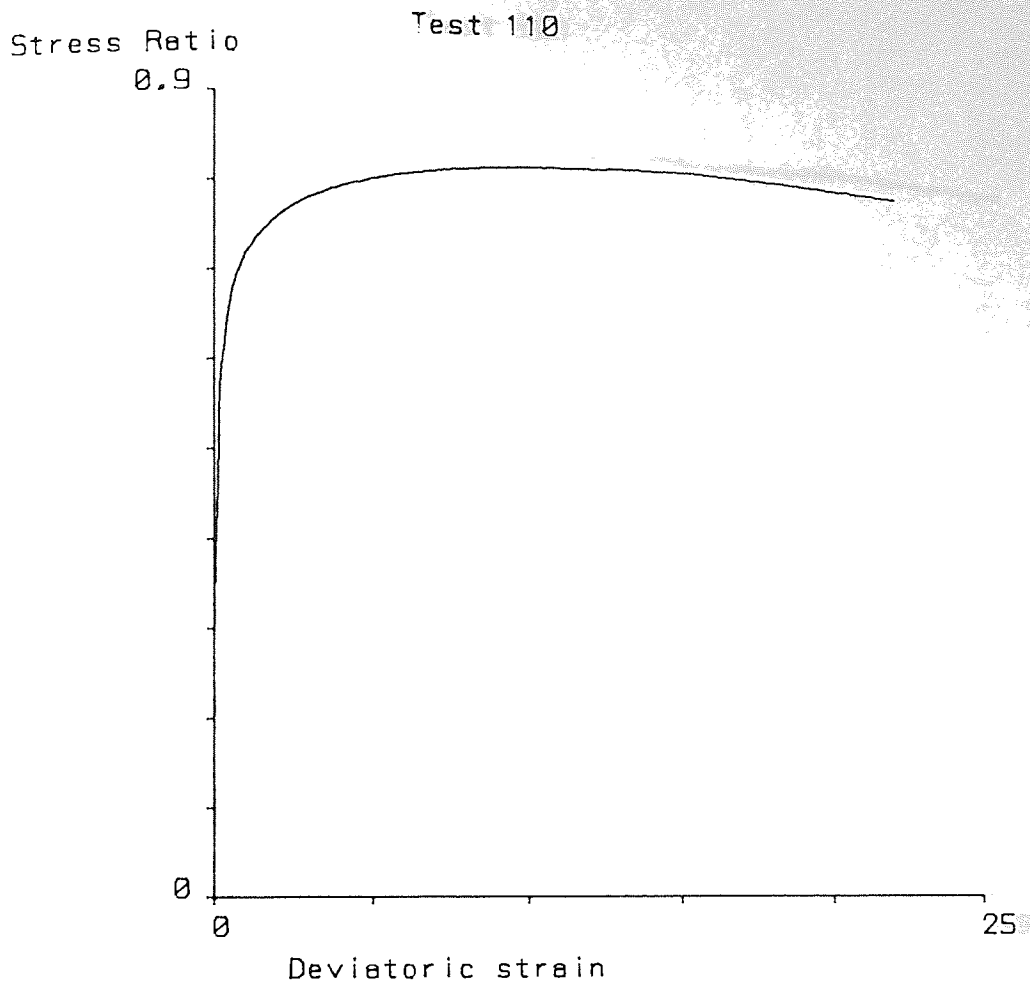
Deviatoric strain

Figure 4.1 Test 110: Stress Ratio/Deviatoric strain

Volumetric strain

Test 110

1

0

-9   25

0
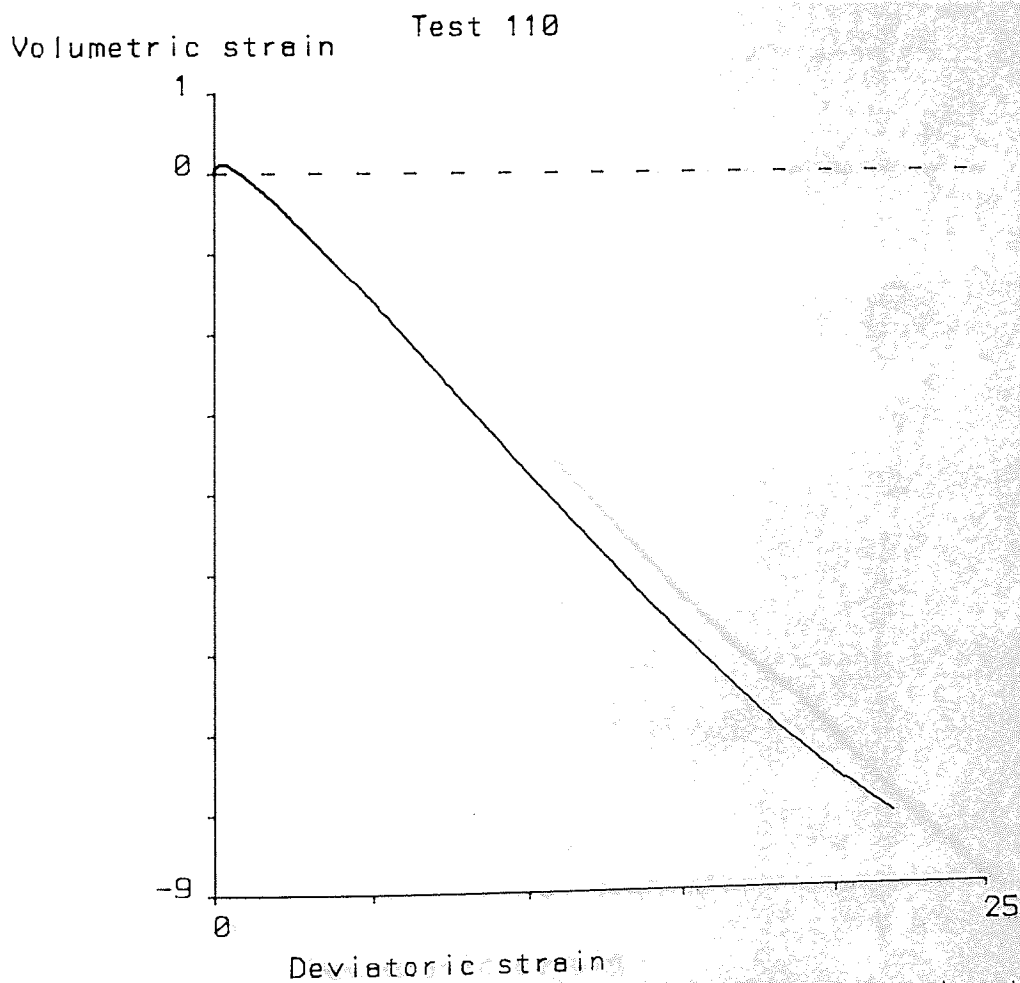
Deviatoric strain

Figure 4.2 Test 110: Volumetric strain/Deviatoric strain

Stress Ratio

Test 88

0.9

0

0   25
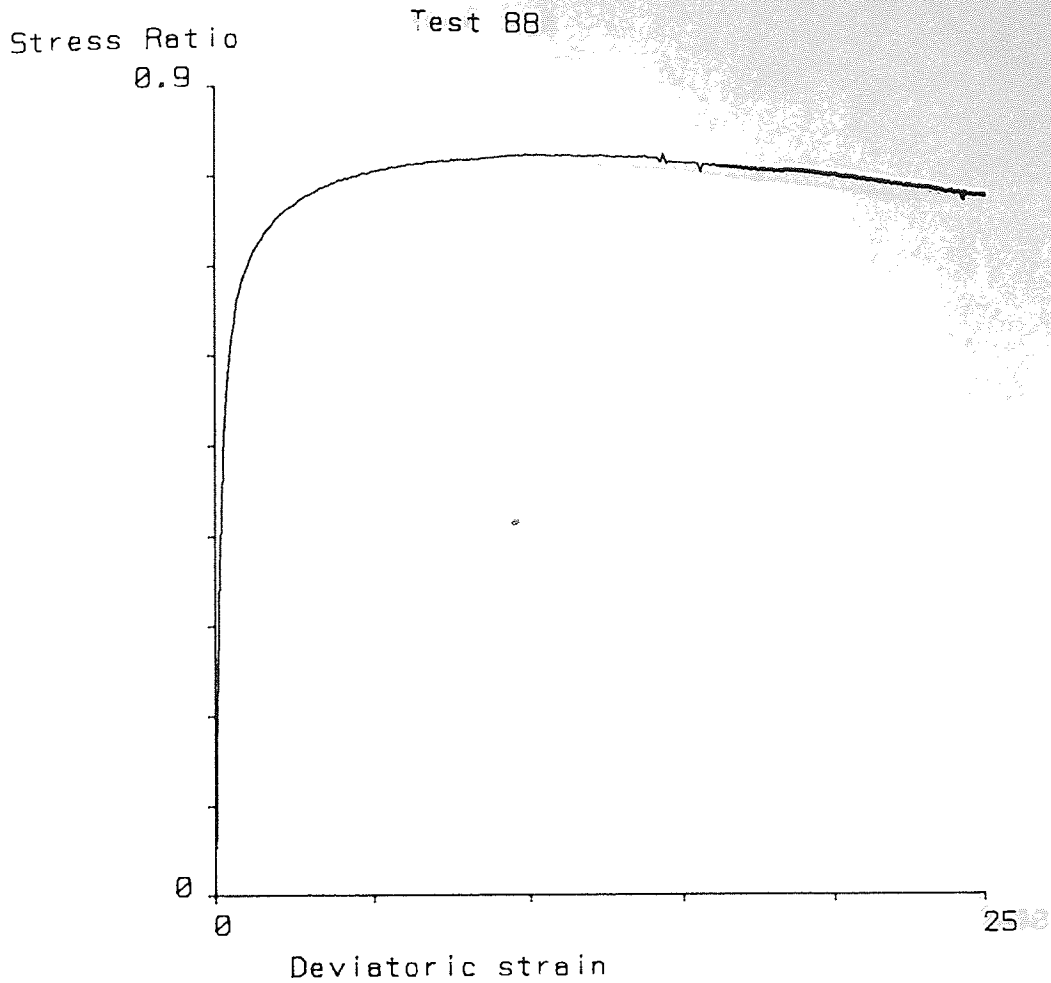
Deviatoric strain

Figure 4.3 Test 88: Stress Ratio/Deviatoric strain

Test 88

Volumetric strain

1

0

-9

0   25
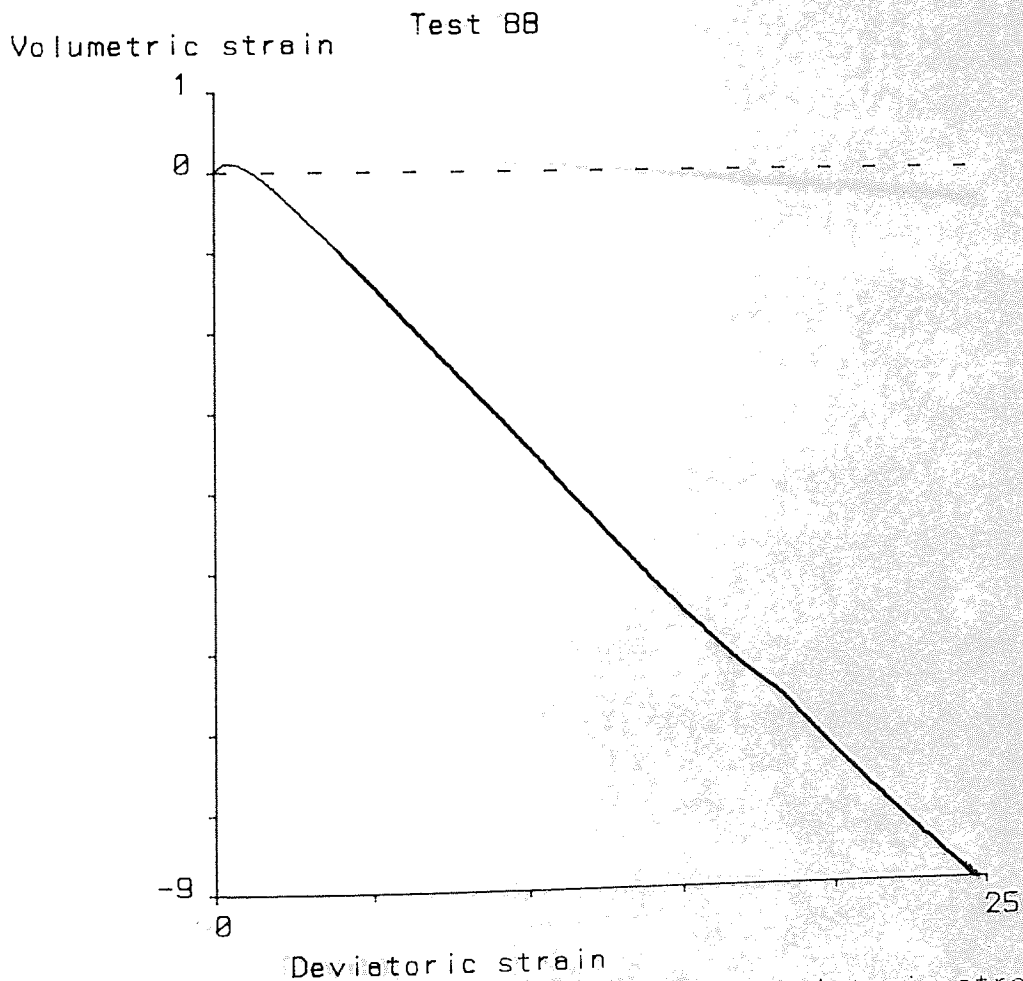
Deviatoric strain

Figure 4.4 Test 88: Volumetric strain/Deviatoric strain

Test 110

Stress Ratio
0.9

Events

0

0   7000
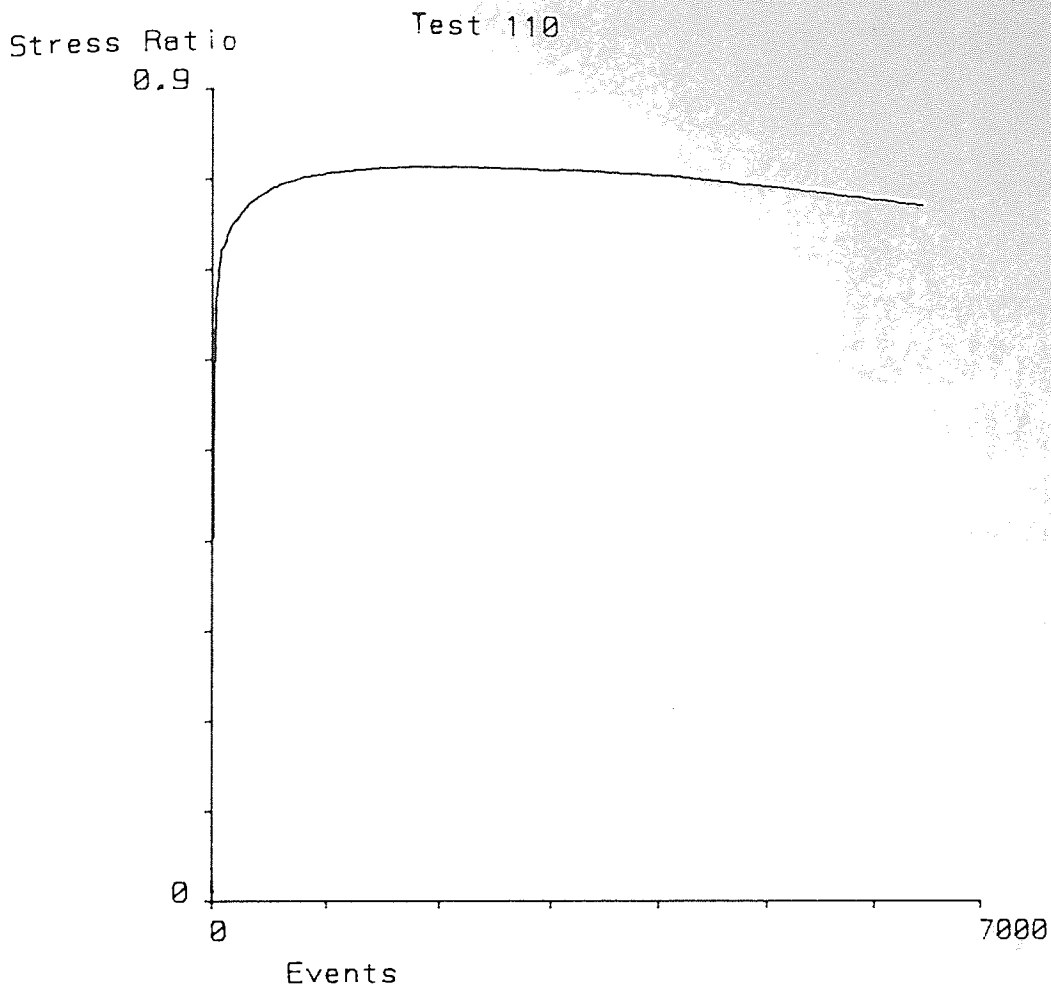
Figure 4.5 Test 110: Stress Ratio/Events

Test 88

Stress Ratio
0.9

Events

0

0   14000
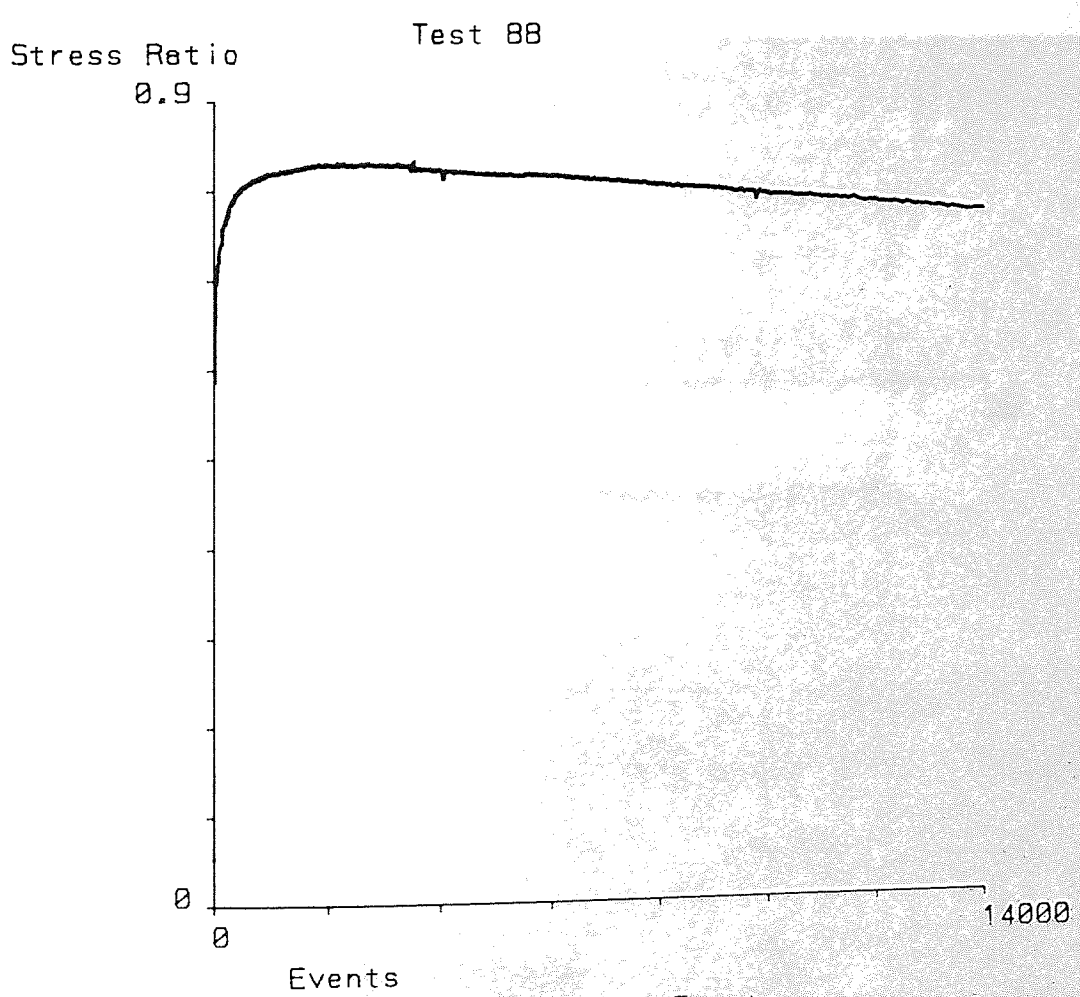
Figure 4.6 Test 88: Stress Ratio/Events

62
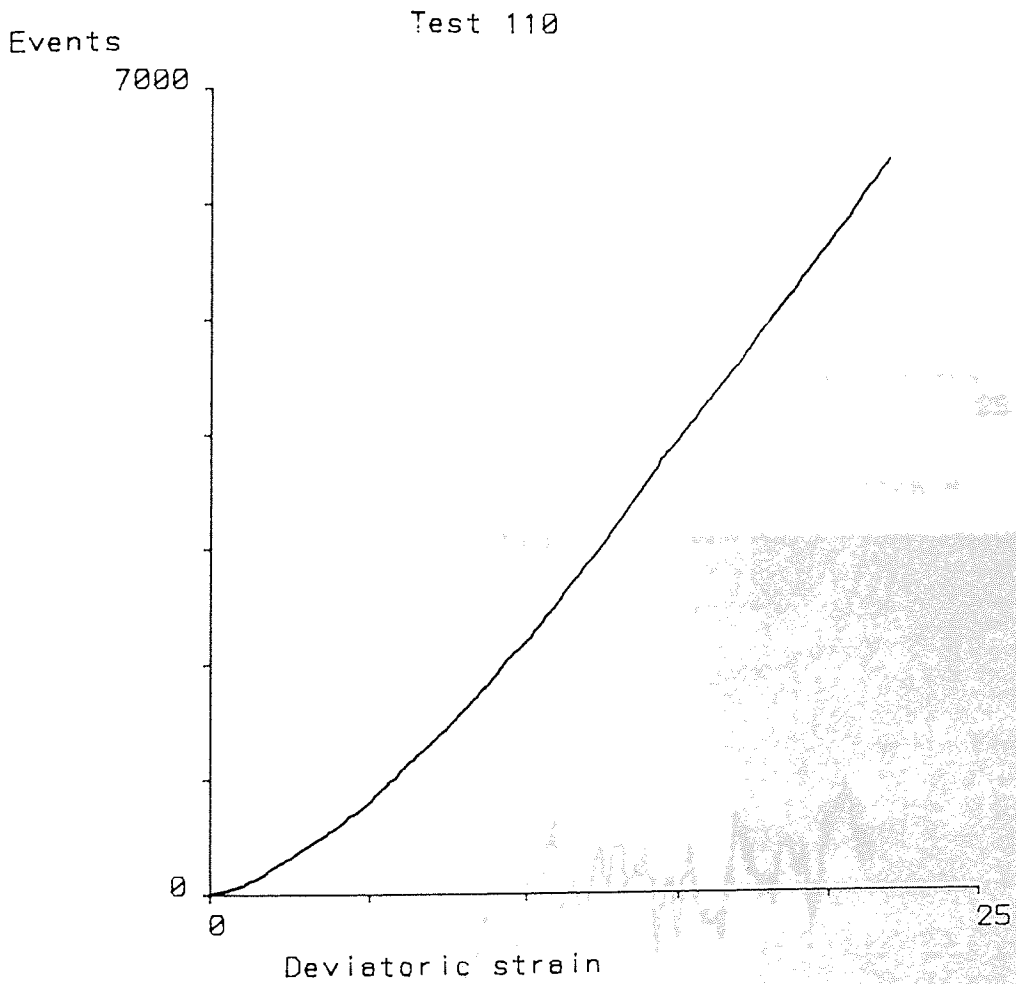
Test 110

Figure 4.7 Test 110: Events/Deviatoric strain

Test 110

Event rate
50
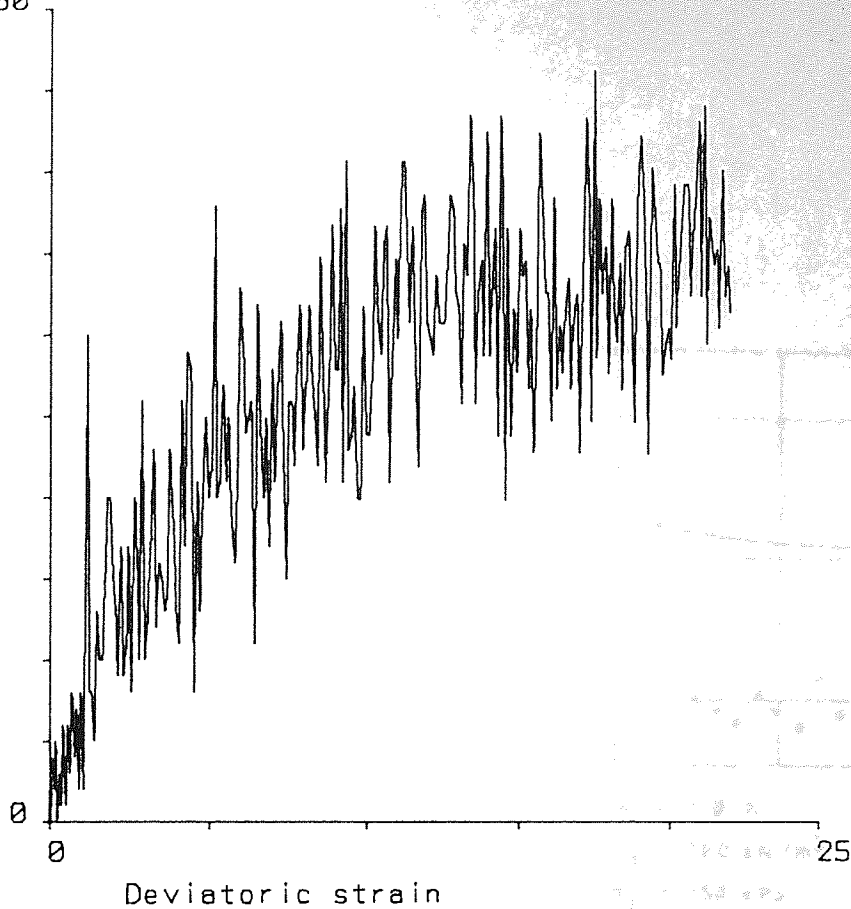
Deviatoric strain

Figure 4.8 Test 110: Event rate/Deviatoric strain

Event rate (averaged) Test 110
50
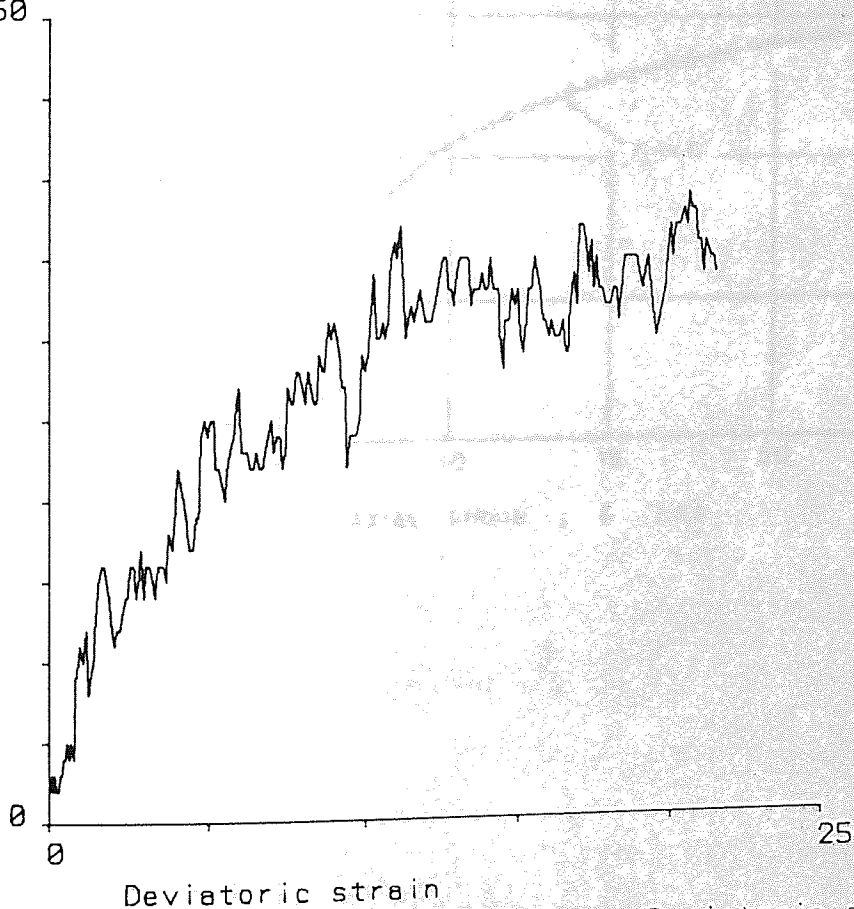
Deviatoric strain

Figure 4.9 Test 110: Average Event rate/Deviatoric strain
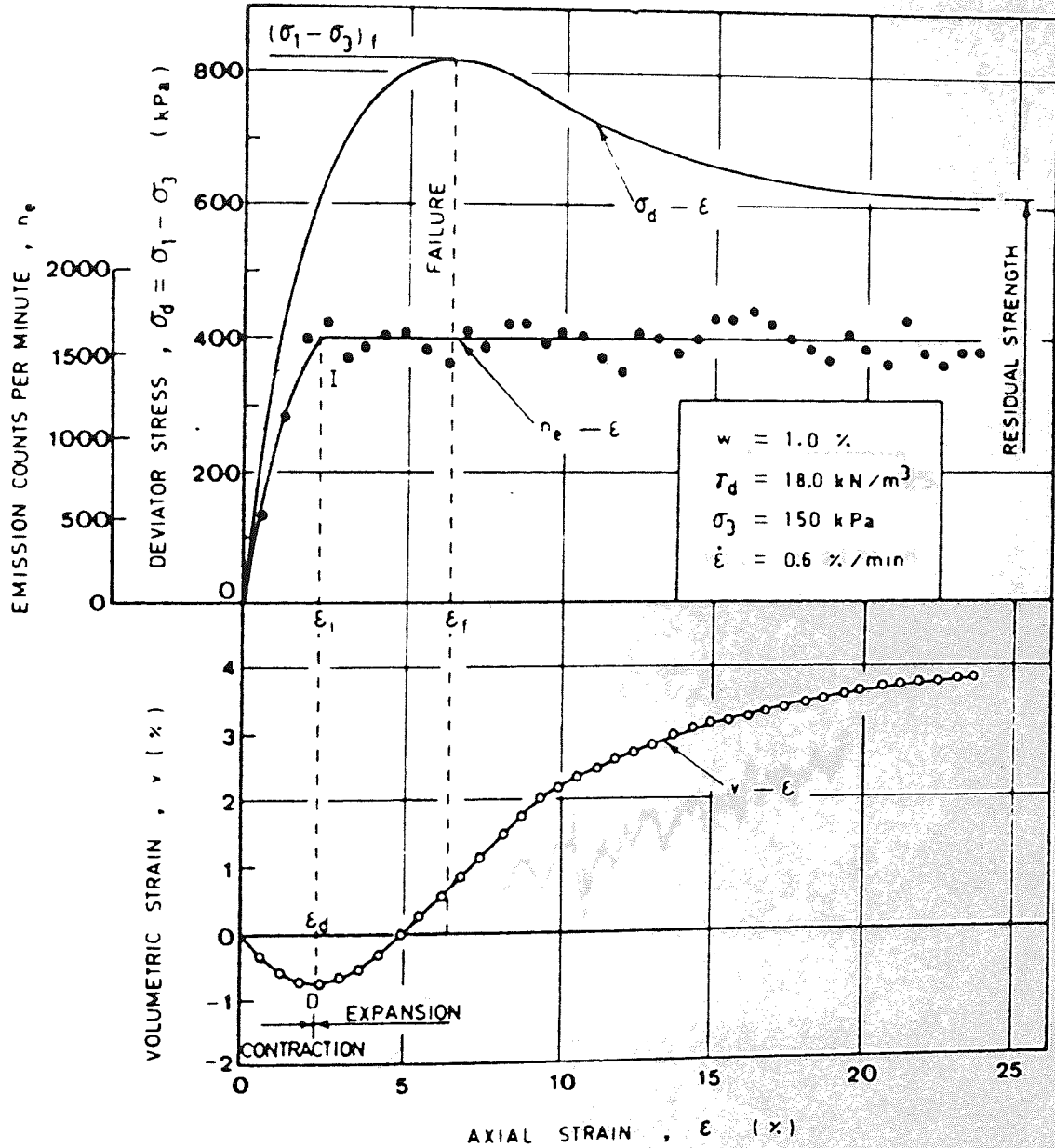
Figure 4.10 After Tanimoto and Nakamura (1981a)

65

Stress Ratio
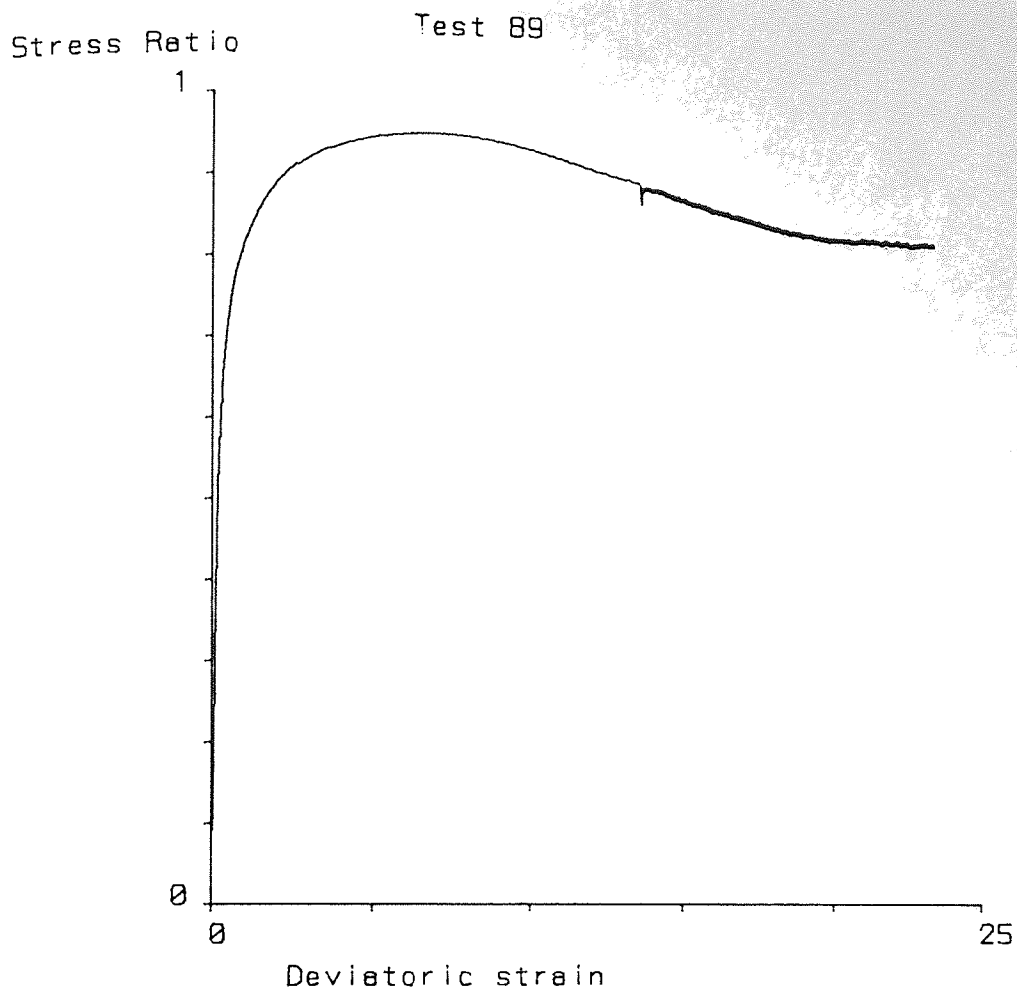
Test 89

Figure 4.11 Test 89: Stress Ratio/Deviatoric strain

Event rate (averaged)
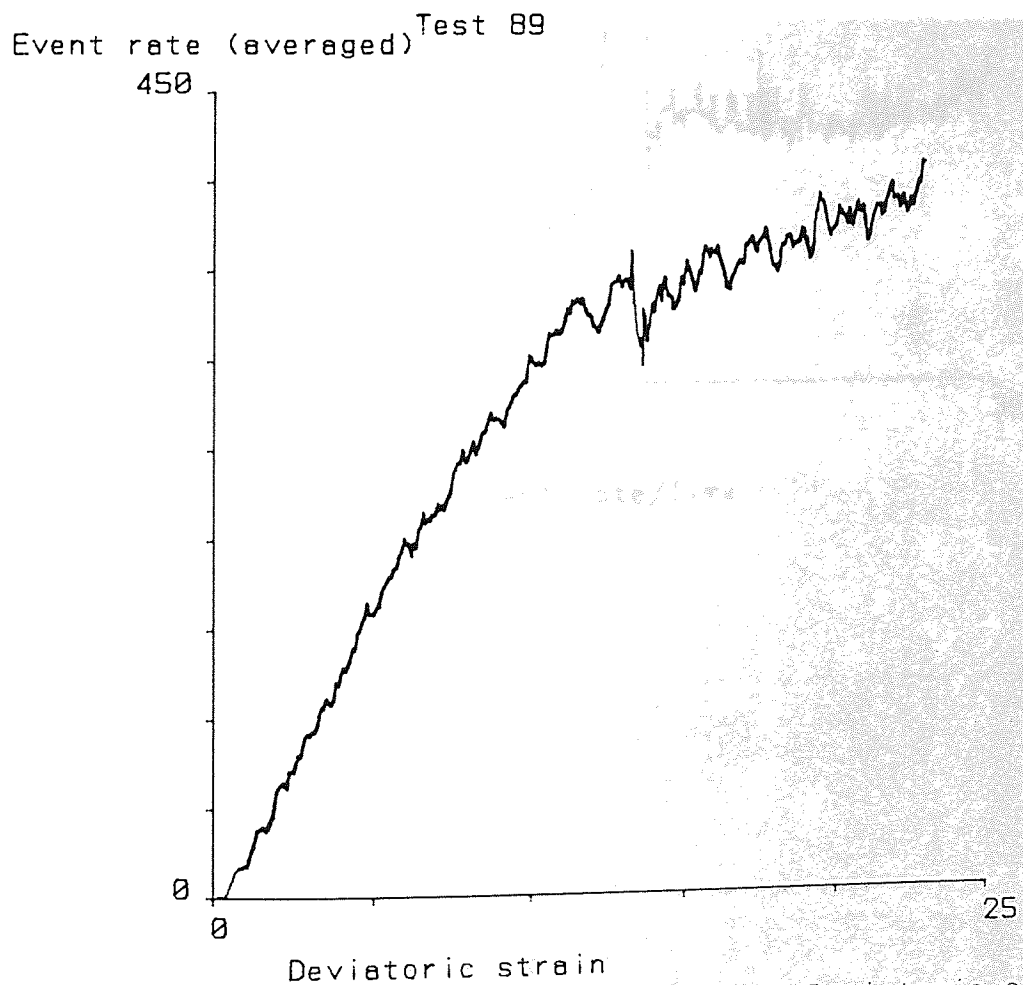
Test 89

Figure 4.12 Test 89: Average Event rate/Deviatoric strain
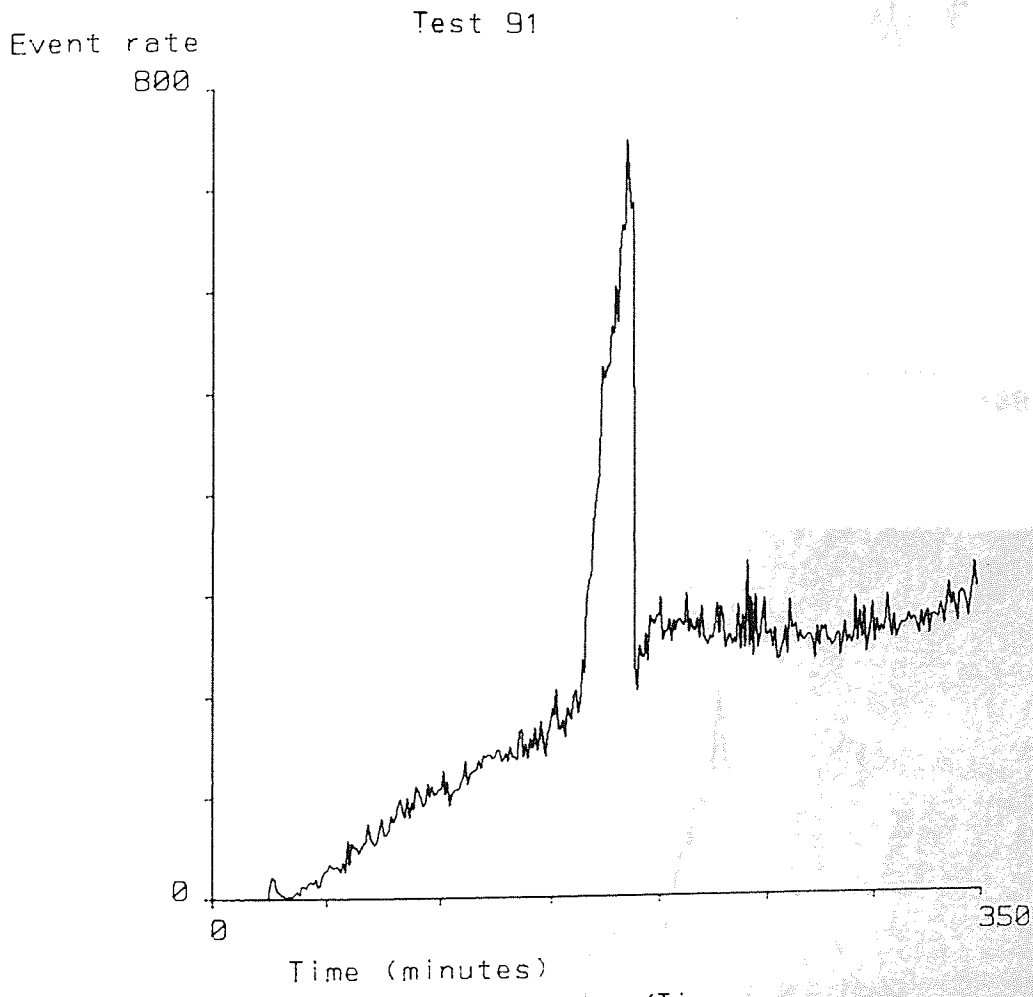
Figure 4.13 Test 91: Event rate/Time
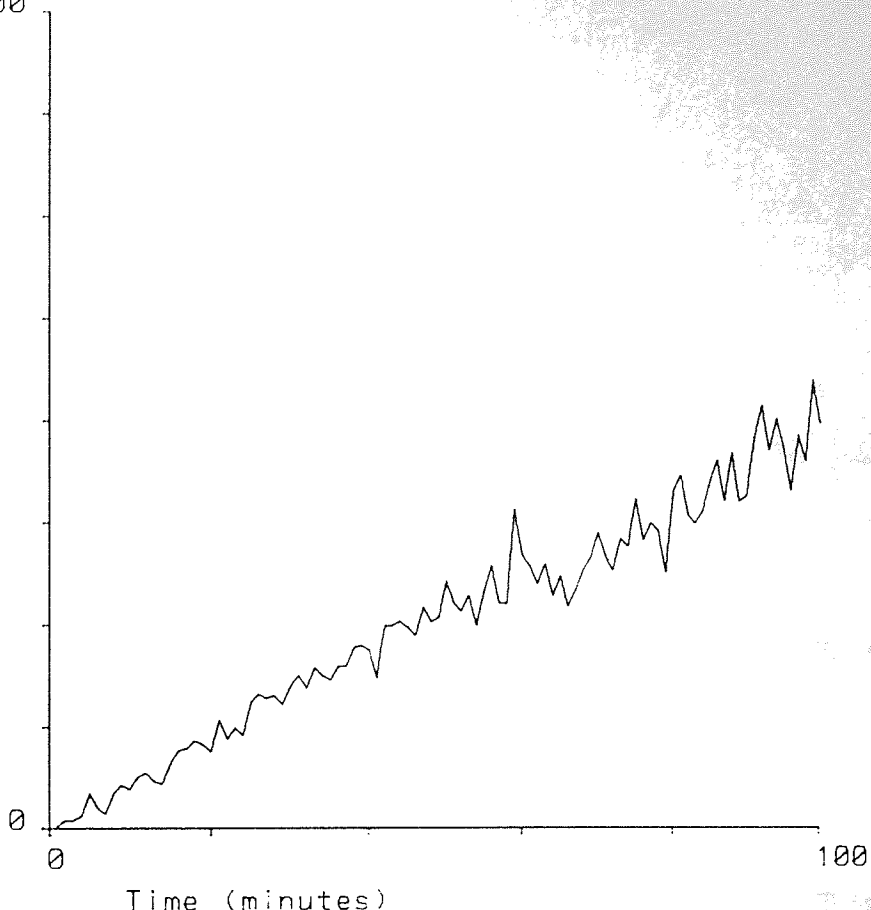
Figure 4.14 Test 92: Event rate/Time
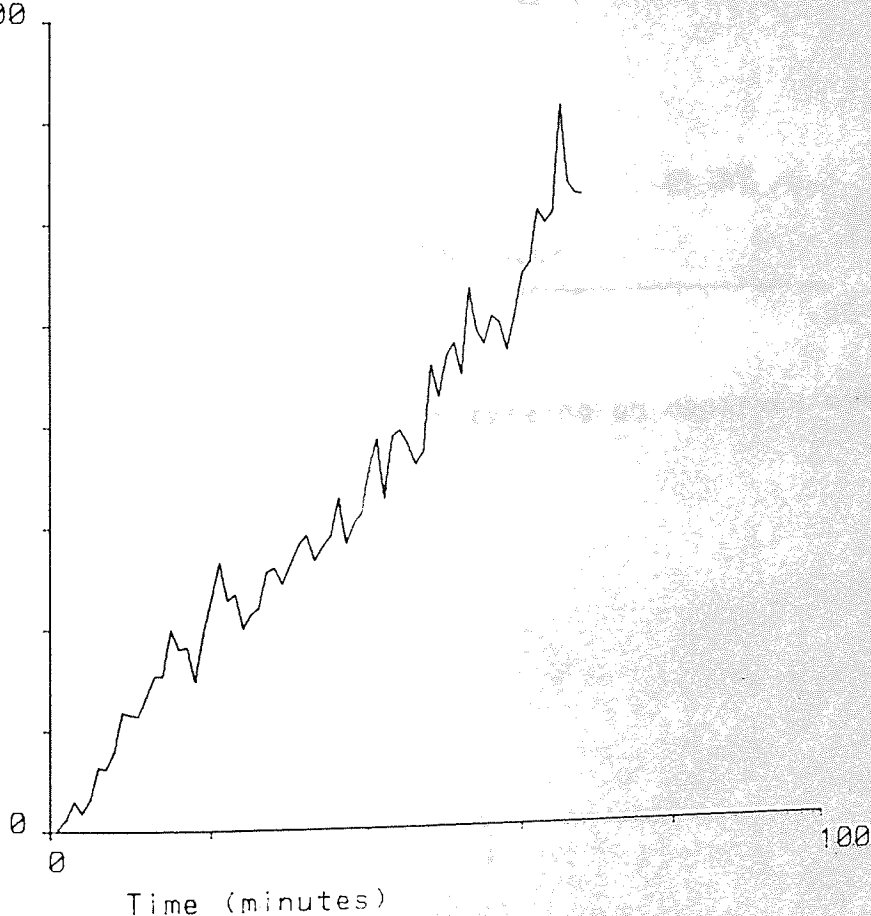
Figure 4.15 Test 93: Event rate/Time
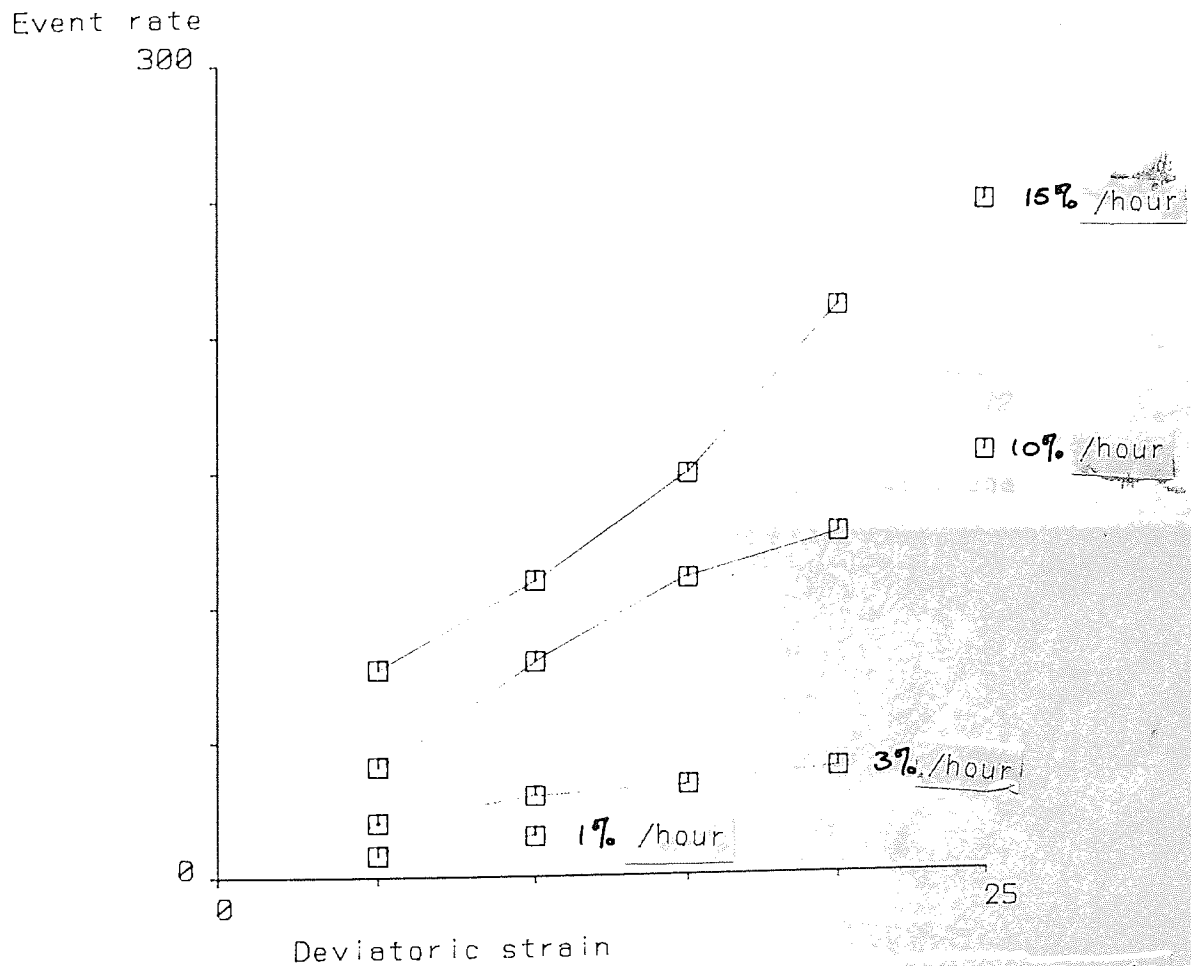
Figure 4.16 Effect of rate of testing on observed event rate
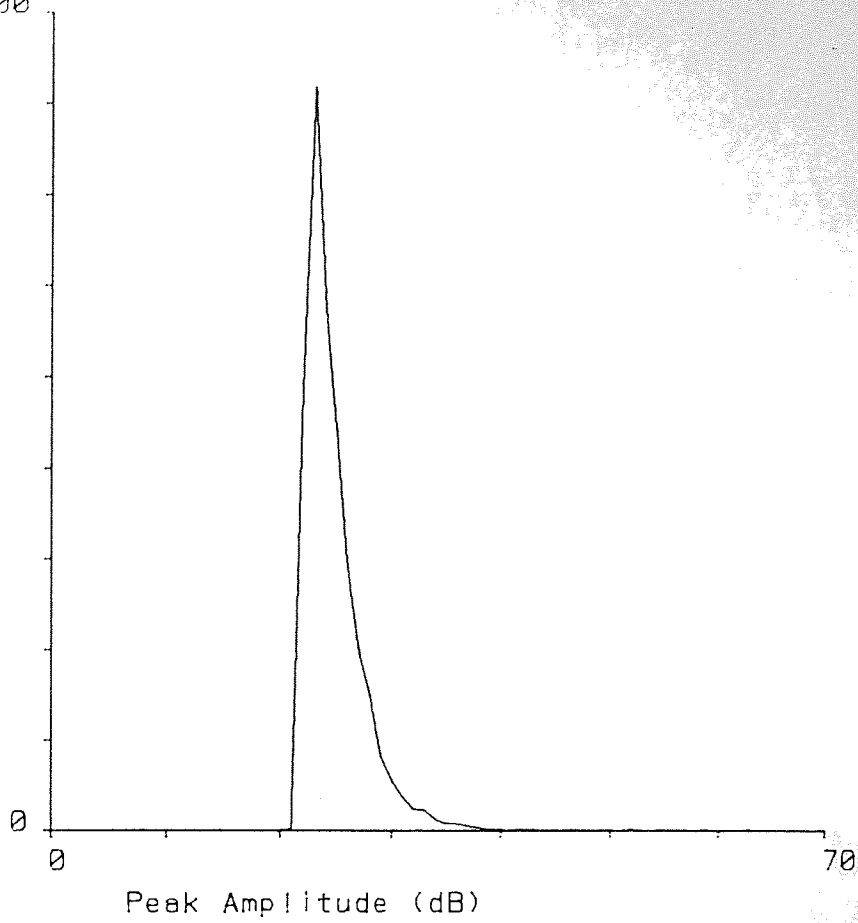
Figure 4.17 Test 110: Distribution by peak amplitude
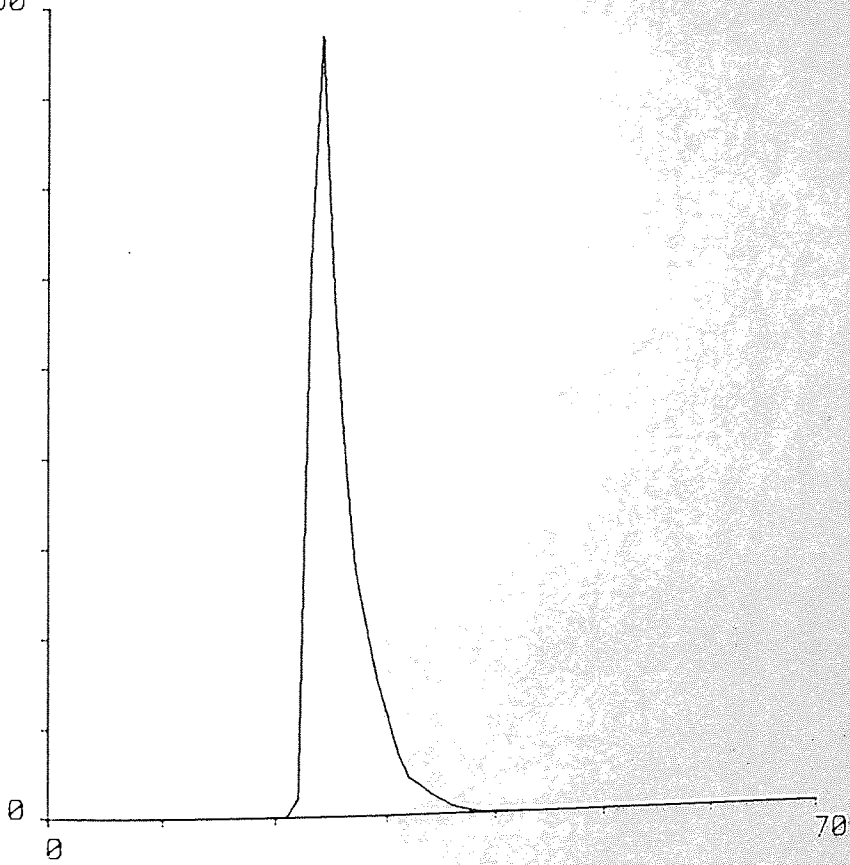
Figure 4.18 Test 88: Distribution by peak amplitude

Test 110 (Simulated Distribution)

Events/dB
1800

0

0   70
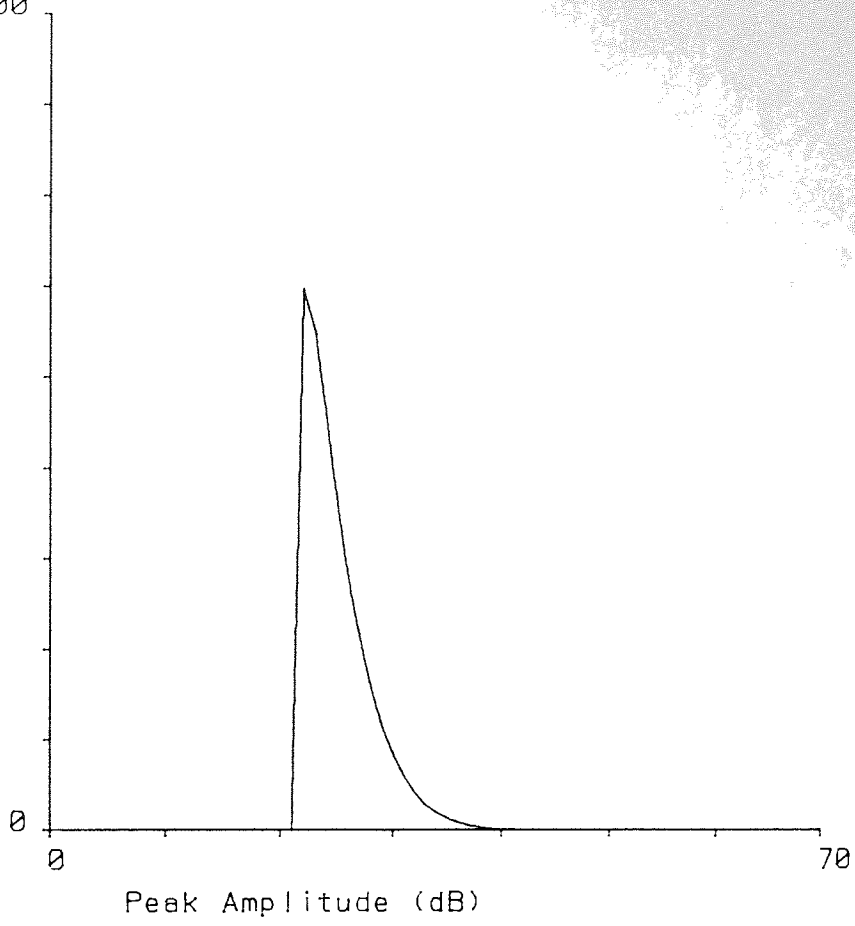
Peak Amplitude (dB)

Figure 4.19 Test 110: Beta Distribution by peak amplitude

Test 88 (Simulated Distribution)

Events/dB
4500

0

0   70
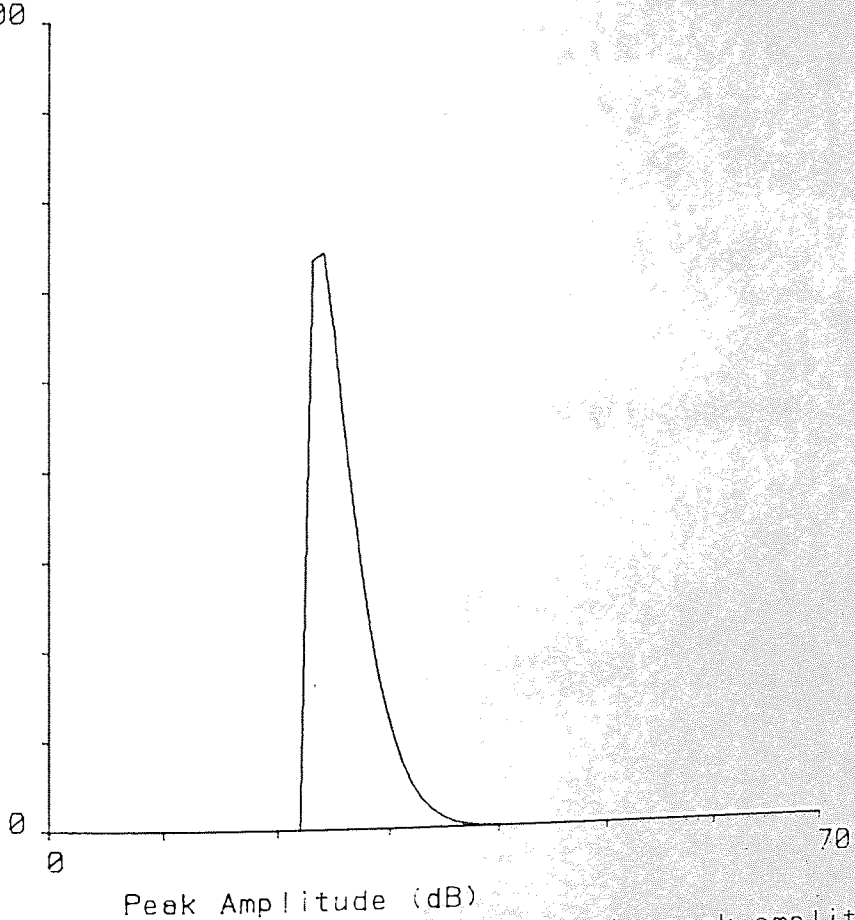
Peak Amplitude (dB)

Figure 4.20 Test 88: Beta Distribution by peak amplitude
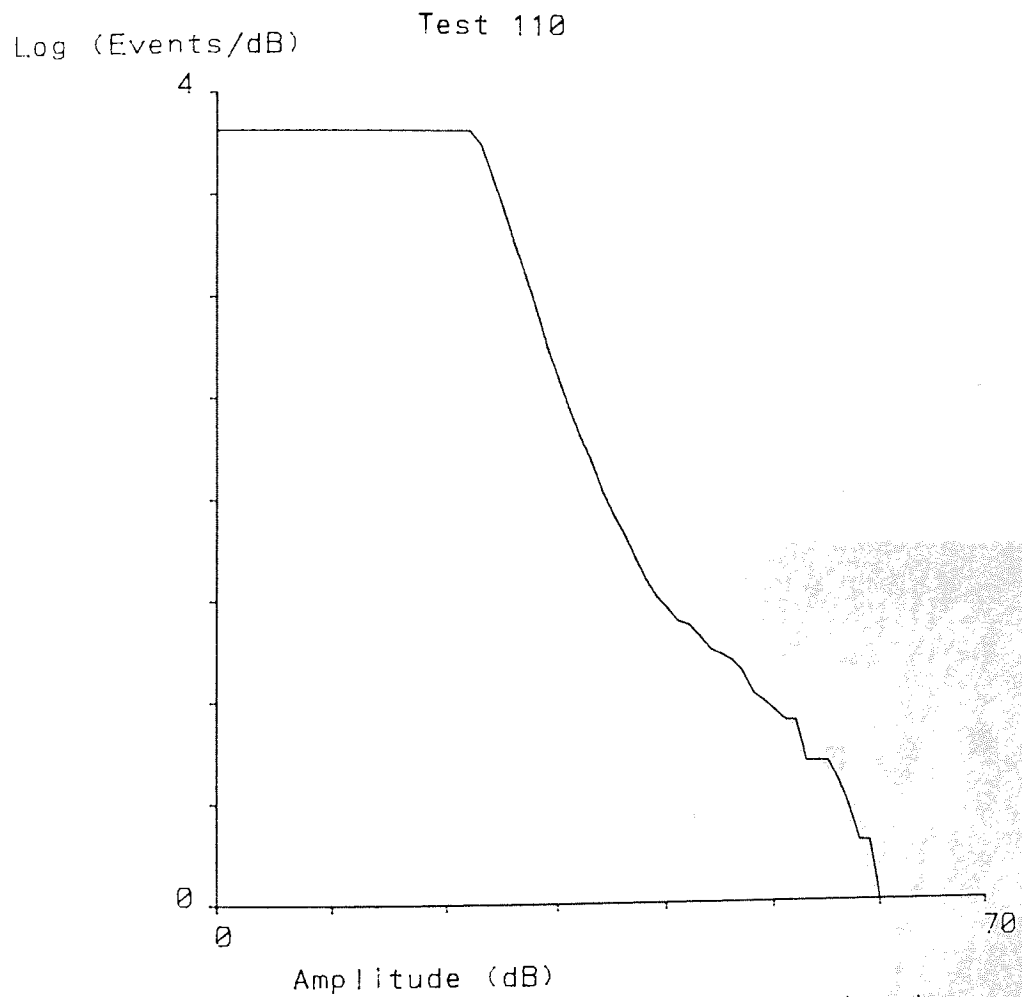
Figure 4.21 Test 110: Log Cumulative Distribution

Test 110

b value

Time (Hours)
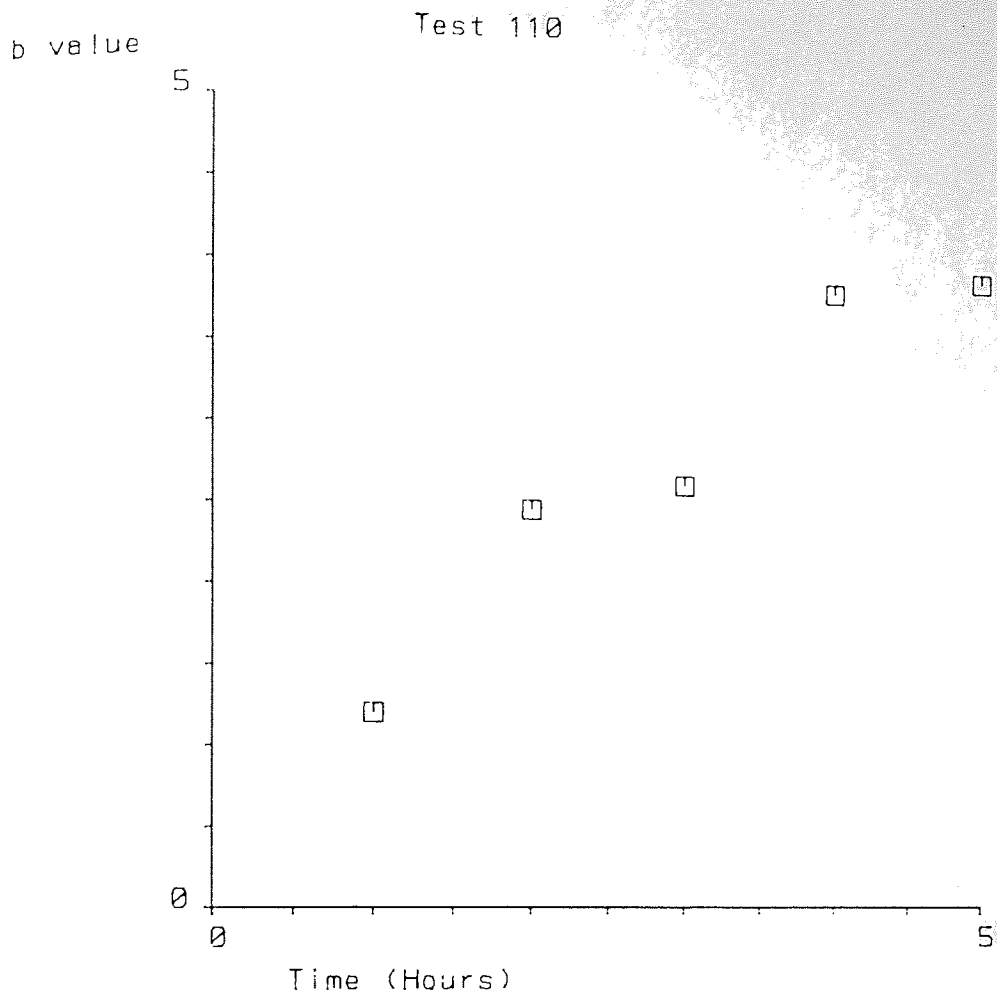
Figure 4.22 Test 110: Variation of b over test

Test 88

b value

Time (hours)
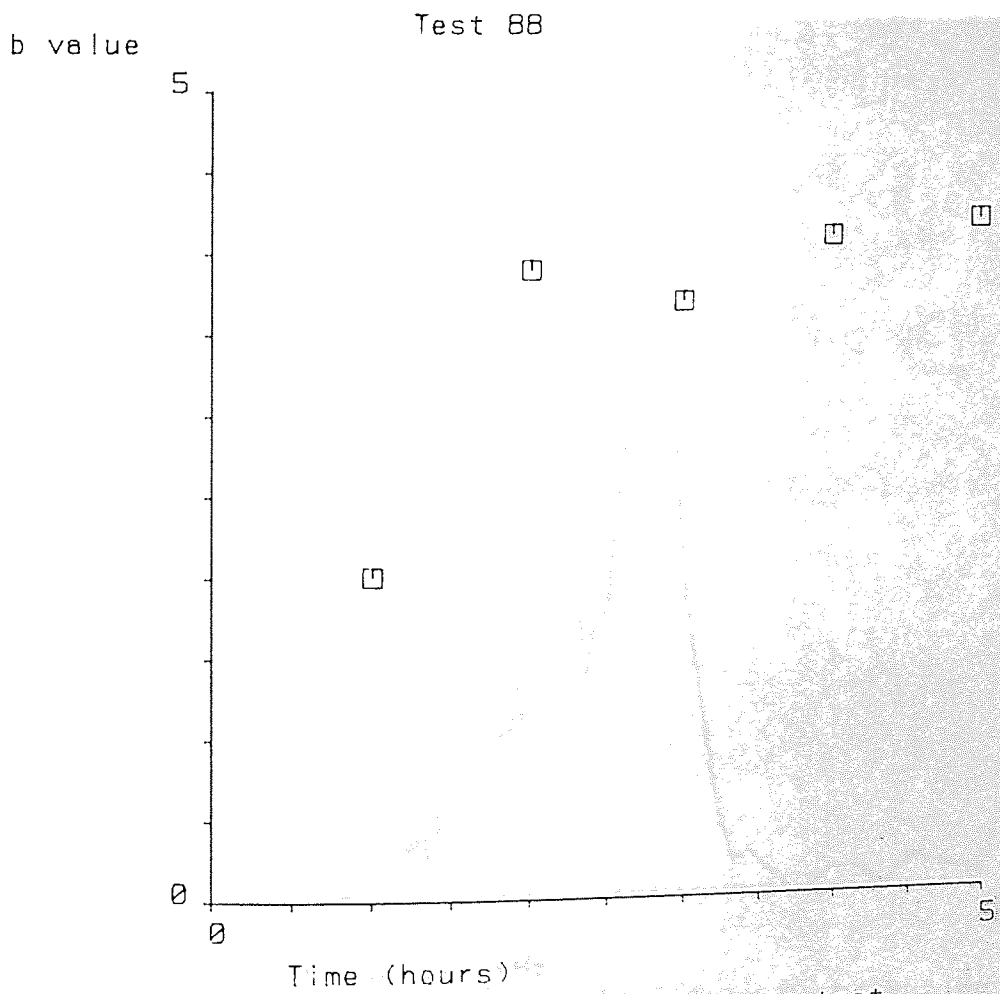
Figure 4.23 Test 88: Variation of b over test

Test 110

Events

250
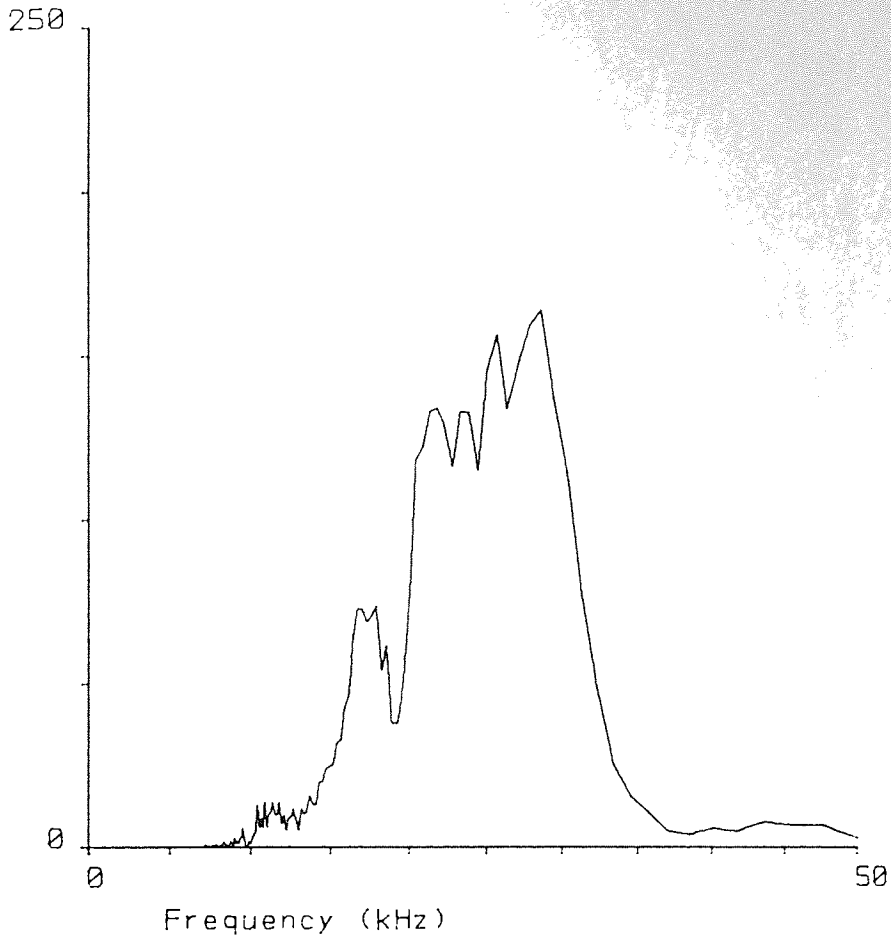
Frequency (kHz)

Figure 4.24 Test 110: Psuedo Frequency Distribution

Test 102

Events

80
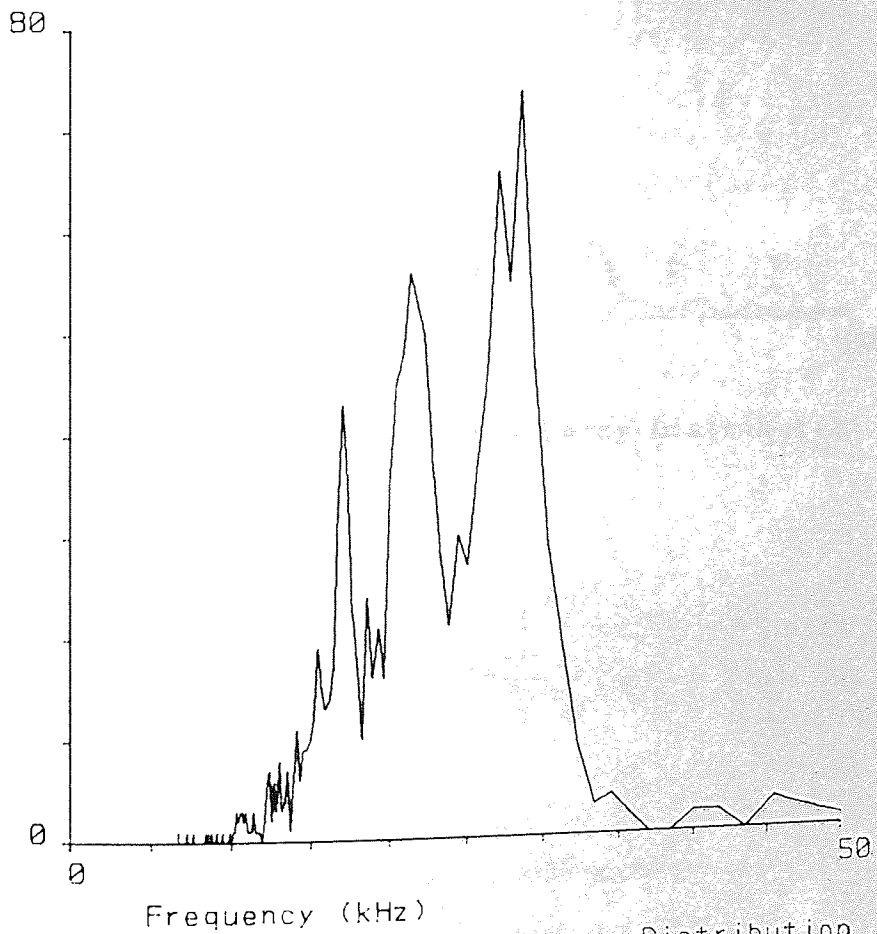
Frequency (kHz)

Figure 4.25 Test 102: Psuedo Frequency Distribution
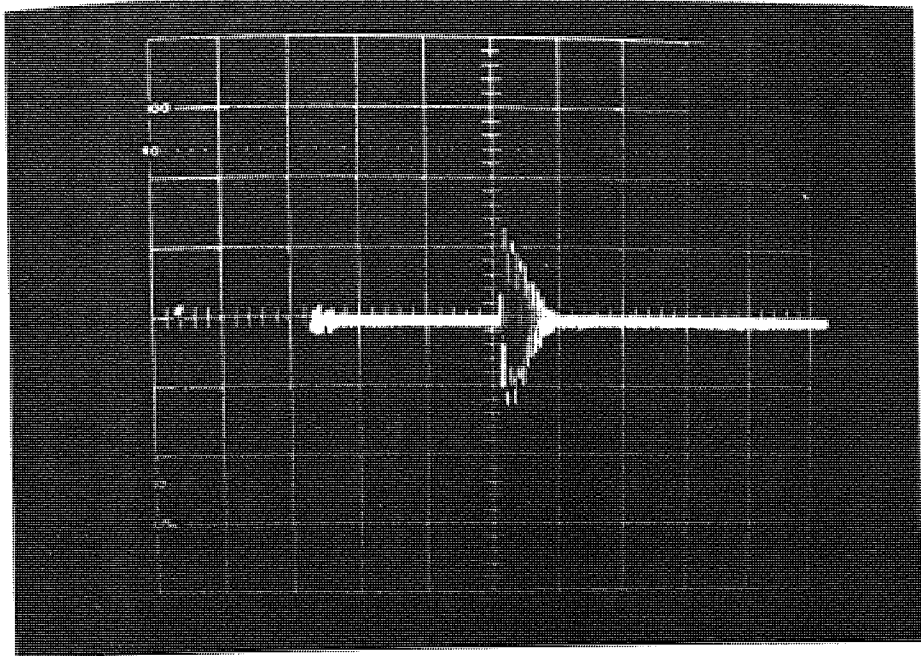
74
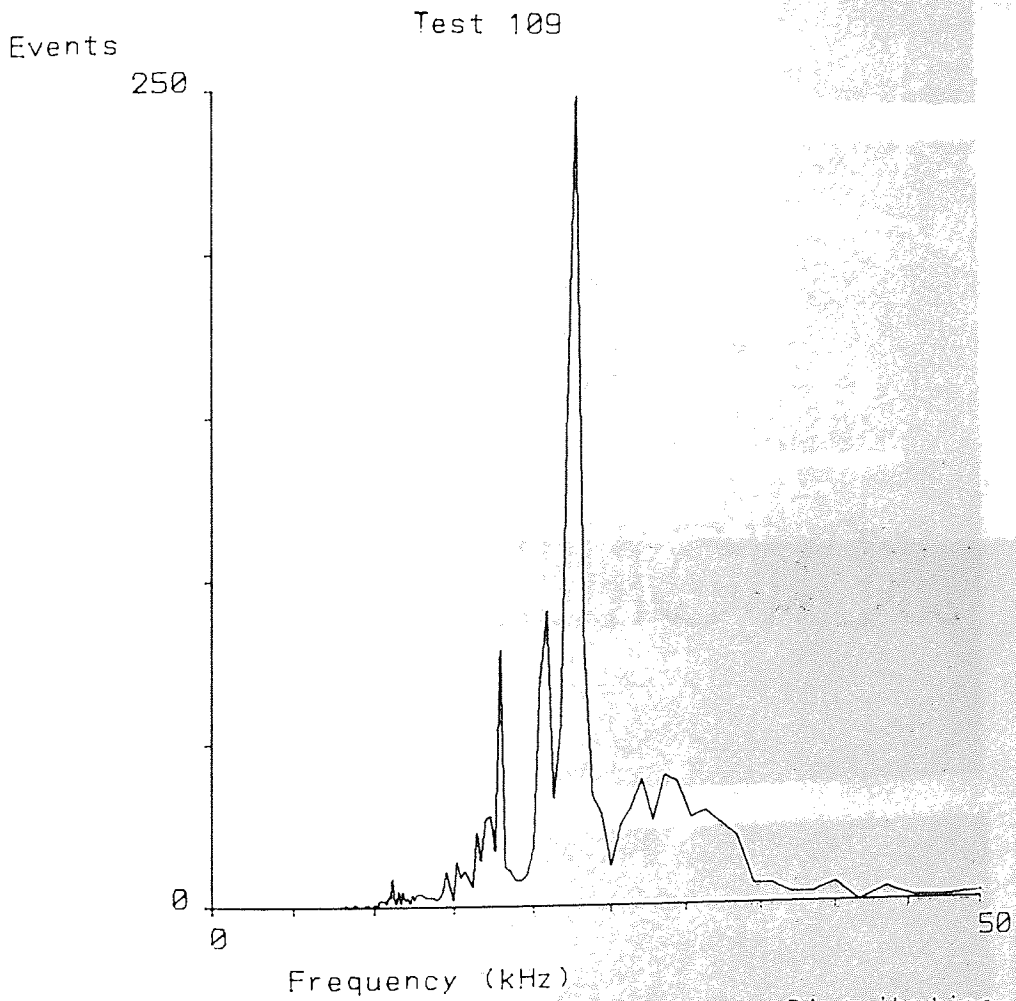
Figure 4.26 Test 109: Psuedo Frequency Distribution
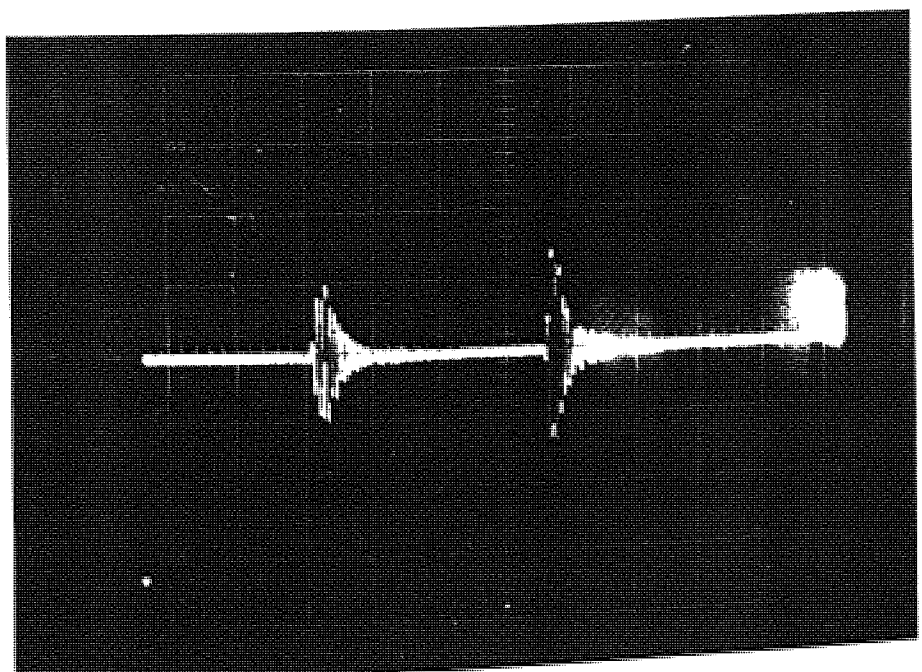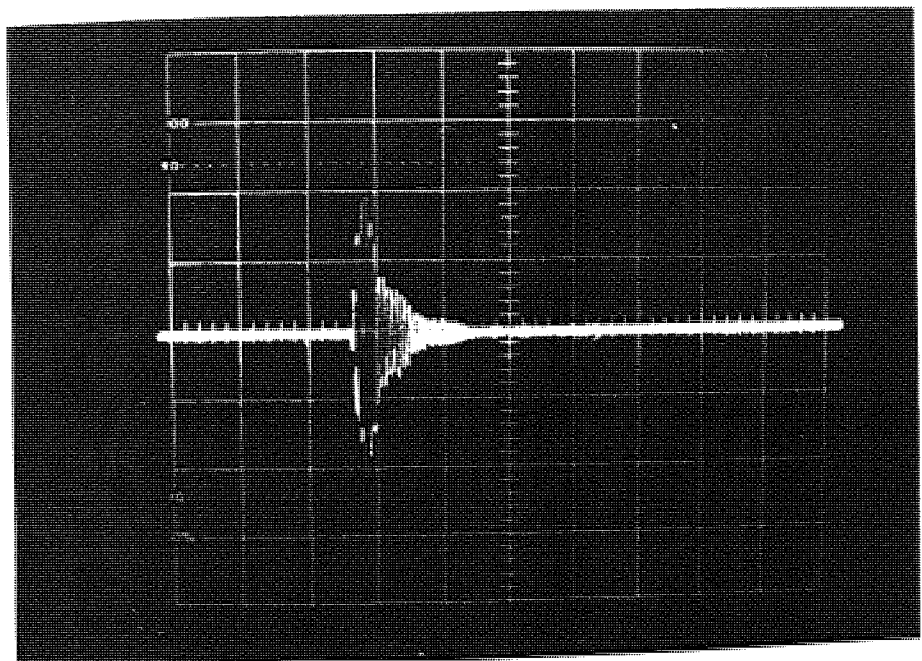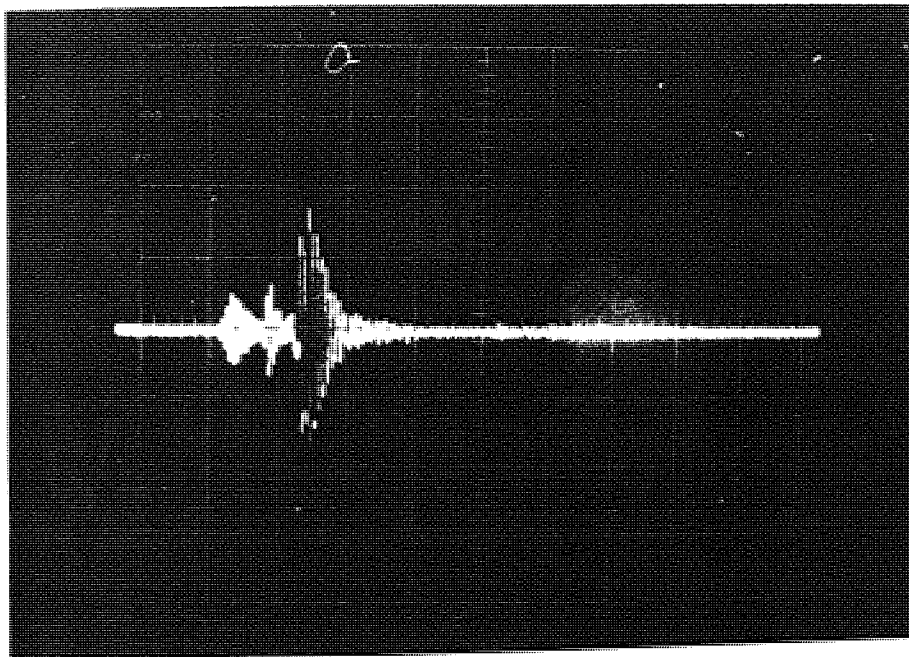
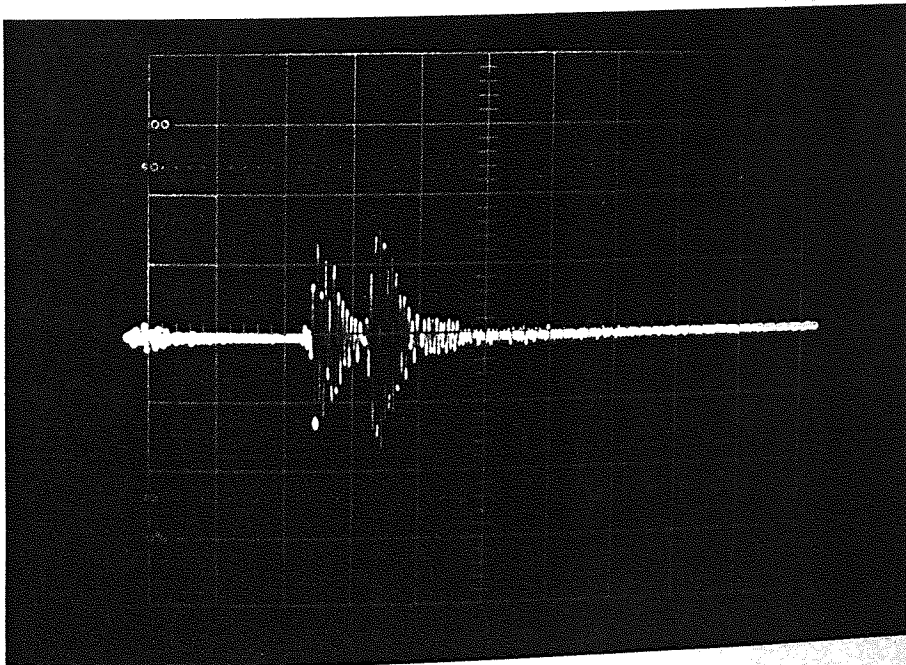Figure 4.27 Typical acoustic emissions

Figure 4.28 Coalesence of events

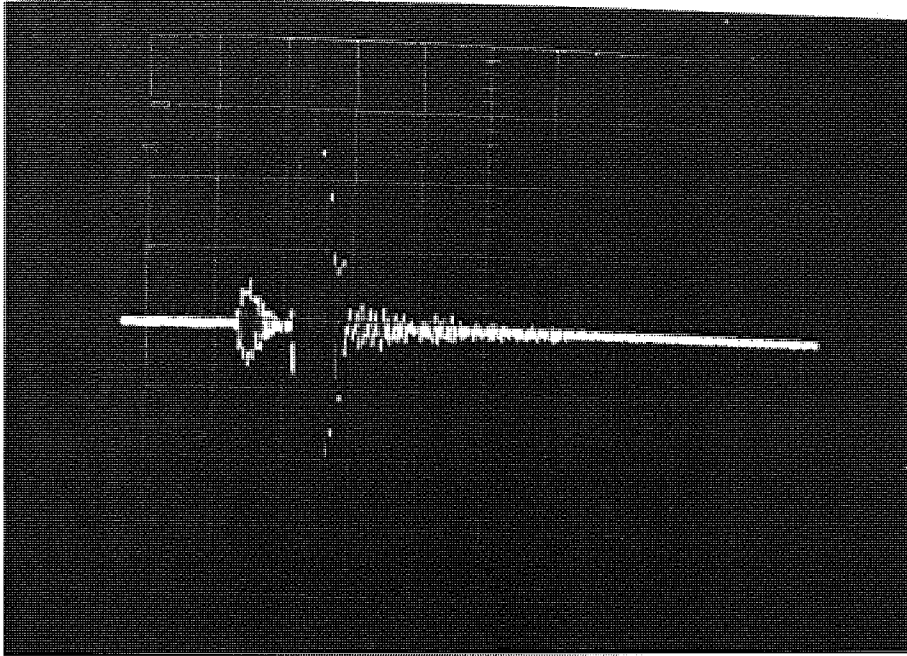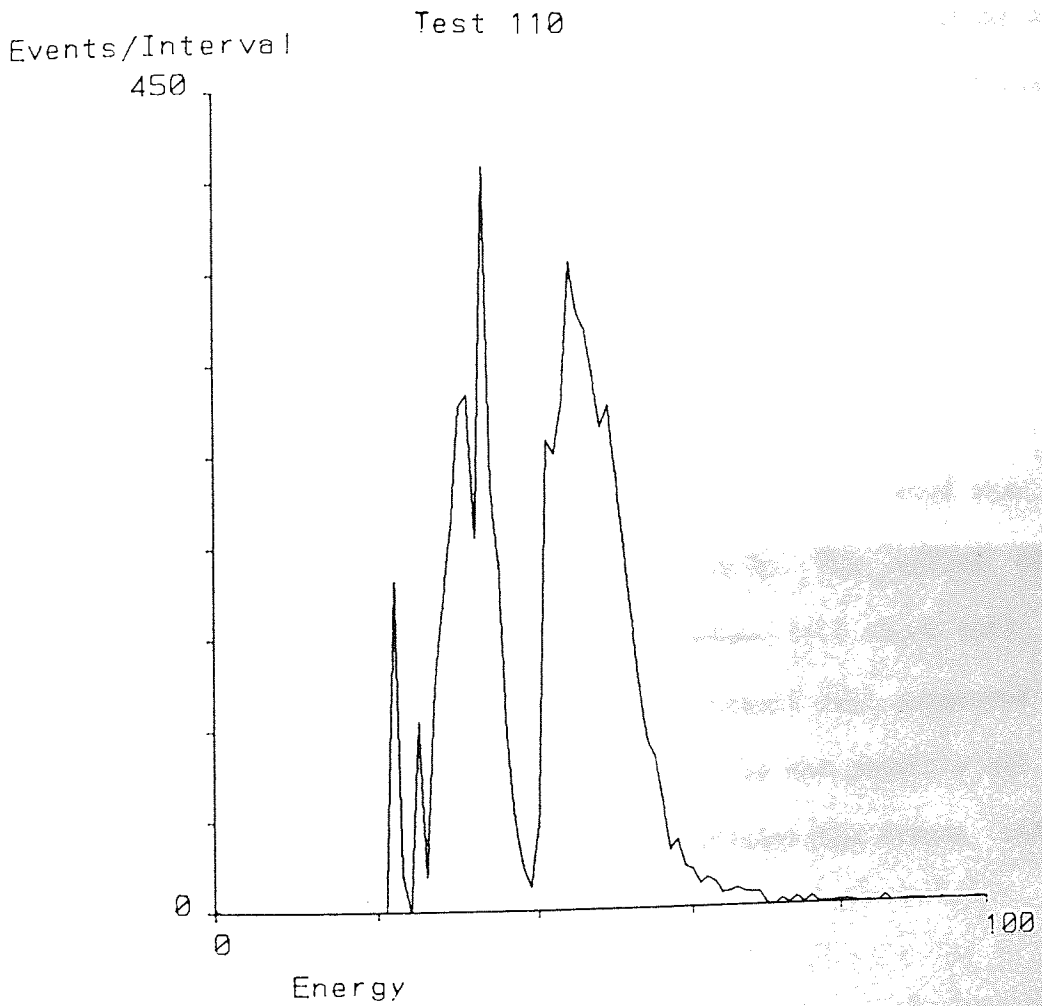Figure 4.29 Coalesence of events

78

Figure 4.30 Distribution by energy

Effect of mean stress and stress path

5.1 Introduction.

One of the principal aims of the research program was to use Acoustic Emission (AE) as a method of identifying yield in sand. In order to do this it was anticipated that tests involving complex stress paths would be performed. However, the effect of varying stress levels on the Acoustic Emission response of the sand was not known. Therefore, several series of tests were carried out to examine the effects of stress level and stress path on the AE behaviour.

5.2 Effect of cell pressure.

Chapter 4 described the observed AE behaviour of sand when tested at a constant cell pressure of 100kPa. The effect of cell pressure on the AE behaviour was studied in a short test series (Tests 46, 55, 40) conducted at constant cell pressures of 50, 100, and 200kPa respectively. So far as was possible all other controls remained the same; in particular the strain rate was 1%/hour.

Figures 5.1 - 5.3 show the stress ratio and volumetric strain/deviatoric strain curves for these tests, each sample exhibiting the classical behaviour of dense sand. In this test series post-peak deformation was not considered. Also, although Tests 40 and 46 show unload/reload cycles the AE response during these cycles will not be commented on here but will be dealt with in Chapter 6. From a comparison of these figures it can be seen

that the maximum rate of expansion decreases with increasing cell pressure. An increase in cell pressure also leads to a decrease in the maximum stress ratio, implying that the sand tested has a curved Mohr Coulomb failure envelope.

Figures 5.4 - 5.6 show events/deviatoric strain for each of the tests. Inspection of each graph individually shows that, independent of cell pressure, the shape of the curves is similar. However, a comparison of the graphs shows that as the cell pressure is raised more events are received. Figures 5.4 - 5.6 are superimposed in Figure 5.7 to give a clearer indication of this. (Note that information above a strain of 4% has been omitted as this incorporates unloading information for Tests 40 and 46). At 4% deviatoric strain the total events are 50, 240, and 540 for the tests at 50, 100, and 200kPa respectively; the corresponding stress ratios are 0.84, 0.81, and 0.76. Figure 5.7 shows that the event rate increases with cell pressure therefore, it is clear that events are primarily a function of cell pressure, hence mean stress, rather than stress ratio.

5.3 Effect of mean stress.

Section 5.2 showed that a relationship between cell pressure and events exists. However, constant cell pressure tests make an analysis more difficult because the change in mean stress is another variable in the problem. So that the effect of mean stress on AE response could be studied a series of 12 tests was carried out. This series was split into 4 groups of 3, and within each group three different mean stresses were used (100, 200, and 300kPa). Each group was tested at a different threshold voltage

(0.5, 0.75, 1.00, and 1.25V); the threshold voltage was varied as a check on earlier findings (see Chapter 4) and to see if it would aid interpretation of the results. Subsequent inspection of results showed that no significant improvement in interpretation was to be gained by varying the threshold voltage. The analysis in this section will concentrate on the tests which used a threshold voltage of 1.00V; the other tests will only be used where additional confirmation of a particular point may be required.

Figure 5.8 shows the stress paths for Tests 59, 67, and 73 at mean stresses of 100, 200, and 300kPa respectively. It may be seen that in each case the actual mean stress follows the desired mean stress fairly closely but a few significant deviations do occur. The variation was brought about because of the equipment used; there was no facility for the continuous monitoring of the data representing the state of the sample, only data at periodic intervals. Therefore, the cell pressure could only be adjusted to the required value at the end of a recording interval although, with experience, a reasonable estimate could be formed. Also, because the mercury pot system controlling the cell pressure could only be adjusted by fixed amounts, due to the teeth on the ratchet, adjustment in the later stages of the test caused fluctuations in the deviator stress. The effect of these limitations was reduced by using a strain rate of 1%/hour and checking the cell pressure every minute.

The stress ratio and volumetric strain/deviatoric strain graphs are shown in Figures 5.9 and 5.10 respectively. It may be seen that following an initial rapid increase in the stress ratio,

82

the stress ratio increases at a decreasing rate. Also it can be seen that increasing the mean stress decreases the peak stress ratio; this was also found in the constant cell pressure tests. The volume change curves for these tests show little initial contraction was recorded and, once expanding, the curves tend towards straight lines. Inspection of the curves shows that they are less smooth than those shown for constant cell pressure tests but this is an effect of the (relatively) abrupt changes of cell pressure. The position of the volumetric strain curve for Test 67 (200kPa) with respect to Test 59 (100kPa) is anomalous; an inspection of the test record shows that, although it is less dense than the other tests, initial stress control was poor.

Events versus strain are plotted for the individual tests in Figures 5.11 - 5.13 and are superimposed in Figure 5.14 for comparative purposes. Each figure shows a reasonably smooth curve similar to those observed in constant cell pressure tests. However, it is clear that there is a substantial mean stress effect on the AE response. The three tests reported were all tested at different mean stresses and, therefore, the amount of work done by the external stresses will be different. It would seem appropriate to plot events against work rather than deviatoric strain. Also, as acoustic emissions are derived from the release of stored energy, the use of work rather than deviatoric strain would appear to be more relevant. Figure 5.15 shows events/work for the three tests; it may be seen that the mean stress effect is still present.

One way to reduce the difference in events at different mean stresses is to normalise the events (E) by dividing by the mean

stress (p). The normalisation is accomplished by dividing the number of events occurring in a fixed interval by the mean stress in that interval, and adding that result to the total. In fact, it was found that the best correlation was to normalise events by $p^{1.5}$, the results of which are shown in Figure 5.16. The procedure was repeated for the tests at different threshold voltages and Figures 5.17 - 5.19 show the normalised events for tests at threshold voltages of 0.50, 0.75, and 1.25v respectively. It may be seen that, in general, there is good agreement between the normalised events and the work done by the external stresses. Also, reducing the threshold voltage can be seen to increase the number of (normalised) events, and the increase of normalised events with work is seen to be non linear. There does not appear to be a simple relationship between events and the threshold voltage.

5.4 Extension tests.

The tests reported so far in this thesis have all been compression tests, that is to say the vertical stress has been greater than the horizontal stress. However, in order to describe the AE response fully and to aid yield identification it is necessary to perform extension tests in which the horizontal stress is greater than the vertical stress. Extension tests represented no extra problems in testing because of the bayonet fitting which connected the load cell to the top platen.

A constant cell pressure extension test, Test 47, was carried out at 300kPa. The stress ratio and volumetric strain/deviatoric strain graphs are given in Figures 5.20 and 5.21 respectively. It

84

may be seen that the sample expands from the start of loading, unlike a compression test. The peak stress ratio may be compared with a constant cell pressure compression test that had a similar mean stress at peak stress ratio; one such test is Test 110 which had a mean stress of 236kPa, while Test 47 had a mean stress of 220kPa. Test 47 had a peak stress ratio of -0.51 while Test 110 had a stress ratio of 0.81; which indicates that the sand tested shows good agreement with the Mohr-Coloumb failure criterion. Additionally it can seen that the volume change curve would form a continuous curve if it were plotted with a compression test; this is illustrated schematically in Figure 5.22.

The events versus deviatoric strain curve is shown in Figure 5.23 and it is clear that the number of events and their rate of emission differ considerably from those which would be recorded in a compression test. It may be seen that there is at least an order of magnitude difference in the number of events received compared with a compression test. Also, the shape of the curve is convex rather than concave but any judgements are very subjective because of the lack of AE data. However, as indicated in section 5.3, the work done by the external stresses influences the AE response, as does the mean stress. Figure 5.24 shows the normalised events/work graph, with the 200kPa mean stress test being shown for the purposes of comparison. It may be seen that there is agreement between the two curves, but the correlation is not as good as that between the mean stress tests.

A number of other extension tests were carried out in case the lack of events was due to a poor testing technique, or a badly prepared sample. However, all the results were consistent with

the results reported here, and the results of Test 47 may be taken to be representative of extension tests. Tanimoto et al (1983) showed that there was a significant difference between compression and extension tests: in the reported results the number of counts received in extension was two orders of magnitudes less than the number received in compression. It was also shown that the peak stress ratio in extension was less than that in compression.

5.5 Constant axial stress test.

Another possible simple stress path is one in which the axial stress is maintained constant. This type of test, in contrast to the others reported above allows the mean stress to decrease while the sample remains in compression.

The stress path for Test 54 is shown in Figure 5.25; Test 54 was tested at a constant axial stress of 300kPa. The same technical problems as in mean stress tests made it difficult to trace the path exactly. The associated stress ratio and volumetric strain curves are shown in Figures 5.26 and 5.27 respectively. The amount of contraction which occurs is larger than is recorded for constant cell pressure (or constant mean stress) tests; since the sample is roughly the same porosity this is an effect of stress path.

The mean stress versus deviatoric strain graph is shown in Figure 5.28; the mean stress develops in a similar manner to that of an extension test, except that the sign of the deviatoric strain is reversed. However, consideration of the events/deviatoric strain

graph (Figure 5.29), shows that the AE response is very different from an extension test and is, in fact, similar to a constant cell pressure test. When the mean stress becomes constant it may be seen that the event rate changes little, and the events/deviatoric curve becomes roughly linear.

5.6 Undrained tests.

During the research period several undrained constant cell pressure tests were monitored for their AE response. While the undrained test is widely applied to cohesive materials, it is used infrequently for tests on cohesionless materials. The tests were thought to be worthwhile since they would provide details of the AE response for a different type of stress path. It should be noted that stresses reported in this section are effective stresses, not total stresses.

The effective stress paths followed for two undrained tests (Tests 57 and 58) are shown in Figures 5.30 and 5.31 respectively. It may be seen that both tests followed the same pattern; the effective stress path leaving a plane of constant mean effective stress, curving over to become asymptotic to a line passing through the origin. The pore pressure/deviatoric strain graphs are shown in Figures 5.32 and 5.33 respectively. It may be seen from the pore pressure curves that the mean effective stress increases at an increasing rate, which is contrary to that observed in drained constant cell pressure tests. The associated effective stress ratio/deviatoric strain curves are shown in Figures 5.34 and 5.35. The stress ratio reached is not as high as that in drained constant cell pressure or constant mean stress

tests but in shape differs little.

The events/deviatoric strain graphs are shown in Figures 5.36 and 5.37 for Tests 57 and 58 respectively. It is apparent that although the initial part of the graphs is similar to that of the constant cell pressure tests, there is a very large increase in the event rate after a deviatoric strain of approximately 1.5%. It is clear that the event rate increases at an increasing rate, suggesting once more that the event rate is strongly mean stress dependent. The increase in the event rate also suggests the AE response is linked with the effective stresses, not the total stresses.

5.7 Discussion of results and summary.

The AE response of sand has been shown to be stress level dependent; this has been demonstrated for constant cell pressure tests and for constant mean stress tests. Koerner et al (1976) also demonstrated that sand exhibited this phemonenon using incremental loading. The AE response has also been shown to be stress path dependent; the number of events recorded in compression tests being an order of magnitude larger than the number recorded in extension.

The stress level dependence of the AE response is not unexpected. The stress path dependence is complex not only because of the stress level effect but also because of the work done on the sample. Acoustic emissions are derived from the dissipated energy, and if the dissipated energy evolves in a similar manner

to total energy the AE response should be affected by the work done on the sample. A strong correlation between (normalised) events and work exists which partially accounts for the differences in mean stress and work done in the different tests. The normalised events/work curves for some of the different types of test presented in this chapter are shown in Figure 5.38. It can be seen that, while the different types are fairly closely grouped, different stress paths cause slightly different AE responses. It is interesting to note that the constant cell pressure tests (compression and extension) fit well after normalisation, as do the initial portions of constant mean stress and undrained (when the stress path follows constant mean stress).

The stress path and stress level dependence of the AE response complicates its use as a method of yield identification, and an increasing event rate does not necessarily imply that the sample is approaching failure. However, it has been shown that, whatever the stress path, the AE response follows a similar pattern. It has also been shown that, while a particular stress path may result in fewer recorded events, it is possible to compensate for this by reducing the threshold voltage or by increasing the gain setting. The threshold voltage provides a means of increasing, or decreasing, the number of recorded events without altering the overall pattern of event recording. In particular it would appear beneficial to reduce the threshold voltage when conducting extension tests so as to maintain a given event level.

Test 46 (50kPa)

Stress Ratio
0.9

0

0   8
Deviatoric strain
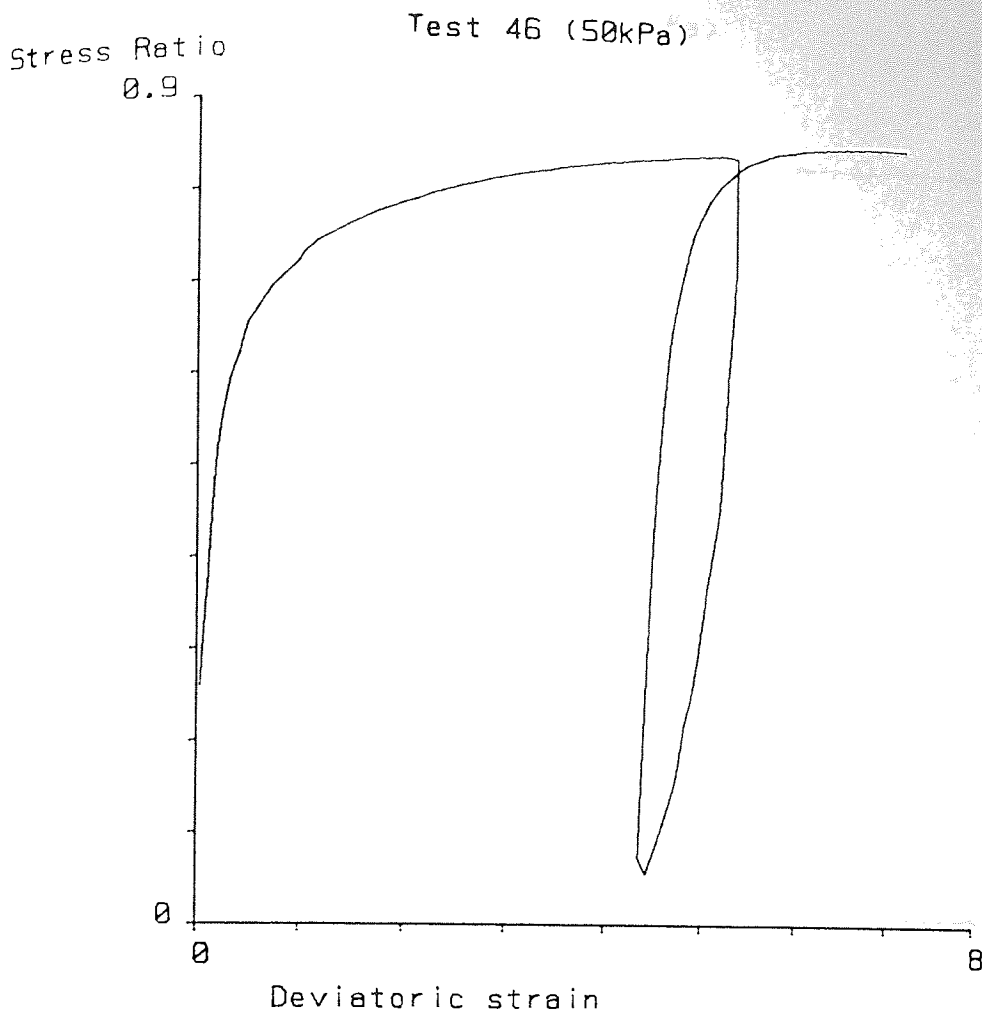
Figure 5.1 Test 46: Stress Ratio/Deviatoric strain

Test 46 (50kPa)

Volumetric strain
0.5

0

-2.5

0   8
Deviatoric strain
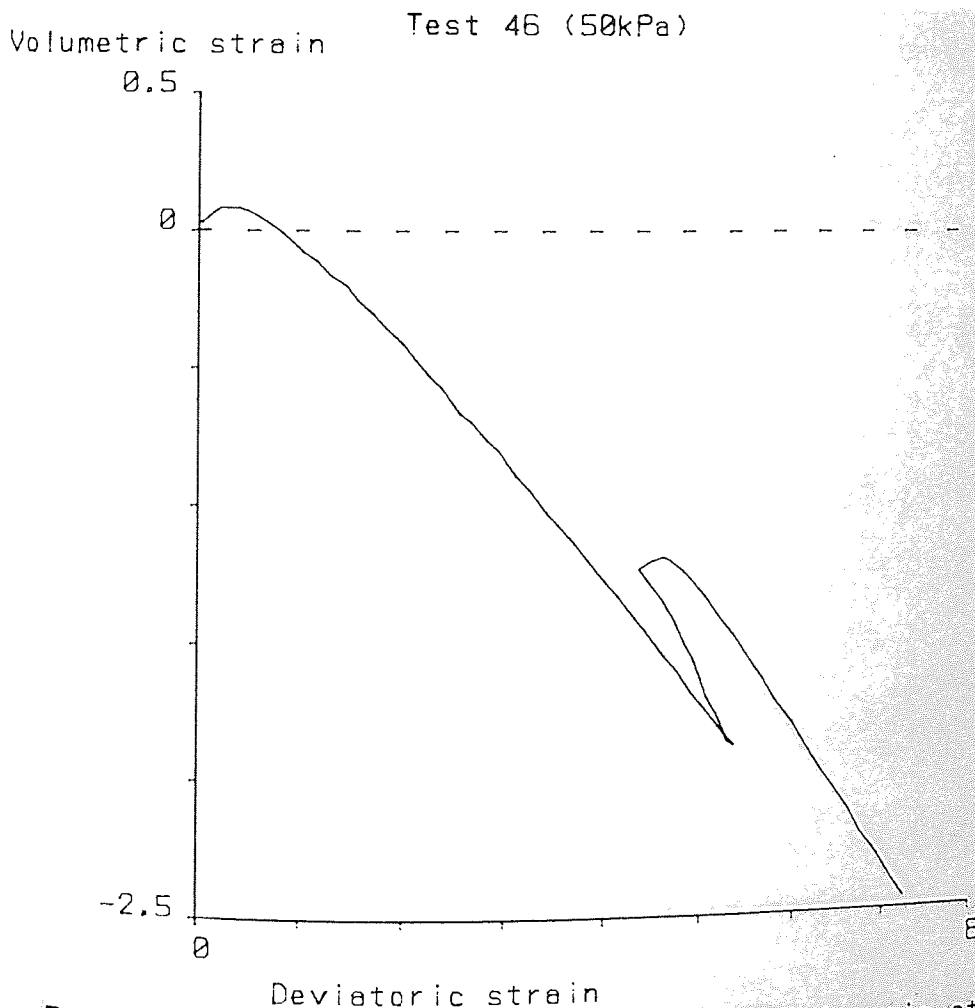
Figure 5.1 Test 46: Volumetric strain/Deviatoric strain

Stress Ratio

0.9
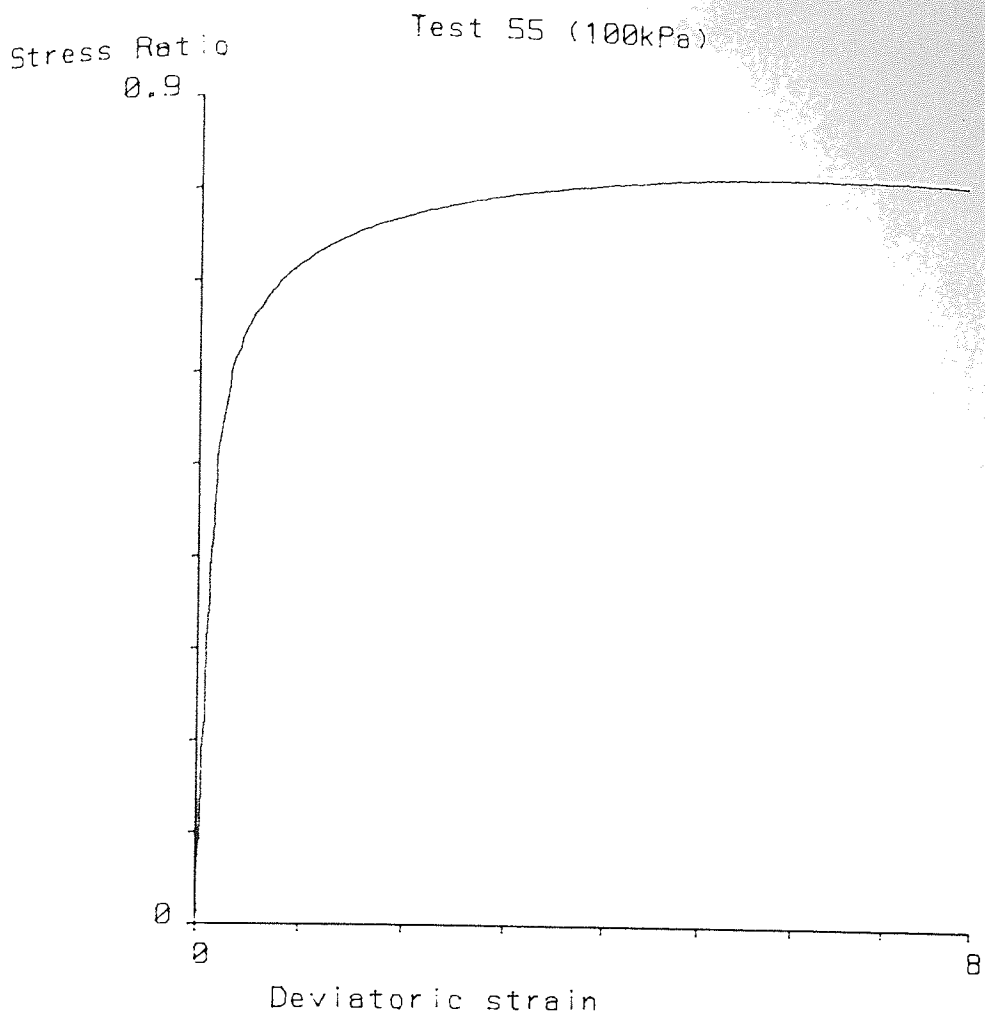
Deviatoric strain

Figure 5.2 Test 55: Stress Ratio/Deviatoric strain

Test 55 (100kPa)

Volumetric strain

0.5

0

-2.5
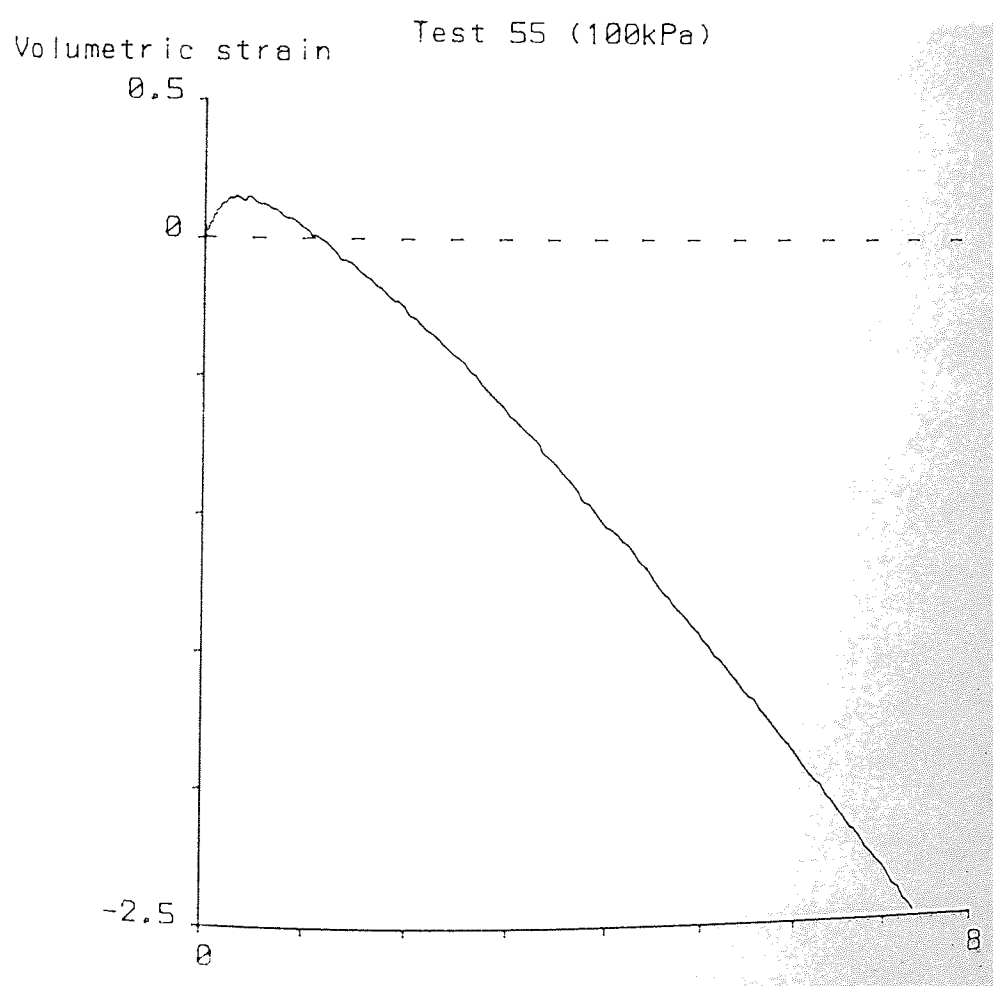
Deviatoric strain

Figure 5.2 Test 55: Volumetric strain/Deviatoric strain

Test 40 (200kPa)

Stress Ratio
0.9
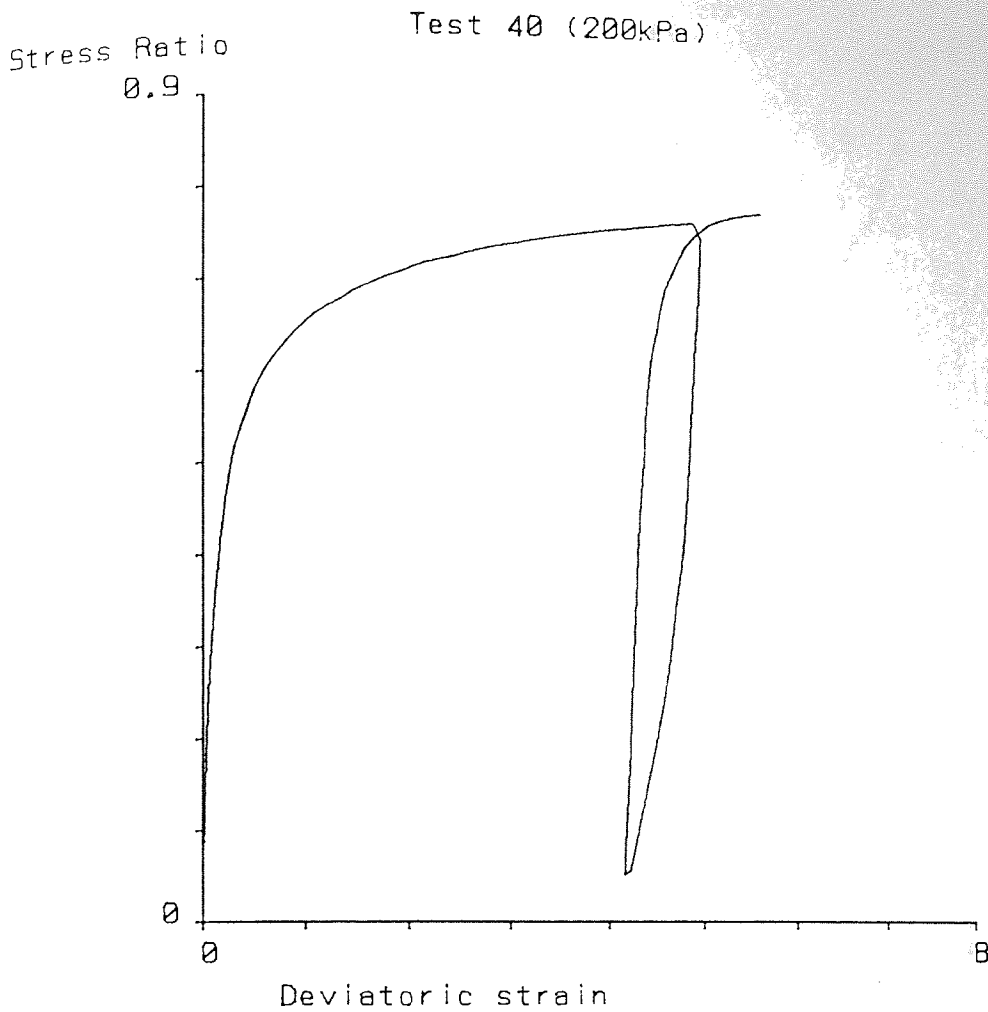
Deviatoric strain
Figure 5.3 Test 40: Stress Ratio/Deviatoric strain

Test 40 (200kPa)

Volumetric strain
0.5
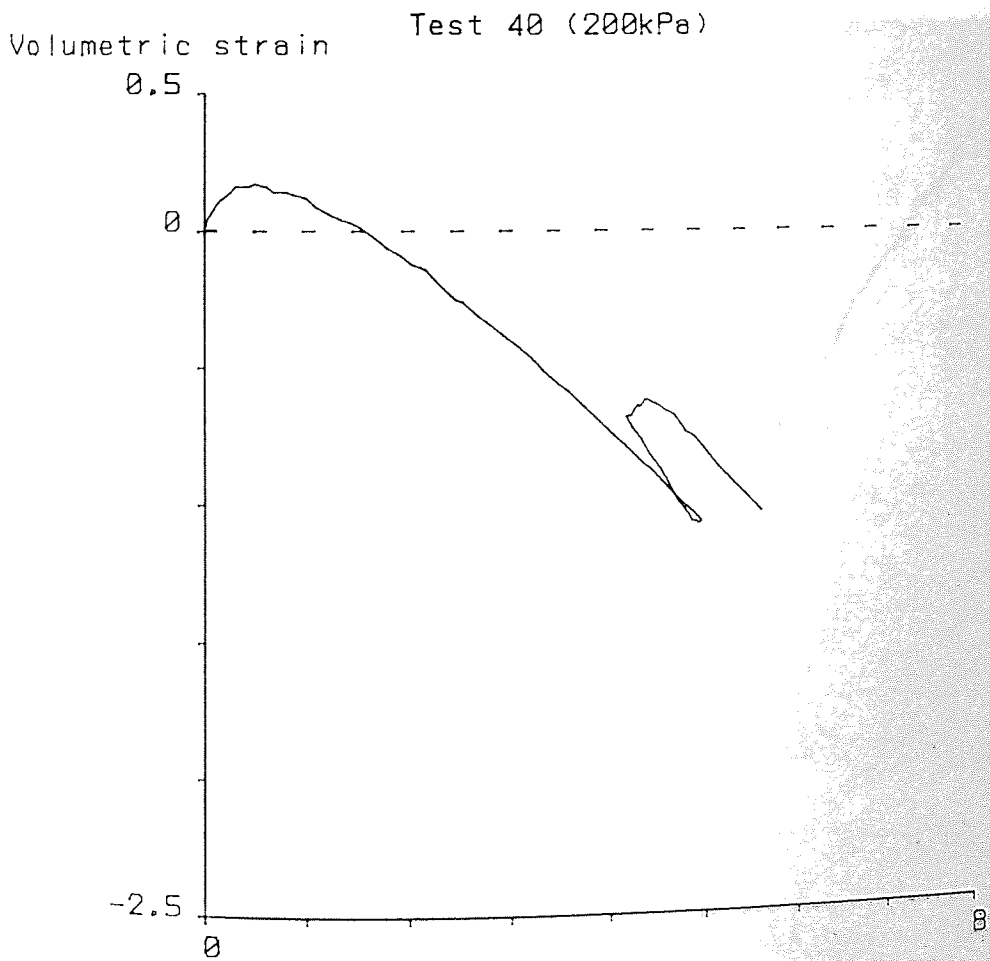
Deviatoric strain
Figure 5.3 Test 40: Volumetric strain/Deviatoric strain

Test 46 (50kPa)

Events

140
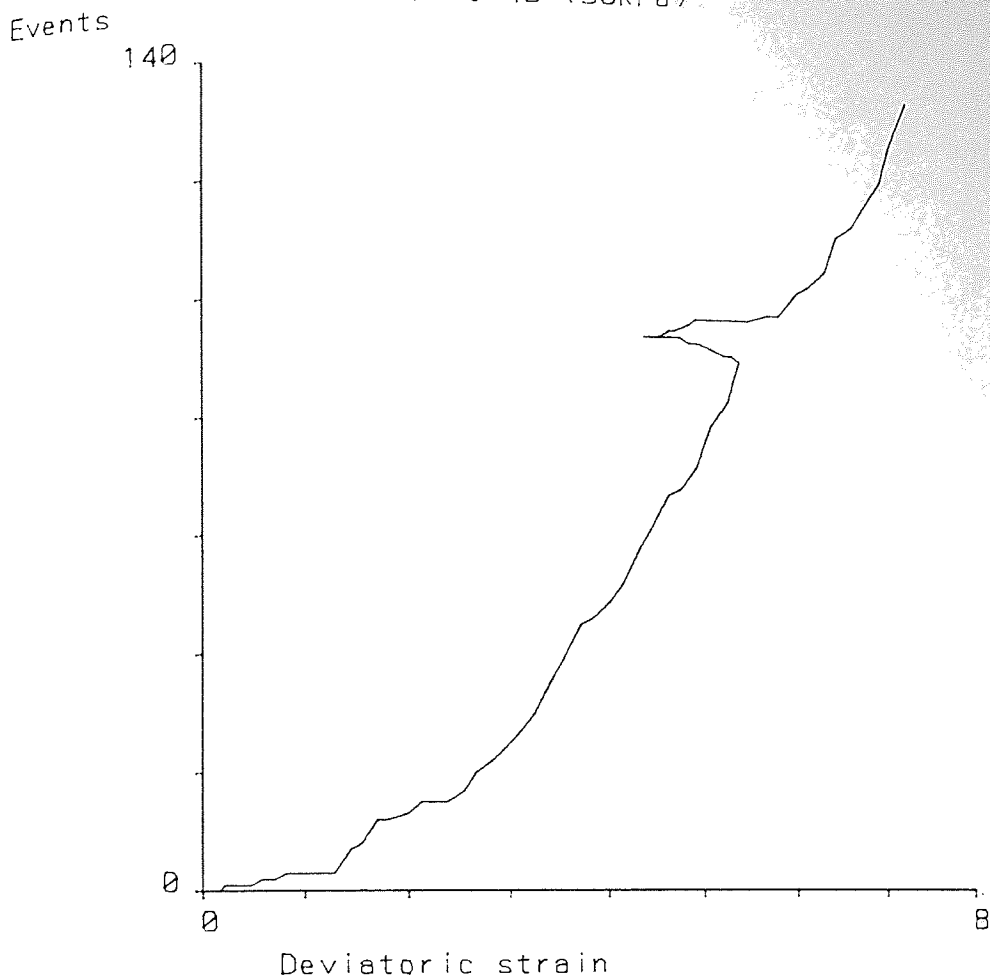
Deviatoric strain

Figure 5.4 Test 46: Events/Deviatoric strain

Test 55 (100kPa)

Events

800
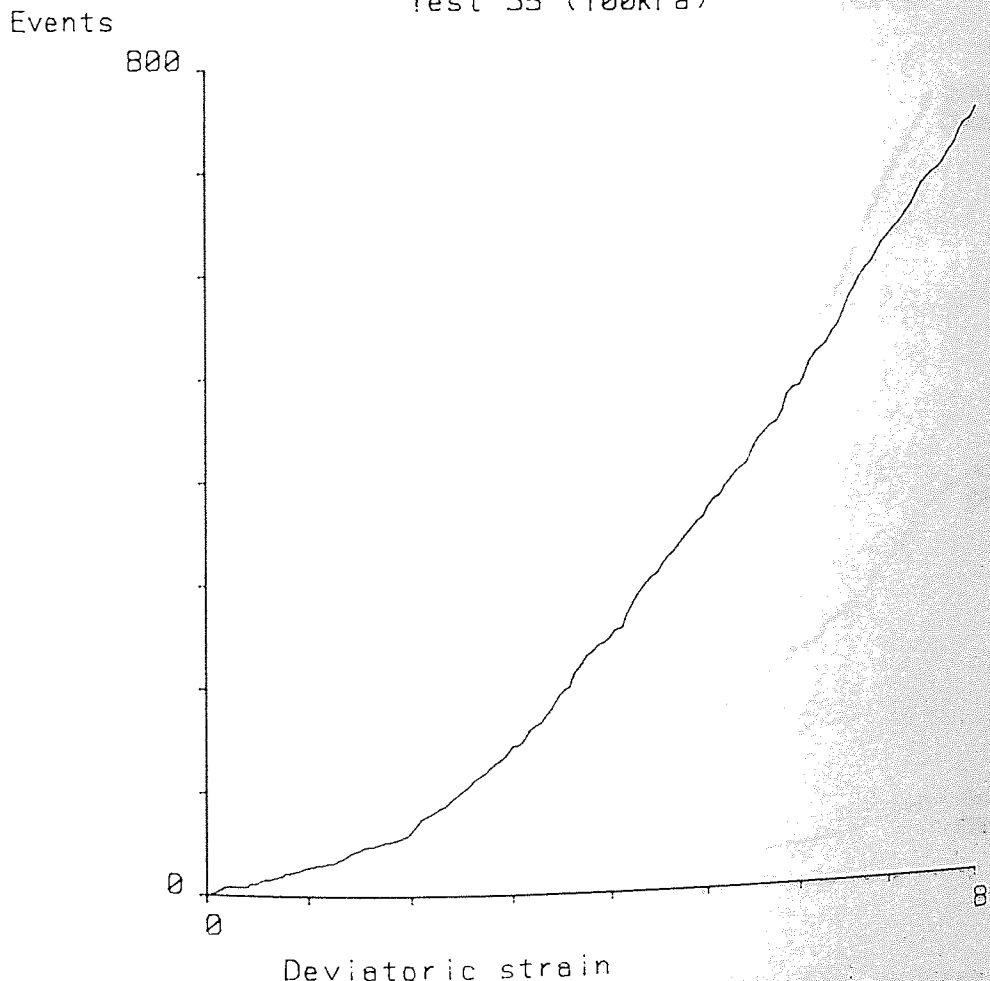
Deviatoric strain

Figure 5.5 Test 55: Events/Deviatoric strain

93

Test 40 (200kPa)
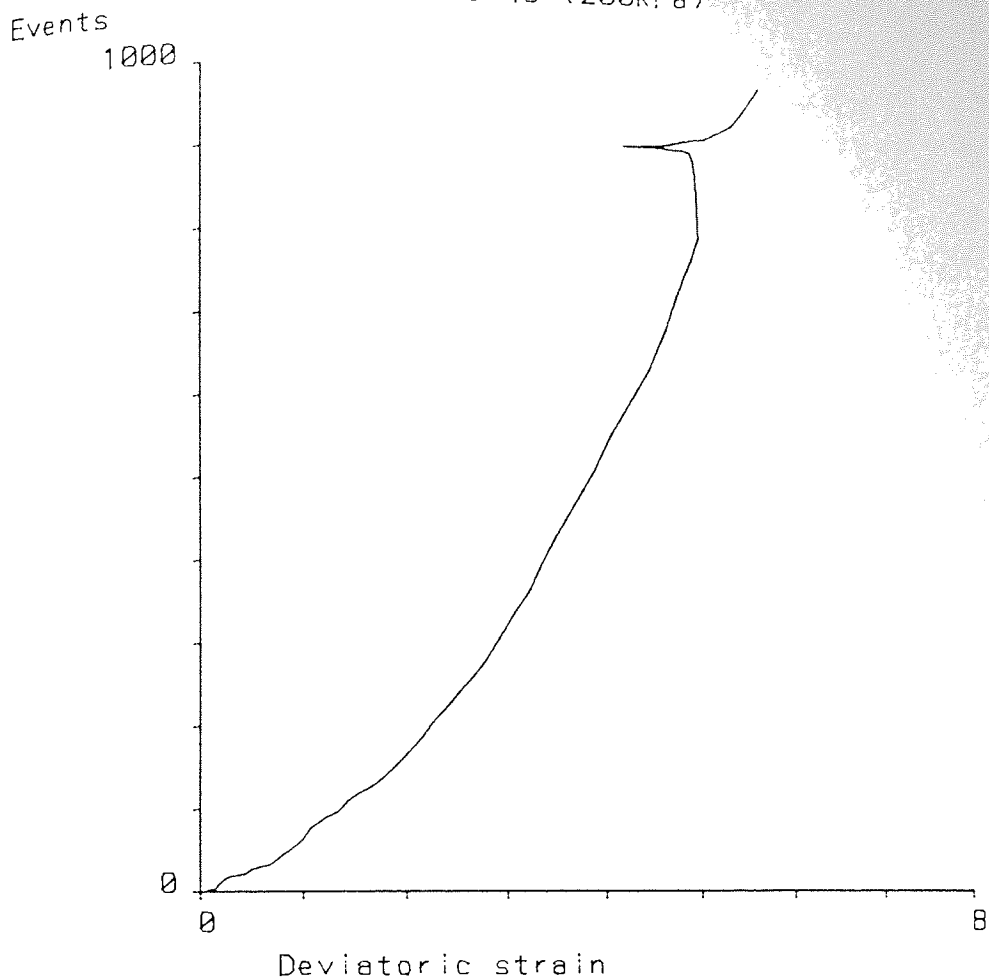
Figure 5.6 Test 40: Events/Deviatoric strain

Constant Cell Pressure Tests
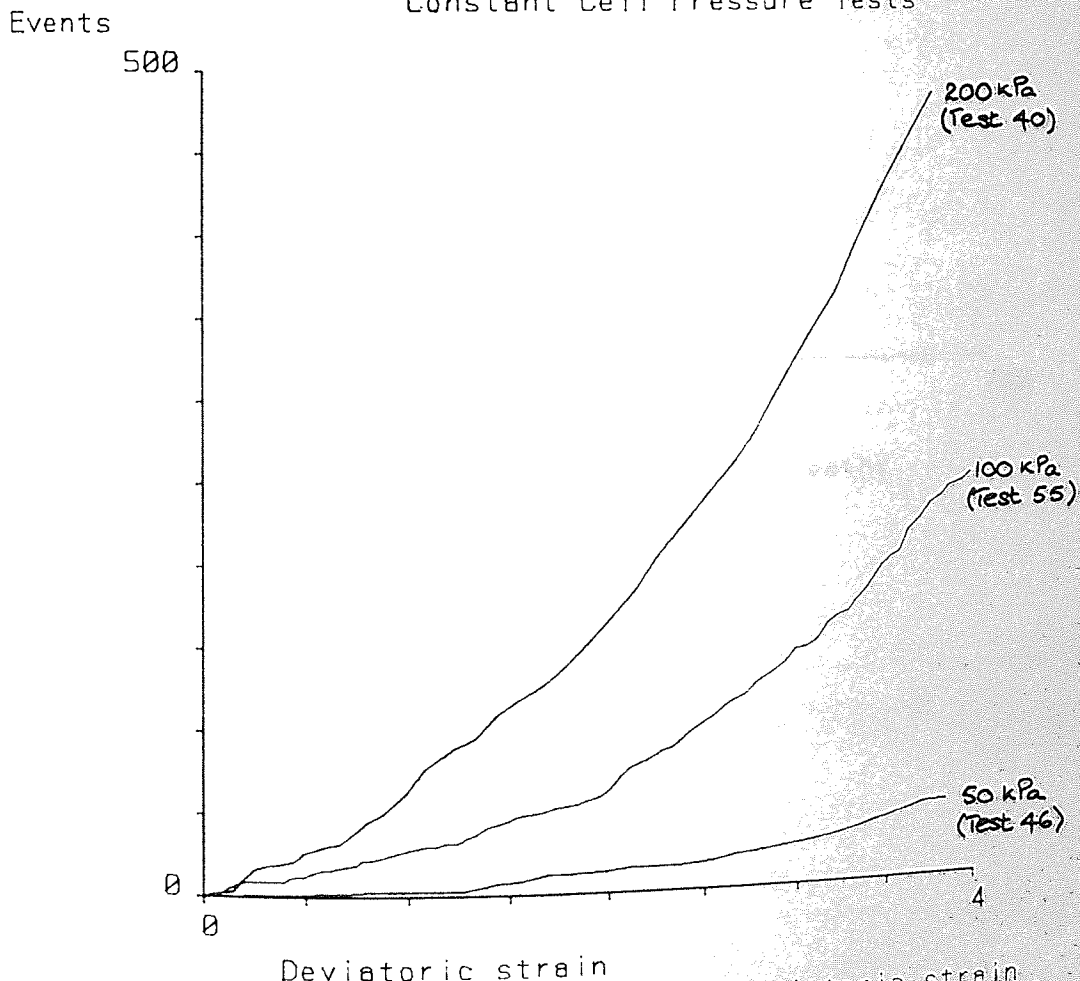
Figure 5.7 Tests 46, 55, 40: Events/Deviatoric strain

Mean Stress Tests

σ'a (kPa)
700

(73)

(67)

(59)

0

0   700

√2.σ'r (kPa)
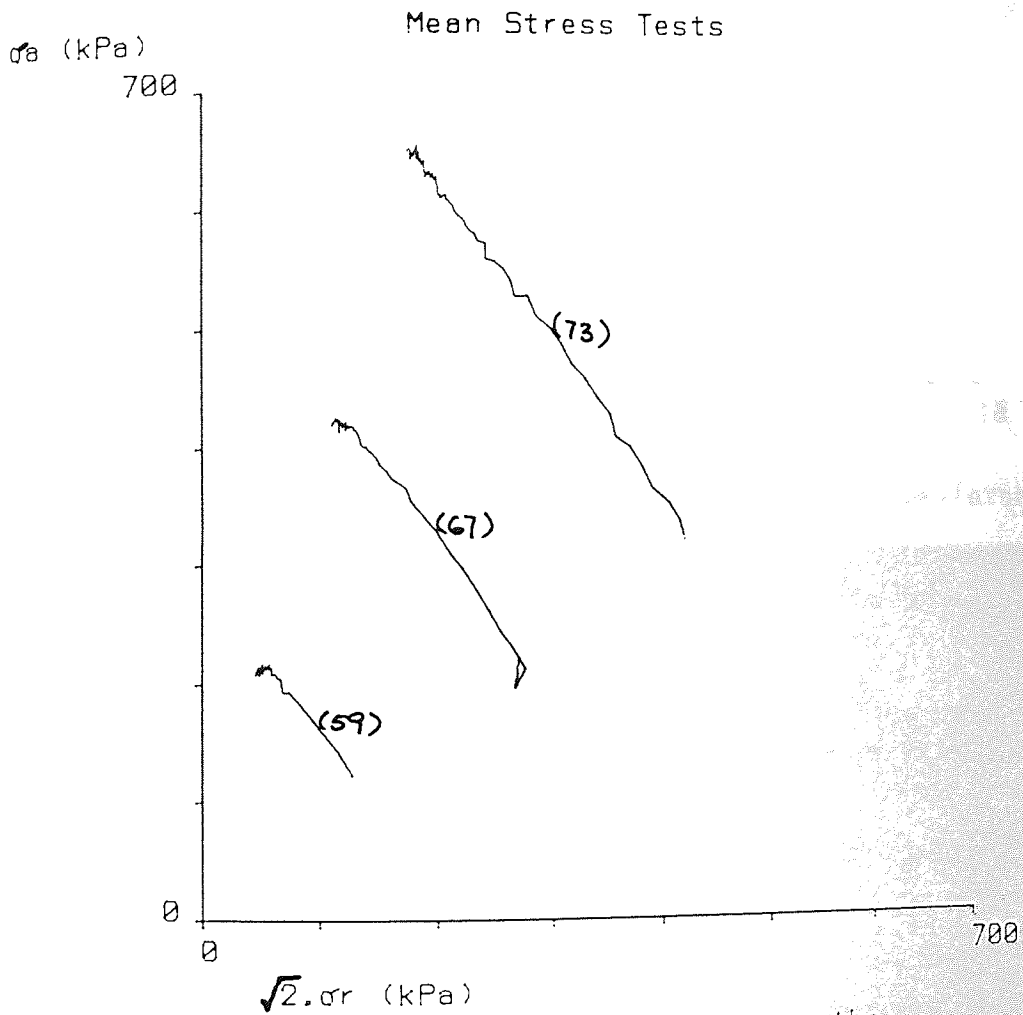
Figure 5.8 Tests 59, 67, and 73: Stress paths
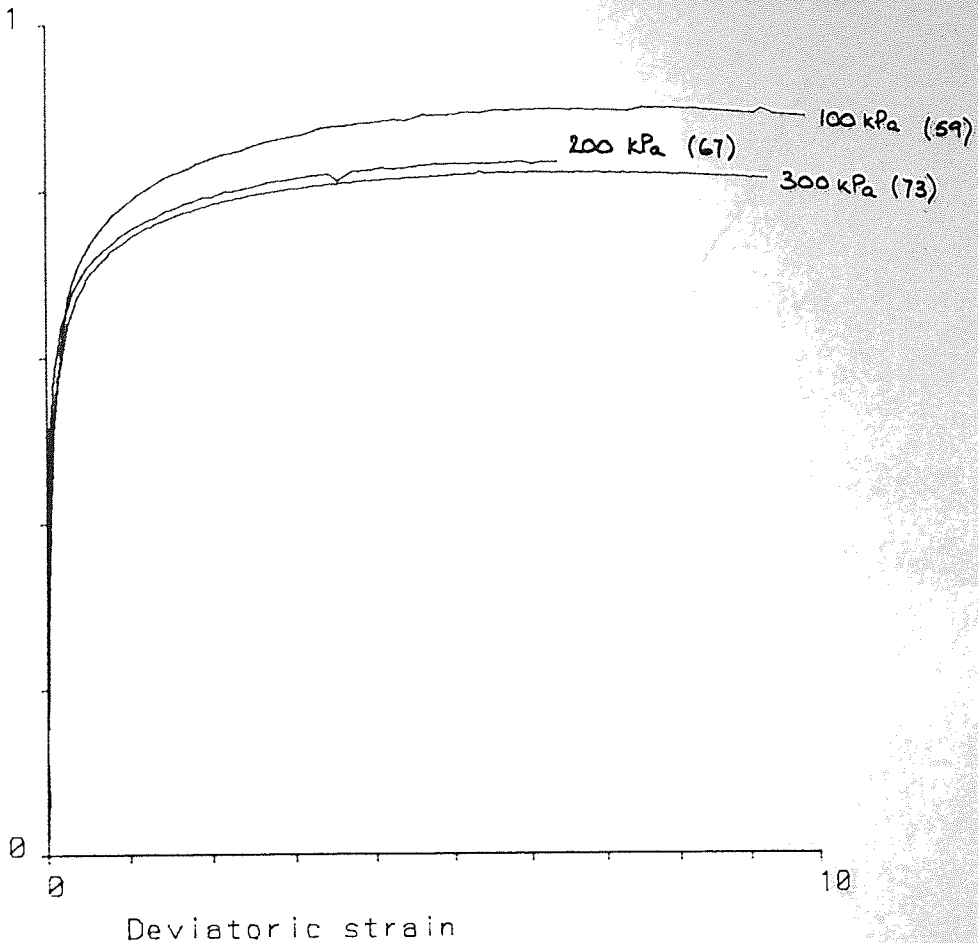
Figure 5.9 Tests 59, 67, and 73: Stress Ratio/Deviatoric strain
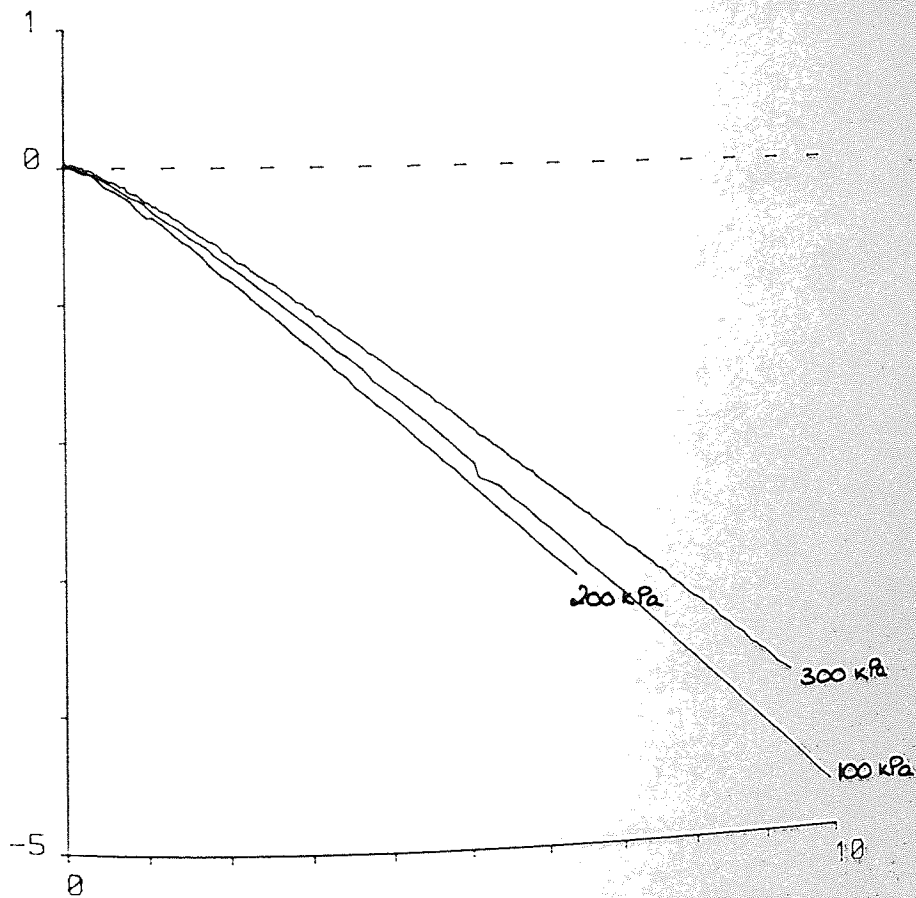
Figure 5.10 Tests 59, 67, and 73: Volumetric/Deviatoric strain

Test 59 (100kPa)

Events
180
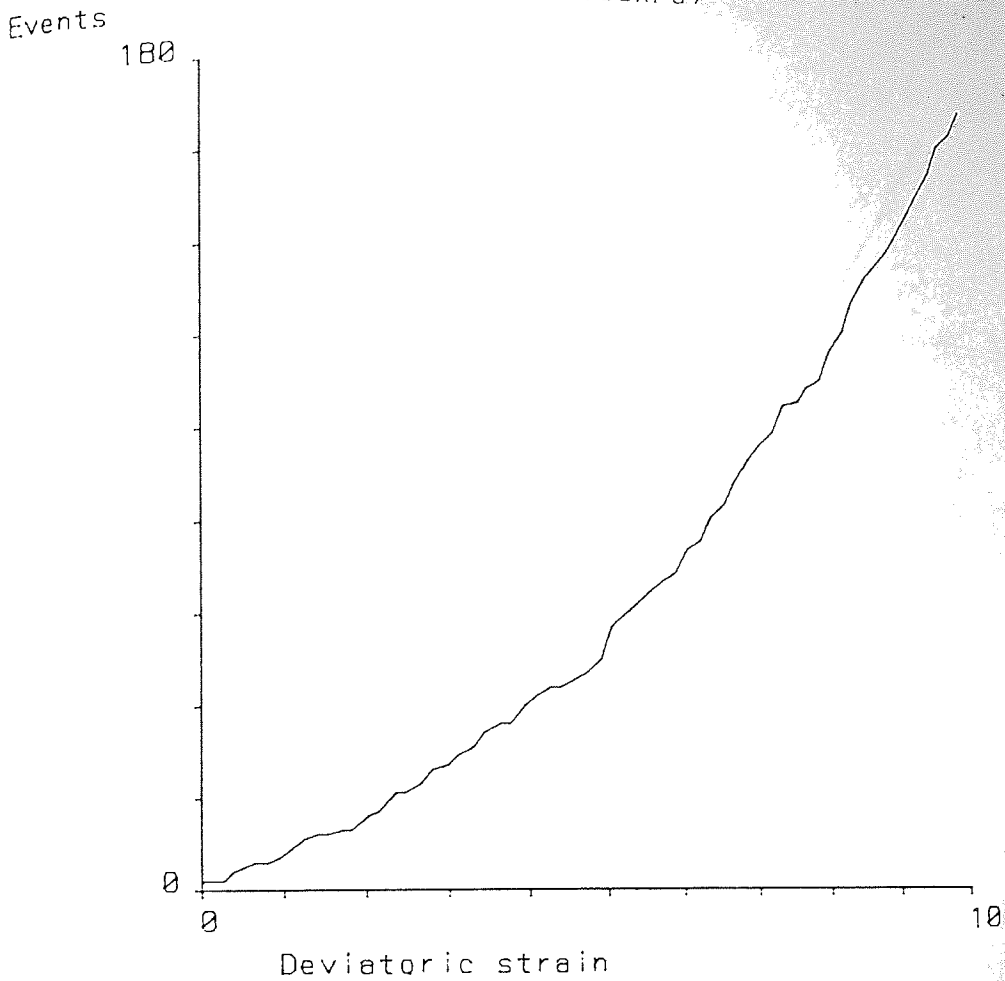
Deviatoric strain

Figure 5.11 Test 59: Events/Deviatoric strain

Test 67 (200kPa)

Events
700
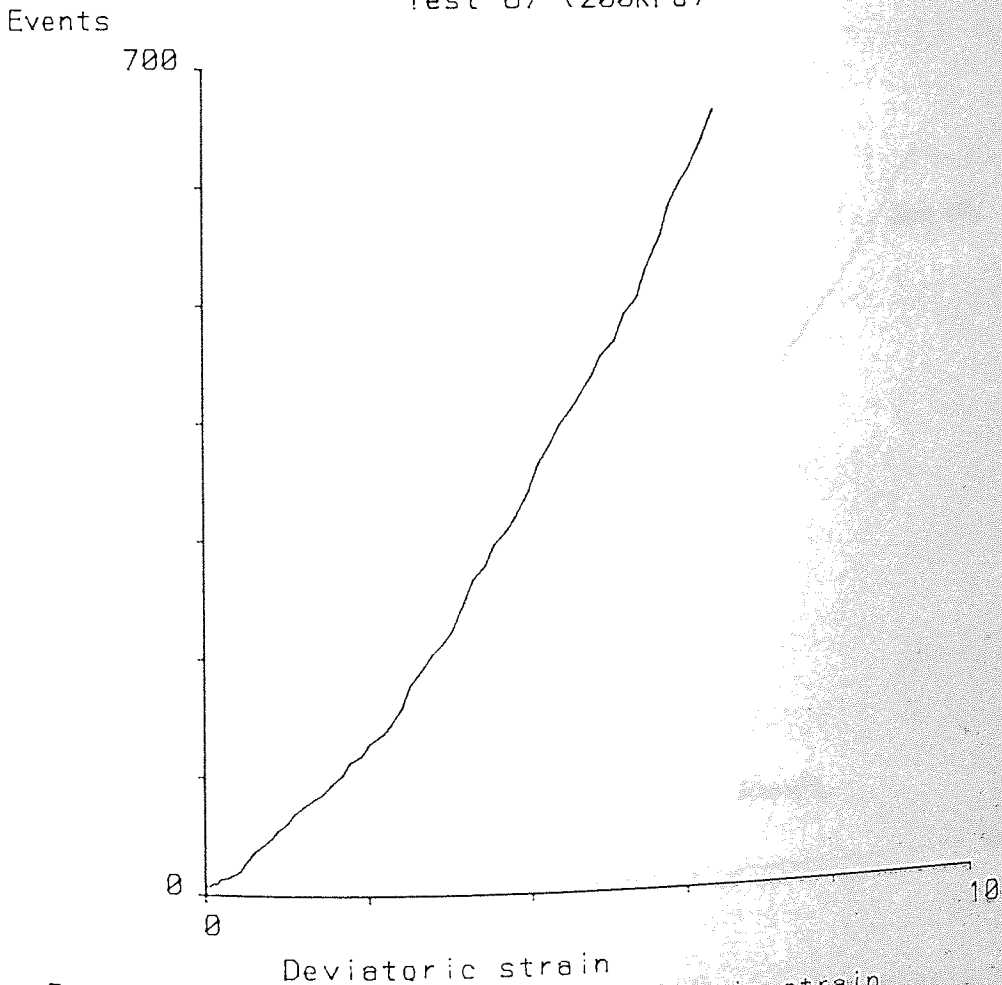
Deviatoric strain

Figure 5.12 Test 67: Events/Deviatoric strain

Test 73 (300kPa)
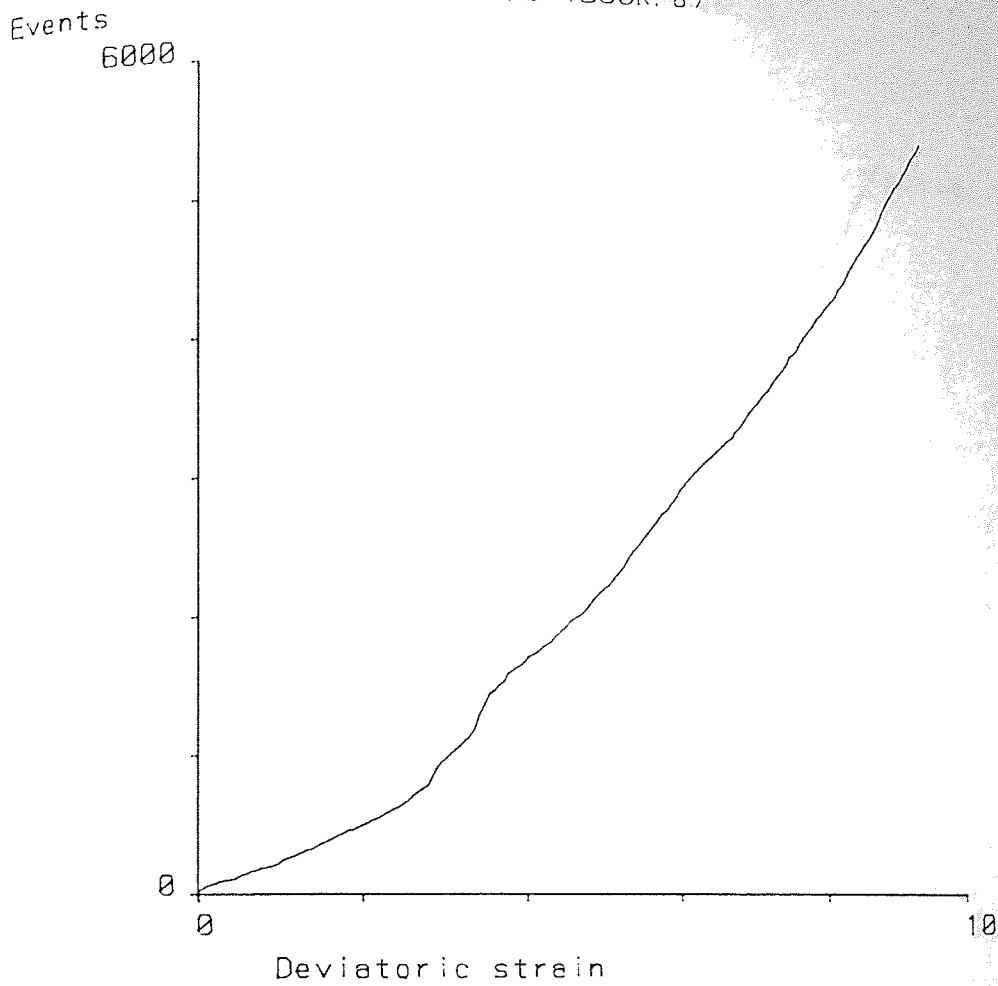
Figure 5.13 Test 73: Events/Deviatoric strain
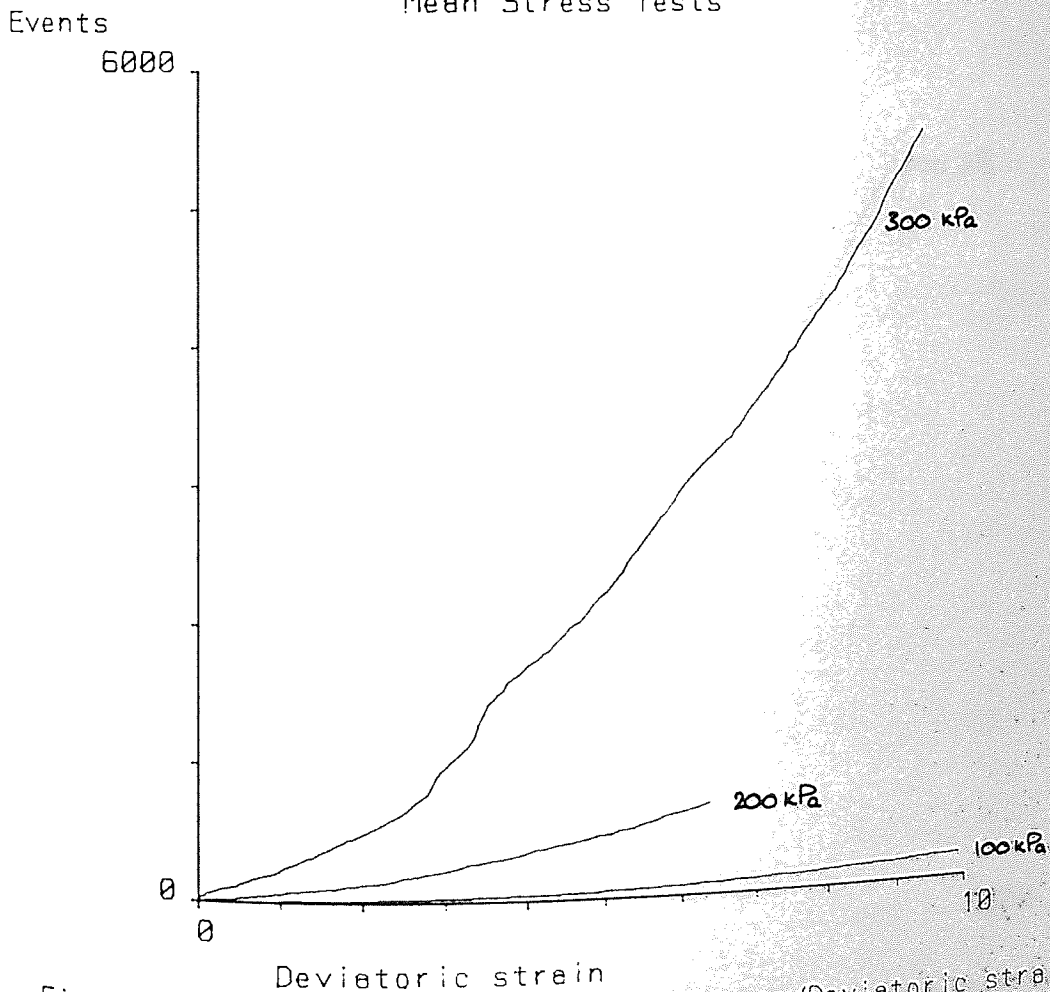
Mean Stress Tests

Figure 5.14 Tests 59, 67, and 73: Events/Deviatoric strain
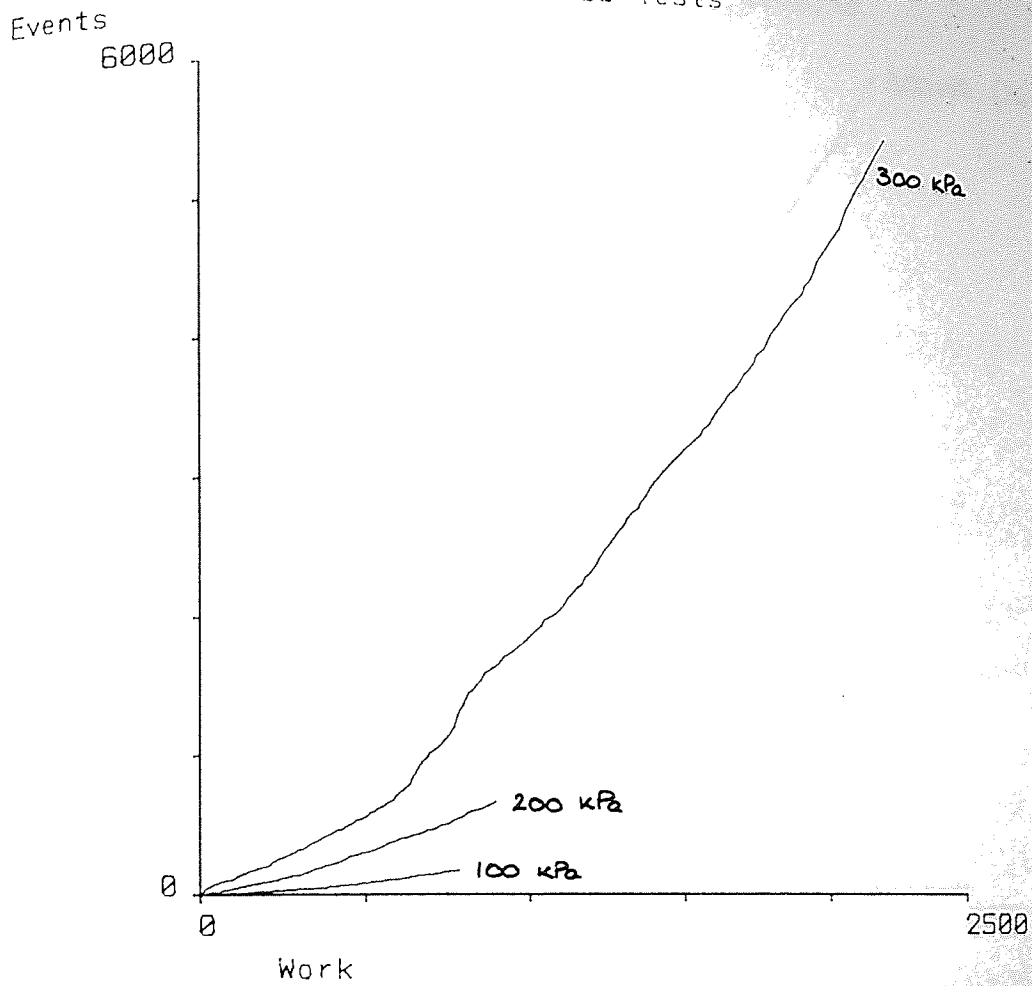
Figure 5.15 Tests 59, 67, and 73: Events/Work
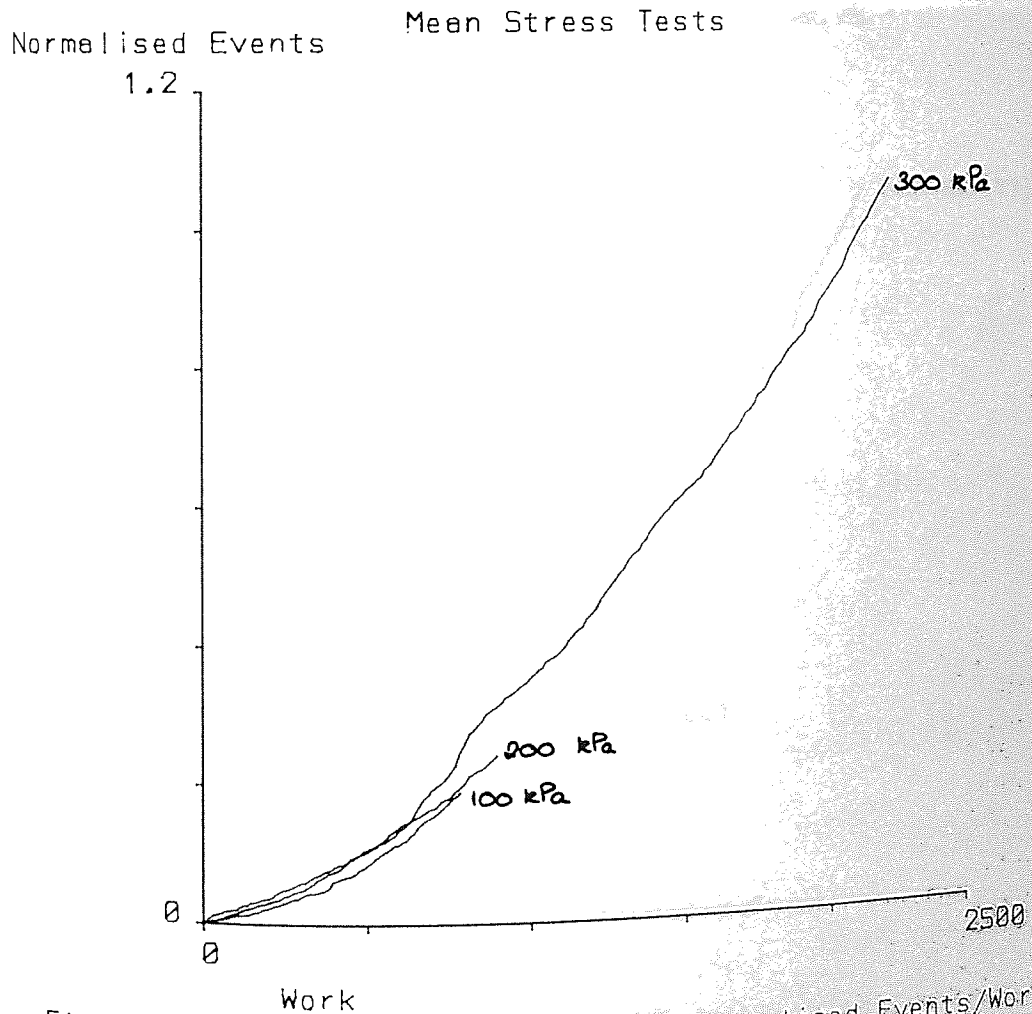
Figure 5.16 Tests 59, 67, and 73: Normalised Events/Work
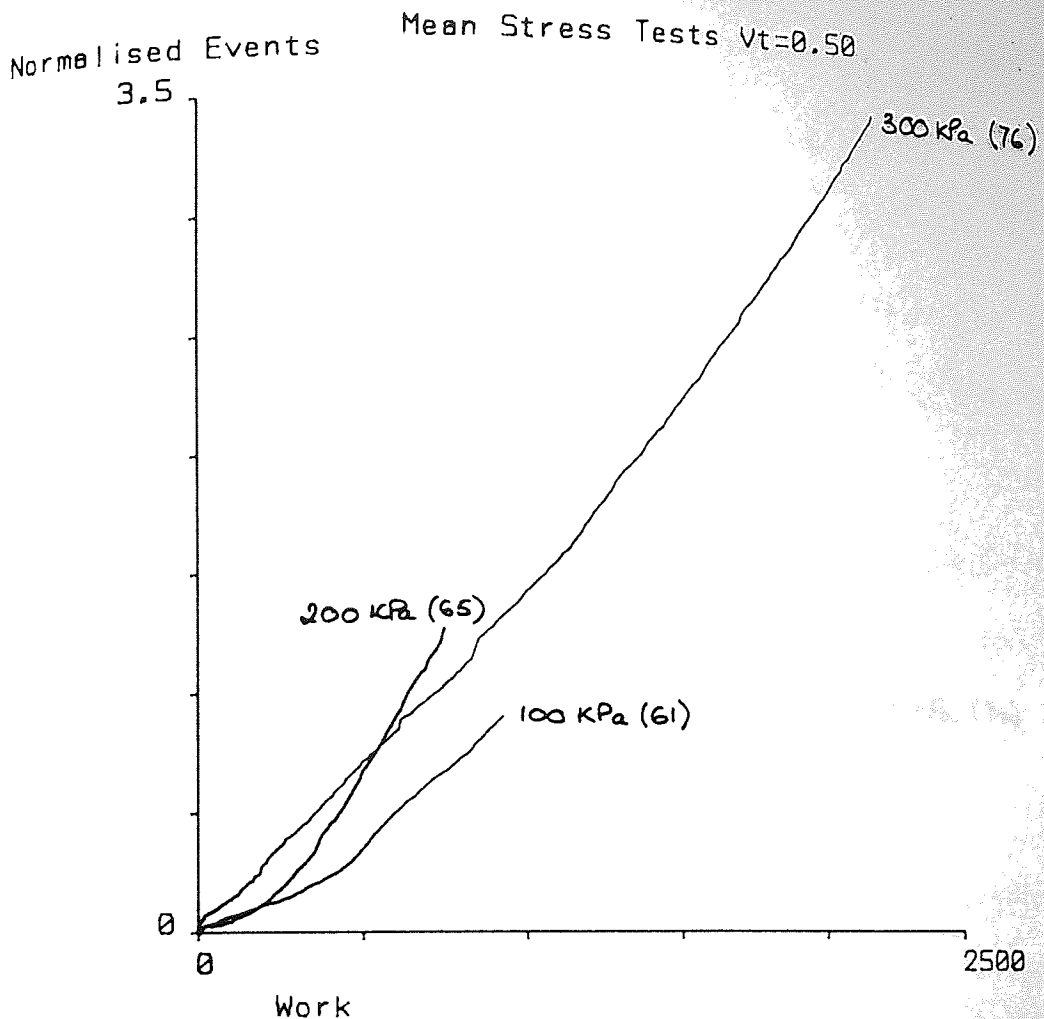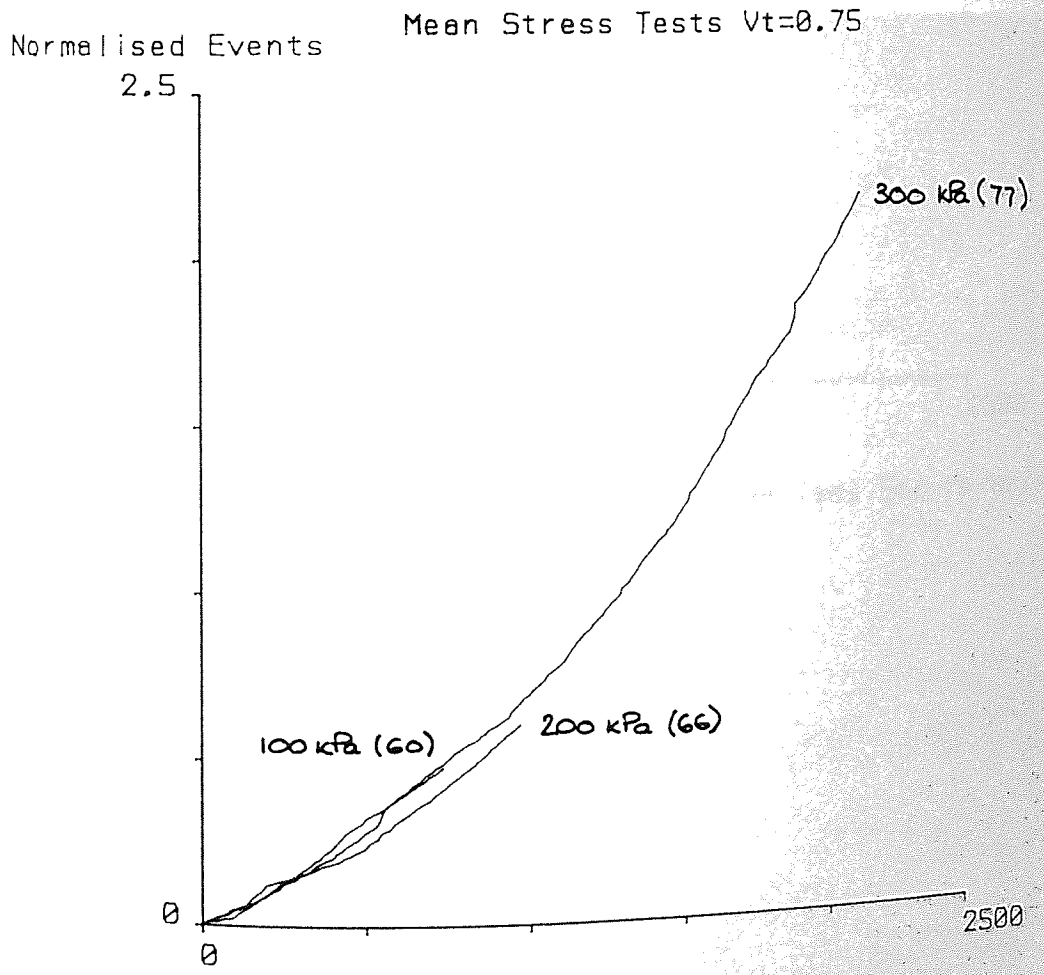
Figure 5.17 Tests 61, 65, and 76: Normalised Events/Work

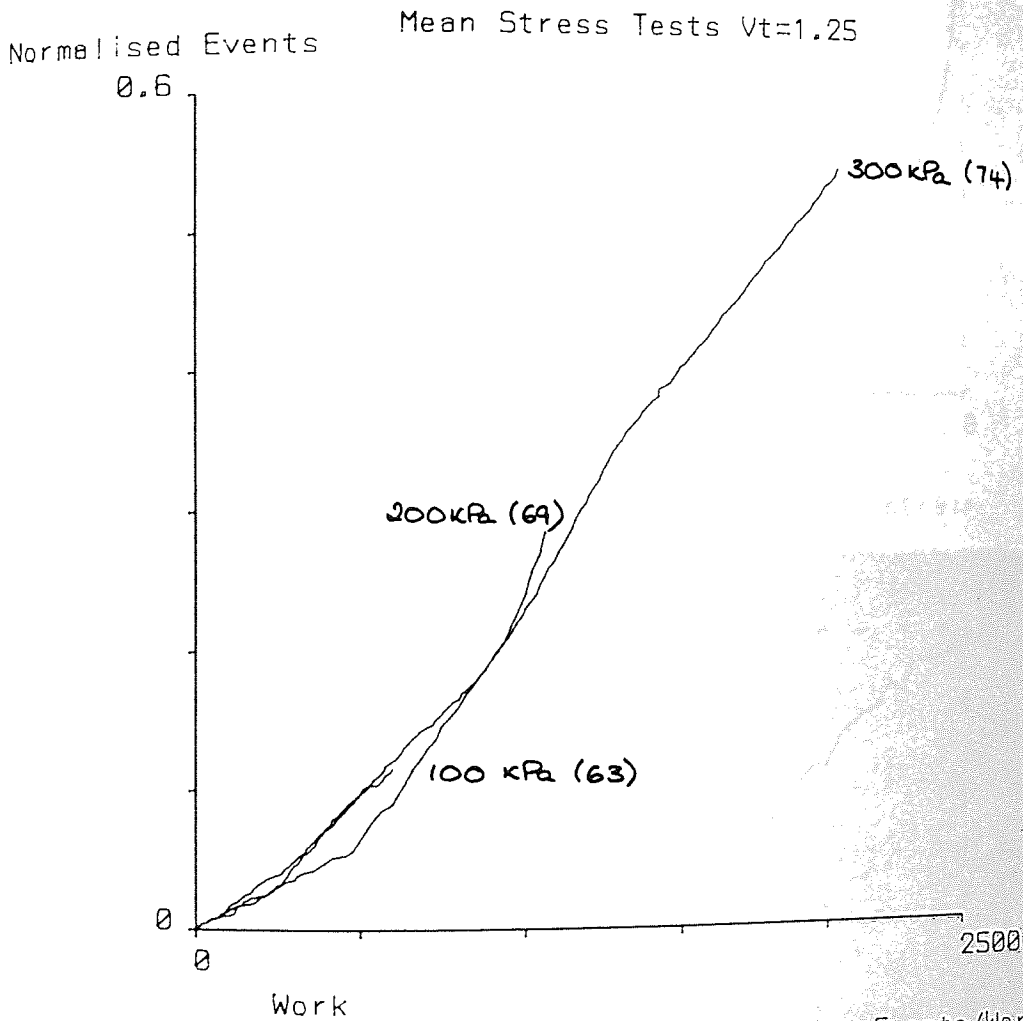Figure 5.18 Tests 60, 66, and 77: Normalised Events/Work

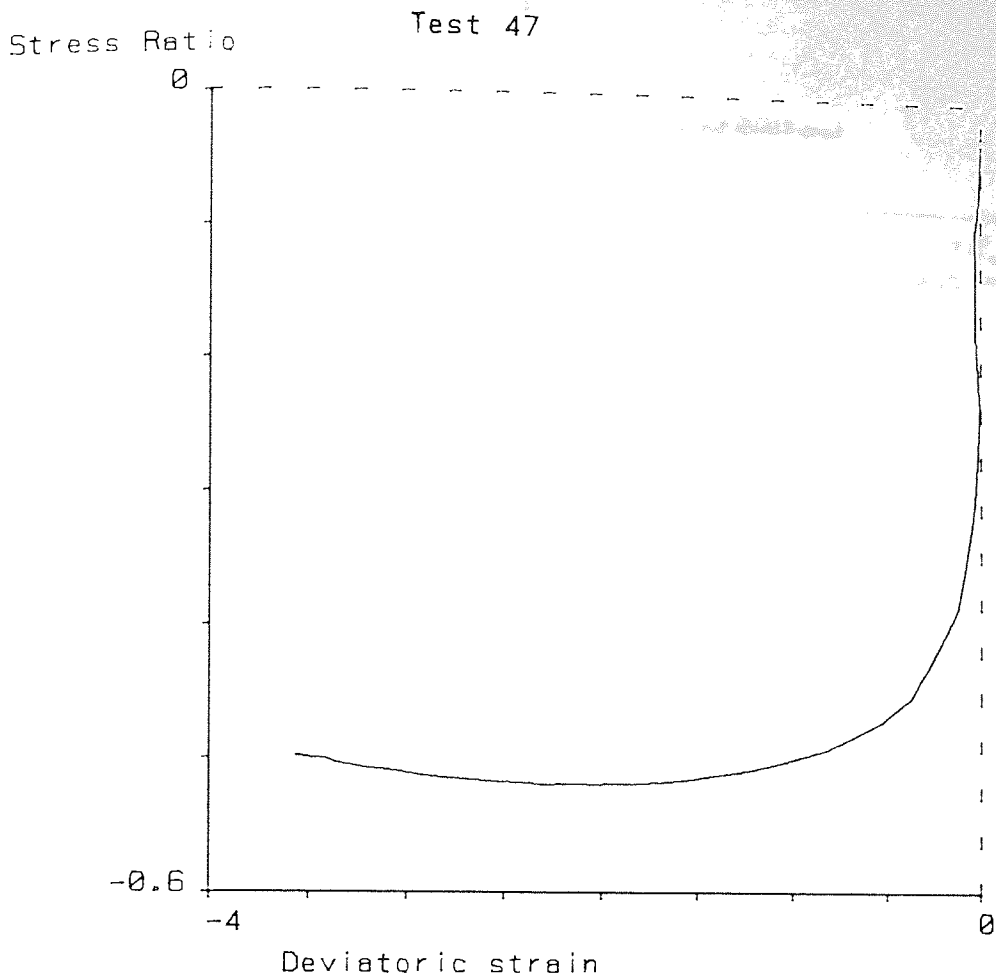Figure 5.19 Tests 63, 69, and 74: Normalised Events/Work

Test 47

Stress Ratio

0

-0.6

-4   0

Deviatoric strain

Figure 5.20 Test 47: Stress Ratio/Deviatoric strain

Test 47

Volumetric strain

0

-1.4

-4   0
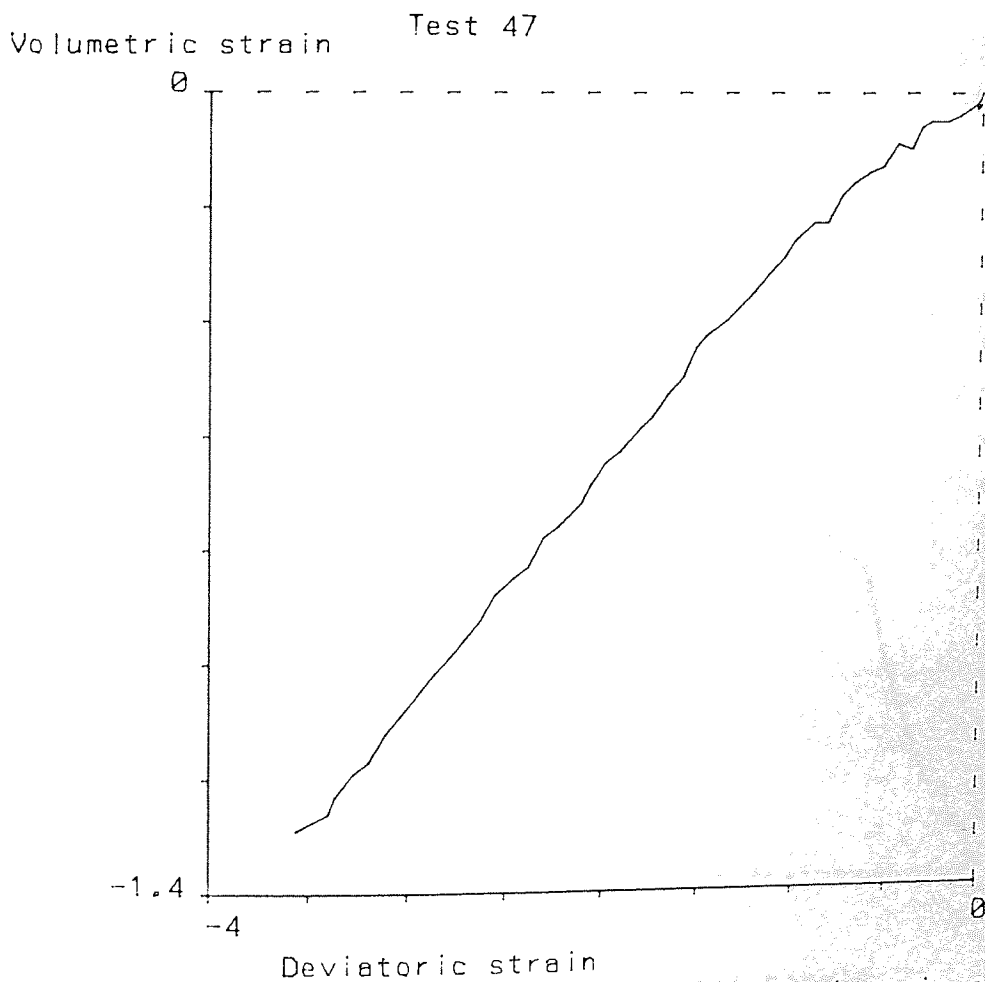
Deviatoric strain

Figure 5.21 Test 47: Volumetric strain/Deviatoric strain

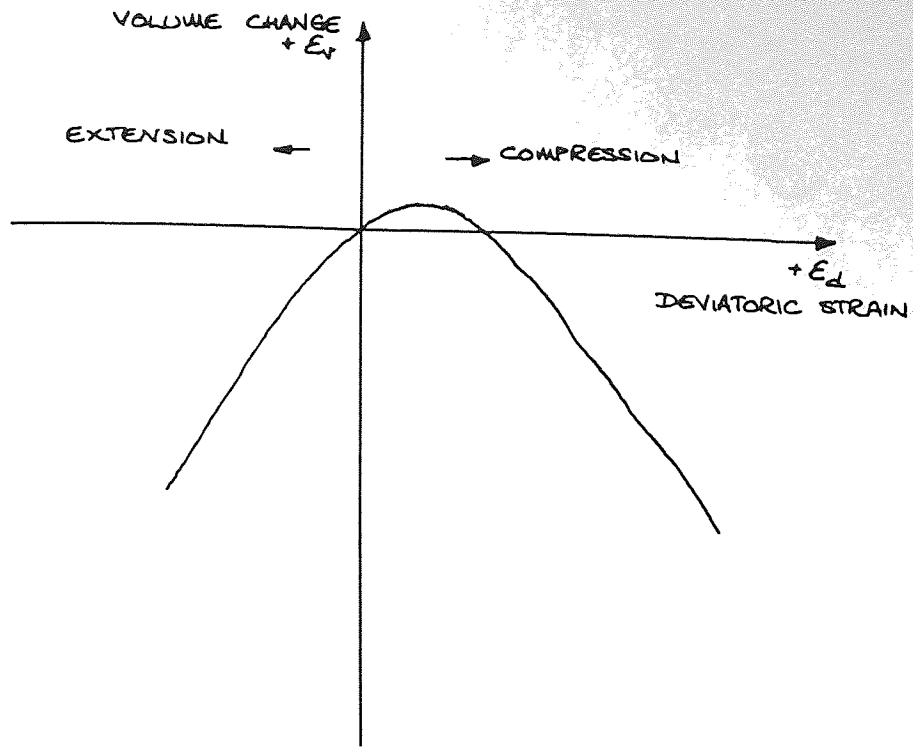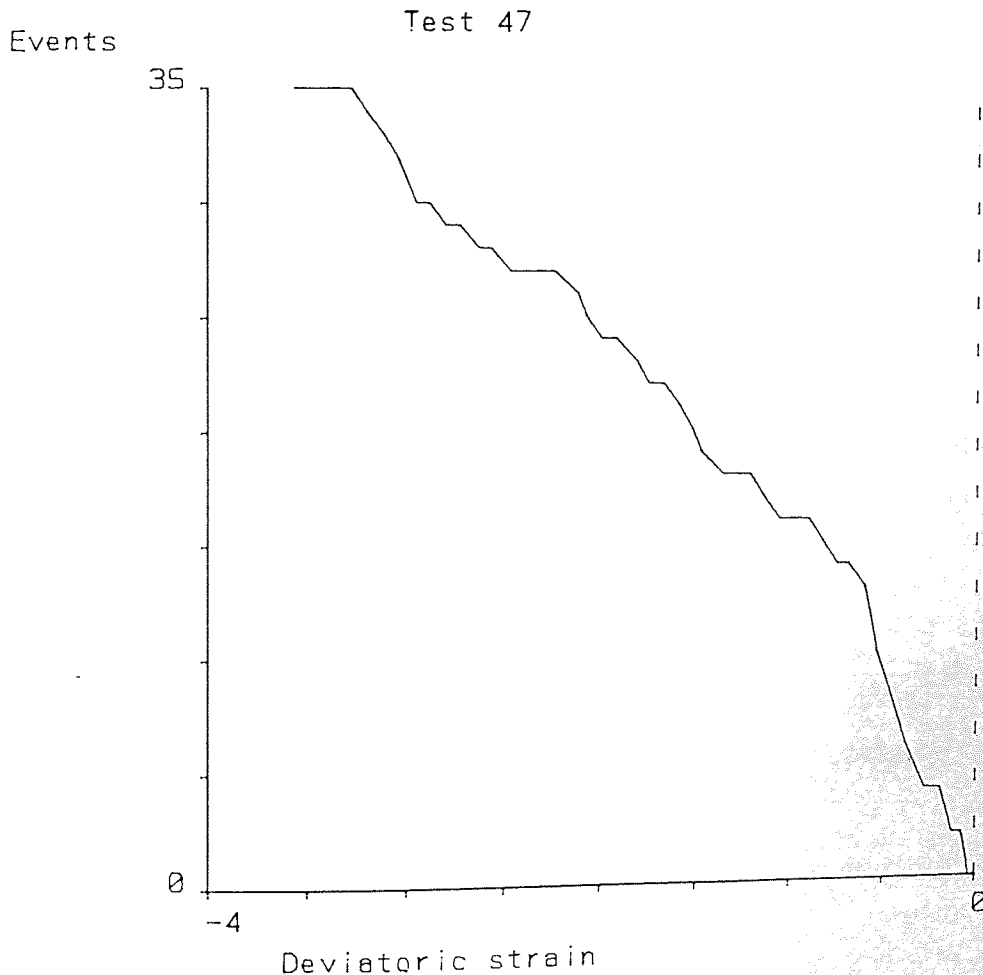Figure 5.22 Schematic diagram of volume change
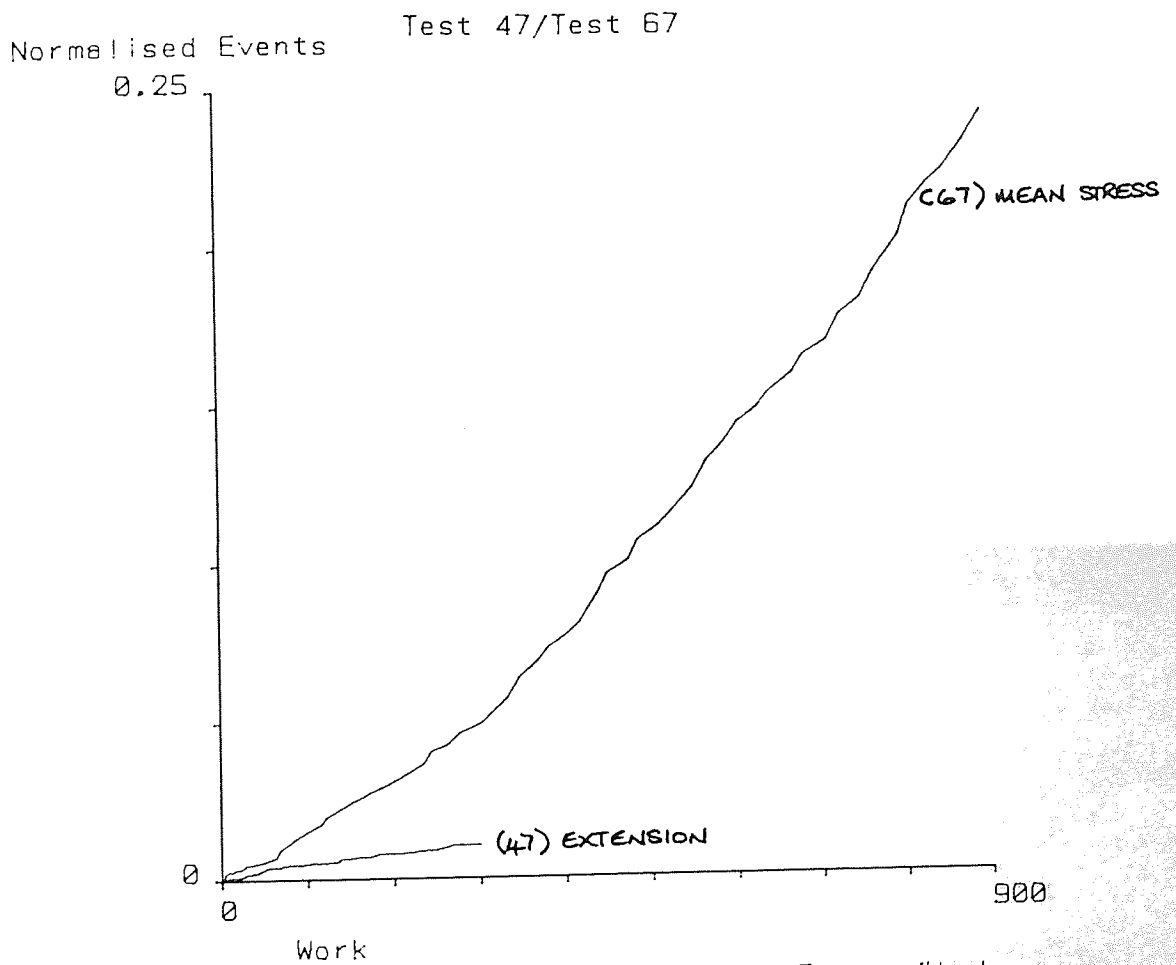

Test 47

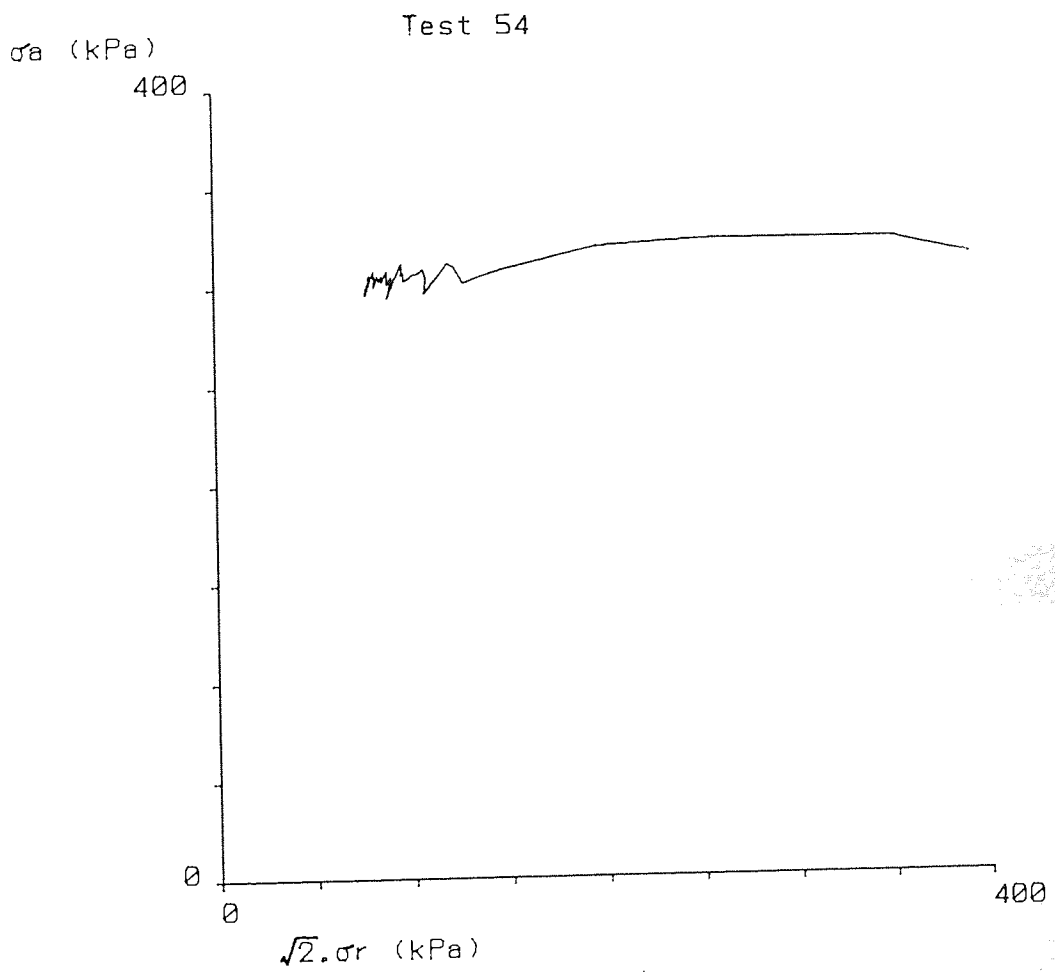Figure 5.23 Test 47: Events/Deviatoric strain

Test 47/Test 67

Normalised Events
0.25

(67) MEAN STRESS

(47) EXTENSION

0

0   900

Work

Figure 5.24 Test 47 and 67: Normalised Events/Work

Figure 5.25 Test 54: Stress path

Test 54

Stress Ratio
0.9

0

0   10
Deviatoric strain
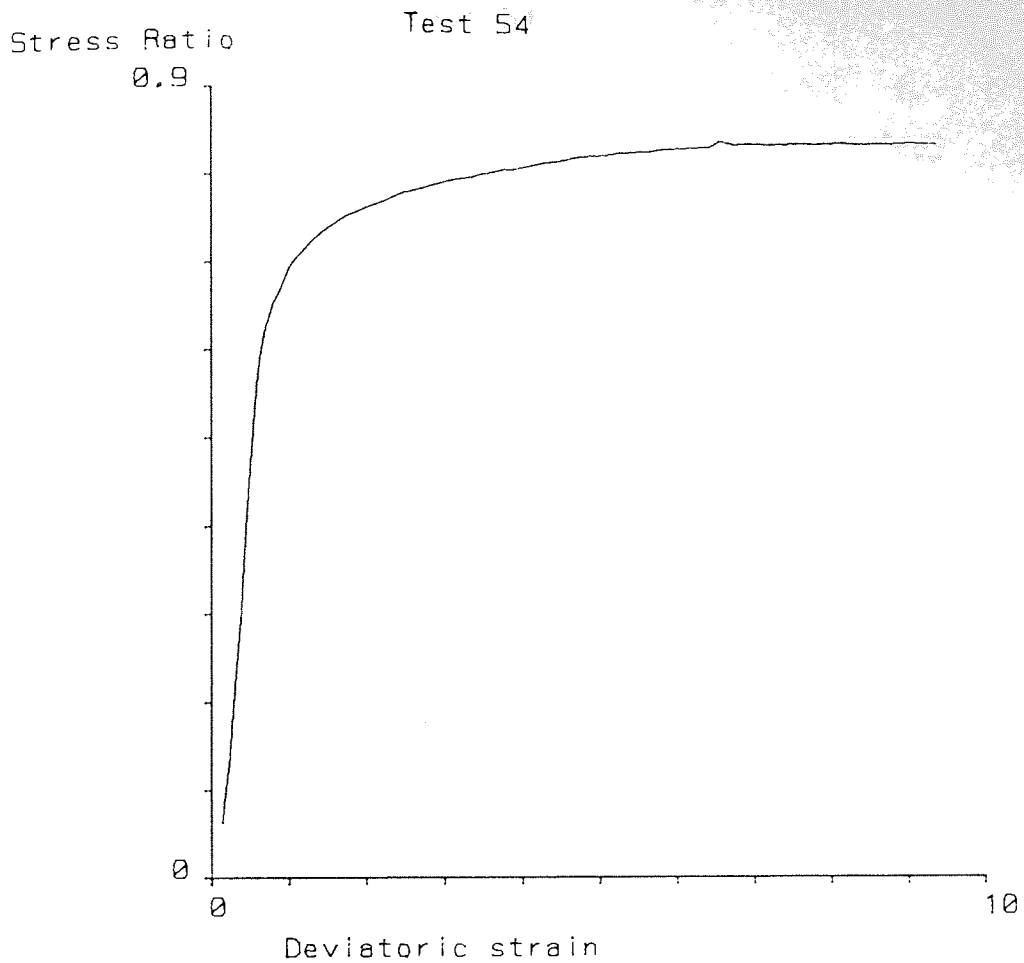
Figure 5.26 Test 54: Stress Ratio/Deviatoric strain

Test 54

Volumetric strain
0.5

0

-2

0   10
Deviatoric strain
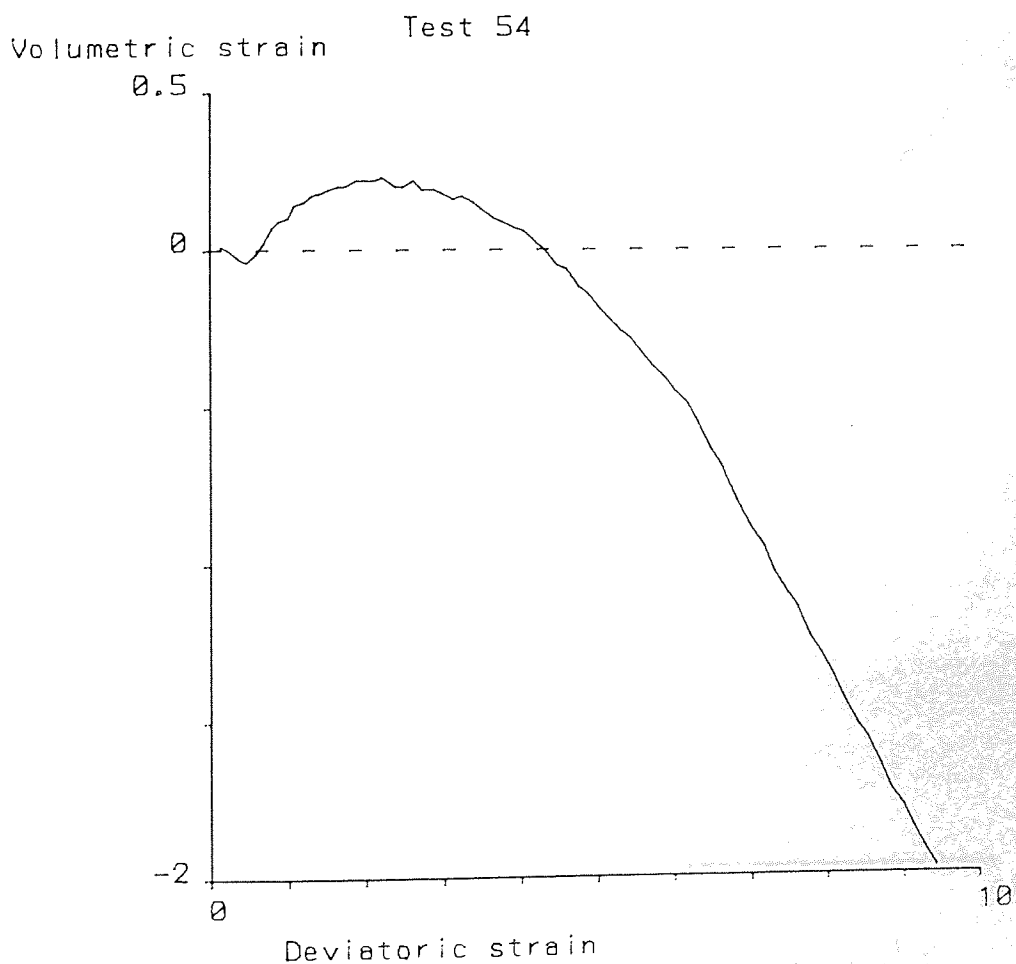
Figure 5.27 Test 54: Volumetric strain/Deviatoric strain

Mean Stress (kPa)

Test 54

Deviatoric stress
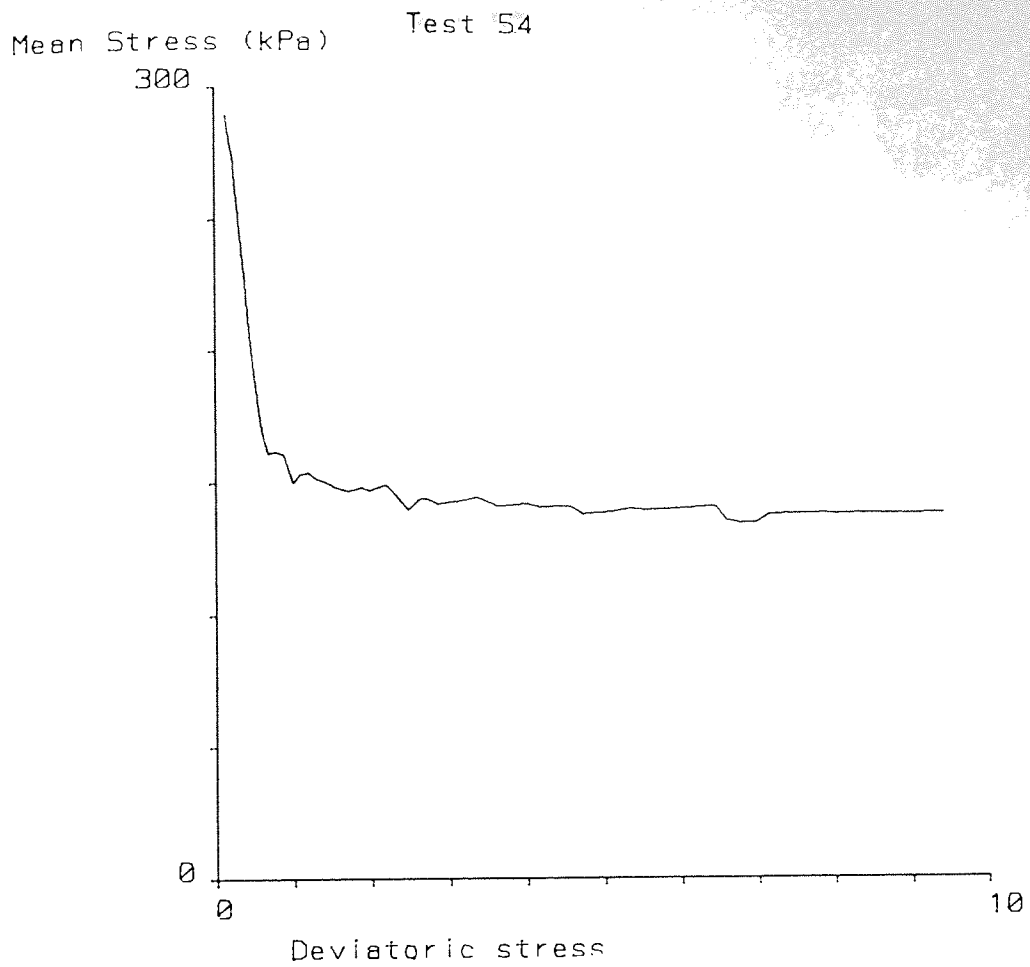
Figure 5.28 Test 54: Mean stress/Deviatoric strain

Test 54

Events
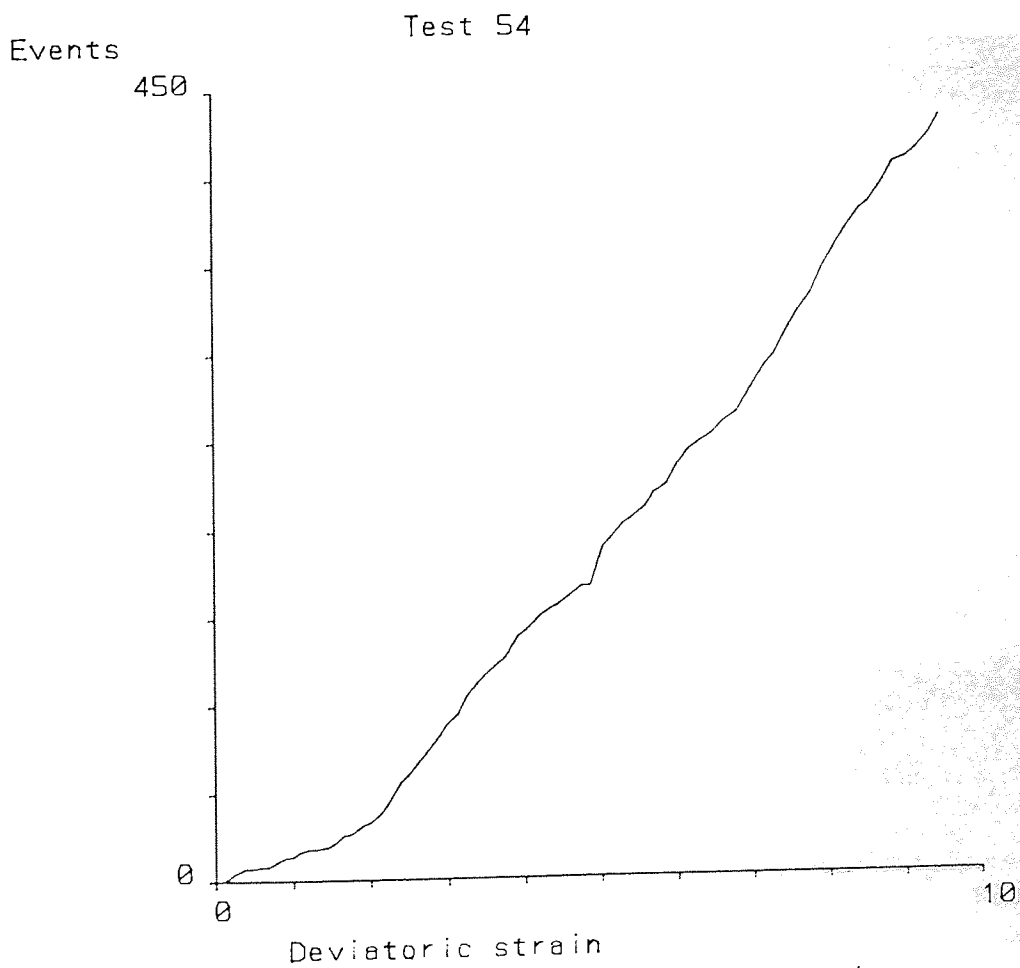
Deviatoric strain

Figure 5.29 Test 54: Events/Deviatoric strain

Test 57

σ'a (kPa)

1600

0

0   1600

$\sqrt{2}.$σ'r (kPa)
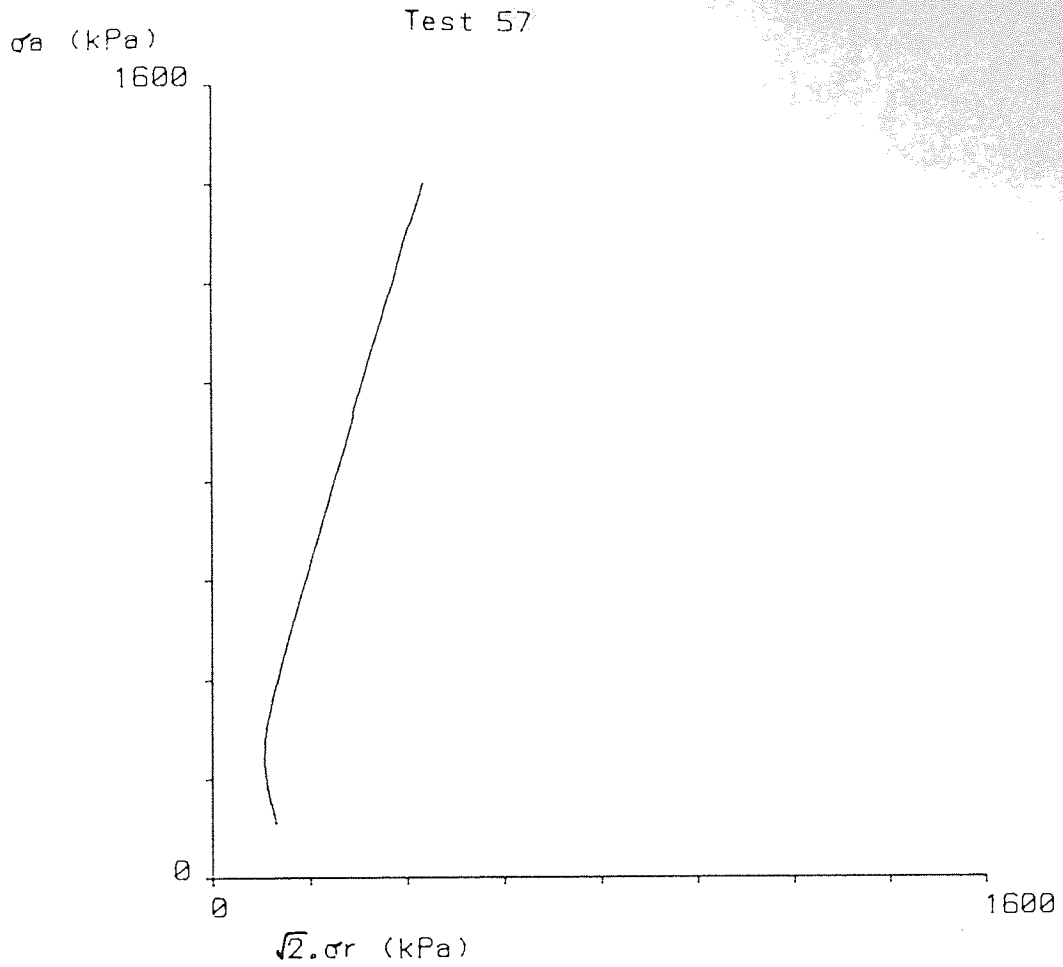
Figure 5.30 Test 57: Stress path

Test 58

σ'a (kPa)

1600

0

0   1600

$\sqrt{2}.$σ'r (kPa)
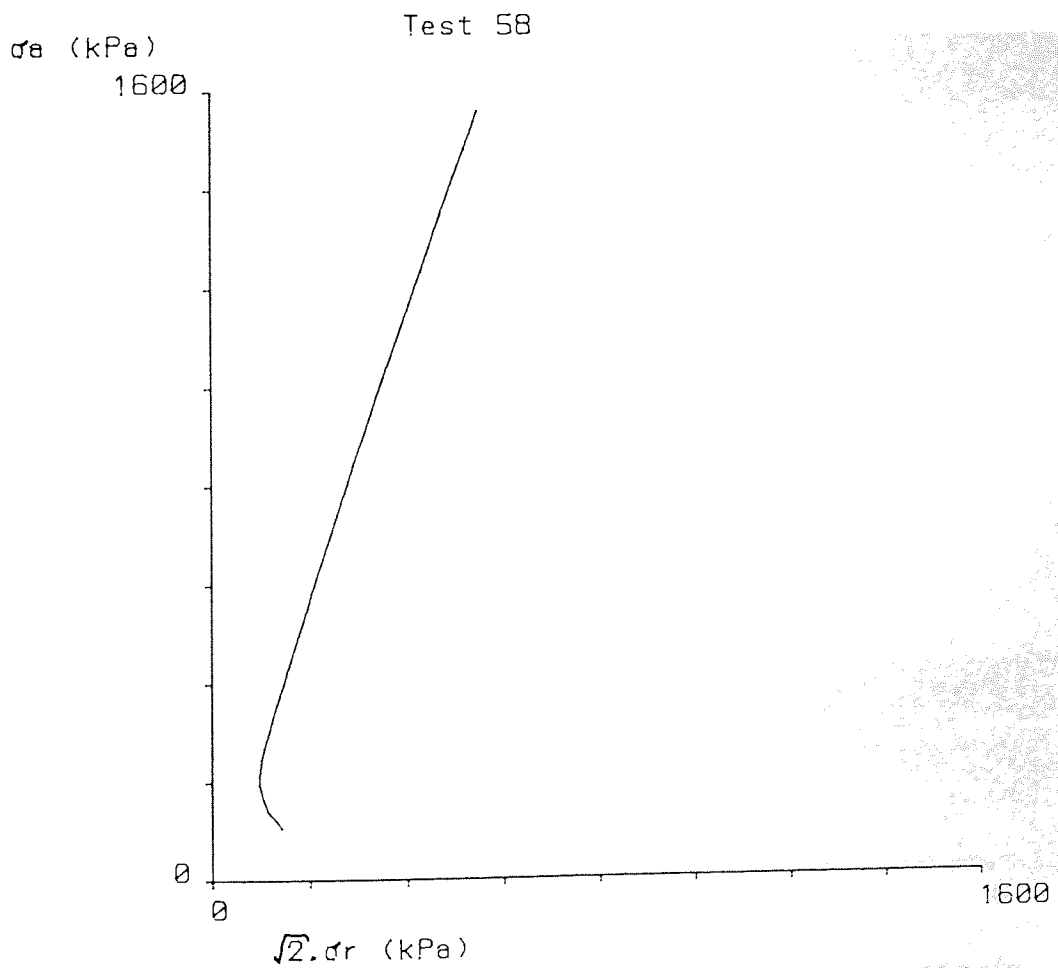
Figure 5.31 Test 58: Stress path

Pore water pressure (kPa) Test 57

350

Deviatoric strain

Figure 5.32 Test 57: Pore pressure/Deviatoric strain

Pore water pressure (kPa) Test 58

350
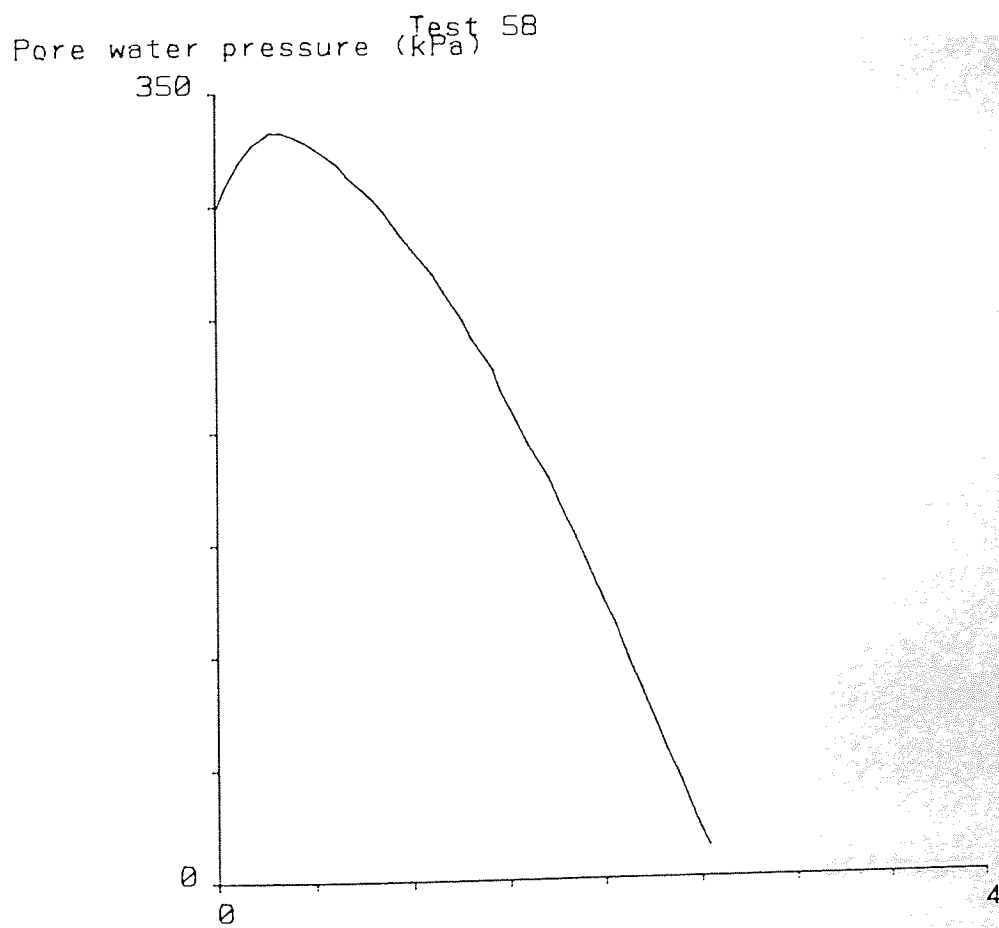
Deviatoric strain

Figure 5.33 Test 58: Pore pressure/Deviatoric strain
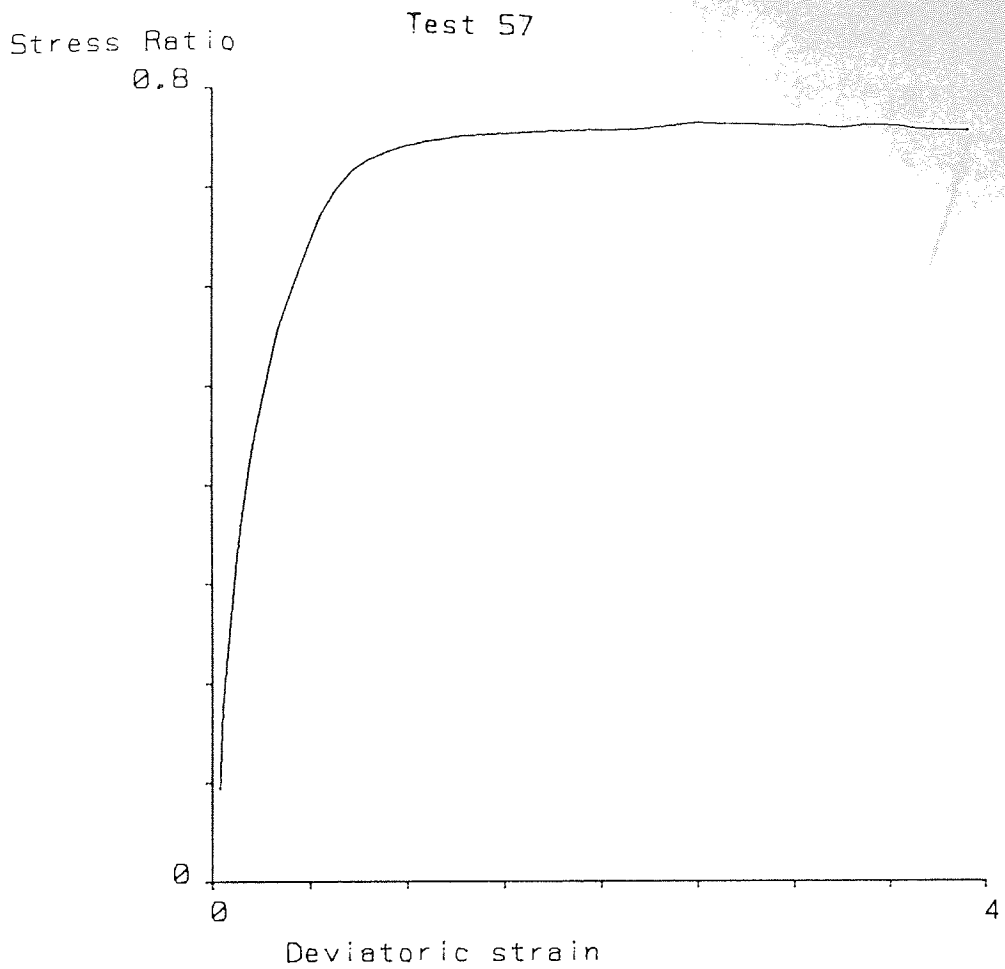
Test 57

Figure 5.34 Test 57: Stress Ratio/Deviatoric strain

Test 58

Figure 5.35 Test 58: Stress Ratio/Deviatoric strain

Figure 5.36 Test 57: Events/Deviatoric strain
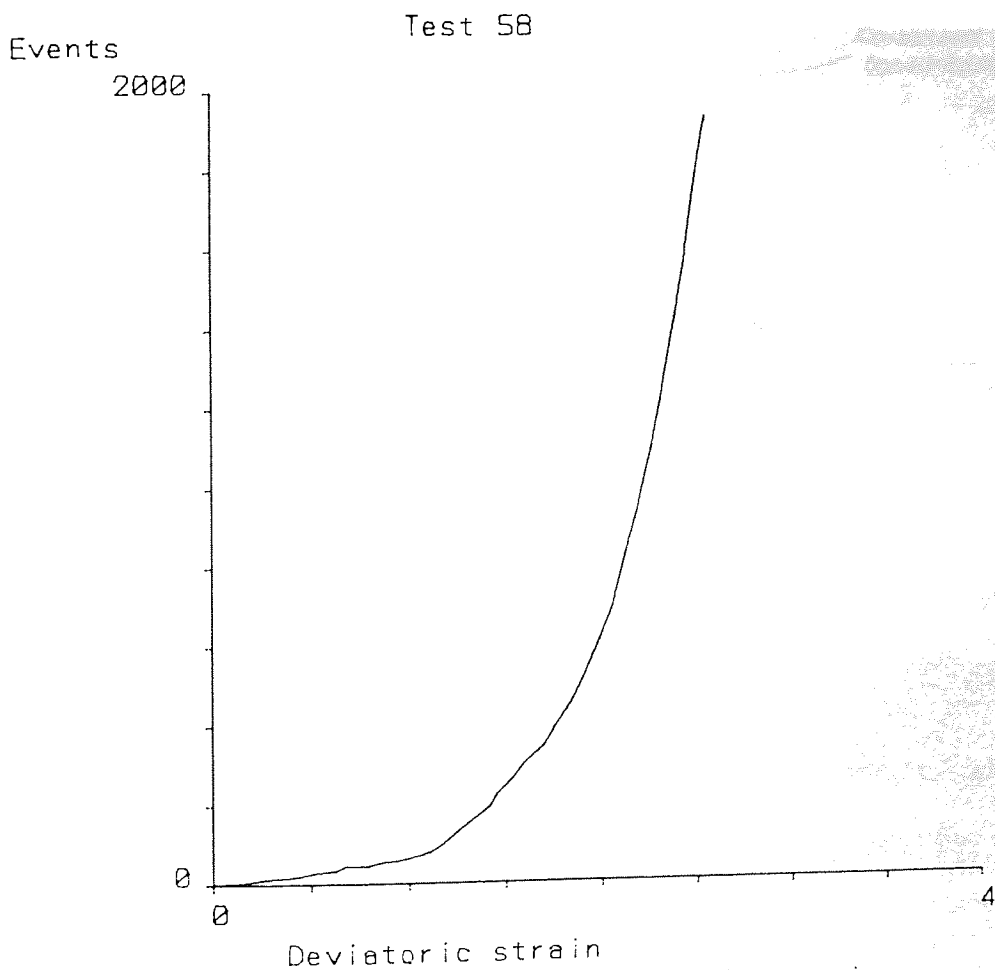
Figure 5.37 Test 58: Events/Deviatoric strain

Normalised Events
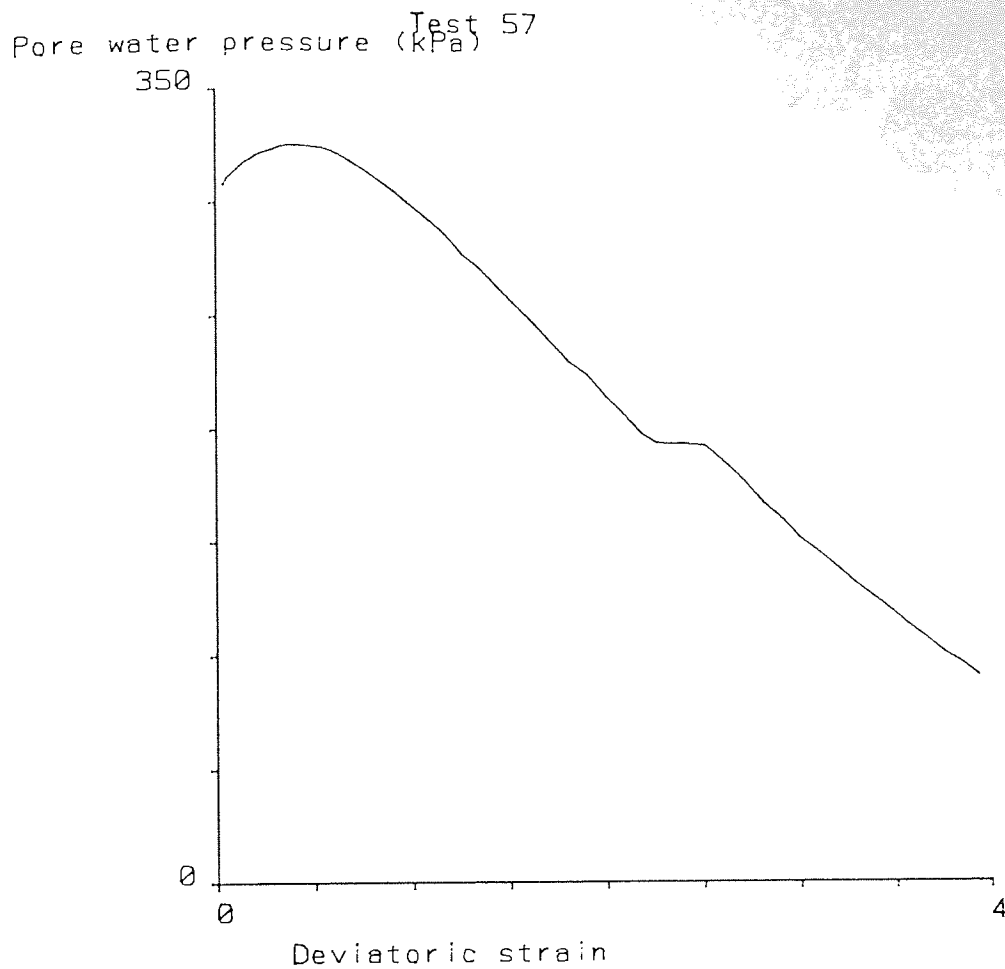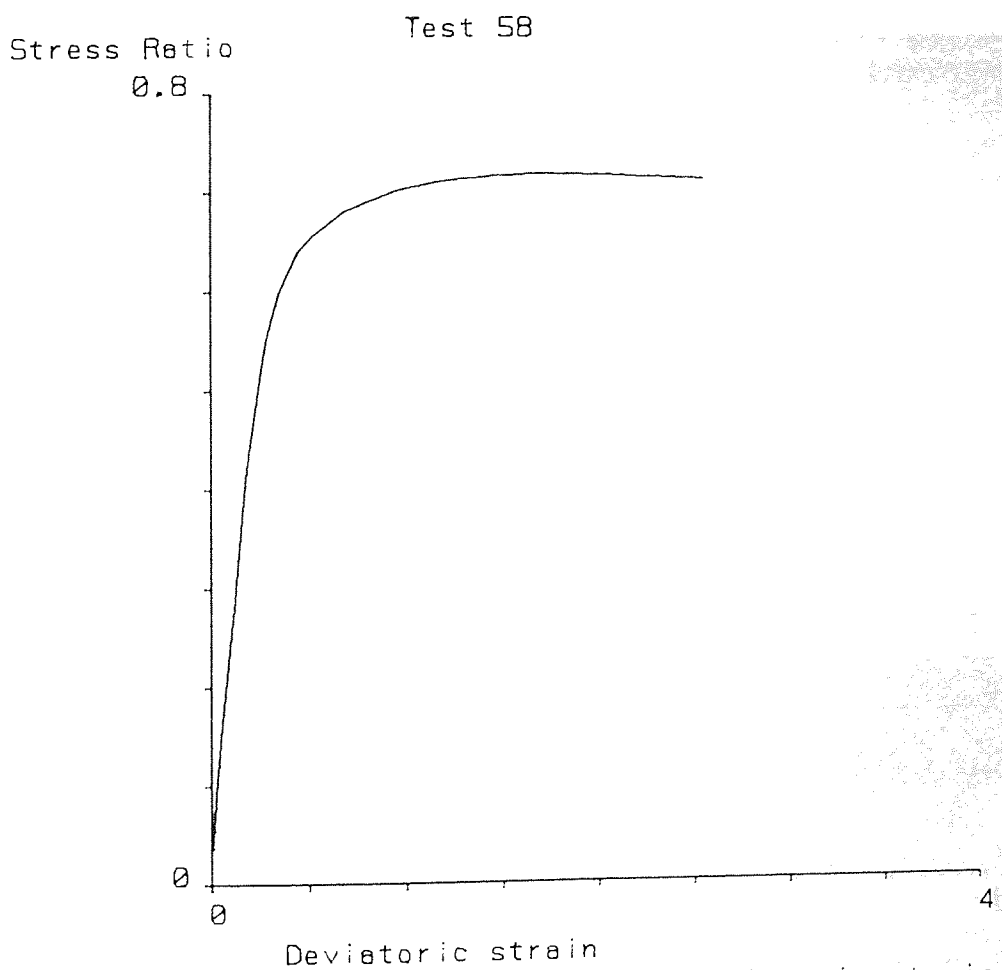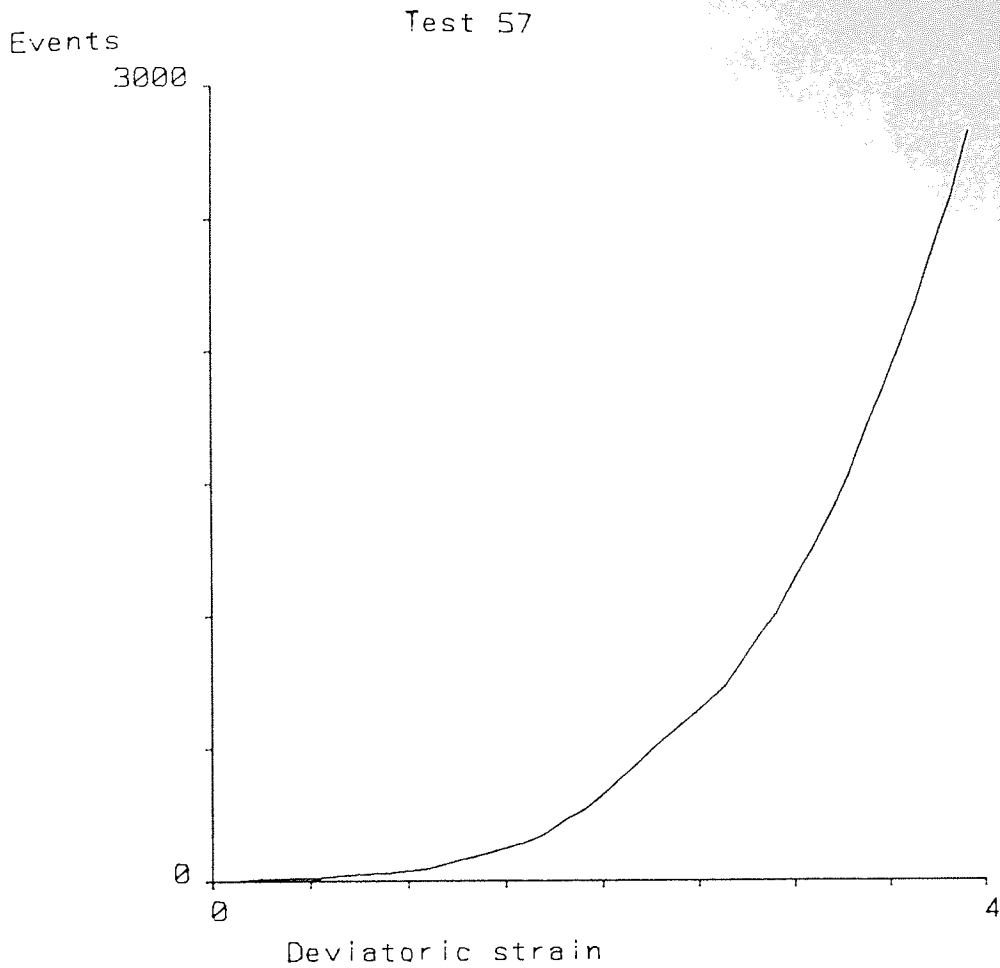0.3
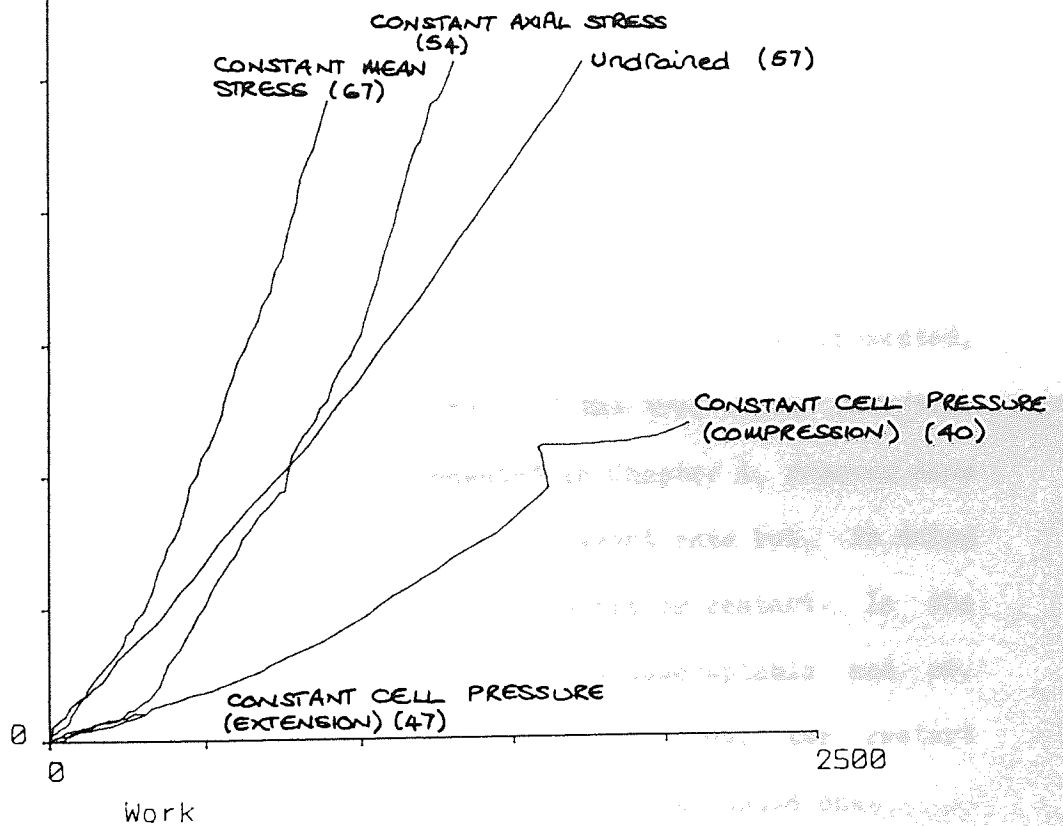
CONSTANT AXIAL STRESS
(54)
CONSTANT MEAN
STRESS (67)
Undrained (57)

CONSTANT CELL PRESSURE
(COMPRESSION) (40)

CONSTANT CELL PRESSURE
(EXTENSION) (47)

0

0   2500

Work

Figure 5.38 Normalised Events/Work

Chapter 6

Yield Point Identification

6.1 Introduction.

So far the tests reported in this thesis have concentrated on the more basic aspects of the Acoustic Emission/soil behaviour. However, one of the aims of the research was to use AE as a means of identifying yield in sand. A short introduction to the concepts of plasticity theory is given in the following section; a full review being beyond the scope of this thesis. One possible aid in identifying yield is the Kaiser effect, mentioned in Chapter 2, which is examined further in this chapter. Yield points are then investigated through two series of tests involving complex stress paths.

In this chapter graphs depicting event rate/time are presented, all those shown are moving averages of the true event rate/time graphs. This method, first presented in Chapter 4, removes some of the variability associated with the event rate but, in doing so, shifts the point at which events start or restart. In the yield point identification this shift is unacceptable and so, although the graphs presented have been averaged, the restart point identified is the actual point, not the adjusted one.

6.2 Concepts of Yield and Plasticity.

When a material is stressed two types of deformation may occur: recoverable (elastic) or irrecoverable (plastic). Theories describing elastic behaviour are well established but theories

for plastic behaviour have only been proposed relatively recently.

The point, in principal stress space, which separates the recoverable strain from the irrecoverable strain is known as the yield point, and the set of all such points describes the yield surface. Inside the yield surface only elastic deformations may occur, and attempts to move outside the yield surface result in plastic deformation. Stress states outside the yield surface cannot exist: the material would not be in equilibrium. One of the requirements of plasticity theory is to describe the shape and the position of this yield surface. Figure 6.1 shows the stress-strain curve and the yield surface (on the deviatoric plane of principal stress space) for a hypothetical material. The material behaves elastically in the region A-B and, when it reaches point B, yields plastically. At point C the material is unloaded to point D and then reloaded, yielding again at point E. The path C-D-E is entirely elastic. Yielding continues after point E as the material is strained further. Viewed on the deviatoric plane the yield surface is represented by a circle, on this plot points B, C, and E are identical. Although the yield function is represented by a circle this is only for the purpose of explanation: the shape of the yield surface is dependent on material properties and could be any continuous function. One limitation on the yield surface shape is that it must be convex, Hill (1950).

For metals, yield is often assumed to be independent of the mean stress, thus in the example given above the yield surface would be represented by a cylinder whose axis coincided with the space

114

diagonal. However, for granular materials such as sand, this is
not the case and yield is dependent on mean stress. In the
example above the yield surface could be represented by a cone
aligned on the space diagonal. The geometric interpretation of
the yield surface is useful as an aid to visualisation, but it is
necessary to represent it mathematically by a yield function such
as:

$$F(\sigma) <= 0 \qquad\qquad\qquad (6.1)$$

where σ represents the stress tensor describing the state of
stress at a point.

When $F(\sigma) = 0$ the material is yielding, and when $F(\sigma) < 0$ the
material is deforming elastically. The yield function, by itself,
is insufficient to describe the material behaviour, as to
define the plastic behaviour of a material completely it is
necessary to define the deformations associated with the state of
stress. In the simple example given above the position and shape
of the yield surface were unaffected by the act of yielding, and
a material behaving in this manner is described as perfectly
plastic. However, the yield surface may change its shape, size,
and position when undergoing yield. If, for example, the yield
surface expands then hardening is said to occur, conversely if it
contracts softening occurs.

A number of different hardening theories have been proposed and
some of the more common are represented in Figure 6.2. Figure
6.2a represents the case of no hardening (perfect plasticity) in
which the yield surface remains fixed in size and position. One
popular theory is shown in Figure 6.2b; the material is loaded as
before and behaves elastically in the region A-B, yielding at

115

point B where the initial yield surface is located. However, at
point B, the act of yielding causes the yield surface to enlarge
uniformly. Loading continues to point C, at which point the
material is unloaded, through point D and yields again at point
E. During the unloading phase the material response is elastic
and plastic deformation does not recommence until point E. This
type of hardening theory is known as isotropic hardening.

An alternative theory is shown in Figure 6.2c, which demonstrates
kinematic hardening. Here, instead of the yield surface expanding
uniformly, the yield surface translates rigidly in the direction
of the applied stress path. Elastic deformation occurs in the
region A-B, yielding at point B. Plastic deformation and
hardening continue as the material is loaded to point C.
Unloading occurs at point C, passing through D and yielding again
at point E. The distance A-B is equal to half the yield locus
diameter (on this deviatoric plane) and the distance C-E is equal
to the (unchanged) diameter of the yield locus.

Another form of hardening theory is shown in Figure 6.2d. Here,
the yield surface distorts when yielding, deforming from a circle
into an ellipse: this is anisotropic hardening. Combinations of
these basic hardening theories are possible, merging in such a
way that the yield surface may translate, distort, and expand
during yielding. The yield function is therefore modified by the
hardening theory and the yield function becomes:

$$F(\sigma, h) <= 0 \qquad\qquad (6.2)$$

where h represents the hardening function. From the descriptions
of the theories given above, it is clear that the hardening
function derives not only from the current stress state but also

from the strain history. The hardening function is commonly represented by a single parameter, although this is a simplification of the true state of affairs.

The yield function and the hardening function do not, by themselves, provide a method of calculating the plastic strain increments. When a material yields it may be considered to flow and, if the flow is considered to be irrotational, it is possible to find a potential function whose partial derivatives give the proportions of strain occurring at that state (rather, the strain velocities). This potential function is known as the plastic potential. As yield occurs as a result of stress, the plastic potential must be a function of the state of stress. Geometrically the plastic potential surface may be interpreted as the surface orthogonal to the strain increment vector at each associated stress point in principal stress space. However, there is a hidden assumption here, which is that the directions of the principal strain increment and the principal stress coincide. This assumption is referred to as coaxiality, without it the geometric definition of the plastic potential is not possible, and the mathematics necessary to describe the interaction of the yield surface and the plastic potential are considerably more complex.

Hence to describe plastic deformation it is necessary to specify a flow rule, which relates the strain rates (or increments) to the stress state. If the plastic potential and the yield surface coincide the flow rule is termed associated, and the normality condition upheld. If the plastic potential and the yield surface are not coincident the flow rule is termed non-associated. Many

plasticity theories assume, for the sake of simplicity, that the yield function is also the plastic potential.

A constitutive law of plasticity is thus described by the yield function, the hardening law, and the flow rule. However, unlike an elastic constitutive law, it does not lead to a unique stress -strain relationship because of its dependence on the deformation history.

The testing of real materials, like sand, provides information which, when combined with an appropriate plasticity theory, allows the material's behaviour to be modelled. The observed behaviour may be used to modify theoretical models as well as to verify them. However, in order to define the plastic deformations accurately, the elastic strains have to be found. The evaluation of elastic strains in sand is acknowledged to be difficult, see for example Holubec (1968), as the elastic properties of the sand depend, partly, on the deformation history. A simple relationship between the applied stresses and the elastic strains is often assumed, see for example Lade and Boonyachut (1982), or alternatively the elastic strains are neglected altogether.

The identification of yield from stress-strain data is not trivial. One conventional method of identifying yield is shown schematically in Figure 6.3, the point P represents the limit of proportionality and the line R - S represents fully plastic deformation. The yield point, Y, is taken to be where 0 - P (produced) intersects with R - S (produced). This technique was

used by Tatsuoka and Ishihara (1974) to identify a number of yield points from the results of cyclic, drained triaxial tests and hence establish the yield loci. Another conventional method of identifying yield is to locate the point of maximum curvature on the stress/strain curve and use a method similar to that adopted when finding the preconsolidation stress (the Casagrande construction). It can be seen that neither of these methods is ideal, and that both may be ambiguous and subjective.

6.3 Preliminary Tests.

The Kaiser effect has been defined as "the absence of detectable acoustic emission until previously applied stress levels are exceeded" by the American Society for Testing Materials (1978). This definition suggests that the effect may be useful in identifying yield points, as Acoustic Emission appears to relate to irrecoverable deformation and not recoverable deformation. The simplest way to try and demonstrate this in a triaxial test is to perform an unload-reload cycle at some point during a constant cell pressure test.

Figures 6.4 and 6.5 show the stress ratio/deviatoric strain and the volumetric strain/deviatoric strain curves for Test 32, which was performed at constant cell pressure. The stress ratio curve shows that the initial unload/reload portions of the curve are steeper than that of the initial loading curve, indicating a change in the stiffness of the sand. The volumetric strain curve shows that, during early unloading, the path followed is almost the reverse of the initial one but diverges as the stress ratio

119

approaches zero. Reloading causes a small amount of contraction prior to expansion which quickly reaches the rate achieved before unloading. The events/deviatoric strain curve is shown in Figure 6.6; during initial loading the events increase steadily but, on unloading, events cease. During the reloading period few events occur, except for one 'blip'. These points are more evident if the stress ratio/events curve is studied (shown in Figure 6.7). The unload point is clearly visible, and it is only during the reload period that events are recorded again. A cursory inspection of this graph might suggest that sand does exhibit the Kaiser effect, events restarting when the former stress ratio is reached. However, a more detailed inspection shows that events restart before the former stress ratio is reached. The events restart point may be found by studying the event rate/time curve (Figure 6.8). The figure shows that there is one burst of events in an otherwise quiet unload/reload period.

Similar behaviour may be seen in the results of Test 36, which are shown in Figures 6.9-6.13. The same general features may be observed in Test 36 as were found for Test 32. The stress ratio/events curve, Figure 6.12, demonstrates the events cease on unloading as was found for Test 32. The various stress ratios and strains may be determined, as for Test 32, and these are tabulated with the results obtained for Test 46 (given in Chapter 5) in Table 6.1. Test 40 is not included in this table because the sample was not sufficiently strained, when reloaded, to obtain all the required values.

TEST	32	36	46
Initial R max.	0.80	0.81	0.85
Initial e max.	7.14	6.10	5.36
Reload R, events restart	0.78	0.78	0.83
Reload e, events restart	7.10	5.92	5.35
Reload R, former event rate	0.80	0.81	0.85
Reload e, former R max.	7.33	6.36	5.67
felicity ratio, F_R	0.98	0.96	0.98

Table 6.1: Stresses, strains, and felicity ratio

From Table 6.1 it can be seen that sand does not conform exactly to the Kaiser effect as defined above. However, it is interesting to note that when the previous maximum stress ratio is reached the event rates are at their former level. In fact, the non conformance of various materials (e.g. fibreglass, rock) to the Kaiser effect has been noted by others, e.g. Wadin (1982) and this specific deviation is known as the felicity effect. Associated with the felicity effect is the felicity ratio, F_R, which is defined as the percentage of the previous maximum load at which a material starts emitting when reloaded. The felicity ratios for Tests 32, 36, and 46 are given in Table 6.1. Note that 'maximum previous load' has been interpreted as the maximum previous stress ratio, rather than the applied load. From this table, it may be seen that the felicity ratio in sand is 0.96 - 0.98. This value is high in comparison with values for some rocks (0.85) and fibreglass (0.85) where the Kaiser effect is known not to be true. Also from the table it can be seen that, generally, events restart at the maximum previous strain. Admittedly the tests considered are relatively straightforward; the unload-reload paths did not involve any complex or difficult paths, and all the tests were conducted at a constant cell pressure.

Figure 6.14 shows the effective stress path followed by Test 109, an undrained constant cell pressure test. The sample was loaded to a deviatoric strain of about 2.0% and then unloaded. Unloading continued to almost zero deviator stress and then the sample was reloaded. The effective stress ratio/deviatoric strain curve is shown in Figure 6.15. Again, as was the case in the drained tests, the unload/reload curves are steeper than the initial loading curve. The pore water pressure/deviatoric strain curve is shown in Figure 6.16 for completeness. The events/deviatoric strain graph is shown in Figure 6.17, and it is clear that events did not cease upon unloading. Also obvious is that the event rate is much higher than in drained tests; this was also shown by the undrained tests reported in Chapter 5. The AE behaviour during the unload/reload period is more clearly shown by studying the event rate/time graph, Figure 6.18. Here the unload point is still marked by a sharp decrease in the event rate, but throughout the unload/reload period there is some AE activity. The level of the activity is below that measured prior to unloading, and remains below it until the stress ratio and deviatoric strain are at their pre-unload levels (approximately). As events never cease in this test it is impossible to give a valid event restart point.

It is possible, and indeed probable, that AE activity occurs throughout the unload/reload period of a test, be it drained or undrained. However, in the undrained case the level of AE activity is significantly higher than that of the drained case because of the mean effective stress effect, which distorts the results.

The results given above show good agreement with the definition
of the Kaiser effect and therefore suggests that AE can be put to
good use in identifying yield points. No work on this has been
reported in the literature directly, but Tanimoto et al (1981a)
used a Menard pressuremeter adapted for AE to determine the in-
situ stresses in sandy soils. Koerner et al (1984a, 1984b) used
this principle to determine the pre-consolidation pressure in
both sand and clay materials very successfully.

6.4 Yield Point Identification.

Section 6.2 introduced some elements of plasticity theory but
made no specific reference to the shape of the yield locus. Early
plasticity theories, such as that of von Mises, described the
yield surface as a cone or cylinder with no limitation on the
length of the cylinder. While this was satisfactory for metals,
it is not appropriate when considering materials like sand as
sand yields under increasing isotropic stress. One yield surface
which has been suggested by Lade (1982) is shown in Figure 6.19.
Here yield is represented by a capped cone in stress space, and
consists of two distinct surfaces, the cone being known as the
deviatoric yield surface, and the end cap as the isotropic yield
surface.

A series of tests was devised in order to investigate the two
possible distinct yield surfaces. These are now described in the
following subsections. Since all the tests are axisymmetric the
stress state may be depicted in 2-D stress space $(\sigma_a, \sqrt{2}\sigma_r)$ and in
this context the yield surface is more correctly referred to as
the yield locus.

123

6.4.1 Deviatoric Yield Point Identification.

Tests were carried out following different stress paths as shown diagrammatically in Figure 6.20. It may be seen that the tests fall into two groups (Tests 94, 95, 96, and 97) and (Tests 98, 99, and 100). In both groups of tests it was hoped to use the Kaiser effect to identify the yield point when the sample was reloaded since, on the basis of those tests reported in Section 6.3, a change in the event rate should be observable when the sample yields again.

The volumetric strain and stress ratio curves for Test 97 are shown in Figures 6.21 and 6.22 respectively. The volume change curve shows that when the cell pressure is reduced from 200kPa to 100kPa a small amount of volumetric expansion occurs. In Section 6.3 it was seen that the stress ratio after reloading was approximately the same as that before unloading. However, in Figure 6.21, the stress ratio following reload is significantly higher. This, in itself, implies that the yield locus is non linear. The events/deviatoric strain curve is shown in Figure 6.23; it is clear that few events are recorded during the unload period, and that when reloading the event rate never reaches its former level. However, this is expected, as Chapter 5 demonstrated that a change in cell pressure results in a change in the event rate: this serves to confirm that finding. The mean stress effect will obviously influence all the results reported in this section but does not detract from them. The stress ratio/events curve is shown in Figure 6.24, and the same abrupt change in the reload stress ratio curve is apparent as was found for simple unload/reload tests.

124

The event rate/time curve is shown in Figure 6.25 and there are several points of interest arising from this. Upon unloading the event rate drops to one, not zero, but this is a feature of the moving average method: the actual event rate/time curve has values oscillating between zero and two. There is a clear 'events restart' point and, perhaps more significantly, a sharp change in gradient a short time after this. Unlike the tests reported in Section 6.3 the restart point does not correspond to the maximum previous strain. However, it is noted that this sample has been subjected to a different loading history. The restart point is marked R on the stress ratio curve figures, and the change of gradient is marked as K. The yield point, as determined from the method described at the end of Section 6.2, is marked as Y on the same figures, and it may be seen that the values of Y and K are approximately the same.

Test 94 followed a similar stress path to that of Test 97 except that the initial loading was conducted with a horizontal stress of 300kPa, reduced to 100kPa on reloading. Figures 6.26-6.30 show the graphs for this test. The stress ratio and volume change curves show the same features as those of Test 97. The events/deviatoric strain curve also shows the effect of mean stress on event rate as in Test 97 with the effect being even more marked. The event rate/time graph shows this difference even more clearly. A change in gradient is still evident during reloading, but slightly distorted by the large event rate in the initial portion of the test. The event restart, change of gradient, and yield points are marked R, K, and Y as before, on the appropriate figures. Unlike other tests reported previously

it can be seen from Figure 6.26 that the events restart at a stress ratio higher than that attained during initial loading. Comparing the two event rate figures of Tests 97 and 94, it may be seen that towards the end of the tests the rates are approximately the same, although the event rate for Test 97 post-peak is more erratic. This further supports the findings given in Chapter 5 regarding mean stress and work effects, and since the two tests were subjected to different loading histories, provides useful confirmation of the repeatability of the AE method.

Tests 96 and 95 are the reverse stress paths to those of Tests 97 and 94 respectively. In both cases the initial loading is at a horizontal stress of 100kPa, with the reloading being at 200kPa and 300kPa. The stress ratio and volume change curves for Test 96 are shown in Figures 6.31 and 6.32. The stress ratio curve shows that, during the reloading period, the stress ratio is less than that of the initial loading. This contrasts well with the results for Test 97. The volume change curve shows that there is a significant volumetric contraction when the cell pressure is adjusted. The events/deviatoric strain graph, Figure 6.33, reflects the difference in the event rates at the two cell pressures. The large number of events recorded in this test, compresses the information presented in the stress ratio/events graph, Figure 6.34, which also shows that some events were recorded during the unload period. The event rate/time graph, Figure 6.35, shows the events recorded in the unload period and that in contrast to Tests 97 and 94 reloading produced higher event rates. This once more verifies the effect of mean stress on the event rate. There is a clear event restart point followed by a change in gradient. These two points are marked, as before, by

R and K on the stress ratio graphs together with the point Y. Examination of the event rate data shows that during the increase in cell pressure some events were recorded.

The results for Test 95 are given in Figures 6.36-6.40. The stress ratio curve showing that the reloaded stress ratio is well below that of the initial loading. The disparity in the event rates at the two cell pressures shows up clearly in the events/deviatoric strain graph. As before, the event rate/time curve shows an abrupt change of slope some time after the events restart. Slightly more noticeable in this figure are the events that occurred whilst adjusting the cell pressure. The restart and change of gradient points are identified as R and K in the usual way. One interesting point to emerge from both this, and Test 96, is that, on the stress ratio/events graphs, the reloaded stress ratio curve has a smaller rate of change of gradient after the 'elastic' part than Tests 97 and 94, i.e. is less sharp.

In this group of tests it is noticeable that, in general, emissions do not cease completely when the sample is unloaded. This is in contrast to those tests reported in Section 6.3, excepting the undrained test. One possible explanation for this is that in the drained constant cell pressure tests the strain rate was only 1%/hour whereas in the deviatoric yield group and the undrained test, the strain rate was 3%/hour. Chapter 4 demonstrated that the event rate was affected by the strain rate and, even in unloading, the more rapid reduction in stress may cause events to occur.

Tests 100, 98, and 99 form the second group of the deviatoric test series. The aim of Test 100 was to identify the same yield surface by loading at constant cell pressure, unload and then approach the same point in stress space at constant mean stress. The stress path actually followed is shown in Figure 6.41; the mean stress fluctuations are due to the limitations of the testing technique used (Section 3.4). The stress ratio/deviatoric strain graph is shown in Figure 6.42, and it may be seen that when the sample is reloaded the stress ratio curve almost passes through the pre-unload point. The volumetric strain/deviatoric strain graph is shown in Figure 6.43; some contraction occurred when the cell pressure was adjusted to the required initial mean stress value. The events/deviatoric strain graph, Figure 6.44, shows that events occur during the unloading period, with a burst of events near the isotropic stress. The event rates during the two phases of the test are approximately the same; this is to be expected since the mean stress levels are approximately the same. The stress ratio/events graph, Figure 6.45, shows that the reload section to be sharper than the initial loading section. The event rate/time graph, Figure 6.46, is similar to those tests reported in Section 6.3 when studying the Kaiser effect. However, it may be seen that the event rate develops slowly in comparison with that of initial loading. This is because the mean stress is not changing significantly. In this test the moving average technique used in presenting the event rate hides the kink which occurs after reloading. Therefore, the actual event rate curve is given in Figure 6.47, and the change of gradient point identified on it. The change in gradient of the event rate is less abrupt than that found in Tests 94 - 97, but this is a mean stress effect.

128

The points R, K, and Y are marked on the stress path figure as well as the stress ratio figures.

Tests 98 and 99 represent a slightly different approach to finding the yield surface, in which the initial loading is at constant cell pressure, the sample is then unloaded, and reloaded at constant mean stress. Test 98 was conducted with an initial mean stress of 100kPa, and Test 99 at a mean stress of 200kPa. The stress path followed for Test 98 is shown in Figure 6.48 and mean stress deviations, as before, due to testing technique. The stress ratio/deviatoric strain graph, Figure 6.49, shows that on reloading the curve is sharper than on initial loading and also that the stress ratio during the mean stress part of the test is considerably greater than that during constant cell pressure. The volumetric strain/deviatoric strain curve, Figure 6.50, is provided for completeness. The events/deviatoric strain graph, Figure 6.51, shows that events cease on unloading but recommence almost at once on reloading. The stress level effect is once more apparent from the gradient of the curve. The events occurring during reload result in the stress ratio/events curve, Figure 6.52, not being as vertical initially as in other tests. Nevertheless this is followed by an abrupt change of slope that clearly suggests yield. The event rate/time curve, Figure 6.53, shows that the event rate is very low which makes it very difficult to identify any change of gradient. The actual event restart point, as seen on the figure, represents only one event and corresponds to the start of reloading. Obviously the stress level effect here has hindered rather than helped any interpretation of the results using AE. Rather than attempt to identify any change of gradient the yield point, Y, determined as

before, is plotted on the event rate figure. It is interesting to note that this corresponds to a (local) peak in event rate.

The stress path for Test 99, Figure 6.54, is a much better fit to that required with only relatively minor divergences from the desired path initially. The stress ratio and volumetric strain graphs are given in Figures 6.55 and 6.56 respectively, the forms being similar to Test 98. The events/deviatoric strain and stress ratio/events graphs, Figures 6.57 and 6.58, show few events occurring during the unload/reload period, and that the initial event rate is much higher than in Test 98. Two odd steps in the event rate are seen to occur in the events/deviatoric strain graph. The event rate/time graph, Figure 6.59, shows these two spurious(?) spikes together with the anticipated change in slope during reloading and the event restart point. The spikes are ignored in the following discussion. Points R and K are evaluated and plotted in the usual way. Point R occurs just below the previous maximum stress ratio and point K occurs just as the stress ratio curve levels out; the two points neatly straddling the transition between the vertical and horizontal sections of the stress ratio curve.

6.4.2 Summary.

The results reported in the previous sub-section have presented a great deal of information, and it is useful to assimilate some of this before proceeding. It is clear from all the tests that the sand tested has a curved failure surface indicated by decreasing peak stress ratio with increasing mean stress. This was also indicated by the results of Chapter 5. Also, where samples were

reloaded at a higher mean stress, it may be seen that yield, as identified conventionally, occurs at a stress ratio less than the previous maximum; this agrees with the work of Tatsuoka and Ishihara (1974). In all but one of the tests reported two points were identified from the AE data, an events restart point R, and an event rate change of gradient point K. Table 6.2 gives the stress ratios at yield as determined conventionally (Y on the figures), and from the AE data (K).

TEST	R Y	R K
97	0.82	0.82
94	0.81	0.81
96	0.76	0.77
95	0.74	0.75
100	0.79	0.78
99	0.82	0.80

Table 6.2   Stress Ratios at Yield

There is strong agreement between the yield points determined by the two techniques, and it is interesting to note that the AE method indicates that yield occurs slightly later in tests where the samples are reloaded at a higher mean stress.

6.4.3 Isotropic Yield Point Identification.

The stress paths chosen for this test series are shown diagrammatically in Figure 6.60. The aim of this test series was to try and define the shape of the isotropic yield surface. In each case the initial loading hopefully establishing a deviatoric yield surface which would not 'interfere' with the isotropic yield surface.

The stress path followed for Test 103, Figure 6.61, was an initial loading at constant cell pressure of 100kPa, unloading to isotropic stress, and finally loading on a line at 10° to the constant cell pressure line. In the stress ratio/deviatoric strain curve, Figure 6.62, it can be seen the reload curve is more abrupt than the initial curve and that the stress ratio during the reload period is less than that of the initial loading period. The volumetric strain/deviatoric strain curve, Figure 6.63, shows that during the reload phase the curve is almost parallel with that of the initial loading. In the events/deviatoric strain curve, Figure 6.64, the events cease on unloading and then increase to a much higher level than that of initial loading. This is in keeping with the increasing mean stress affecting the event rate, which is also reflected in the stress ratio/events graph, Figure 6.65. The event rate/time curve, Figure 6.66, shows a similar pattern to Tests 94, etc. On unloading events cease, and at some point during reloading events restart, followed by a change of gradient. These points are indicated in the usual manner, and are shown on the stress path and the stress ratio figures. Studying the stress ratio curves reveals that the points occur in similar positions to those in the deviatoric test series. Also, it is obvious from the stress path plot that K and Y are located on the curved deviatoric yield surface. It would appear that the AE data fails to identify any possible isotropic yield surface.

In Test 101 the same initial loading path was followed but the sample is reloaded on a line at 30° to the constant cell pressure line, the actual stress path is reproduced in Figure 6.67. The stress ratio curve, Figure 6.68, shows that the reloaded stress

ratio is much less than that of the initial stress ratio, but this is expected given the slope of the loading path. The stress path was stopped relatively early in strain terms because the load limit of the load cell was being approached. The volume change curve, Figure 6.69, is noticeably different from previous tests; after behaving normally until just after the start of reloading the sample shows considerable volumetric compression as may be expected from the stress path followed. The stress ratio is replotted against volumetric strain in Figure 6.70 and it is apparent that yield has occurred. The yield point is identified in the conventional manner, but is marked V rather than Y to indicate its derivation. The rate of increase in the events/deviatoric strain curve, Figure 6.71, on reloading is almost vertical which, considering the rate of increase of mean stress, is to be expected. The large event rate increase results in a rapid reduction in the slope of the reload stress ratio/events curve, Figure 6.72. This figure clearly suggests yielding has occurred. Indeed, there is a suggestion of this when stress ratio is plotted against deviatoric strain, Figure 6.68. Figure 6.73, event rate/time, shows that following reloading the event rate increases at an increasing rate (c.f. undrained tests), which is to be expected from the rate of increase of mean stress. A slight change of gradient occurs following reloading but, unlike Tests 94 - 100, this leads to a higher event rate. The events restart point, R is identified and is plotted on the usual figures, with K, V, and Y. R occurs in a similar (relative) position on the stress ratio plot to that of Test 103. The position of K on the stress path figure would seem to be that of the deviatoric yield locus; however, the lack of AE data after this point makes it difficult to draw firm conclusions. V and Y

occur close together, and appear to lie on an isotropic yield locus.

The stress path in Test 102, Figure 6.74, was originally intended to be parallel with the space diagonal but a calculation error meant that the actual path was at about 20° to it. The stress ratio, Figure 6.75, looks odd but this is because the high value of σ_r causes a significant volumetric strain. The volumetric strain/deviatoric strain curve, Figure 6.76, follows the pattern set by Test 101 with, in this case, virtually no deviatoric strain occurring during the reload period but a great deal of volumetric strain. The stress ratio is replotted against volumetric strain in Figure 6.77, and it is evident that yield has occurred but that small fluctuations in stress, due to the testing technique, have been reflected by relatively large changes of stress ratio. Events are plotted against volumetric strain, Figure 6.78, as virtually no deviator strain occurred during the reload period. The stress ratio/events curve, Figure 6.79, shows that on reloading the stress ratio drops to an almost constant value which again is expected from the stress path followed. The event rate/time curve, Figure 6.80, does not exhibit an abrupt change of gradient after events restart, but the event rate increases rapidly from the reloading point. The unevenness of the stress ratio/volumetric strain graph prevents any estimates of where yield occurs being made. However, it is clear that yield has occurred from both the stress ratio/events and stress ratio/volumetric strain figures.

6.5 Discussion and Summary.

The tests reported in Section 6.3 showed that few, if any, events were recorded when a sample was unloaded, and that on reloading events started very close to the former maximum stress ratio. When the stress ratio reached its former level it was found that the event rate was also at its pre-unload level. In materials other than sand, where events start at a significantly lower stress ratio on reloading, the ratio of the previous maximum and restart stress ratios is taken to be an indication of damage to the material and is known as the felicity ratio. The felicity ratio for the sand tested was found to be 0.96-0.98, which indicates (virtually) no damage. The lack of damage is not unexpected as sand is strengthened by changing its structure.

The tests reported in Section 6.4 attempted to identify the position of the yield surface with the aid of AE. The results of Section 6.4.1 showed that the deviatoric yield surface could be identified from a discontinuity in the event rate, which is related to the presence of the Kaiser effect. The discontinuity, marked as K in the figures, agrees well with the yield point identified from conventional methods. In Tests 94-97, where the reloaded cell pressure was different to the initial cell pressure, the difference in the event rates due to the mean stress effect is clearly seen. There is, however, no difficulty in identifying the discontinuity, K. The AE method of yield identification shows the yield surface to be curved, but less than conventional methods might suggest. The non linearity of the yield surface agrees with suggestions made by others, e.g. Tatsuoka and Ishihara (1974), Lade (1982), and Vermeer (1980).

In Chapter 5 it was suggested the gain or threshold voltage could be adjusted to enhance the AE data. A couple of tests were performed in which the gain was adjusted at the appropriate point. However, as the relationship between gain and events is not known, the gain adjustment had to be estimated. The results showed that, in general, the increase in gain was insufficient to match the event rates. Additionally, if the gain was increased too much, background noise became more of a problem. This aspect of AE therefore requires further clarification.

The results of the tests in Section 6.4.3, where it was hoped to identify a possible isotropic yield surface, are disappointing. Test 103 succeeded only in identifying the deviatoric yield surface; this is, perhaps, to be expected from the stress path. The other two tests were handicapped by the mean stress effect and by the testing technique. The rapid development of mean stress suggests that a lower strain rate should have been used in order to exercise finer control over the stresses.

This chapter has provided further evidence for the repeatability and the reliability of the Acoustic Emission method. Tests at similar strain rates and stress levels have produced similar event rates. The influence of stress level on the AE results has once again been made apparent; this point has to be continually borne in mind when any analysis is undertaken. The Kaiser effect has been shown to be present in sand. It has also become apparent that it is the changes in the event rate which are important for the identification of the deviatoric yield surface. A deviatoric yield surface has been identified using the AE method.

No evidence for any of the possible hardening laws has been adduced, as it is necessary to locate both edges of the yield surface for this; this is investigated in the next chapter.
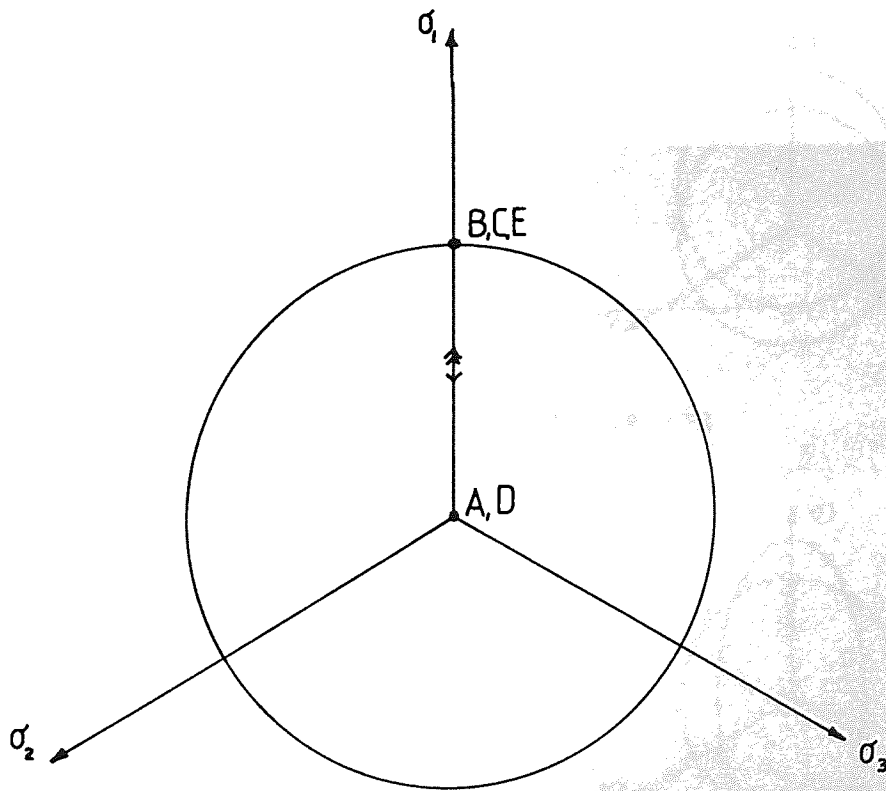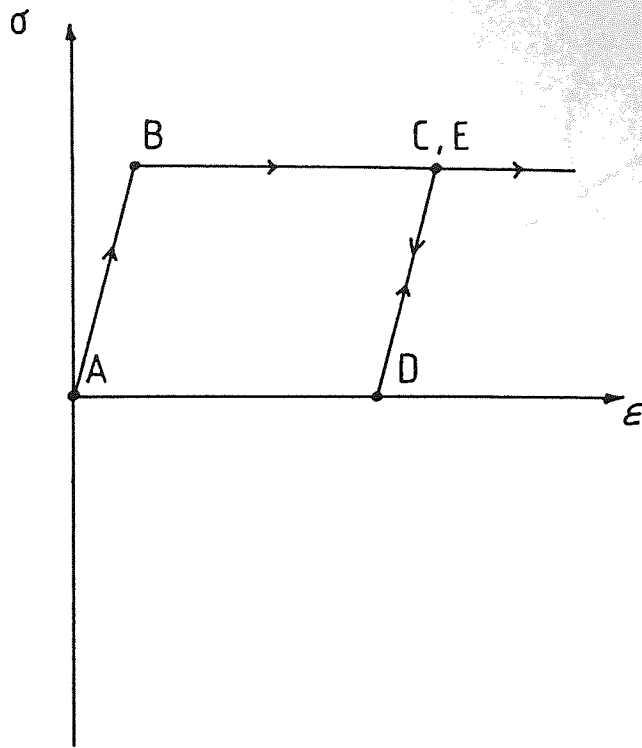
Figure 6.1 Stress/strain curve for a hypothetical material

138

(a) No hardening

(b) Isotropic hardening

(c) Kinematic hardening

(d) Anisotropic hardening
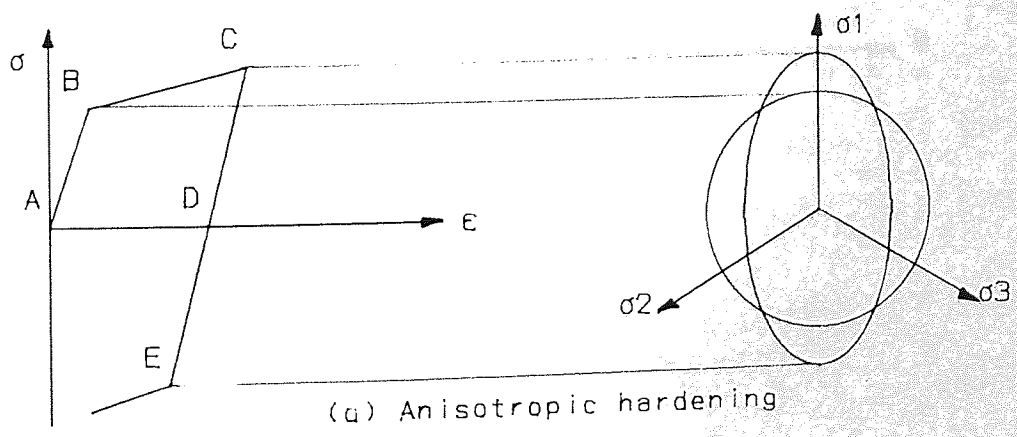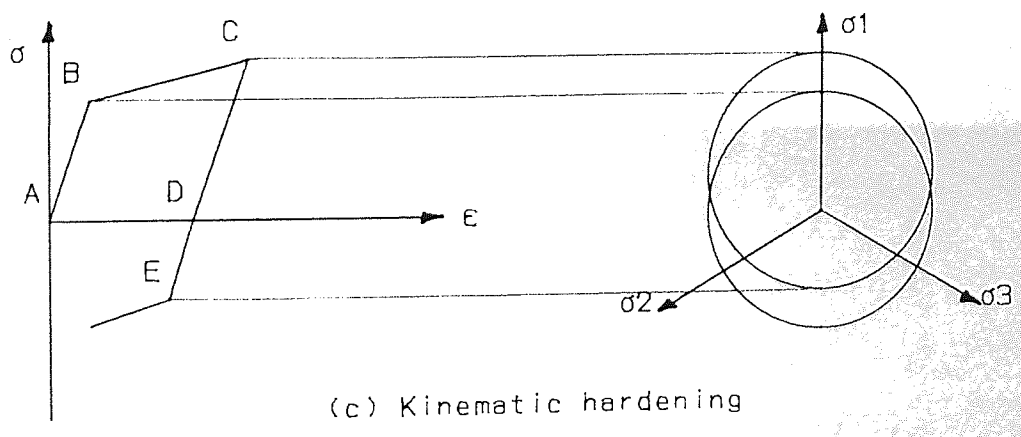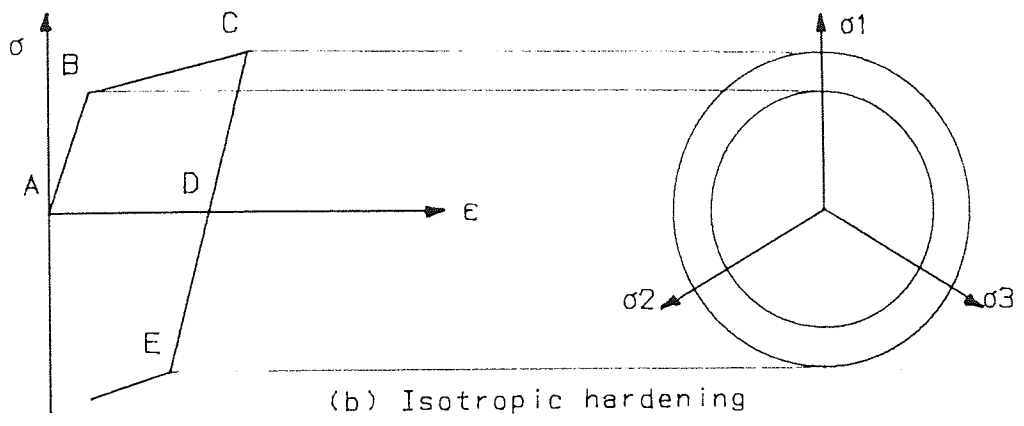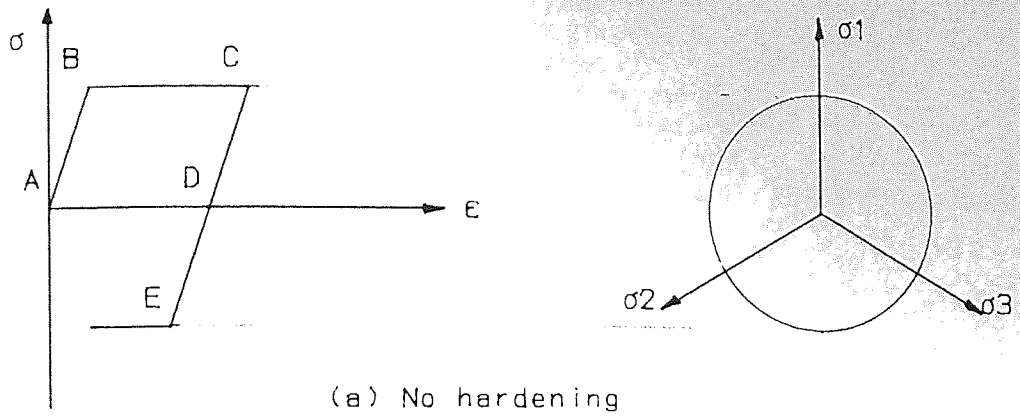
Figure 6.2 Hardening theories
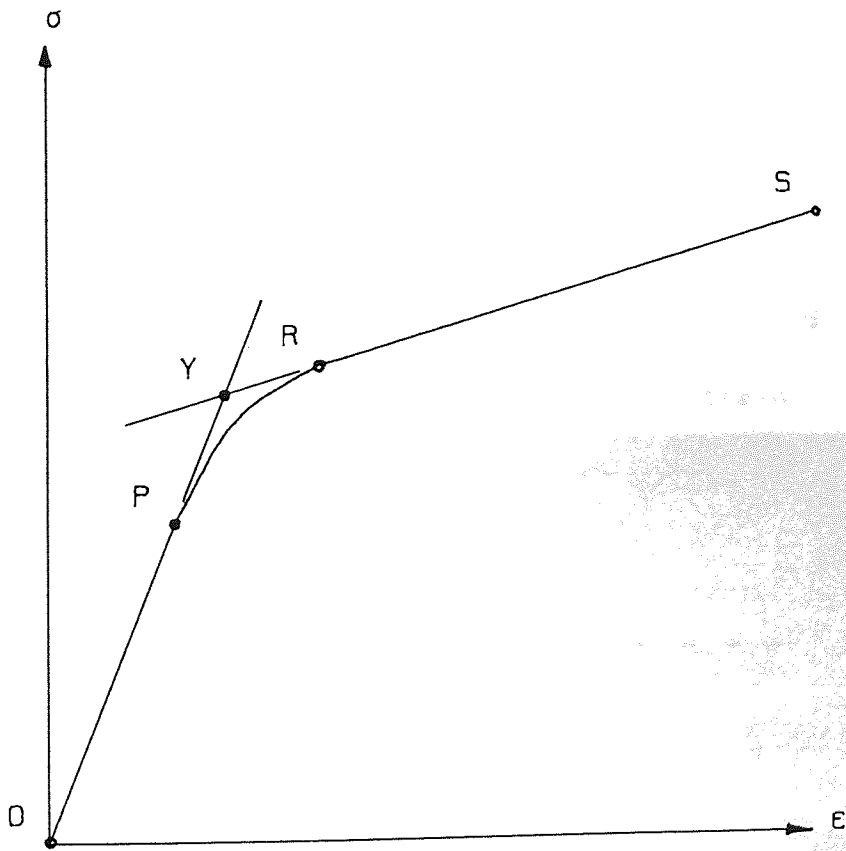
Figure 6.3 Identification of the yield point

140
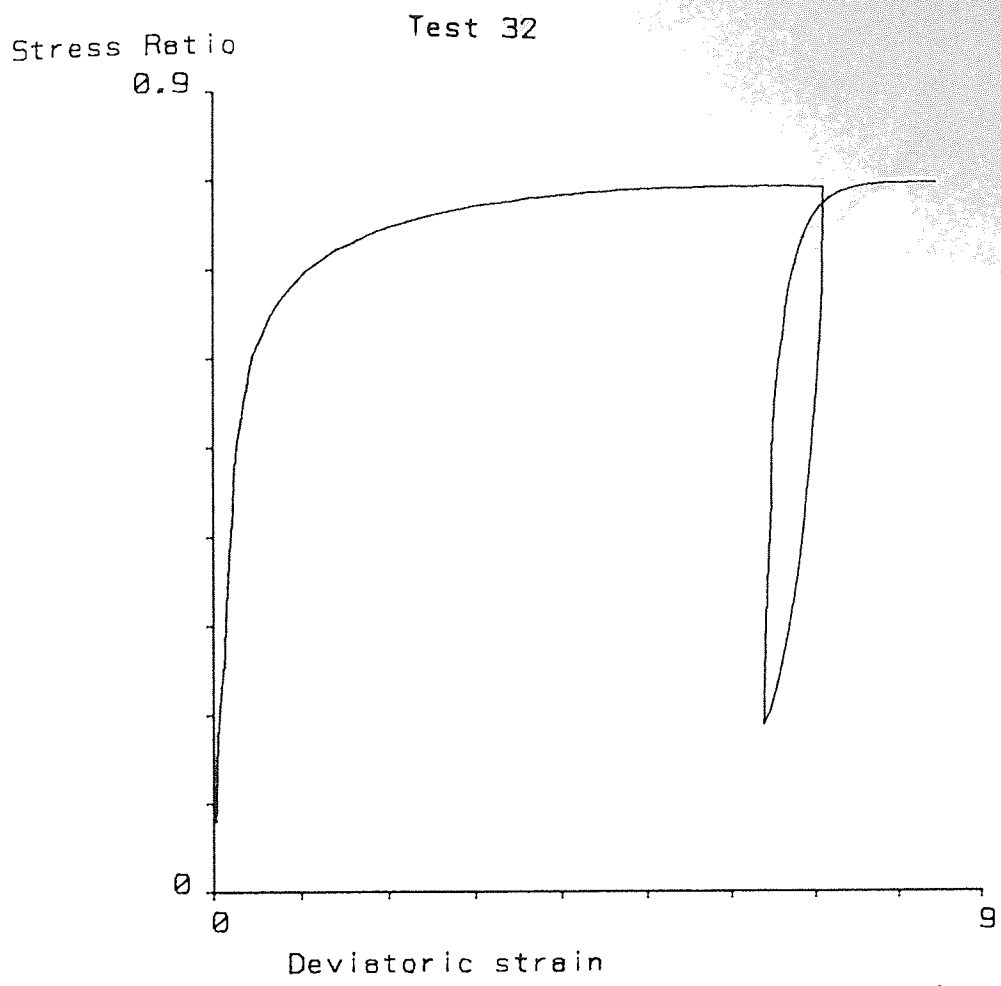
Figue 6.4 Test 32: Stress Ratio/Deviatoric strain
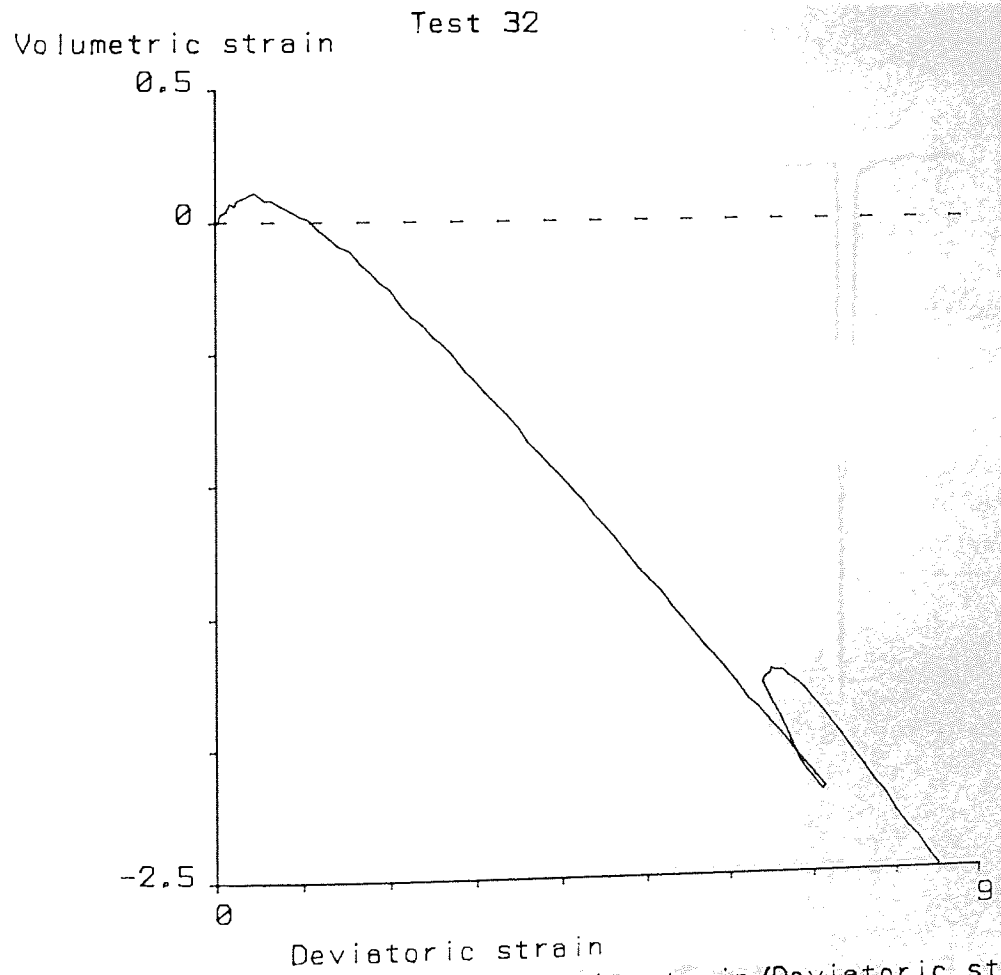
Figure 6.5 Test 32: Volumetric strain/Deviatoric strain

Test 32

Events
1000
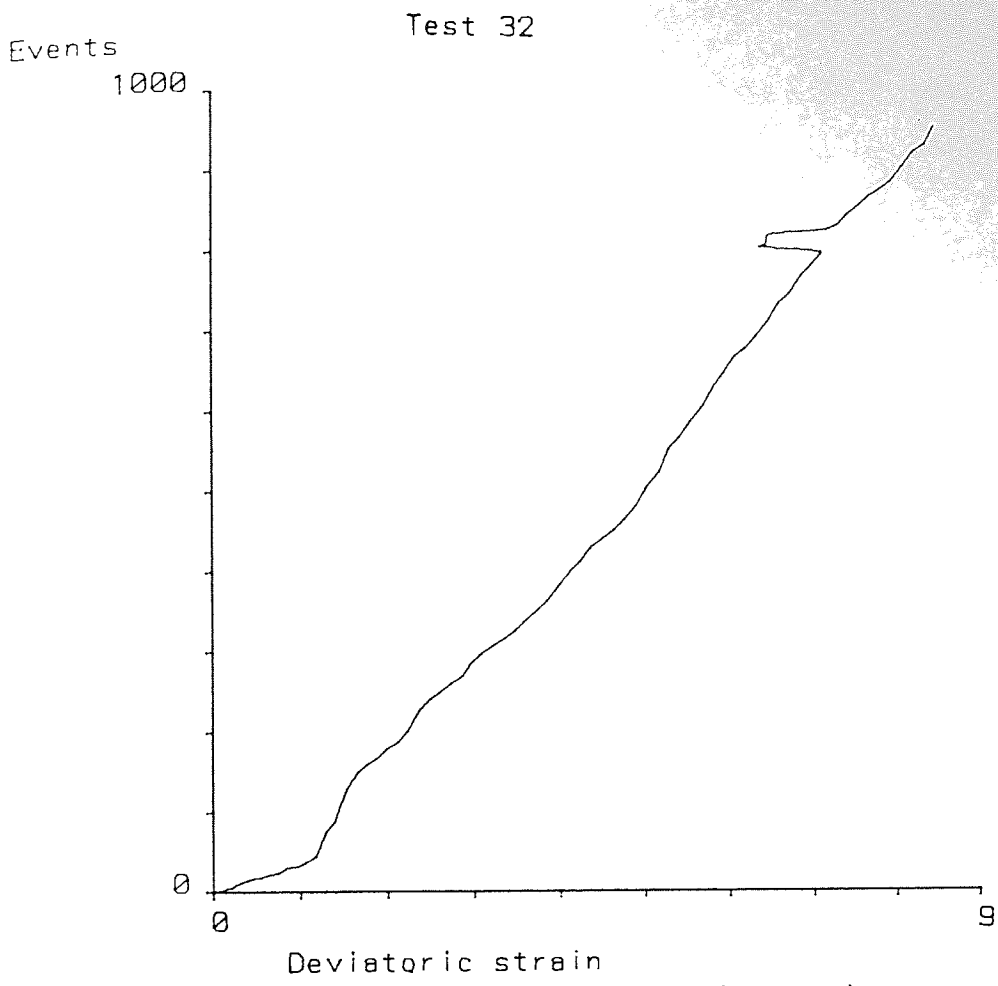
Deviatoric strain

Figure 6.6 Test 32: Events/Deviatoric strain

Test 32

Stress Ratio
0.9
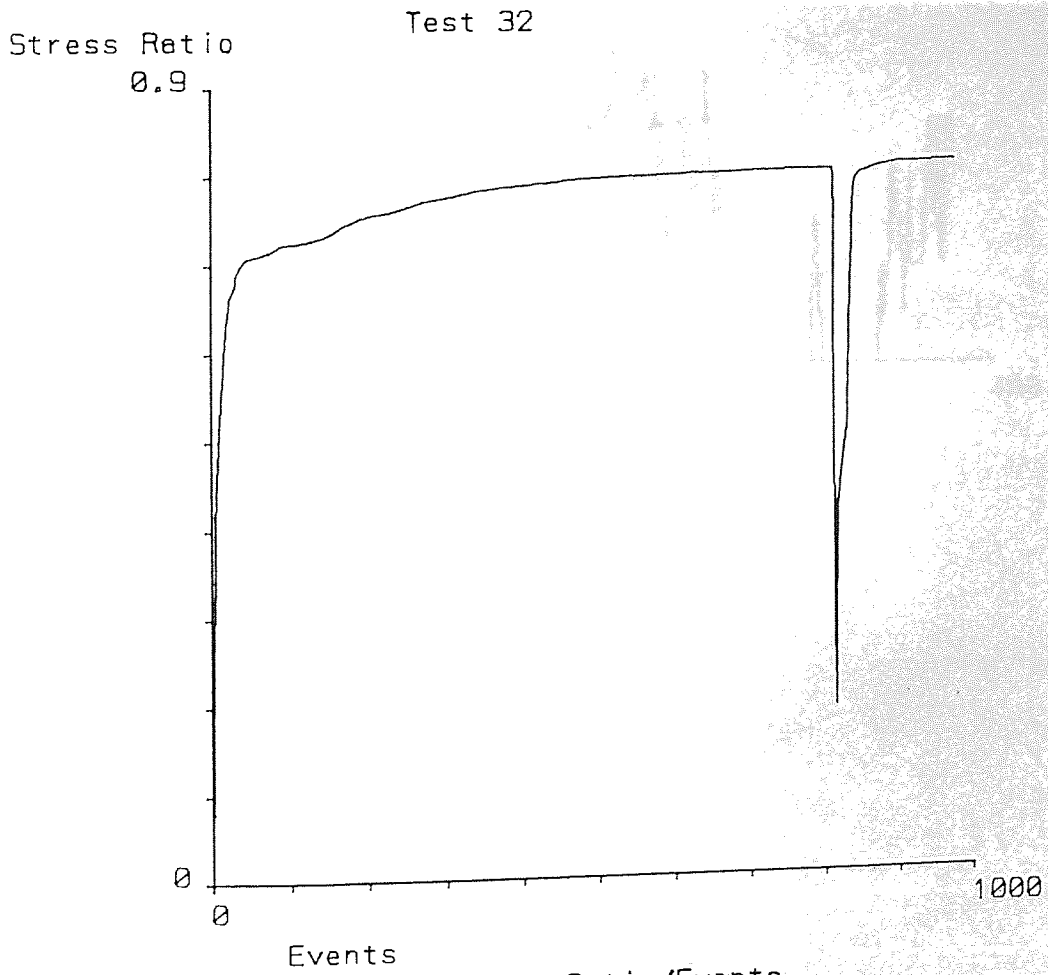
Events

Figure 6.7 Test 32: Stress Ratio/Events

142
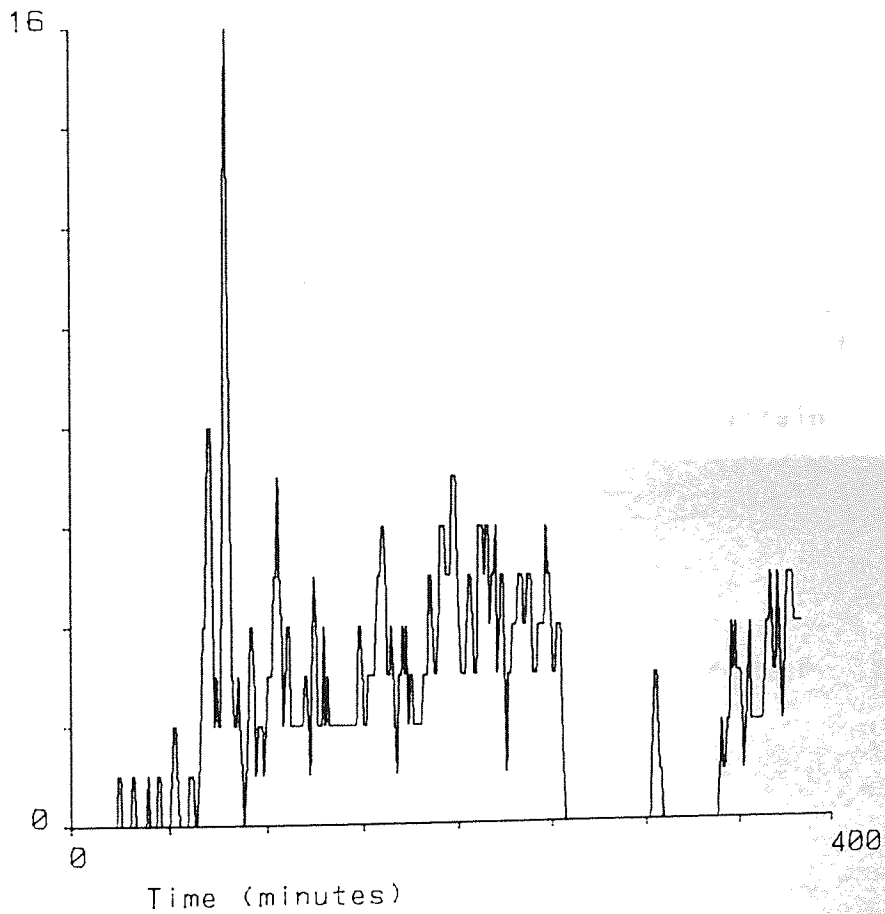
Figure 6.8 Test 32: Event rate/Time

Stress Ratio
Test 36

0.9

0

0
Deviatoric strain
9
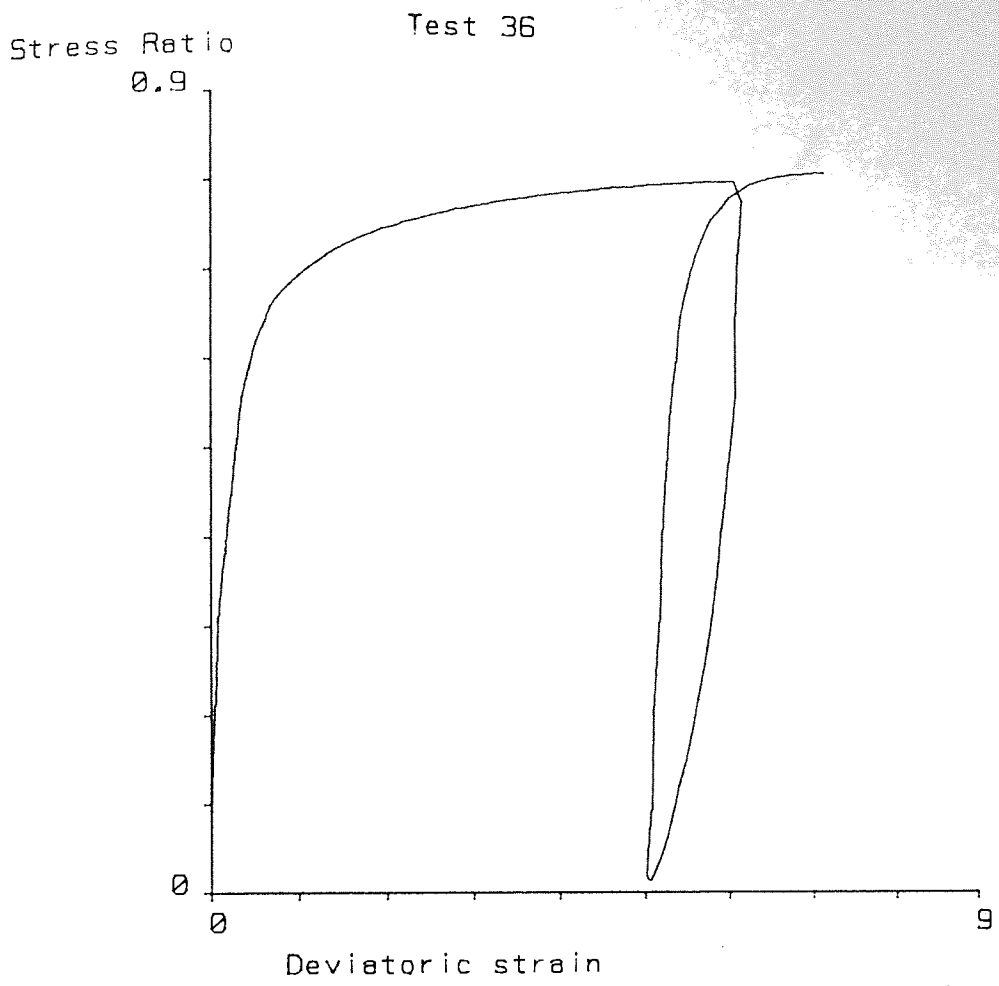
Figure 6.9 Test 36: Stress Ratio/Deviatoric strain

Volumetric strain
Test 36

0.5

0

-2.5

0
Deviatoric strain
9
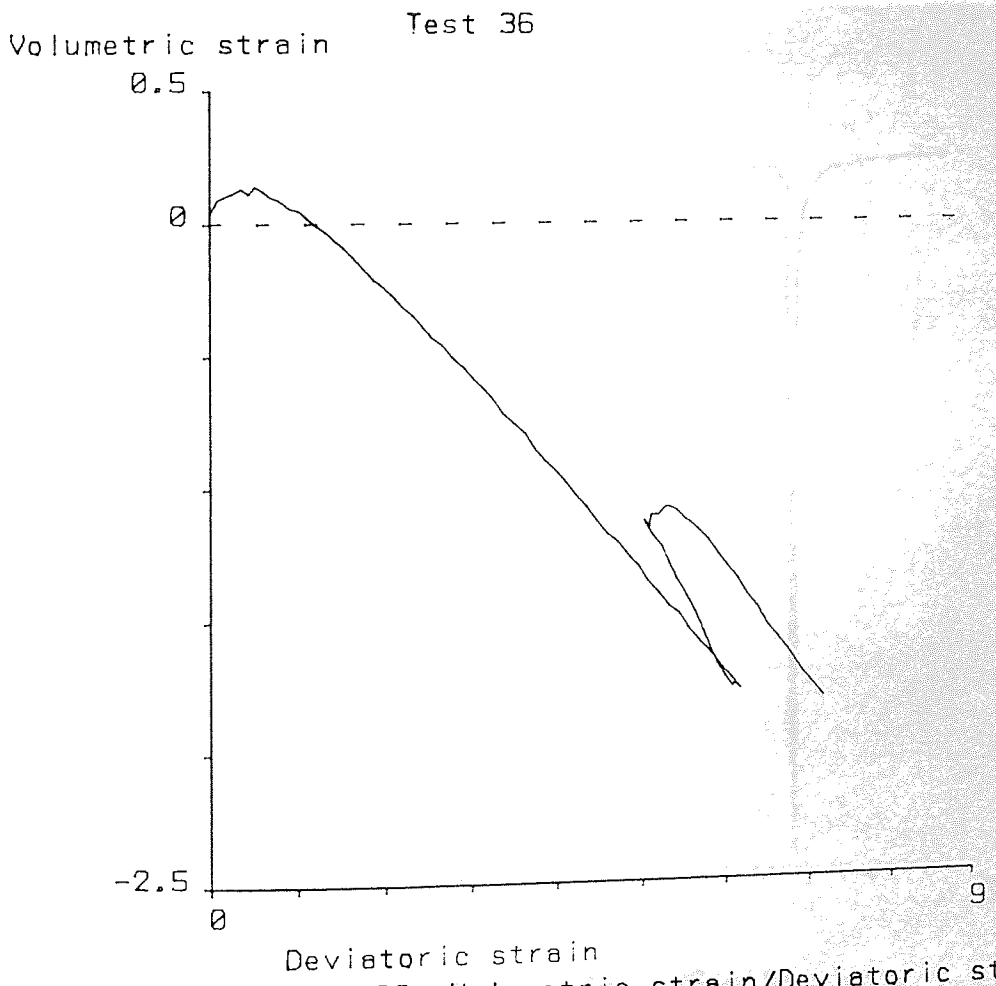
Figure 6.10 Test 36: Volumetric strain/Deviatoric strain

144

Test 36

Events
700

0

0   9
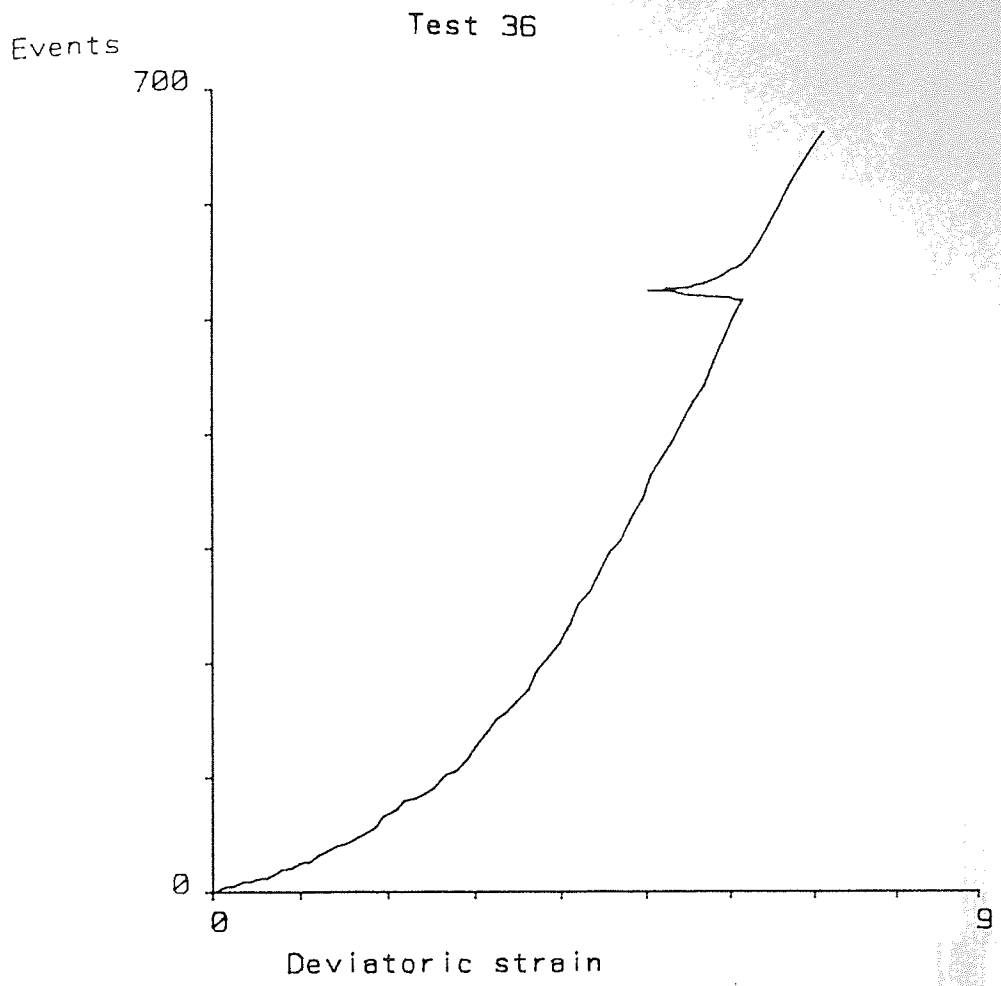
Deviatoric strain

Figure 6.11 Test 36: Events/Deviatoric strain

Test 36

Stress Ratio
0.9

0

0   700
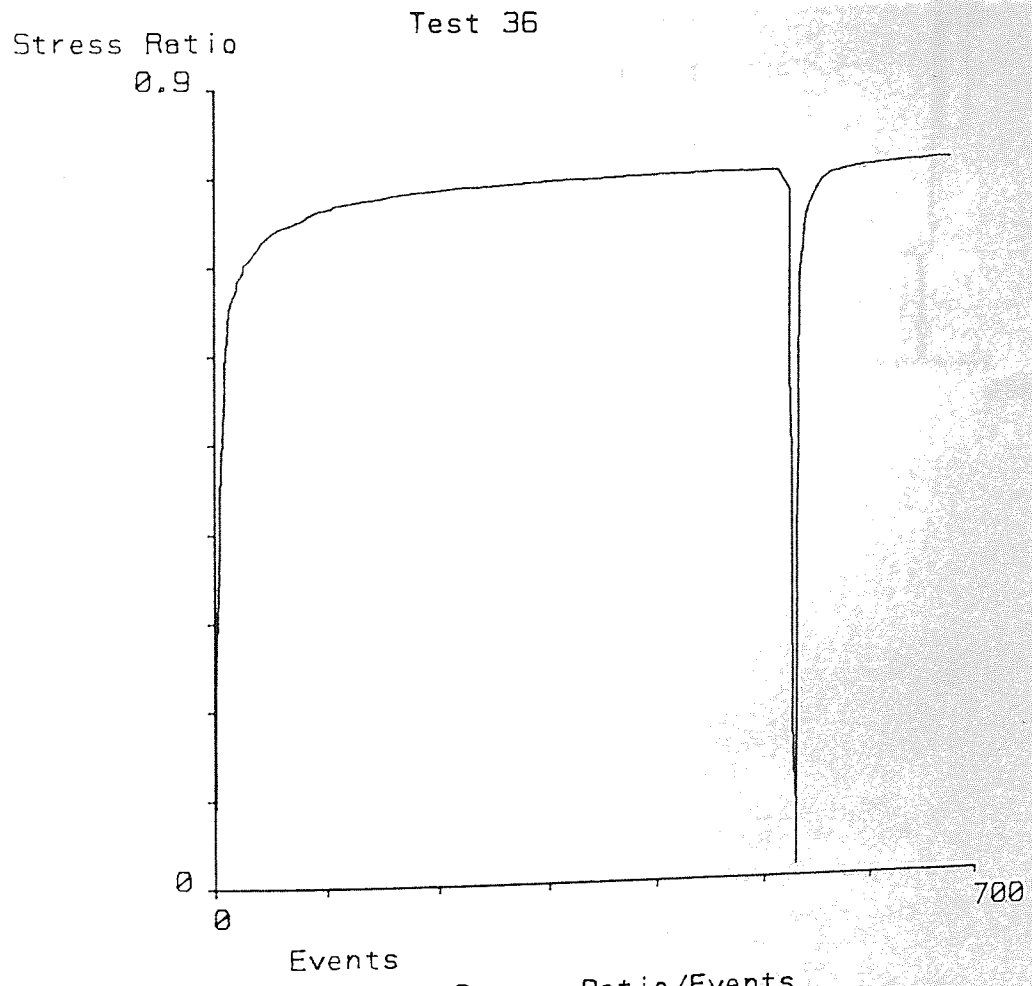
Events

Figure 6.12 Test 36: Stress Ratio/Events

145
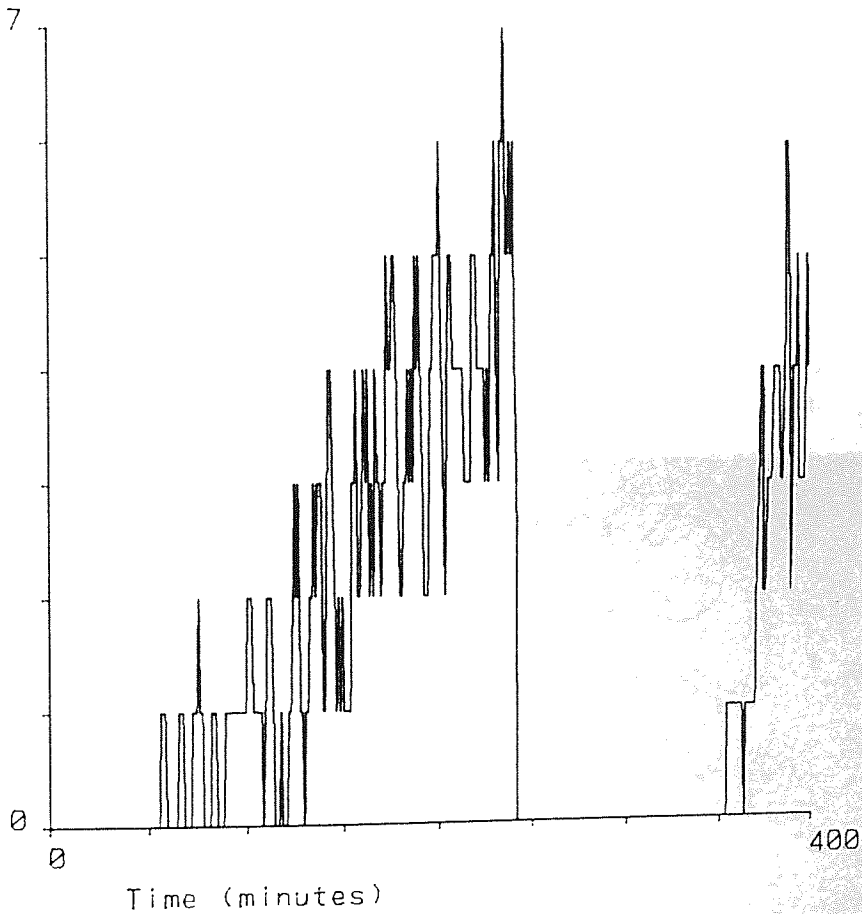
Figure 6.13 Test 36: Event rate/Time
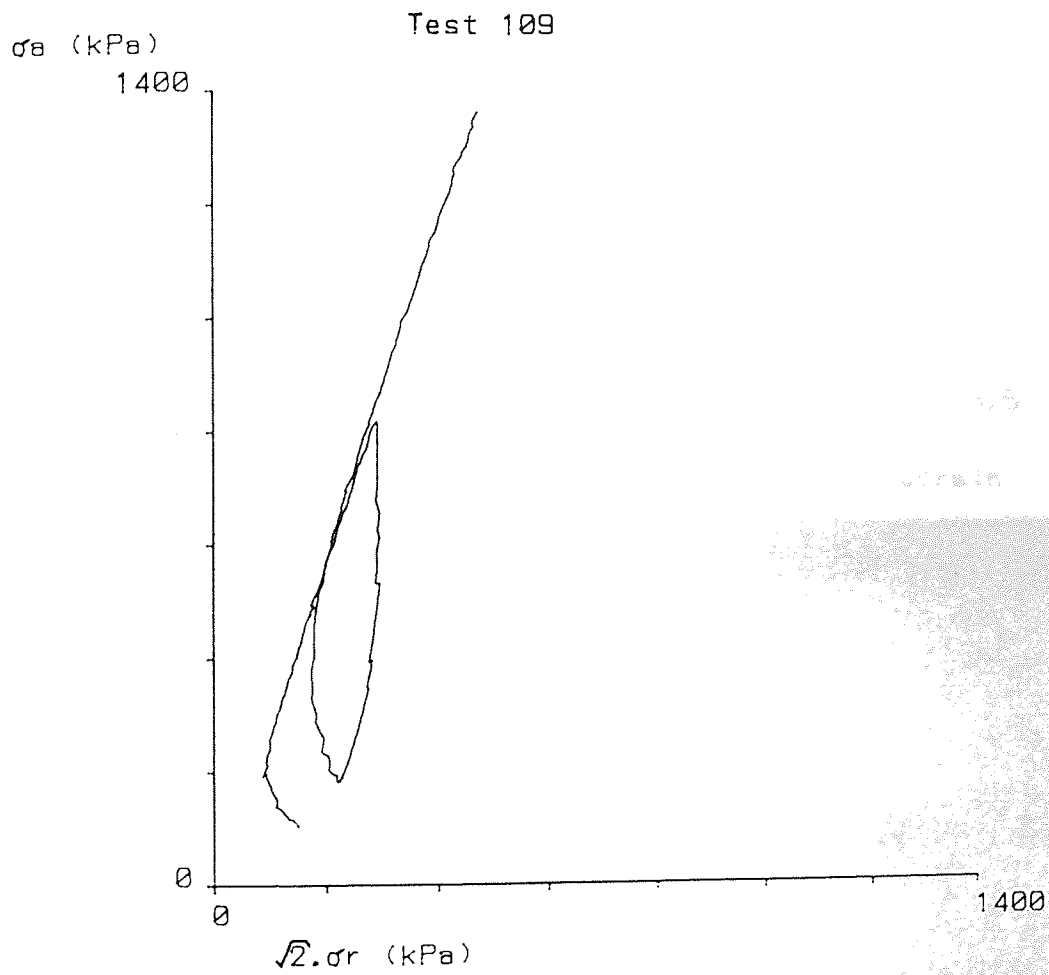
Figure 6.14 Test 109: Stress path

Test 109

Stress Ratio
0.8

0
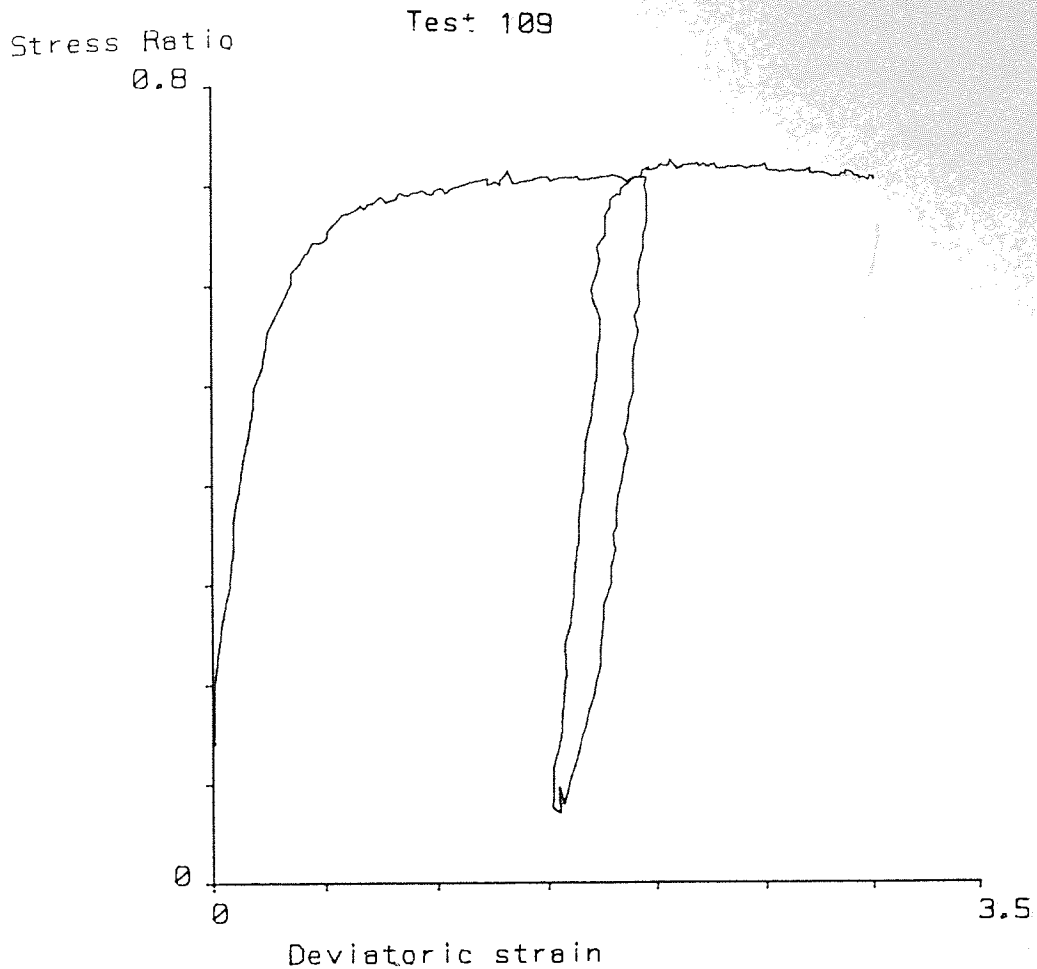
0   3.5
                    Deviatoric strain
Figure 6.15 Test 109: Stress Ratio/Deviatoric strain

Test 109
Pore Water Pressure (kPa)
350

0
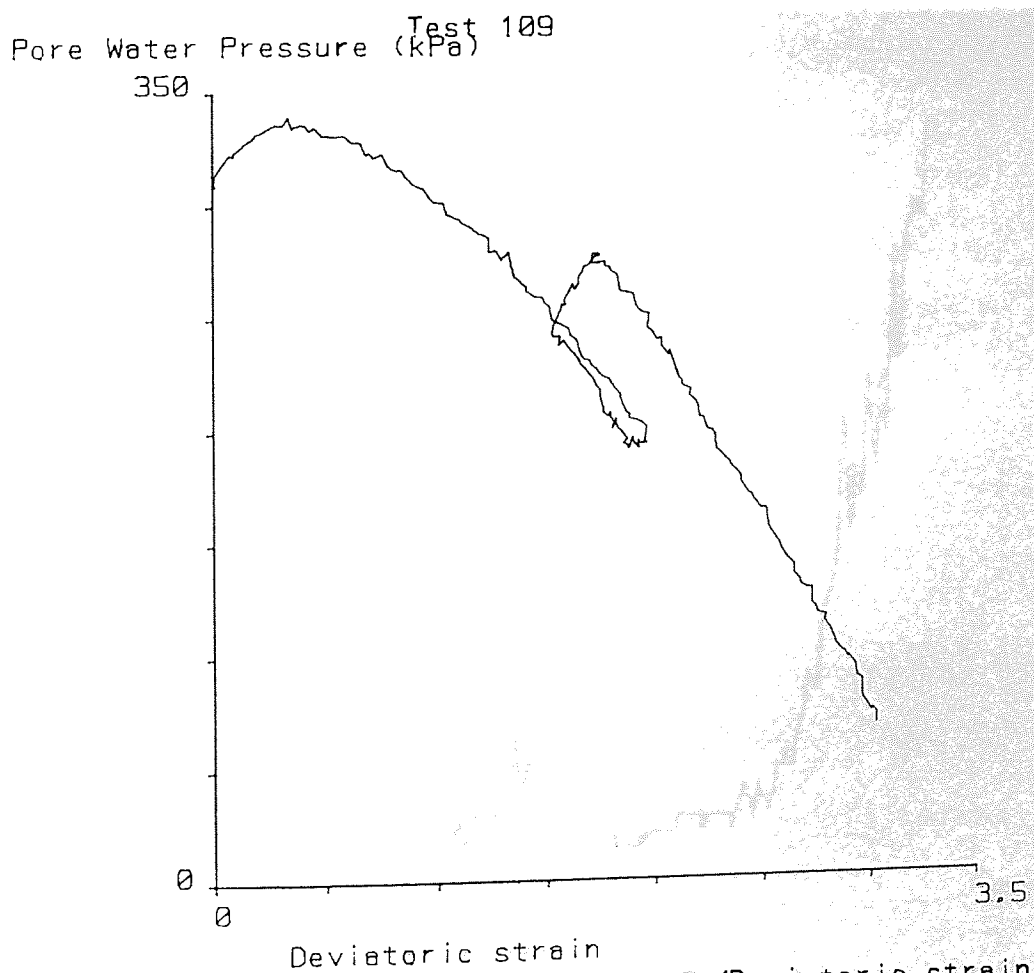
0   3.5
                    Deviatoric strain
Figure 6.16 Test 109: Pore pressure/Deviatoric strain
148
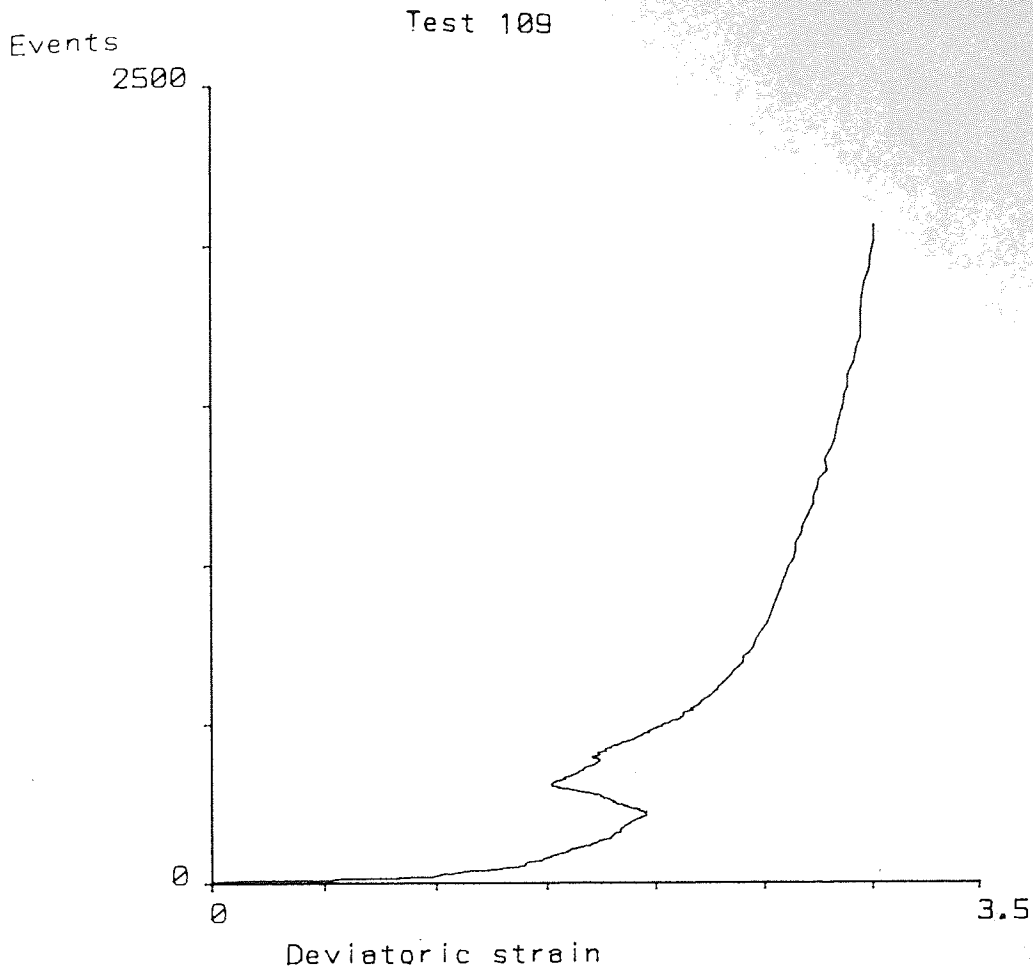
Figure 6.17 Test 109: Events/Deviatoric strain

Time (minutes)
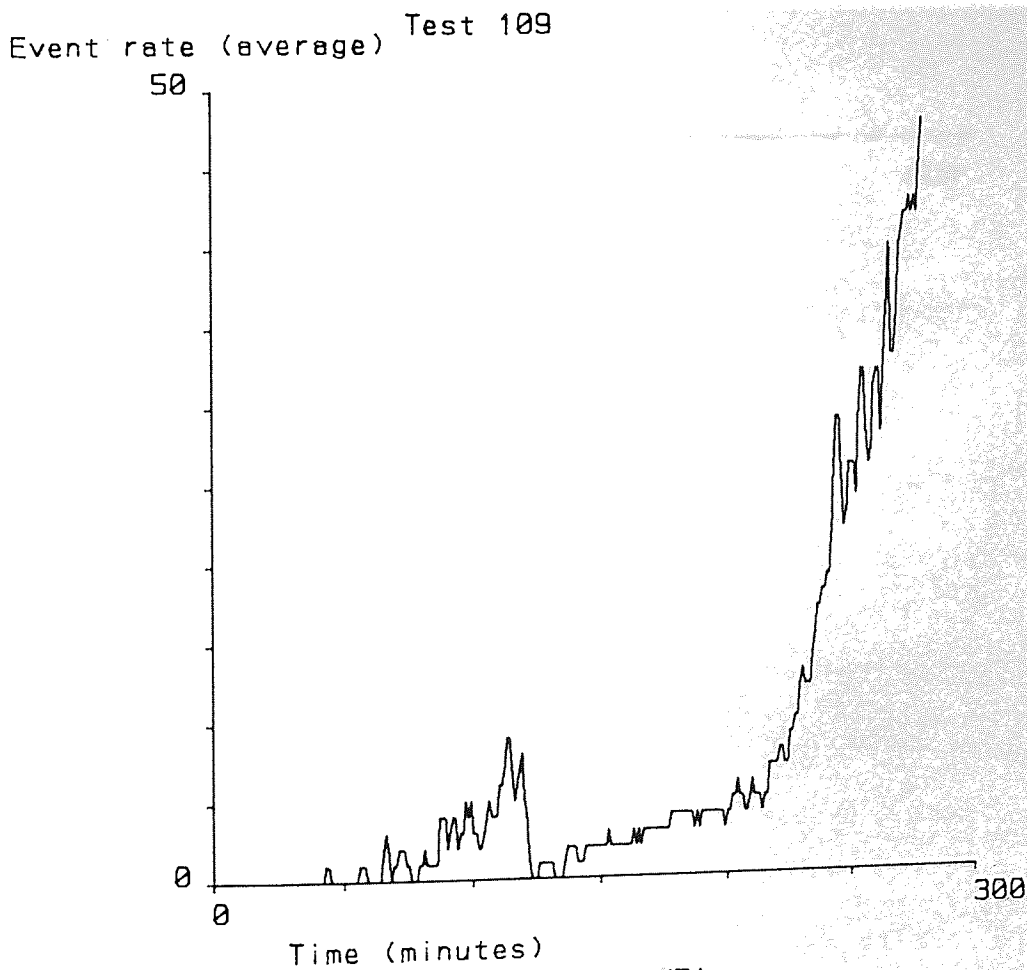
Figure 6.18 Test 109: Event rate/Time

149

σa

Deviatoric Yield Surface

Isotropic Yield Surface

Space Diagonal

$\sqrt{2}\sigma r$
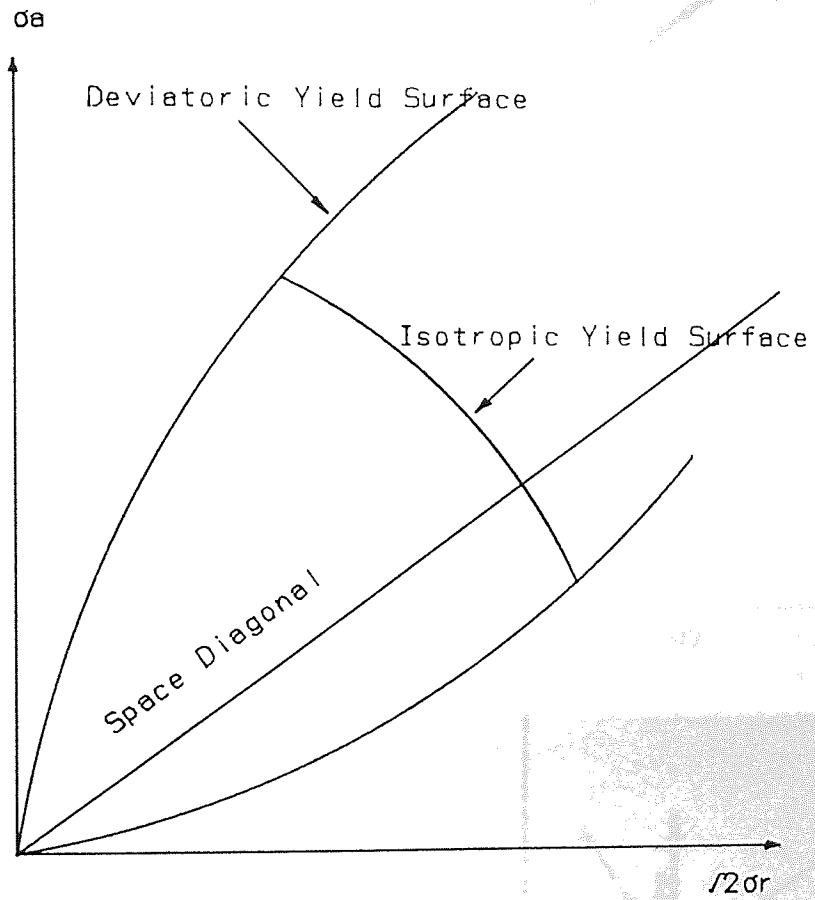
After Lade (1982)

Figure 6.19 Example of yield surface
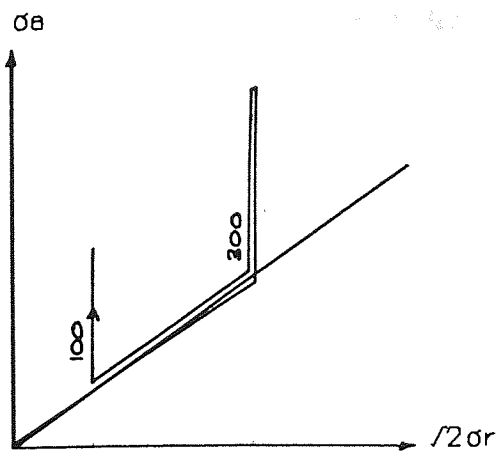
Figure 6.20 Stress paths

Test 97

Stress Ratio
0.9

Y

K

R

0
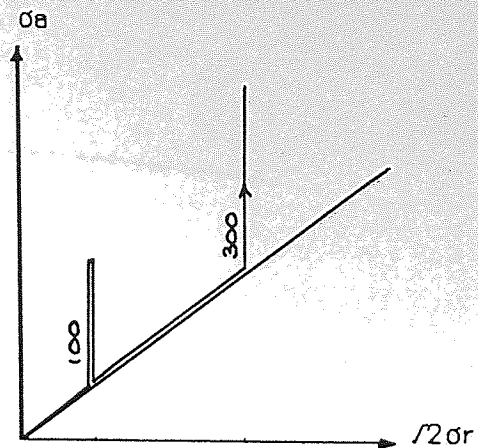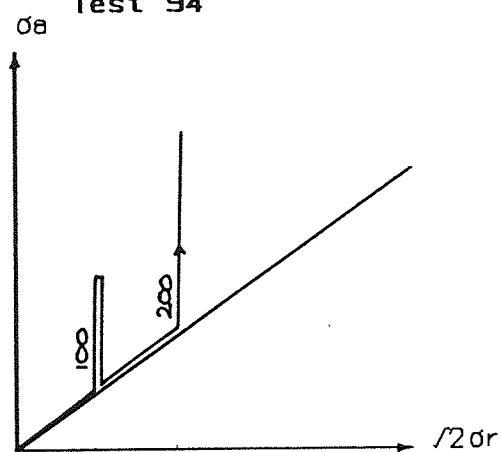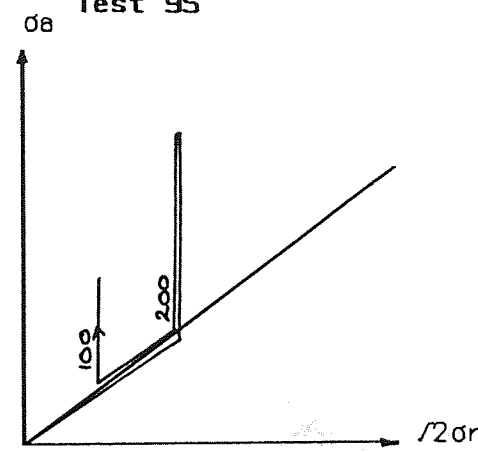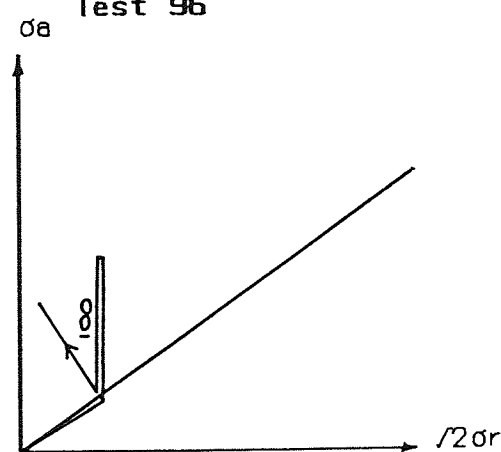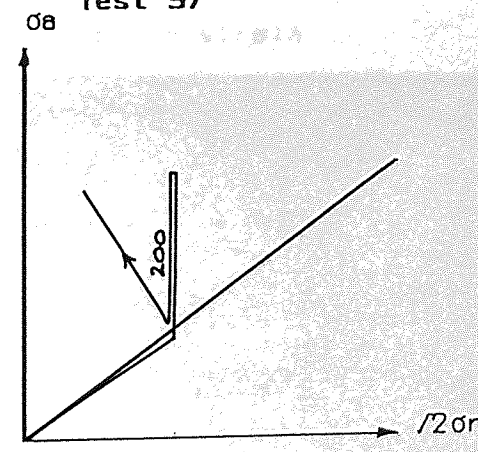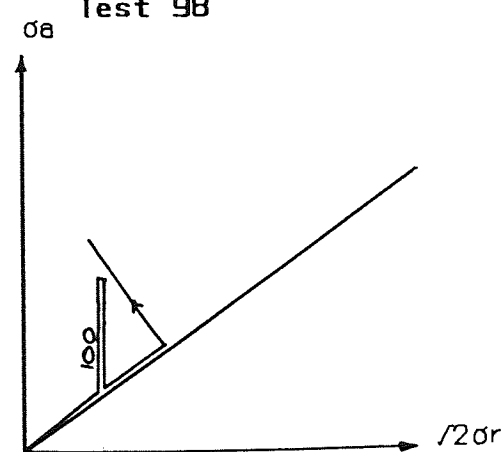
0   Deviatoric strain   25
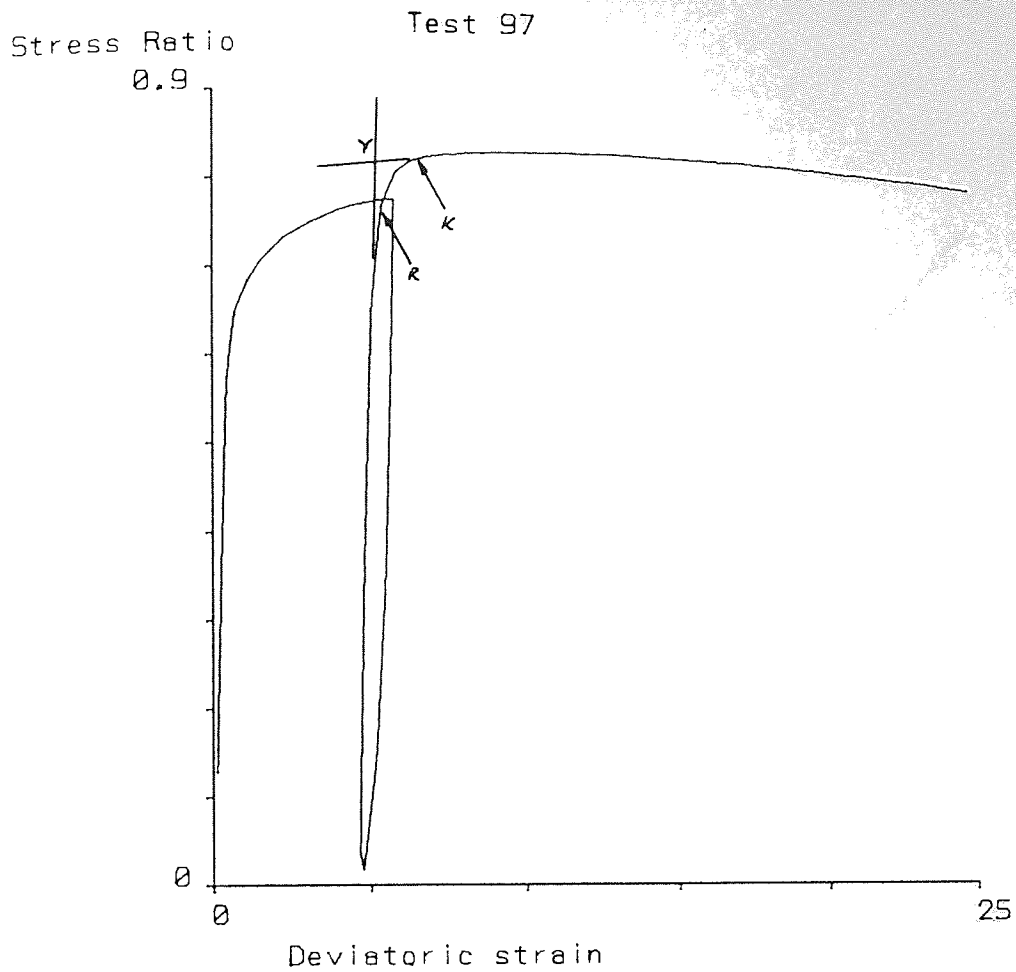
Figure 6.21 Test 97: Stress Ratio/Deviatoric strain

Test 97
Volumetric strain
1

0

-10

0   Deviatoric strain   25
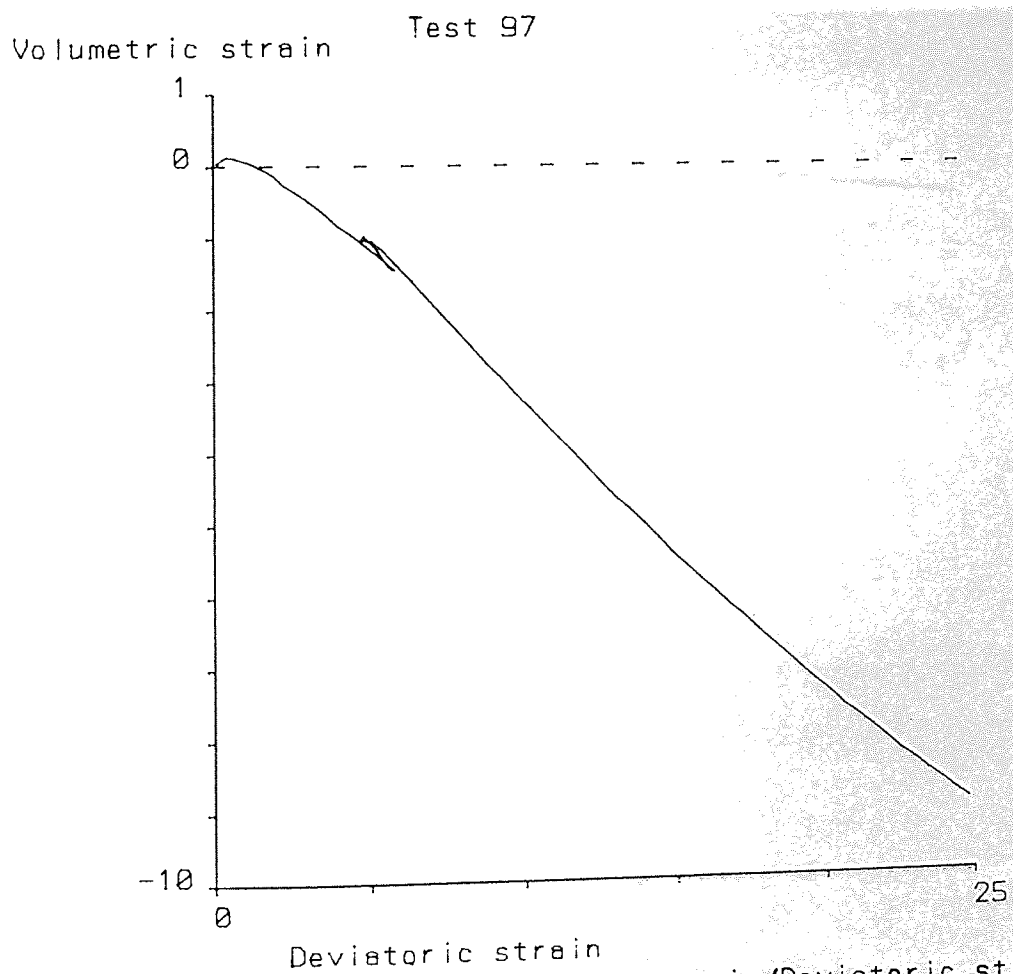
Figure 6.22 Test 97: Volumetric strain/Deviatoric strain

152
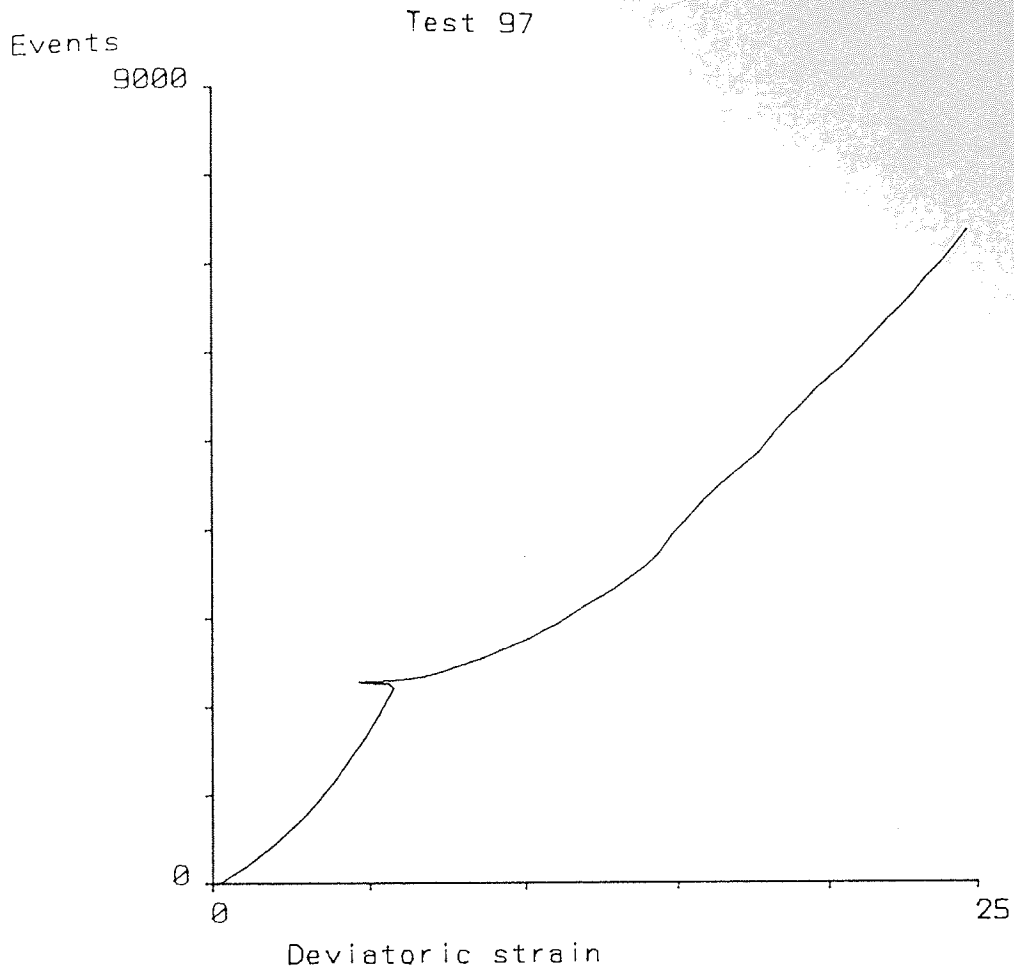
Figure 6.23 Test 97: Events/Deviatoric strain
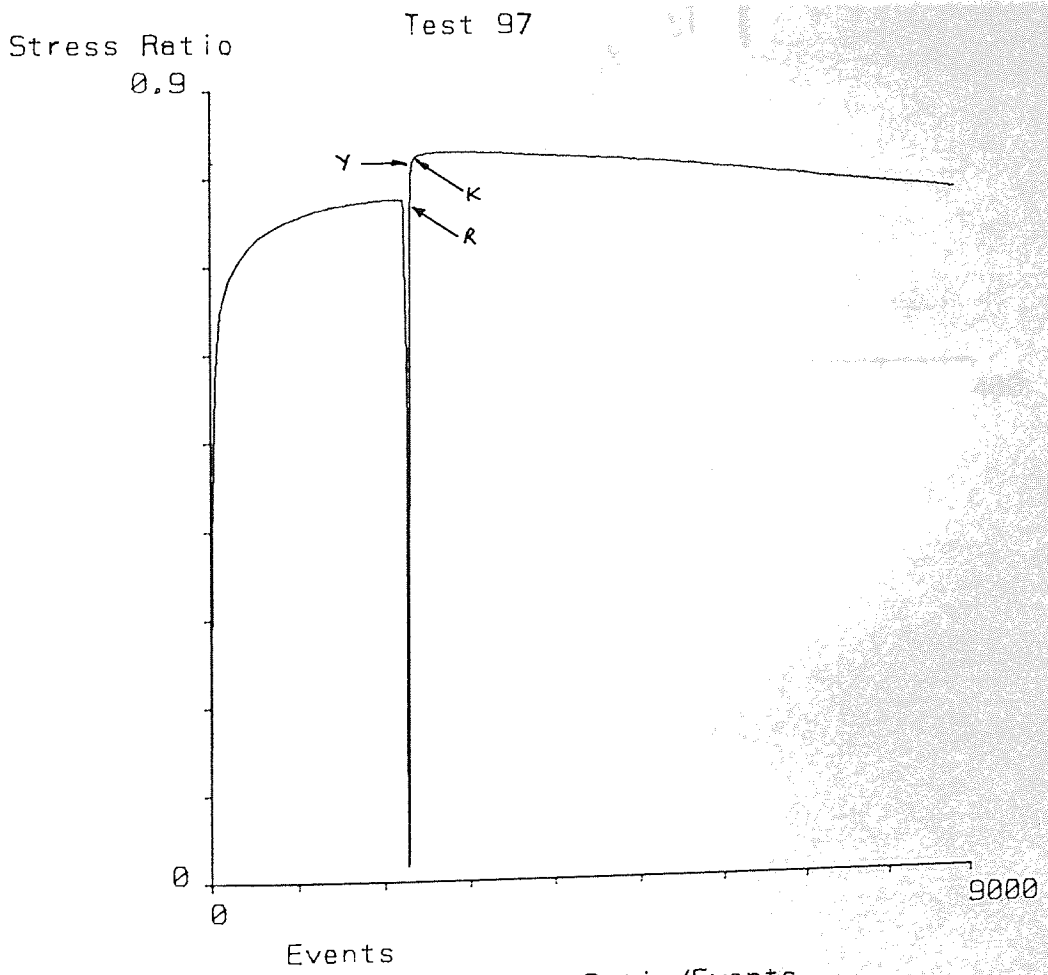
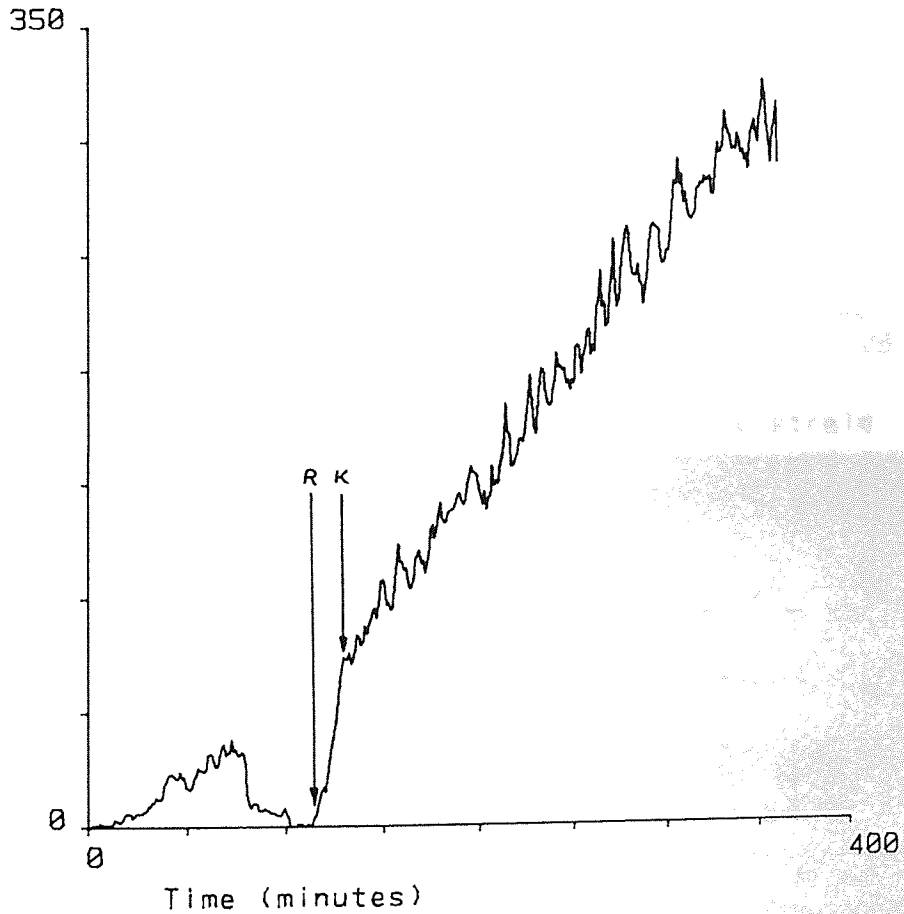Figure 6.24 Test 97: Stress Ratio/Events
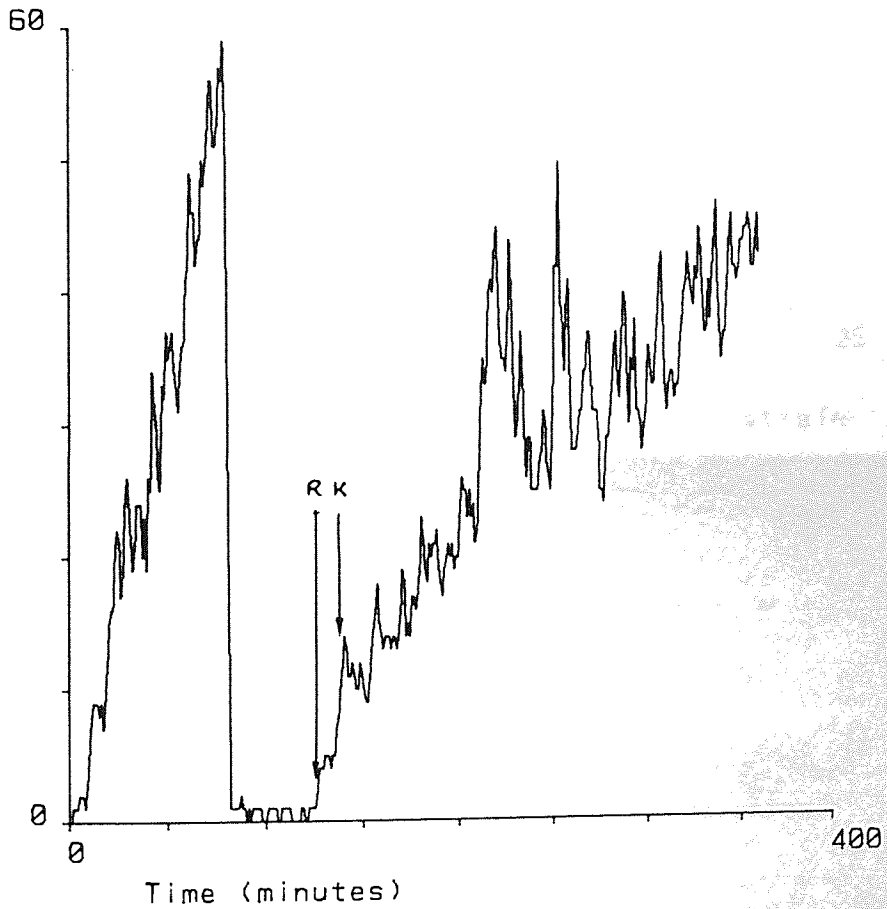
Figure 6.25 Test 97: Event rate/Time
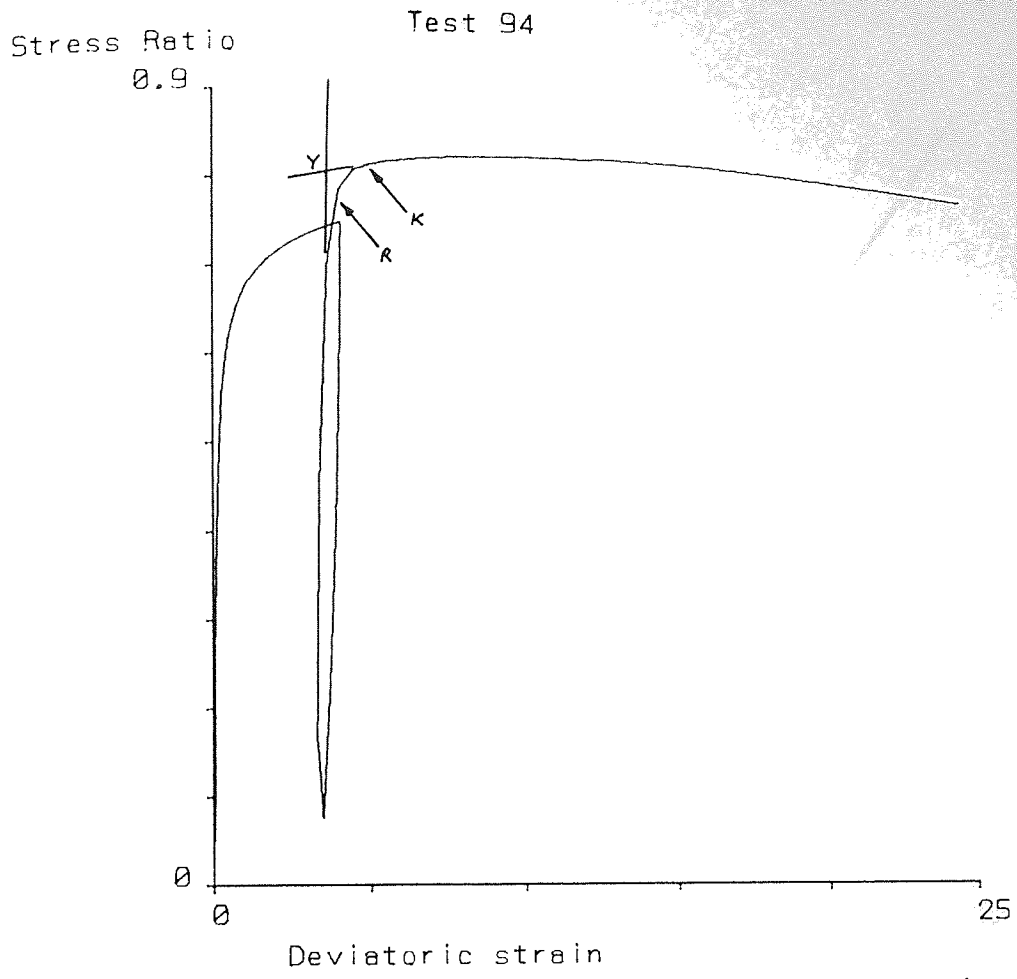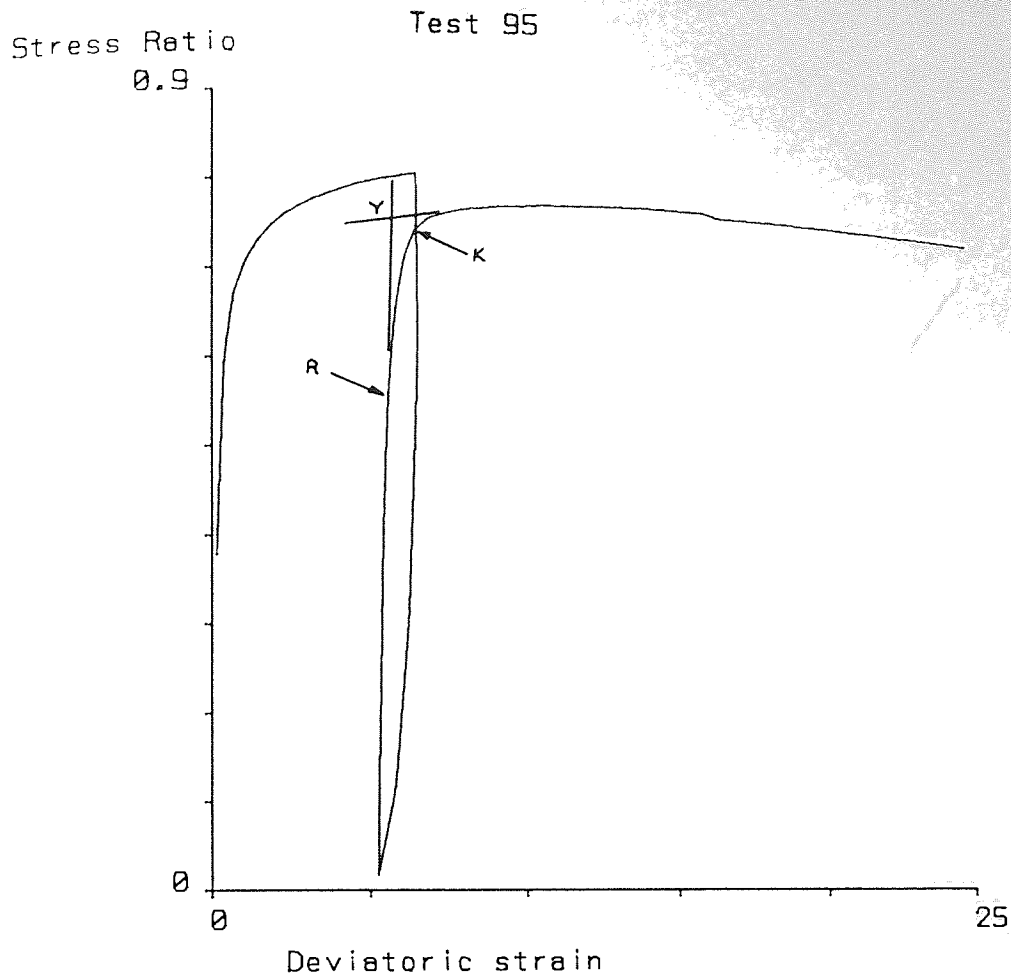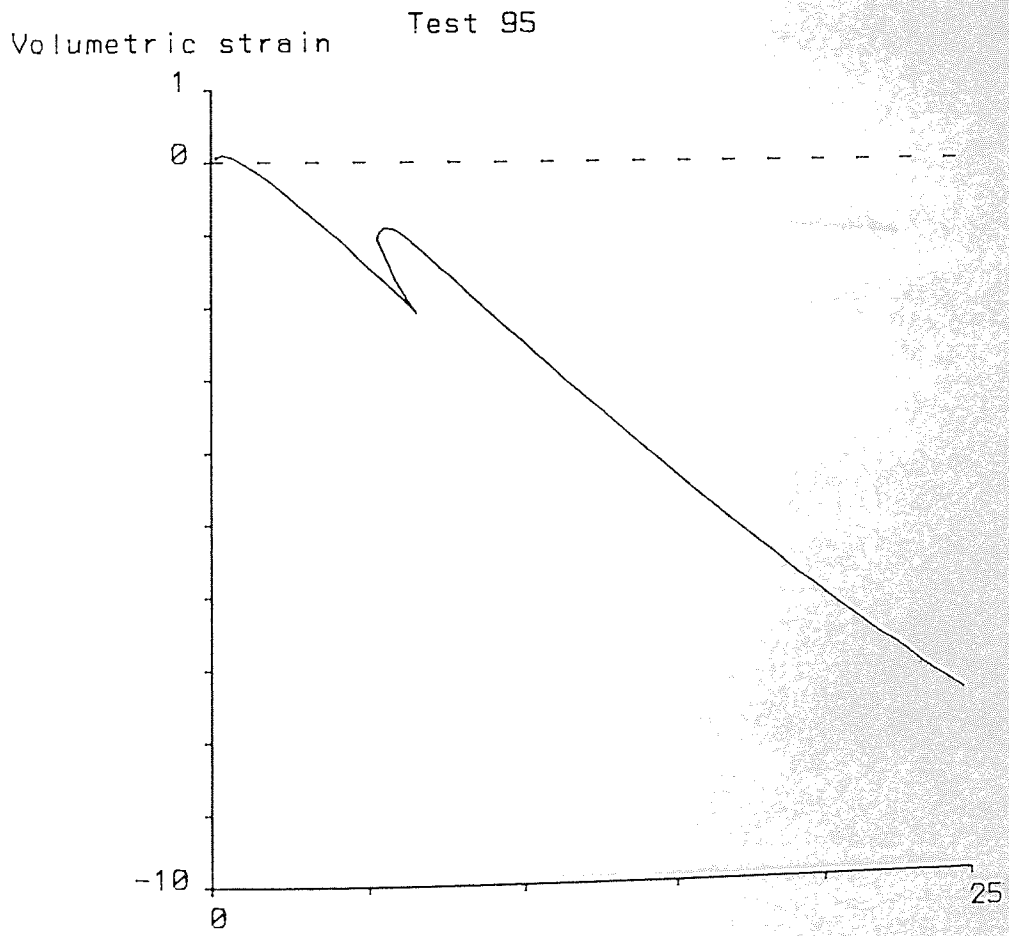
Figure 6.26 Test 94: Stress Ratio/Deviatoric strain
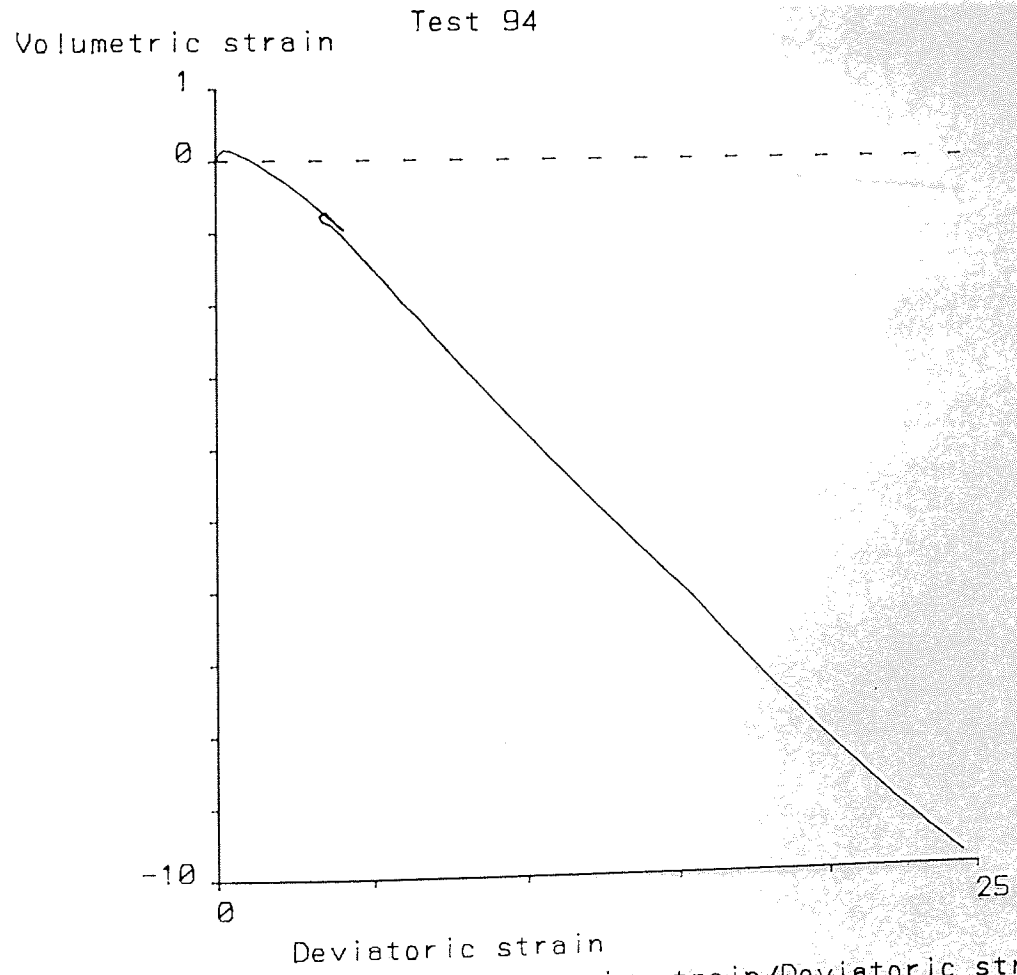

Figure 6.27 Test 94: Volumetric strain/Deviatoric strain

Test 94

Events
12000

0
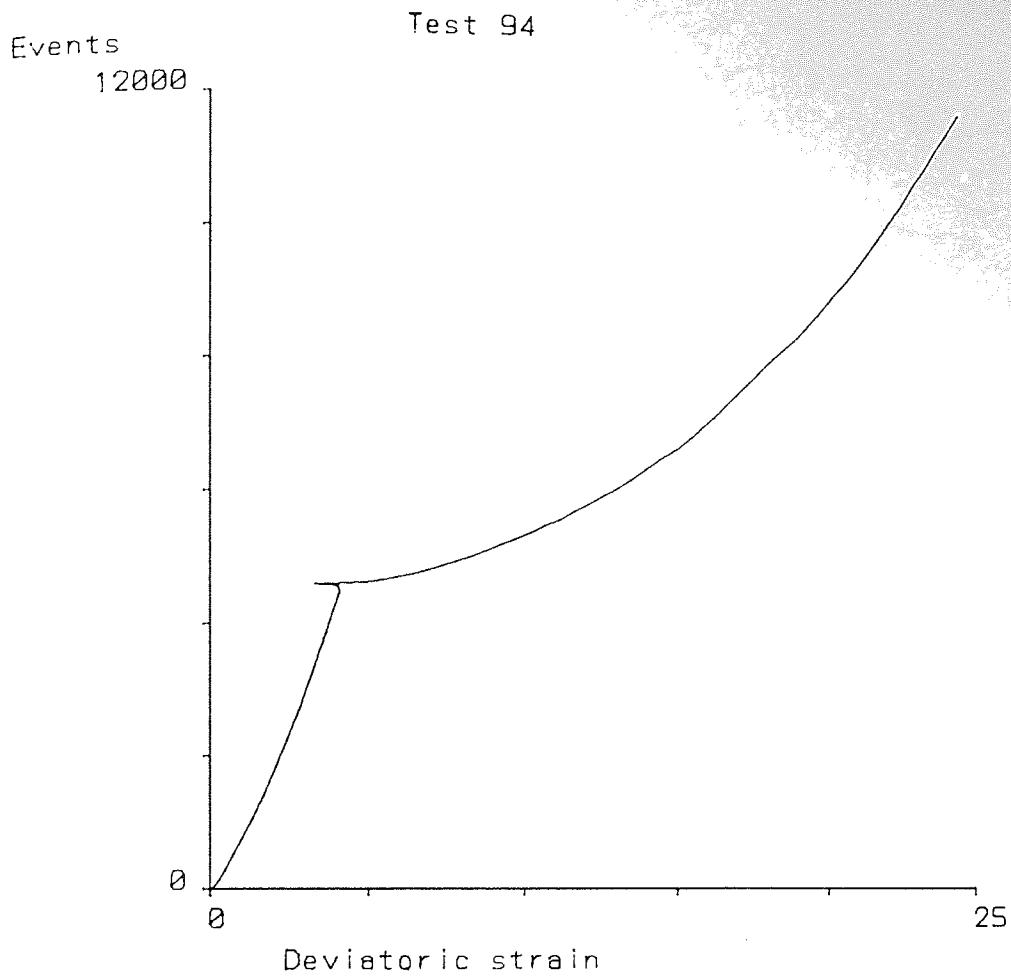
0   25
Deviatoric strain
Figure 6.28 Test 94: Events/Deviatoric strain

Test 94

Stress Ratio
0.9

Y →
K
R

0
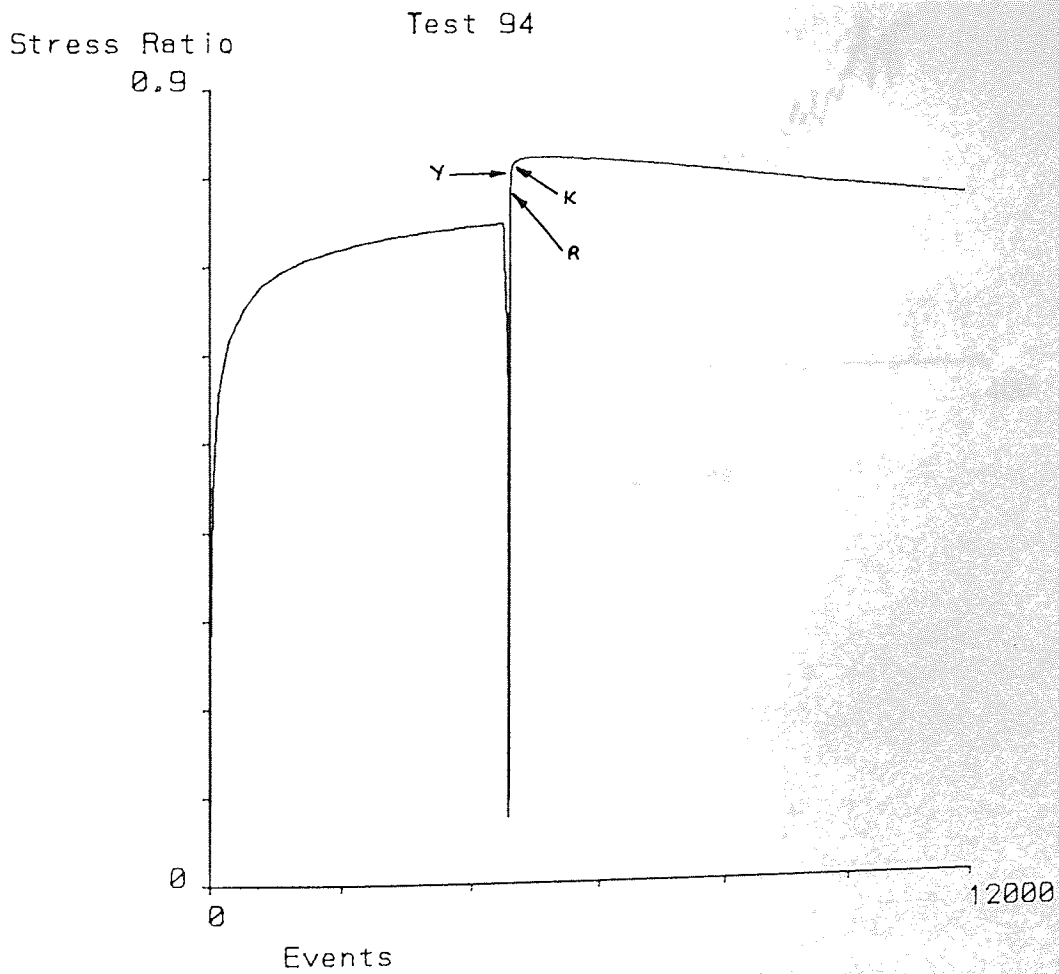
0   12000
Events
Figure 6.29 Test 94: Stress ratio/Events
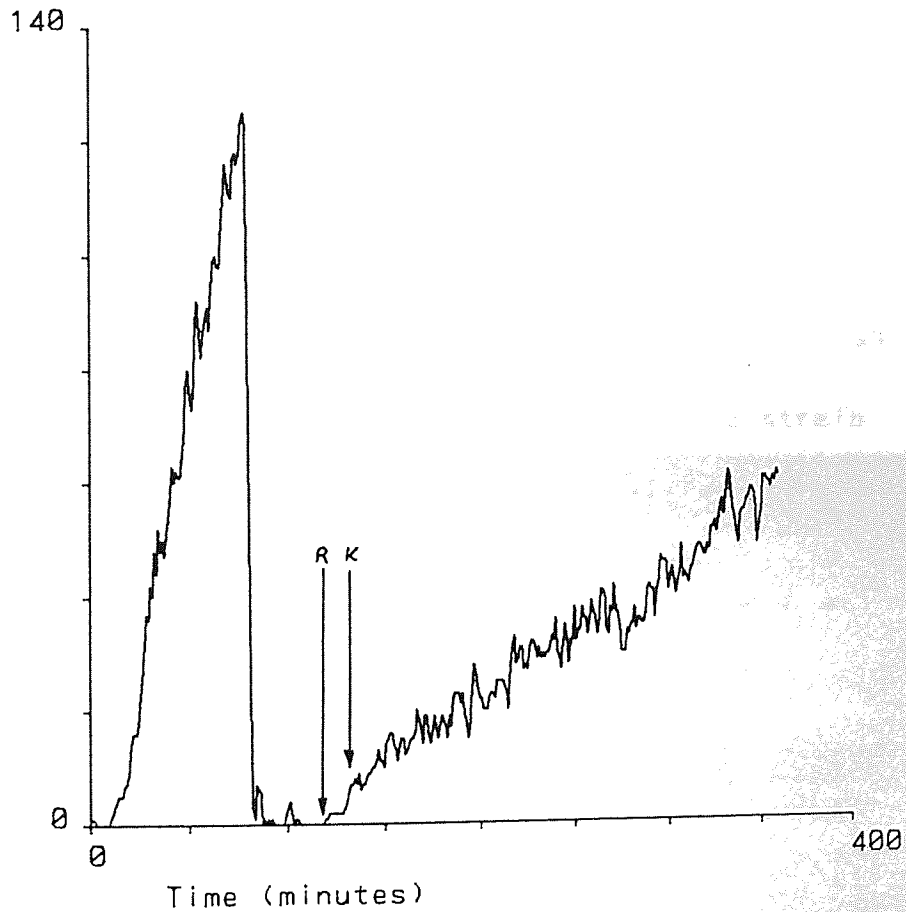
Figure 6.30 Test 94: Event rate/Time

Test 96

Stress Ratio
0.9

Y

k

R

0

0   25
Deviatoric strain
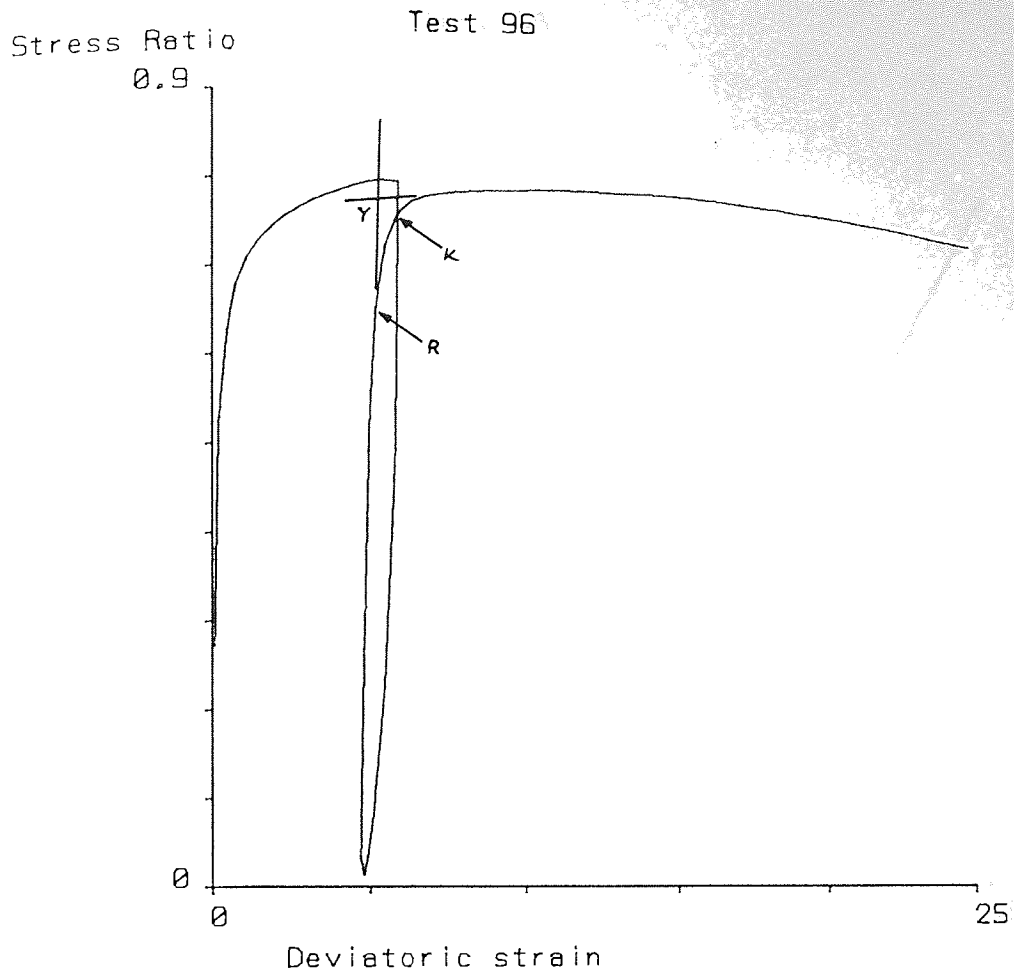
Figure 6.31 Test 96: Stress Ratio/Deviatoric strain

Test 96
Volumetric strain
1

0

-10

0   25
Deviatoric strain
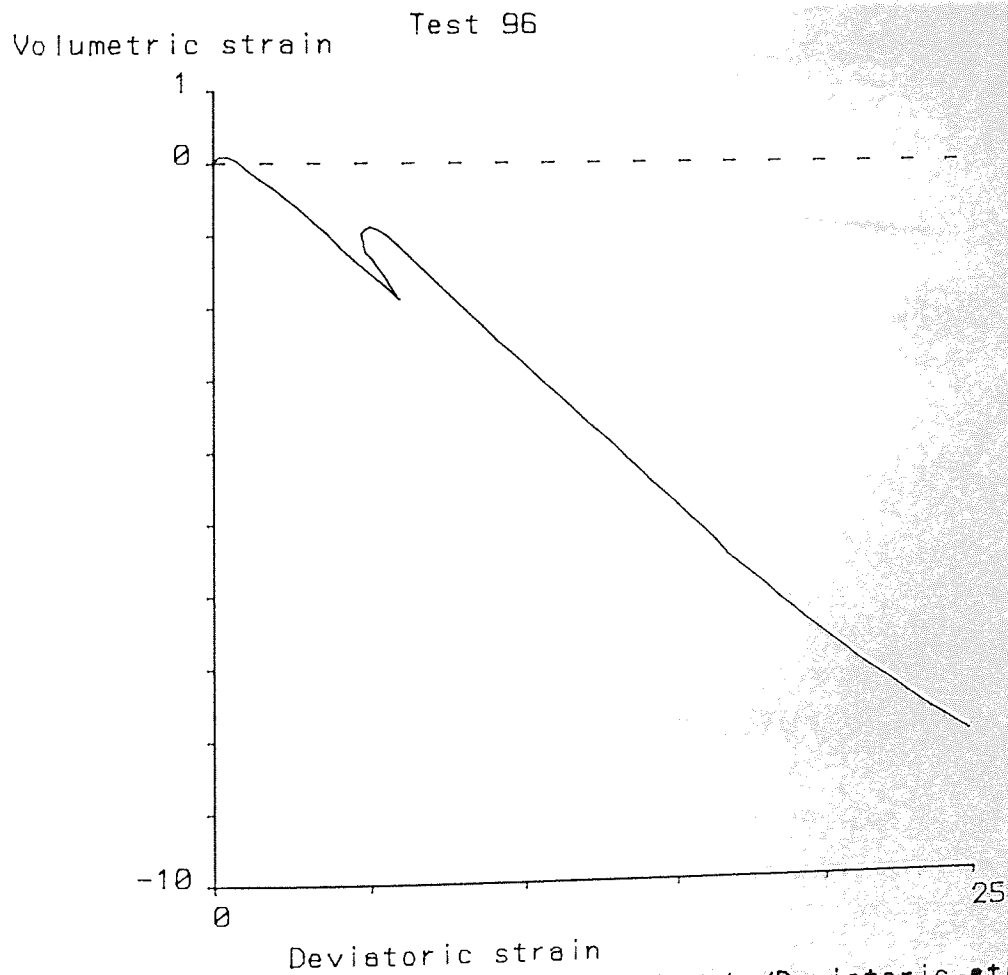
Figure 6.32 Test 96: Volumetric strain/Deviatoric strain

158

Test 96

Events
50000
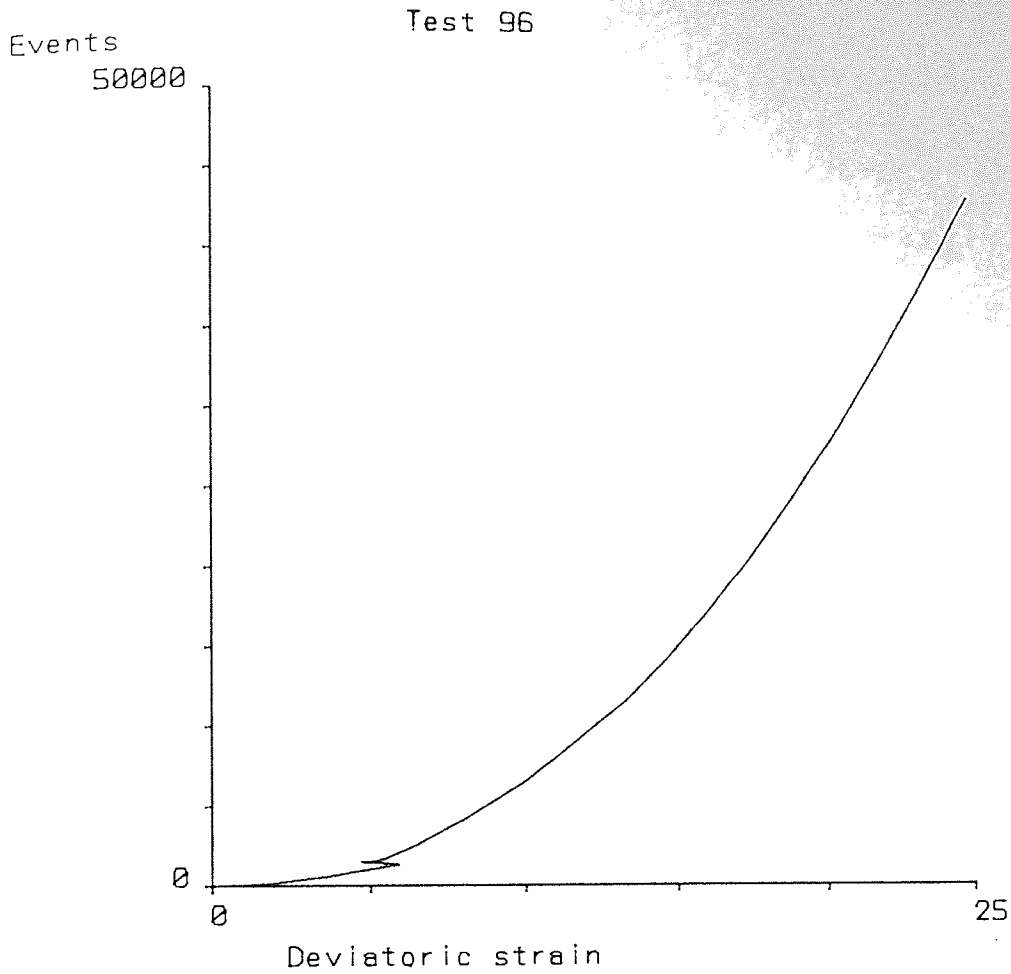
Deviatoric strain

Figure 6.33 Test 96: Events/Deviatoric strain

Test 96

Stress Ratio
0.9

Y
K
R
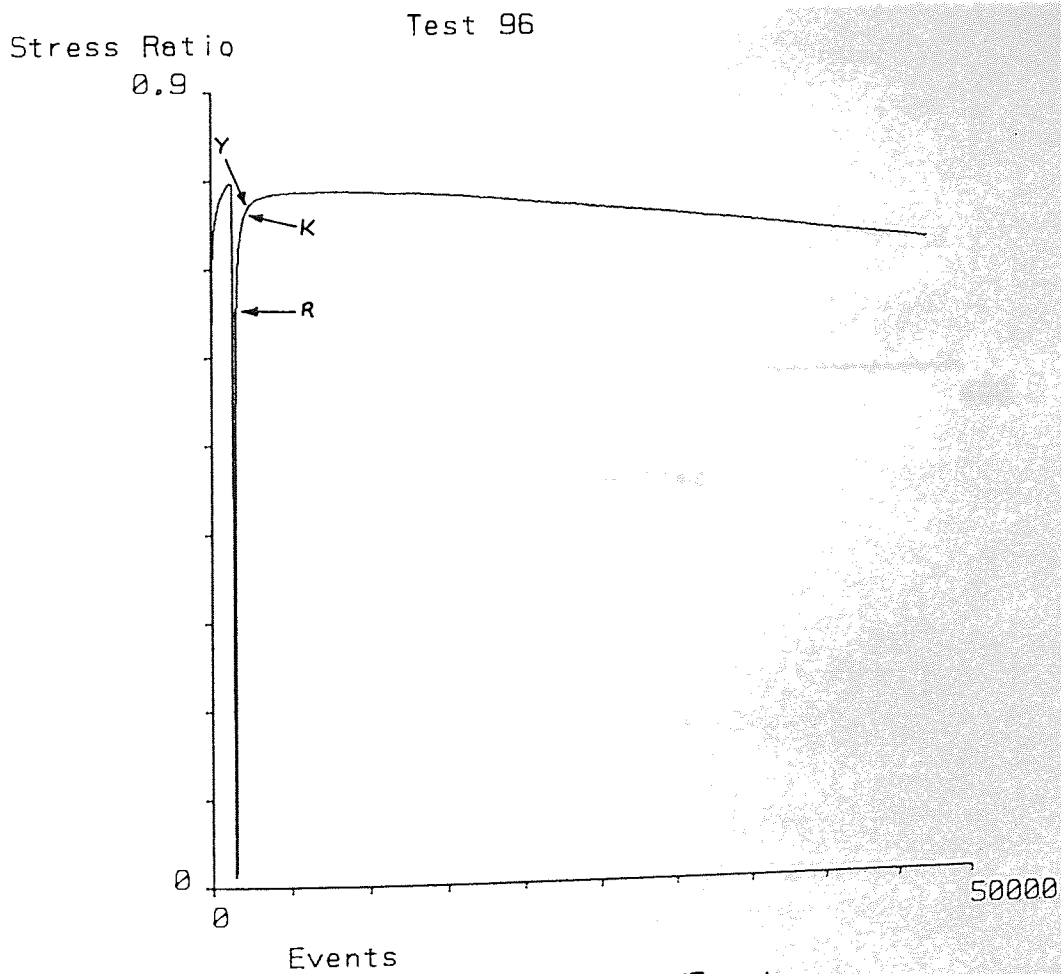
Events
50000

Figure 6.34 Test 96: Stress Ratio/Events

Test 96

Event rate (average)

350

R K

0

0   400

Time (minutes)

Figure 6.35 Test 96: Event rate/Time

Test 95

Stress Ratio
0.9

Deviatoric strain

Figure 6.36 Test 95: Stress Ratio/Deviatoric strain

Test 95

Volumetric strain
1

0

-10

Deviatoric strain

Figure 6.37 Test 95: Volumetric strain/Deviatoric strain

161

Test 95

Events
80000

0
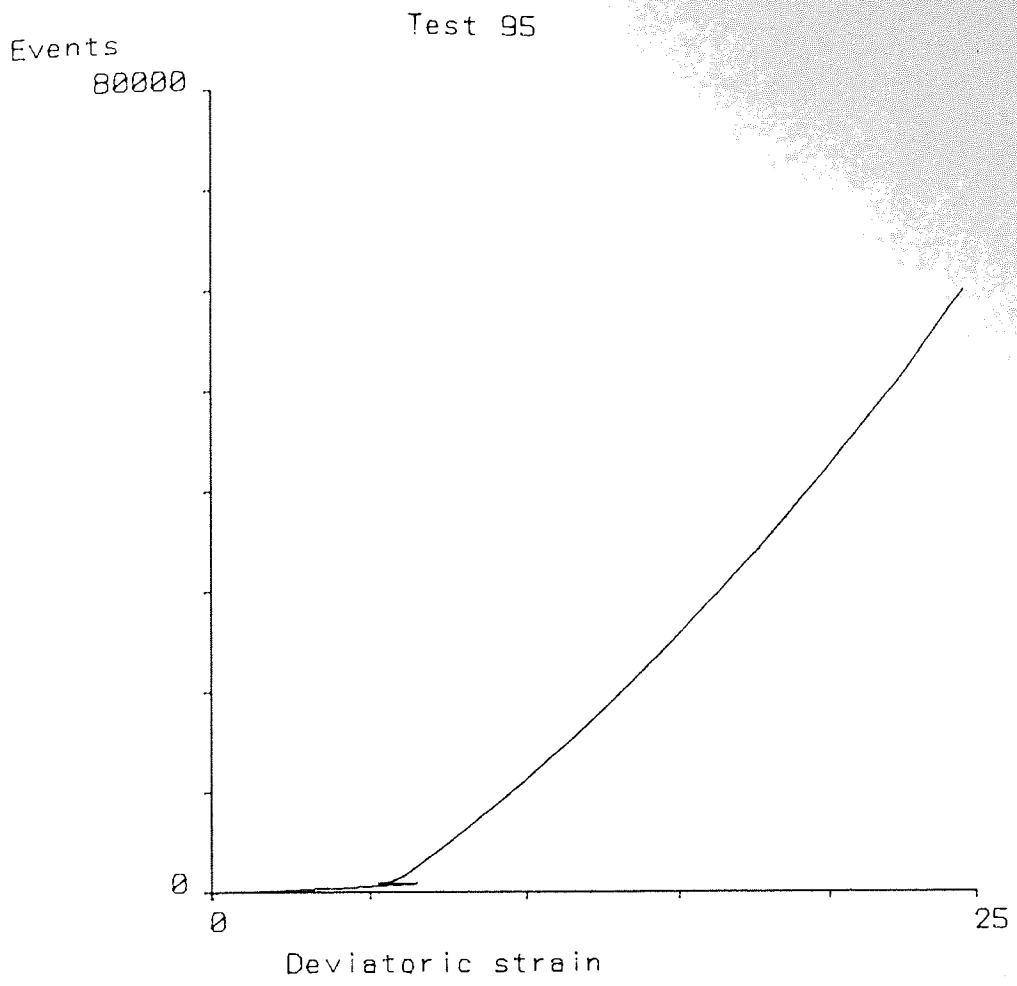
0   25
                  Deviatoric strain
Figure 6.38 Test 95: Events/Deviatoric strain

Test 95
Stress Ratio
0.9

Y

K

R
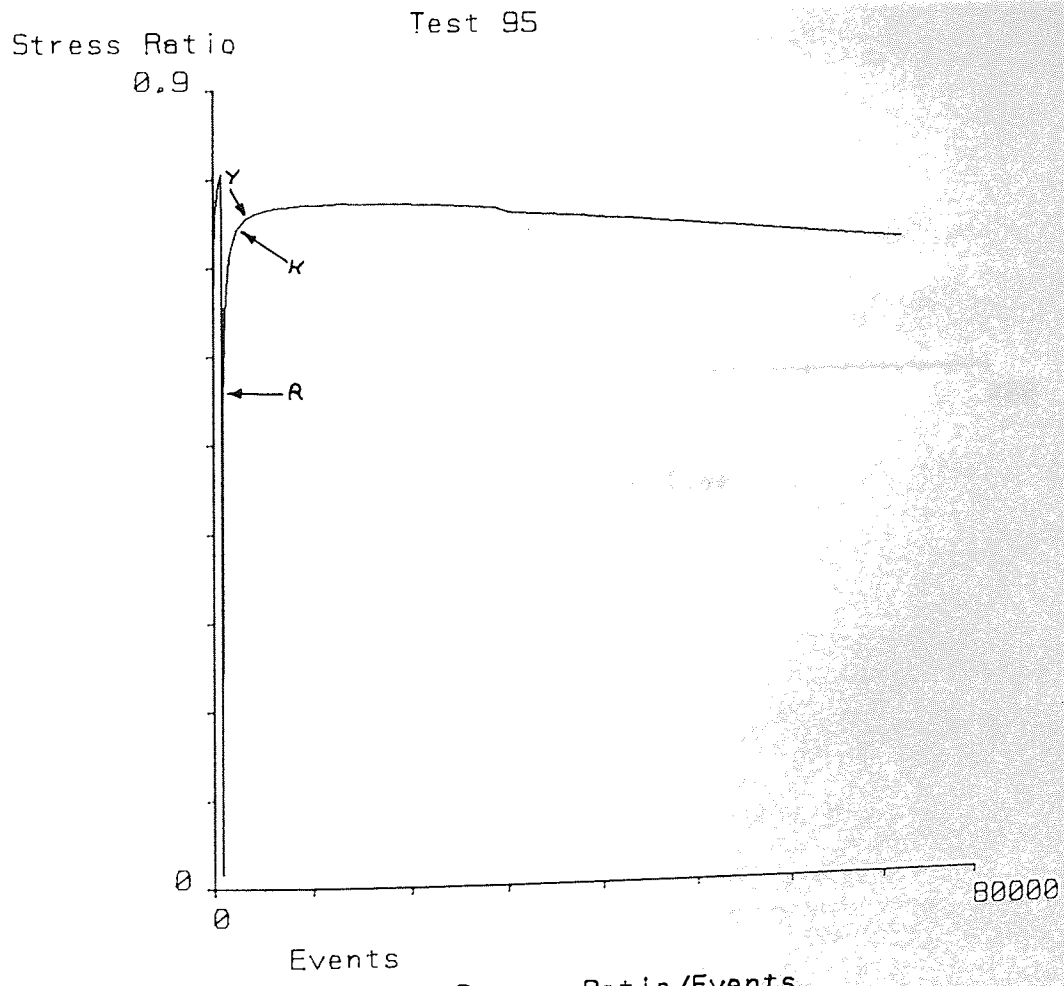
0
0   80000
              Events
Figure 6.39 Test 95: Stress Ratio/Events

162
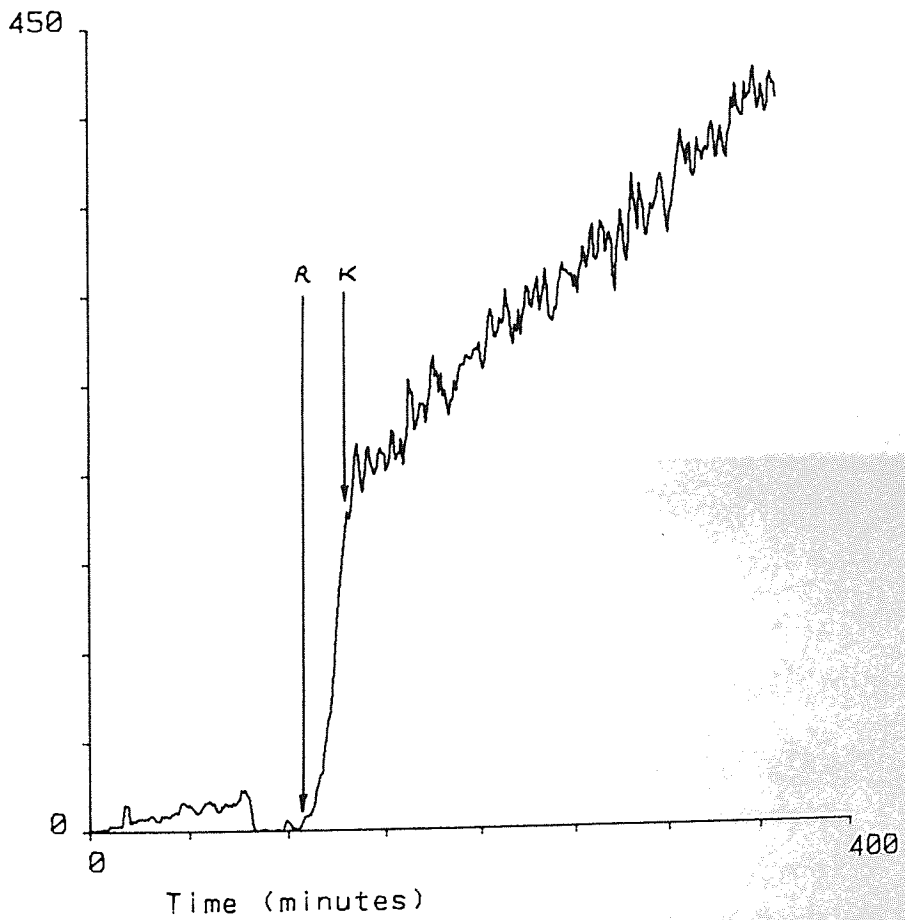
Figure 6.40 Test 95: Event rate/Time
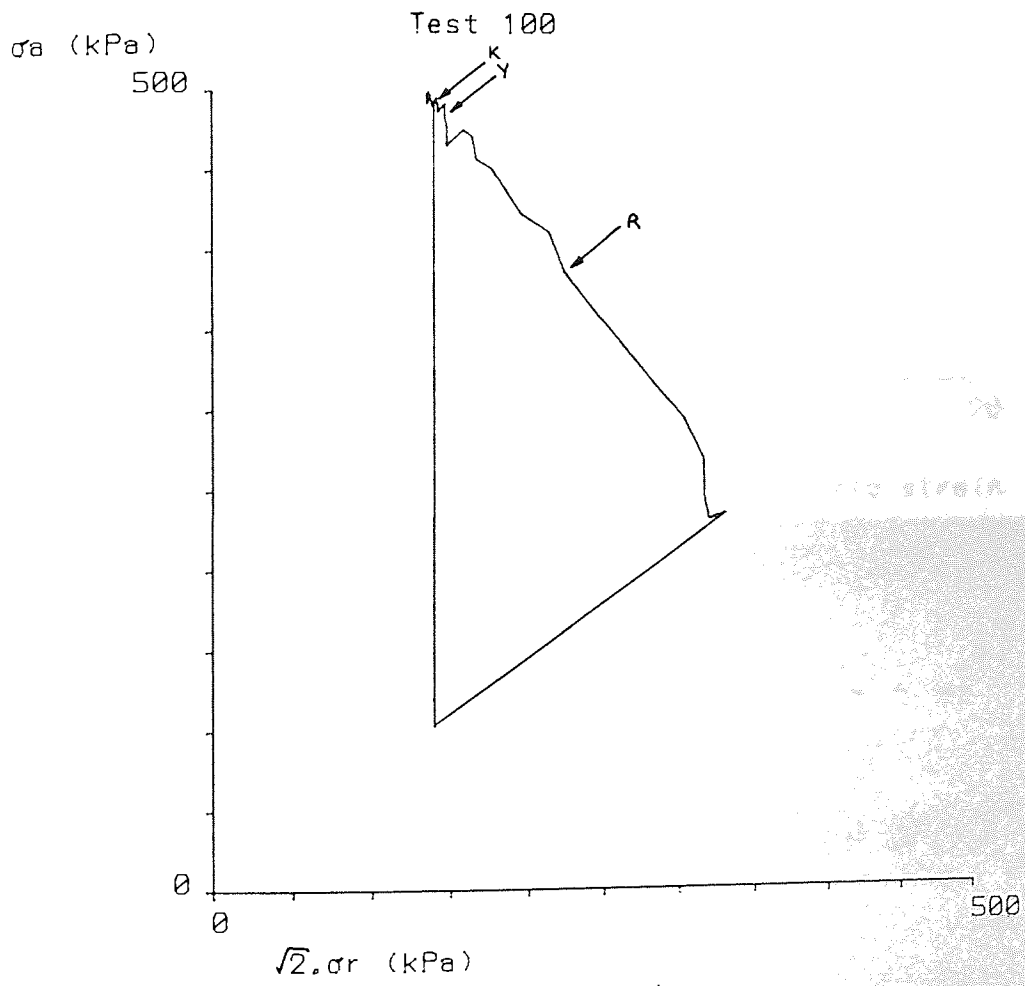
Figure 6.41 Test 100: Stress path
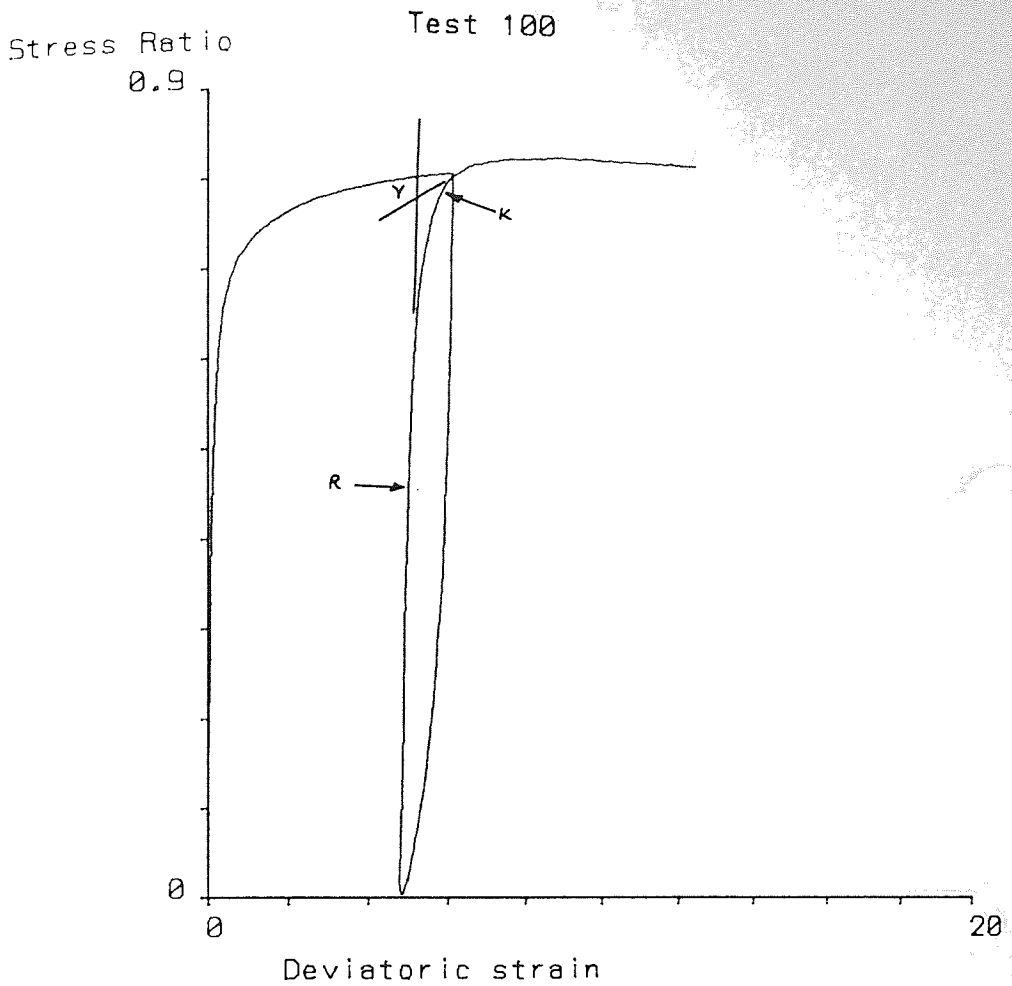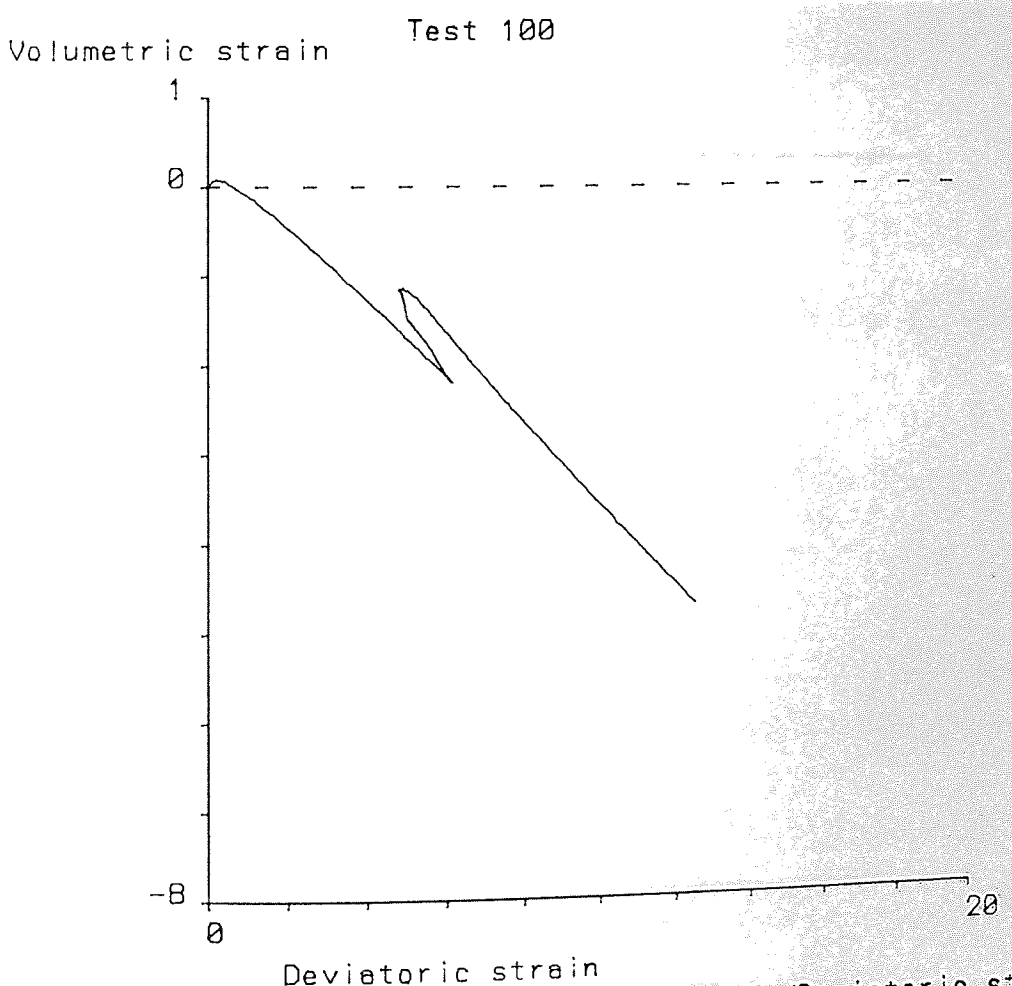
Figure 6.42 Test 100: Stress Ratio/Deviatoric strain

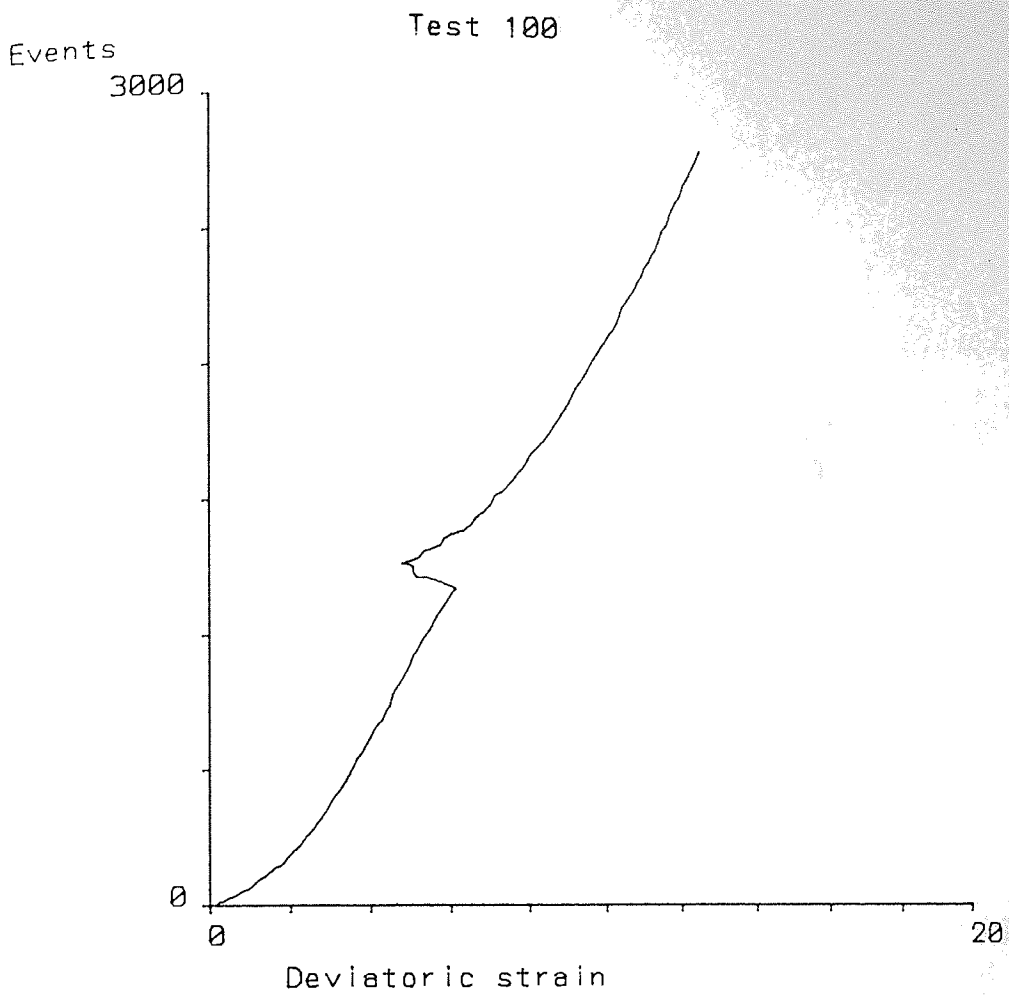

Figure 6.43 Test 100: Volumetric strain/Deviatoric strain

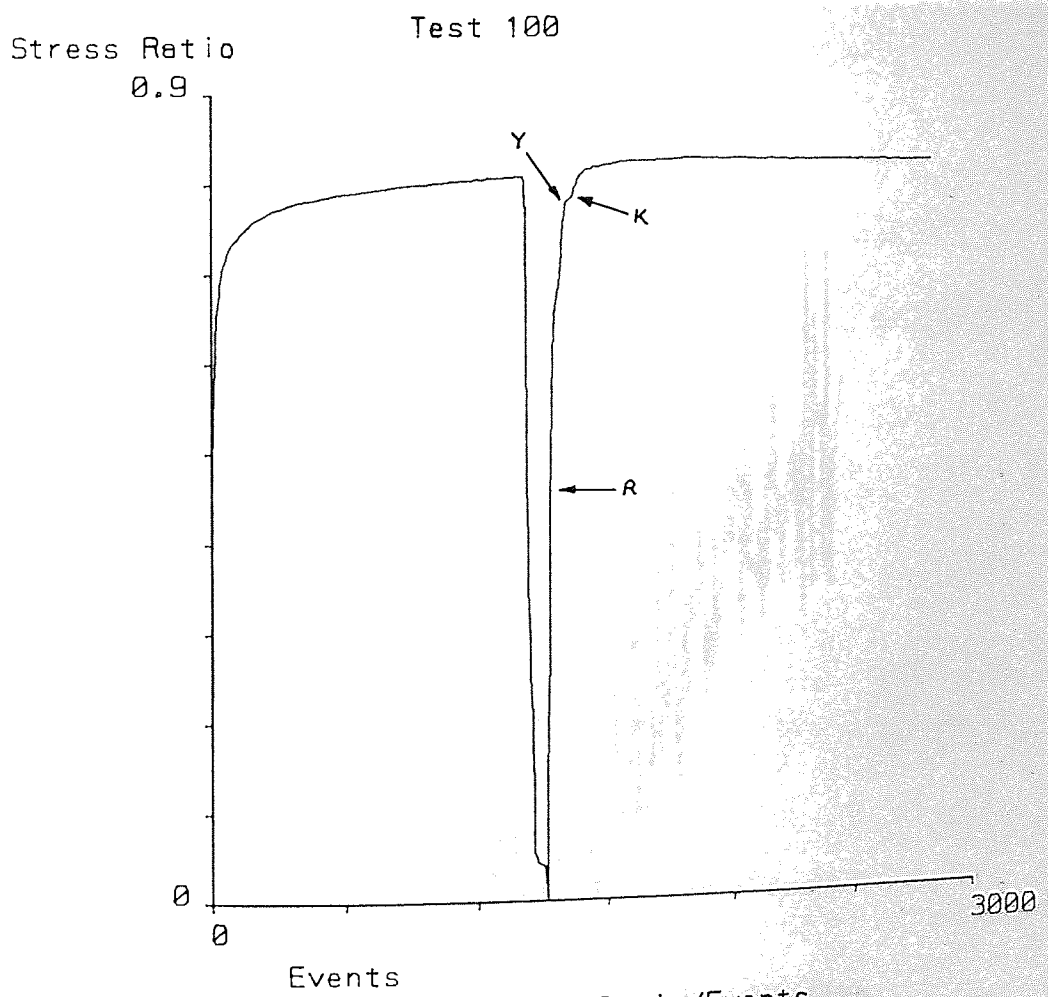Figure 6.44 Test 100: Events/Deviatoric strain

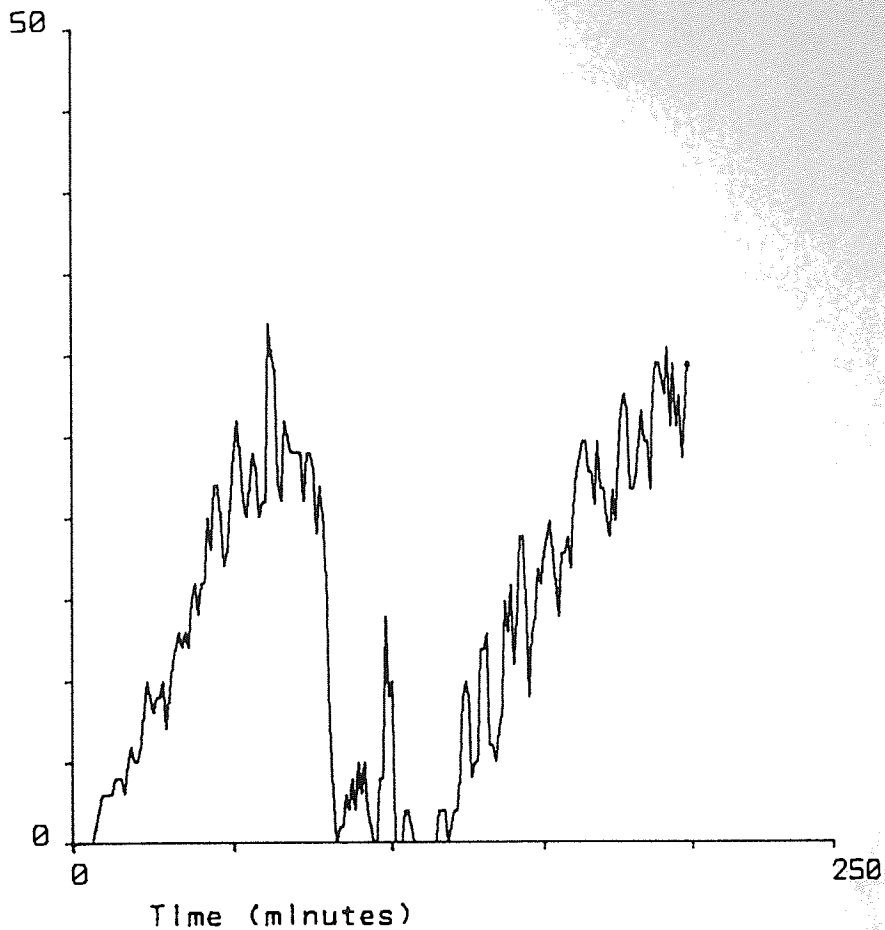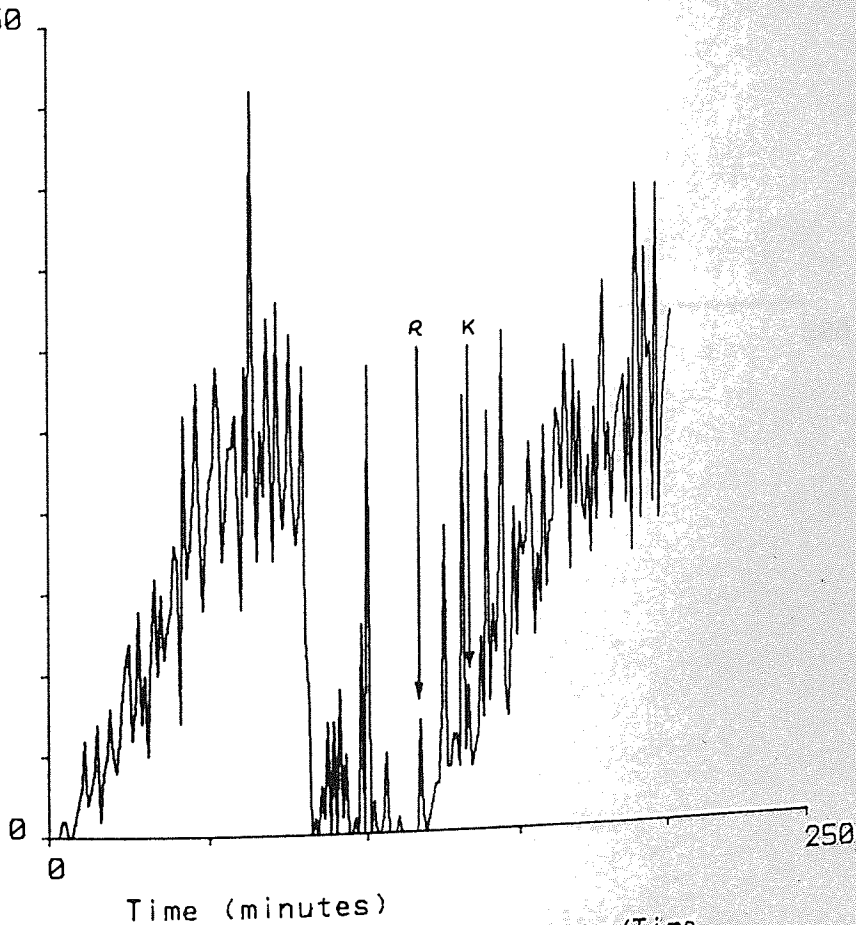Figure 6.45 Test 100: Stress Ratio/Events

Figure 6.46 Test 100: Event rate/Time

Figure 6.47 Test 100: Actual event rate/Time

167

Test 98

σa (kPa)

500

0

0

√2.σr (kPa)

500

Figure 6.48 Test 98: Stress path

Test 98

Stress Ratio
0.9

Y

0

0   20

Deviatoric strain

Figure 6.49 Test 98: Stress Ratio/Deviatoric strain

Test 98

Volumetric strain

1

0

-8

0   20

Deviatoric strain

Figure 6.50 Test 98: Volumetric strain/Deviatoric strain

169

Test 98

Events
1400

Deviatoric strain

Figure 6.51 Test 98: Events/Deviatoric strain

Test 98

Stress Ratio
0.9

Events

Figure 6.52 Test 98: Stress Ratio/Events

170
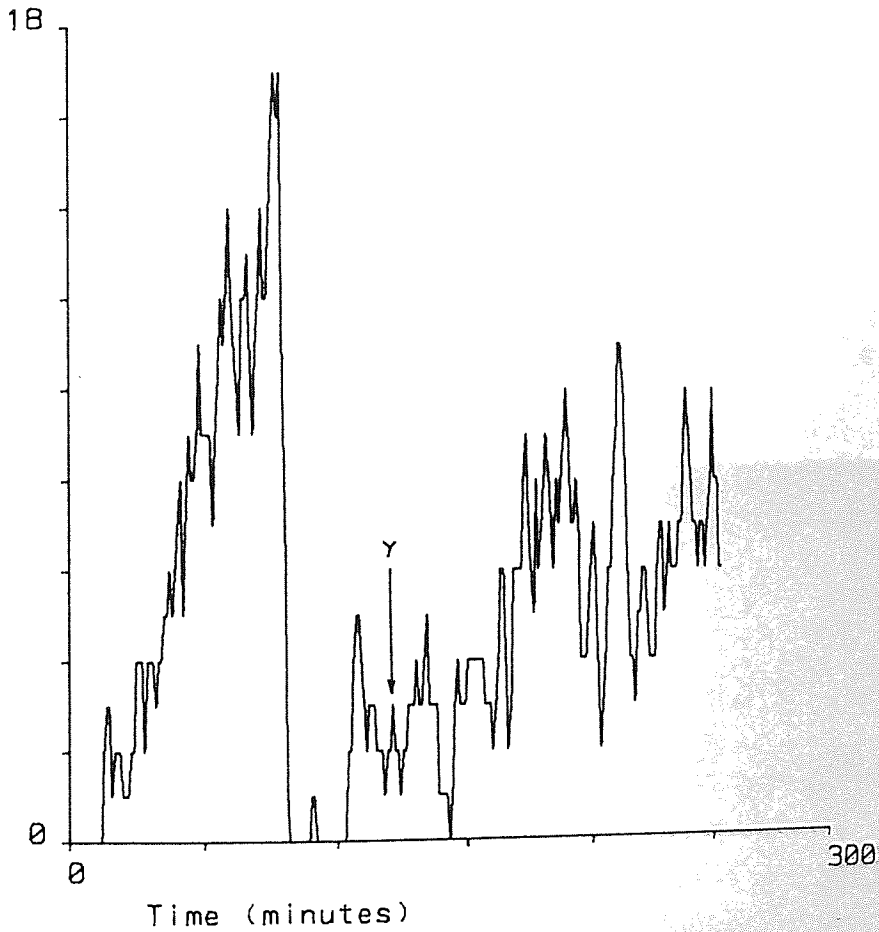
Figure 6.53 Test 98: Event rate/Time

Test 99

σa (kPa)
900

K
R
Y

0

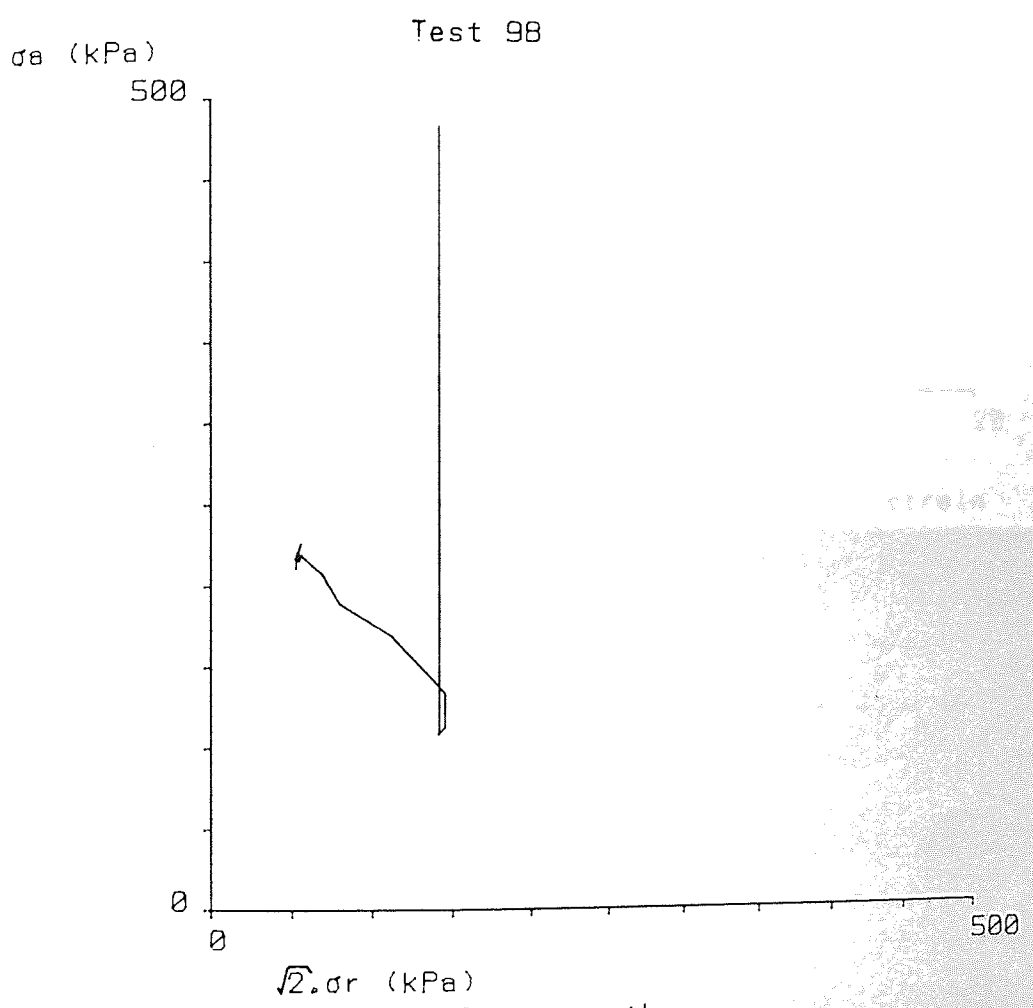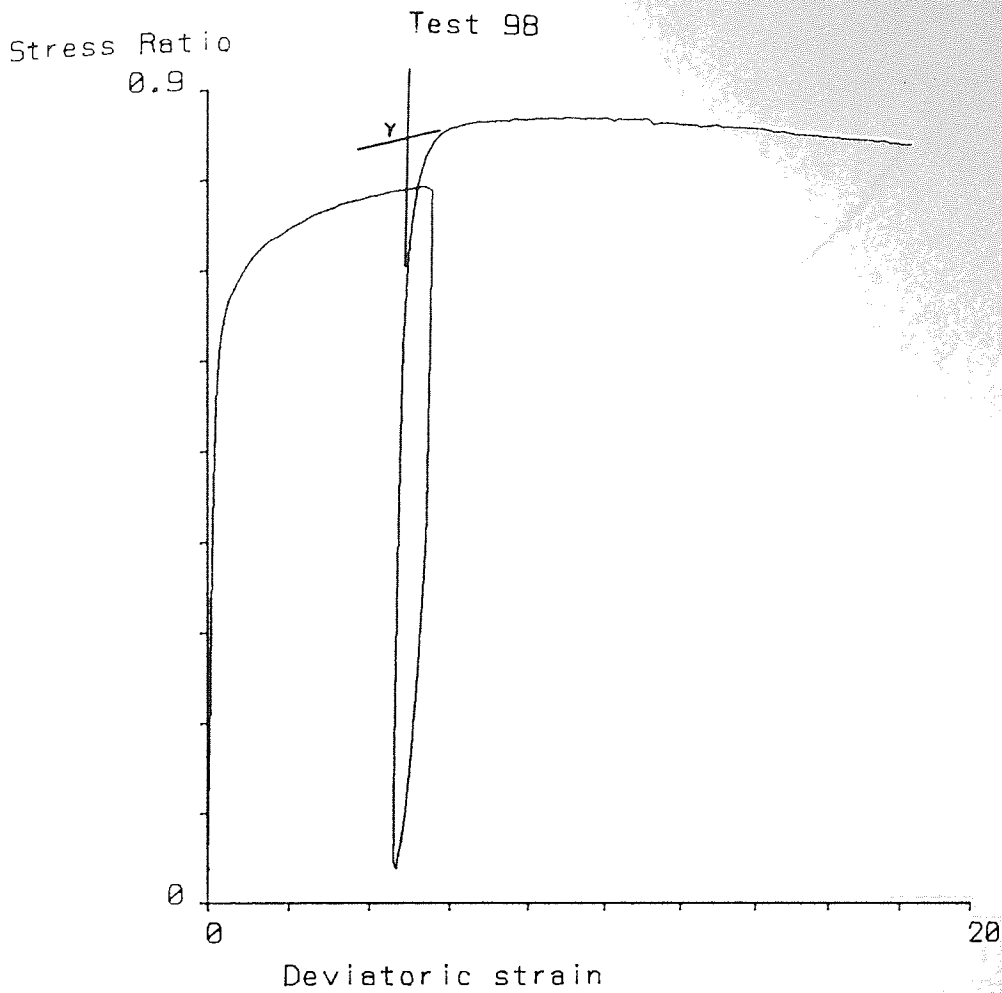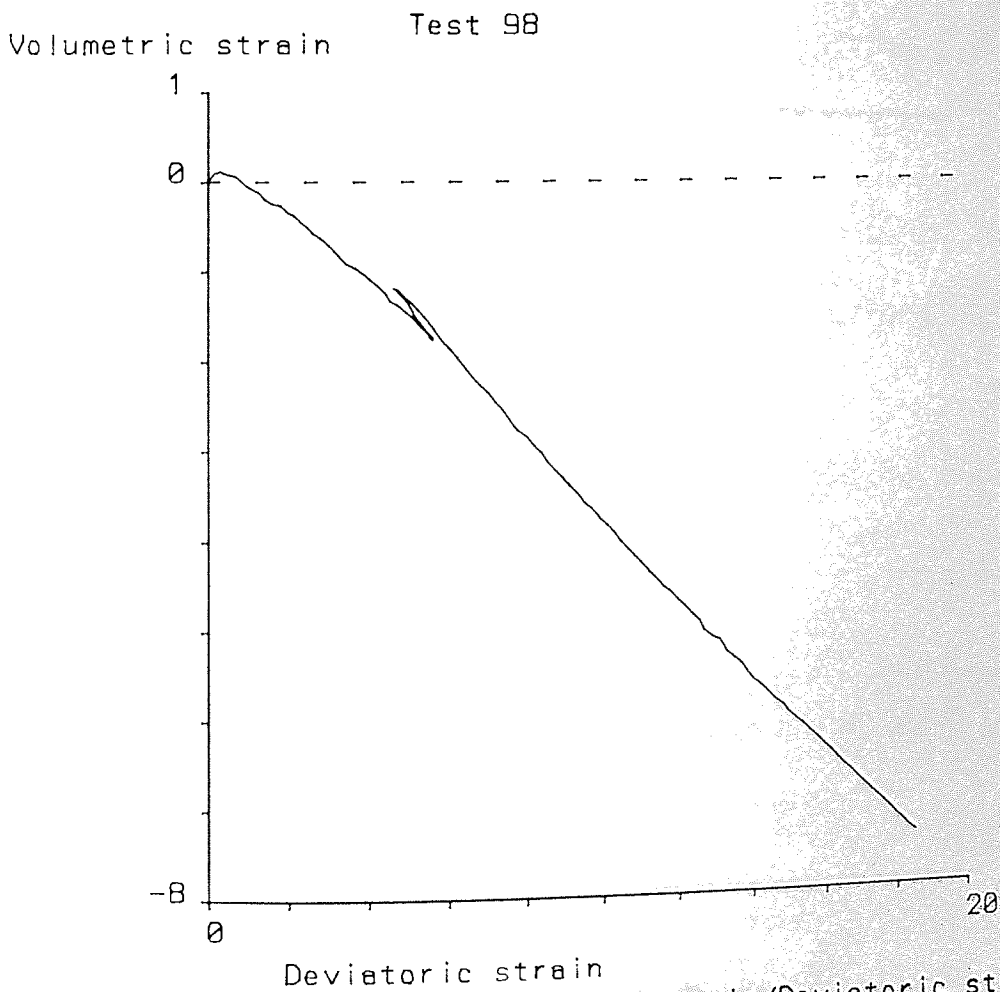0   900

√2.σr (kPa)
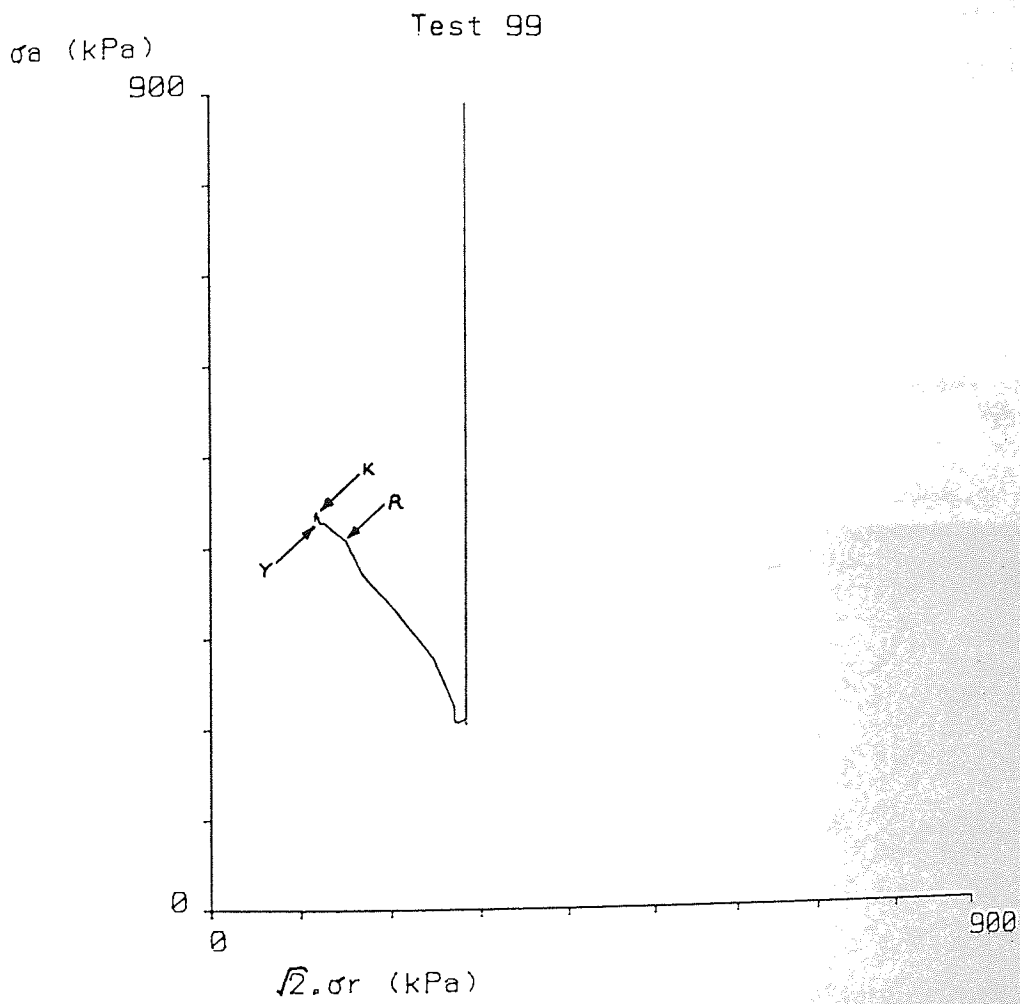
Figure 6.54 Test 99: Stress path
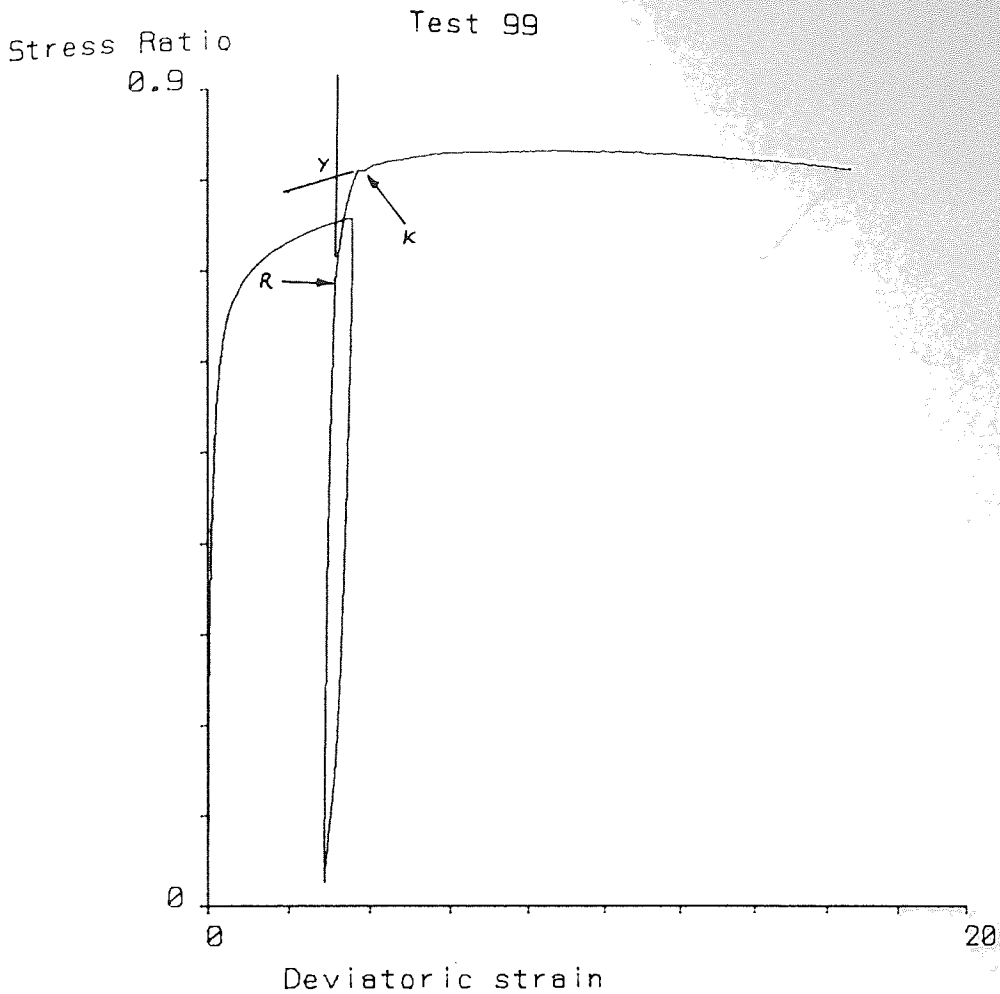
Figure 6.55 Test 99: Stress ratio/Deviatoric strain
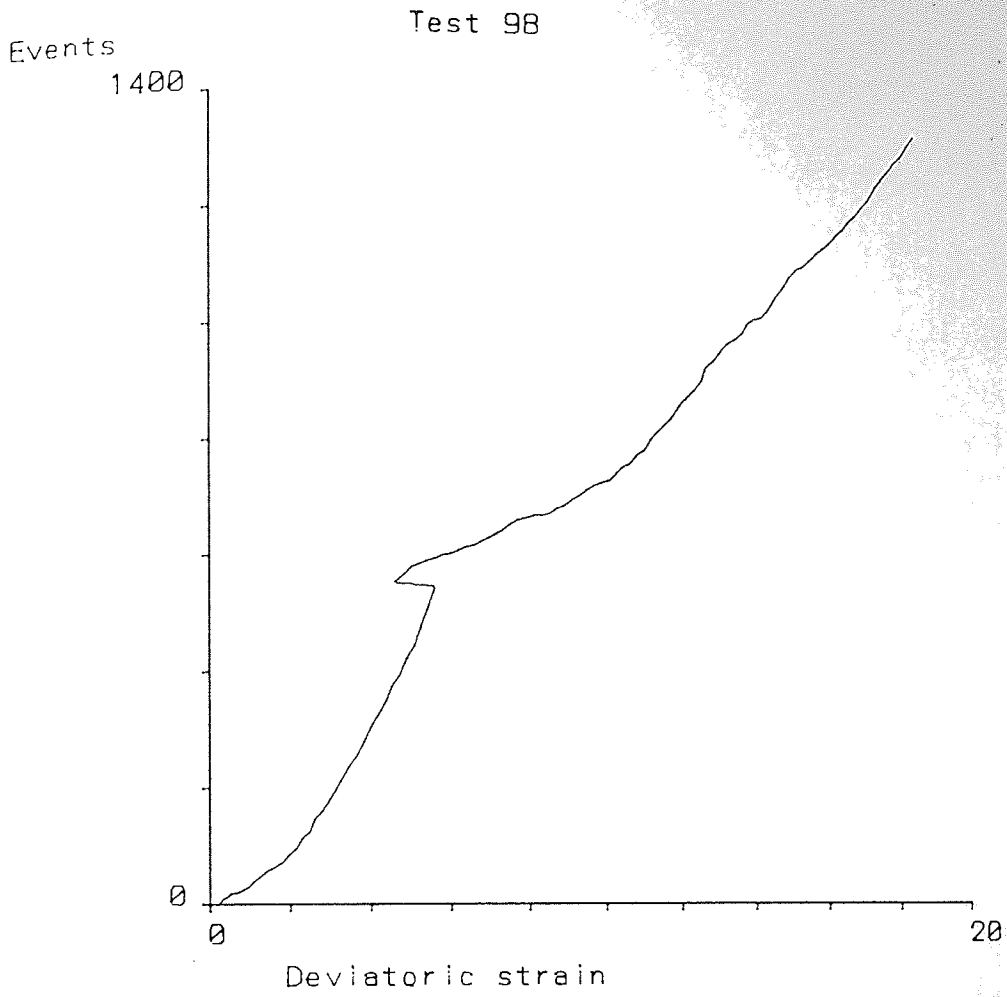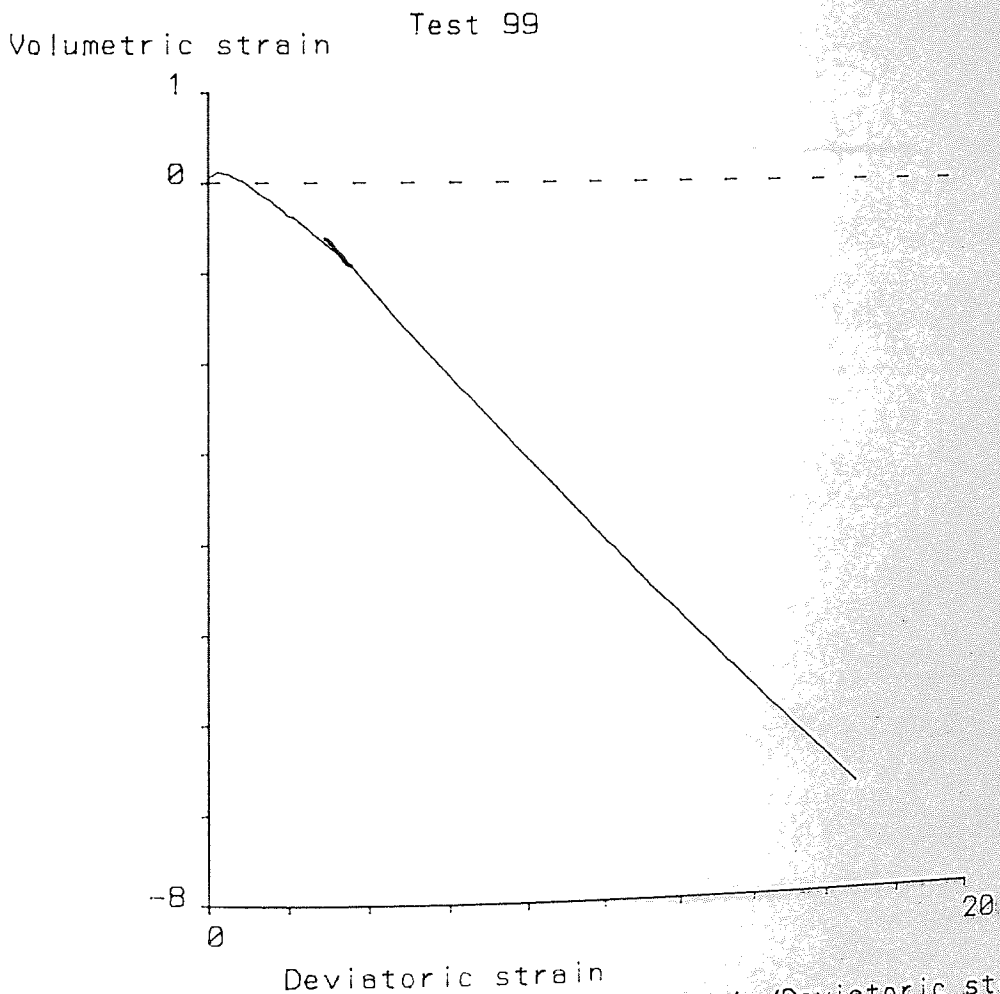

Figure 6.56 Test 99: Volumetric strain/Deviatoric strain

173

Test 99

Events
5000

0

0   20
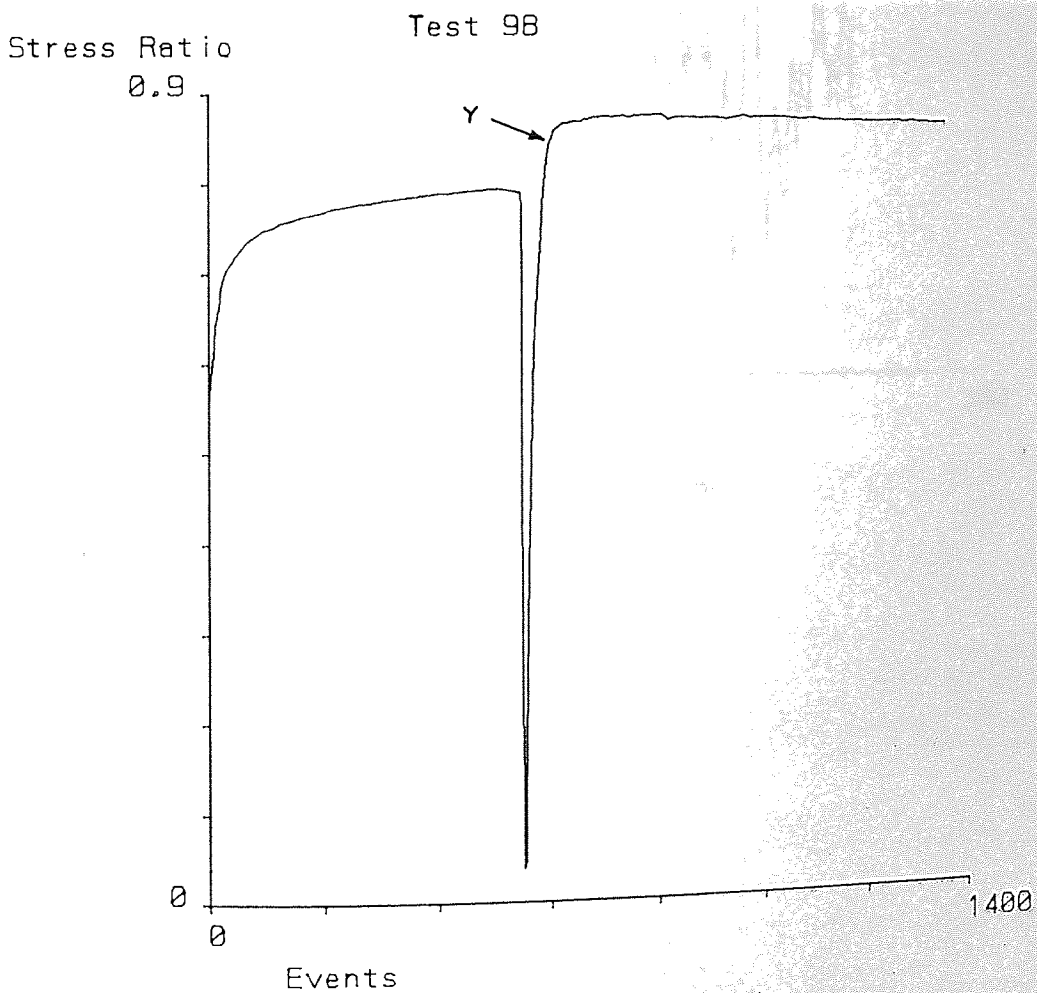   Deviatoric strain
   Figure 6.57 Test 99: Events/Deviatoric strain

Test 99

Stress Ratio
0.9

Y →
         ← K
      ← R

0
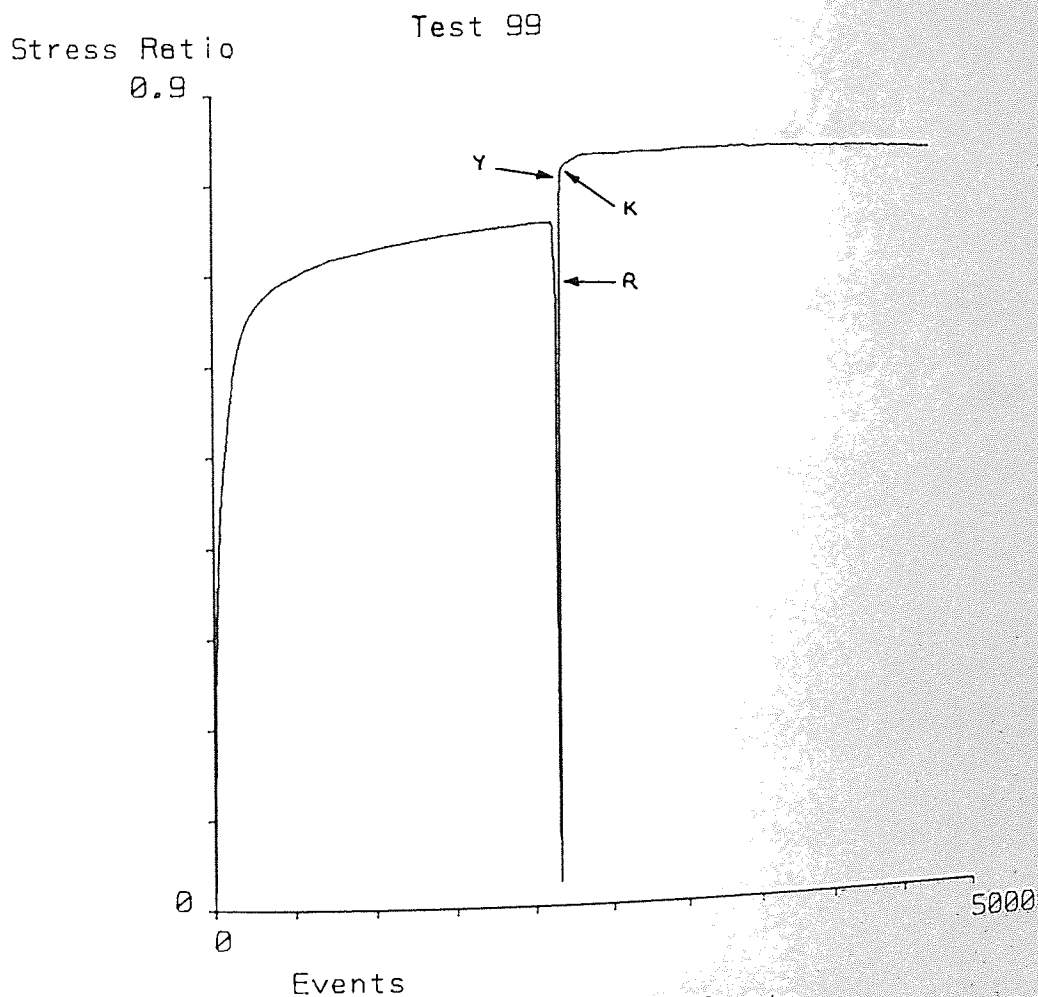
0   5000
                    Events
   Figure 6.58 Test 99: Stress Ratio/Events
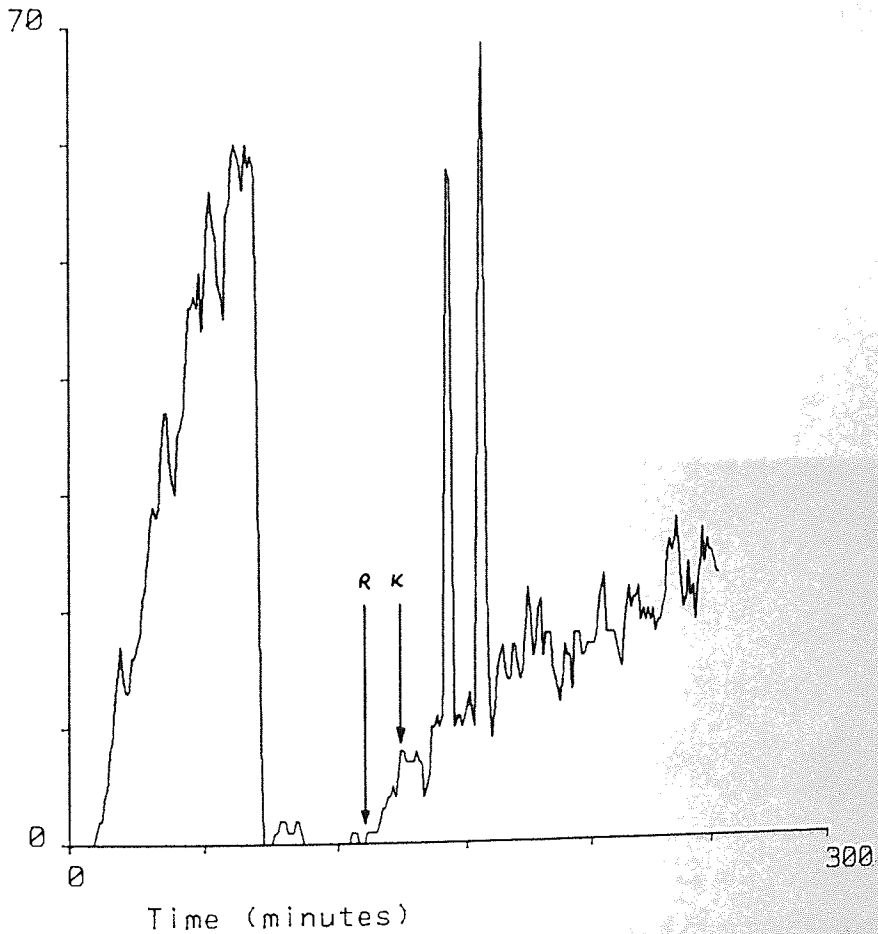
Figure 6.59 Test 99: Event rate/Time
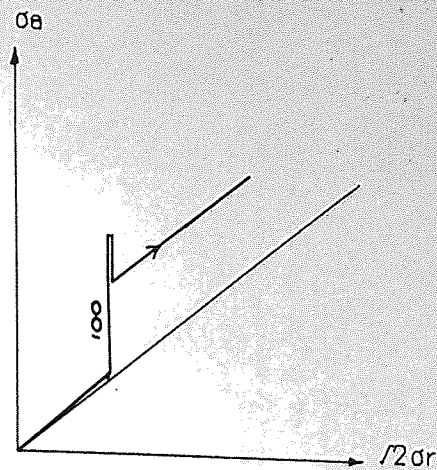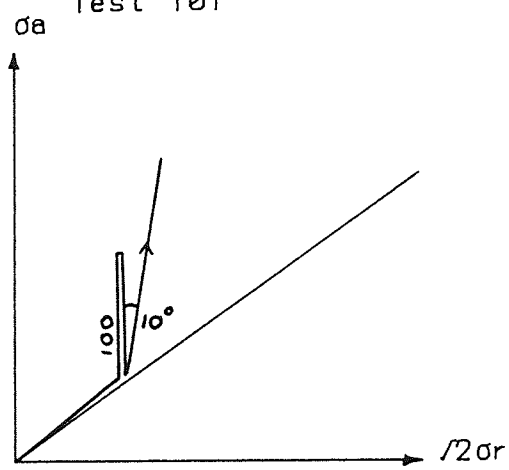
Figure 6.60 Stress paths
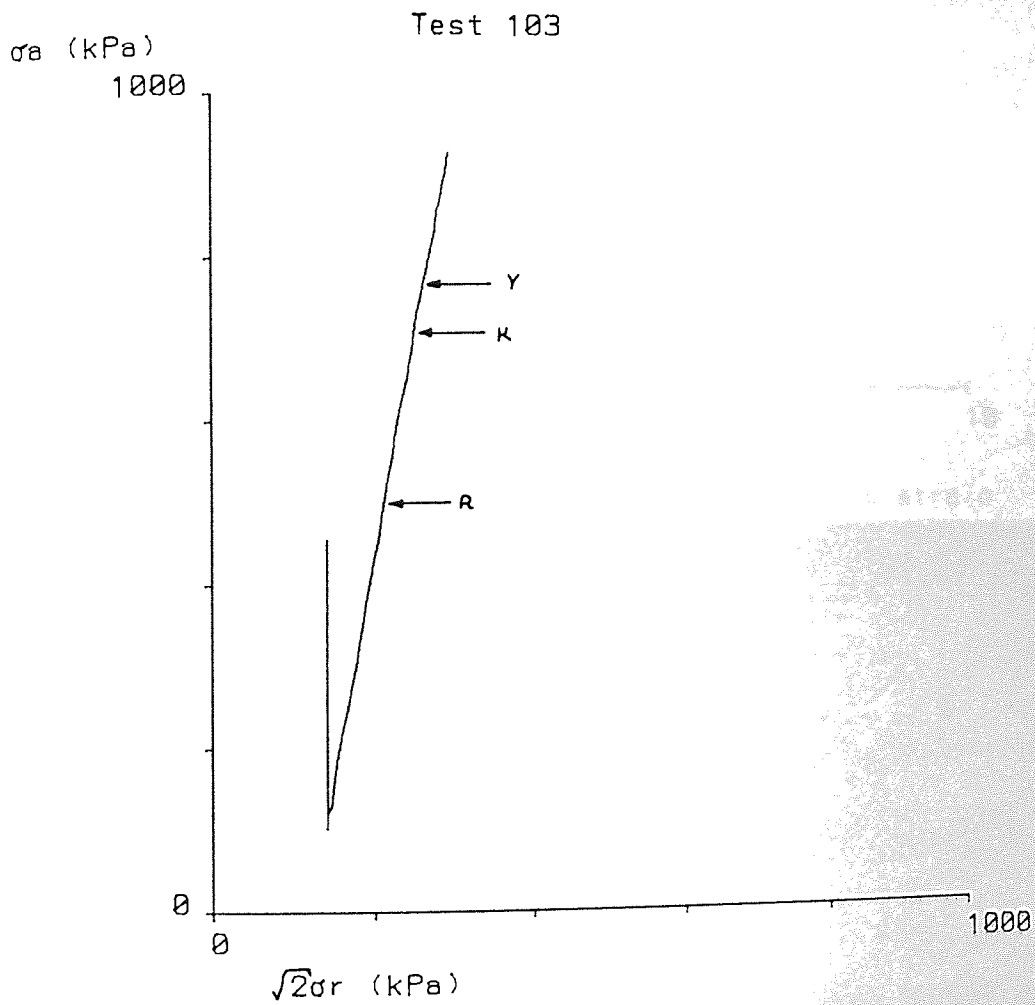
Figure 6.61 Test 103: Stress path

Test 103

Stress Ratio

0.8

Y

K

R

0
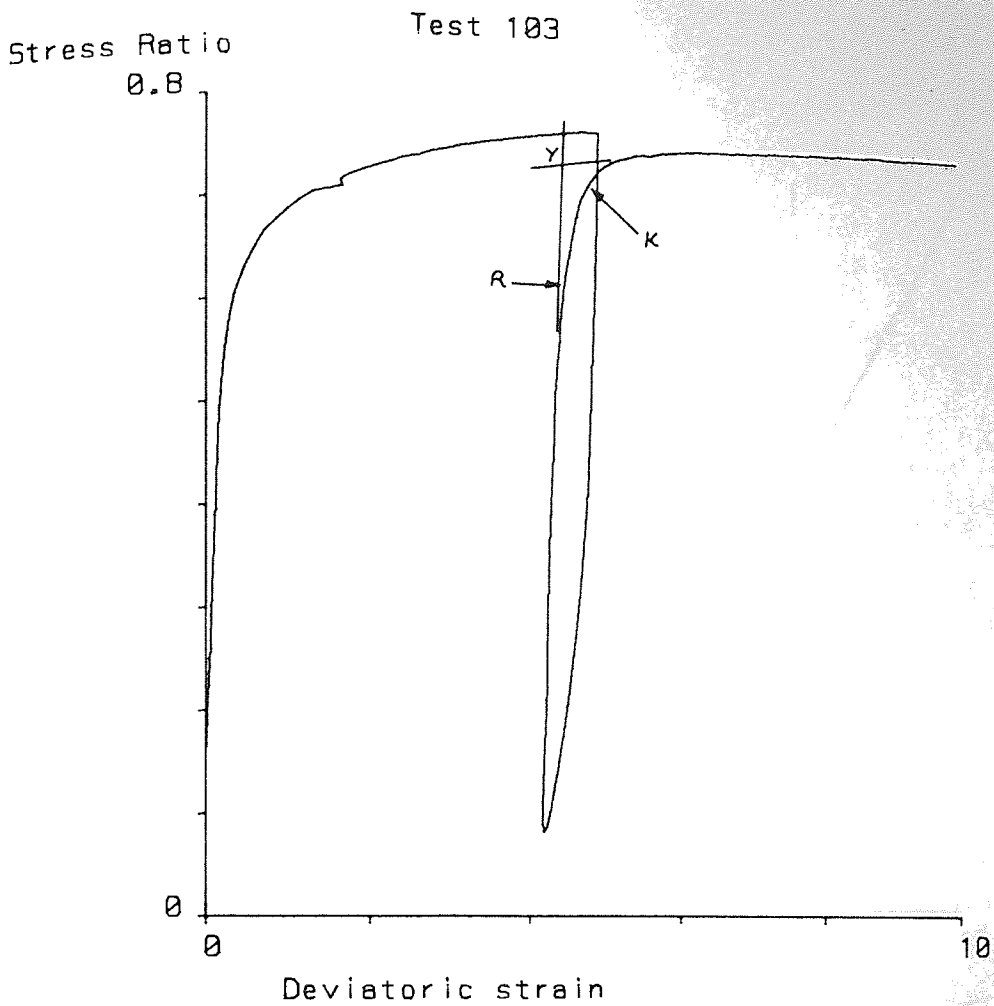
0   10
        Deviatoric strain
Figure 6.62 Test 103: Stress Ratio/Deviatoric strain

Test 103

Volumetric strain

0.5

0

-3.5
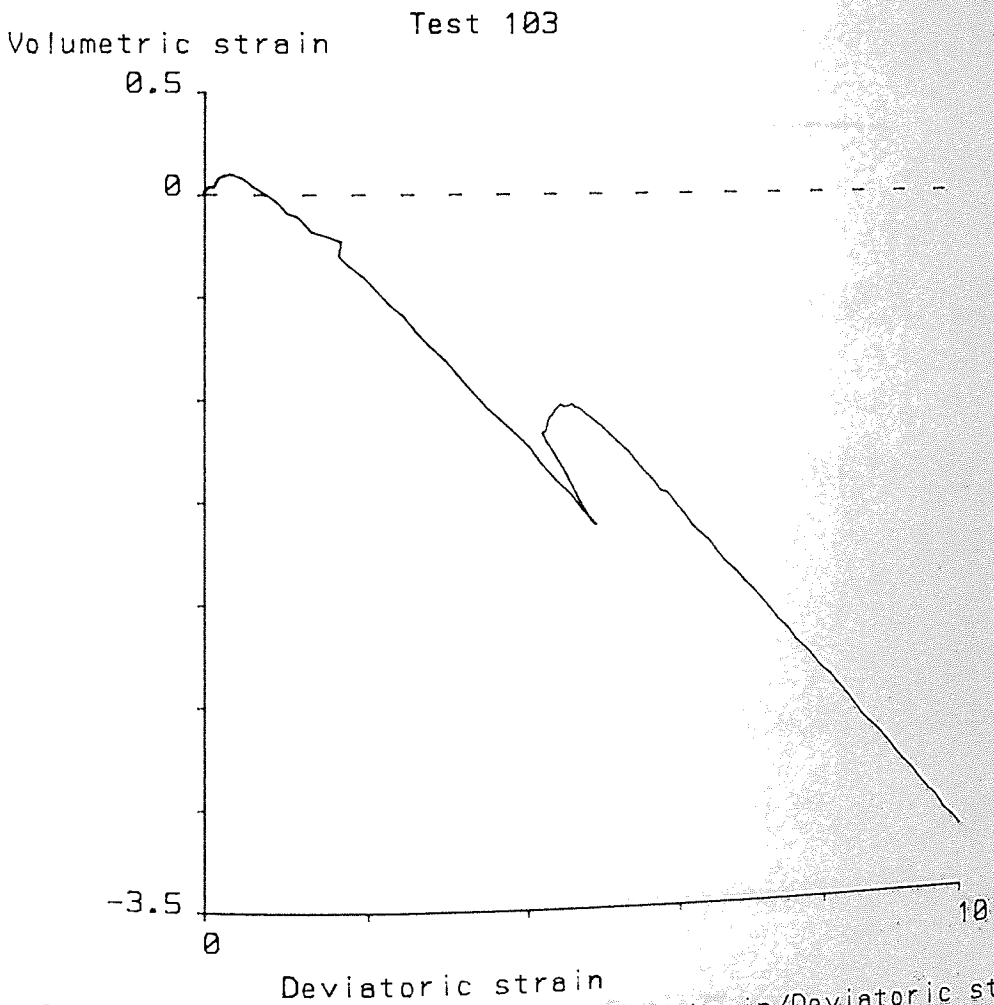
0   10
        Deviatoric strain
Figure 6.63 Test 103: Volumetric strain/Deviatoric strain

Test 103

Events
7000
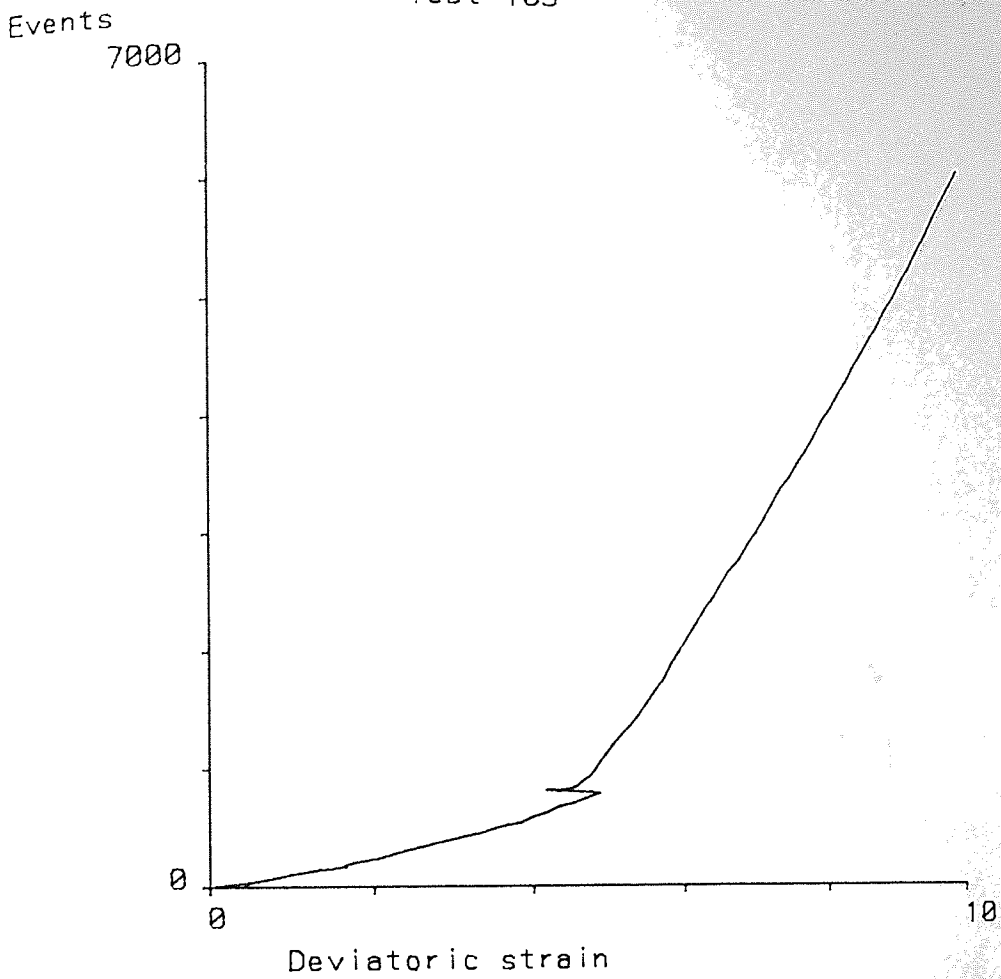
Deviatoric strain
Figure 6.64 Test 103: Events/Deviatoric strain

Test 103
Stress Ratio
0.8

Y
K
R

0

0   7000
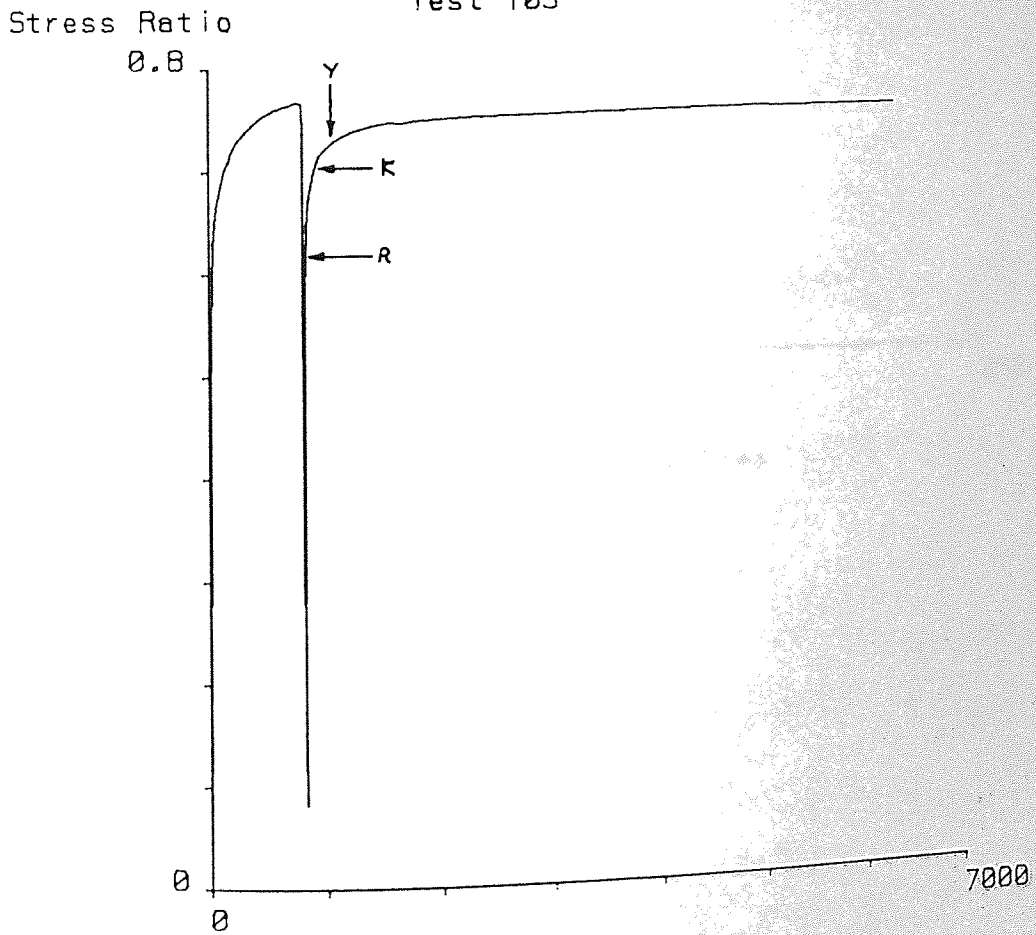
Events
Figure 6.65 Test 103: Stress Ratio/Events
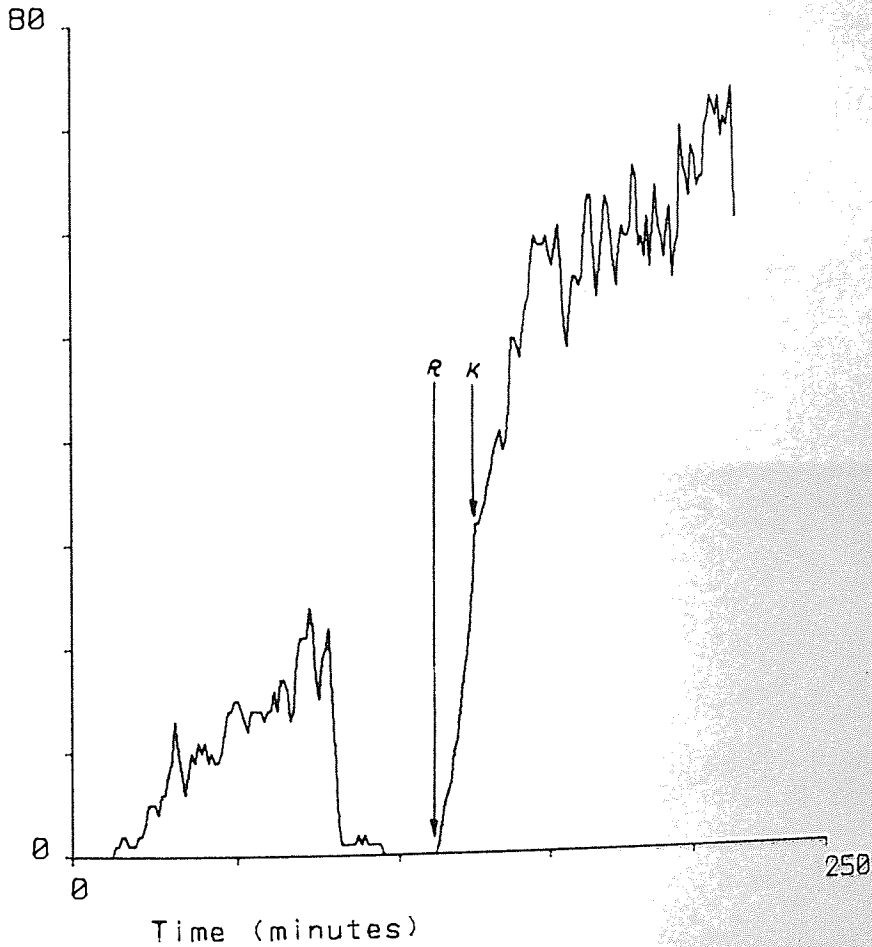
Figure 6.66 Test 103: Event rate/Time
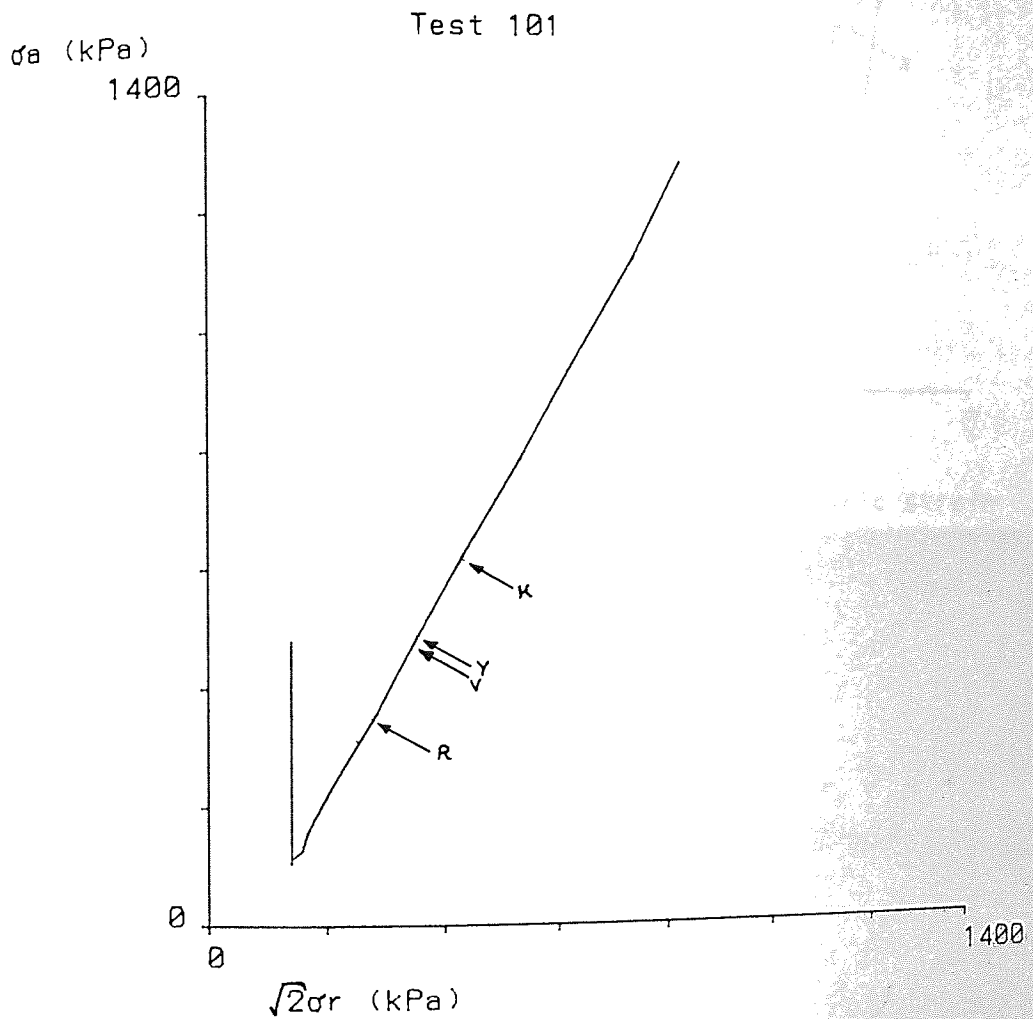
Test 101

Figure 6.67 Test 101: Stress path
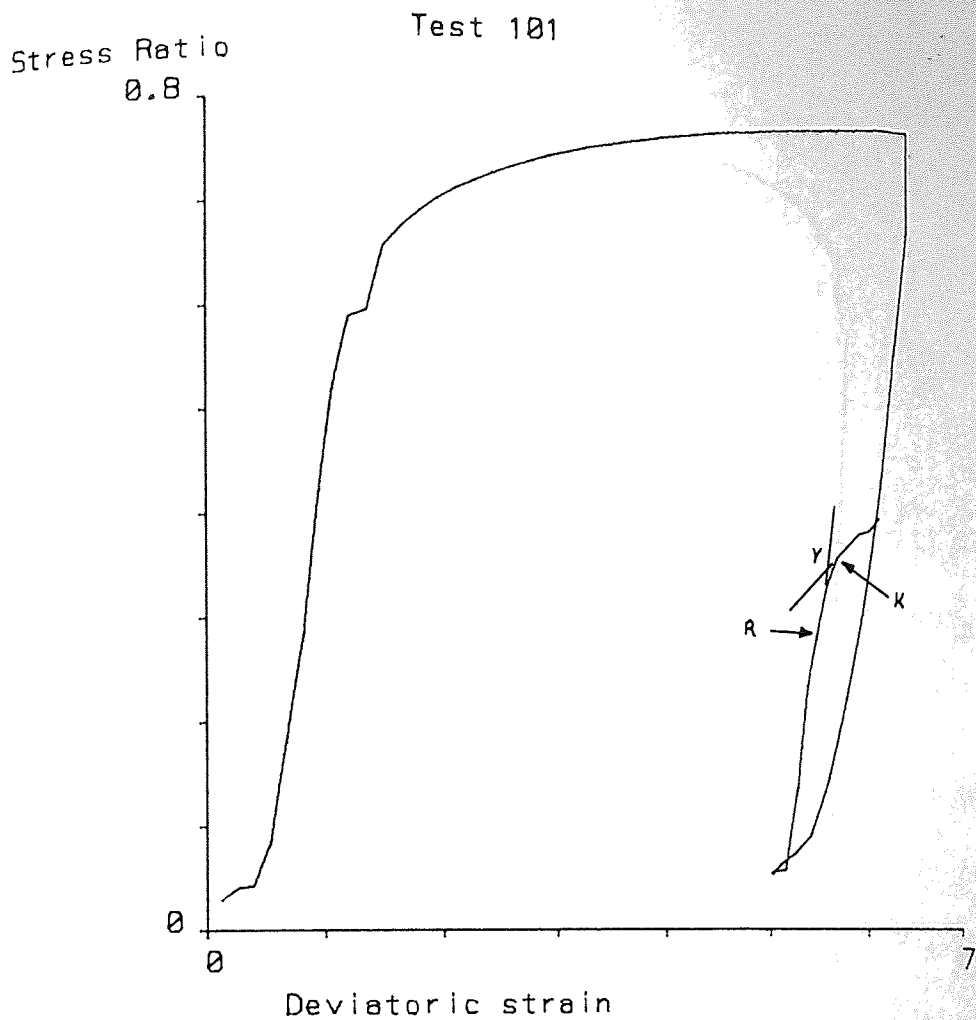
Figure 6.68 Test 101: Stress Ratio/Deviatoric strain
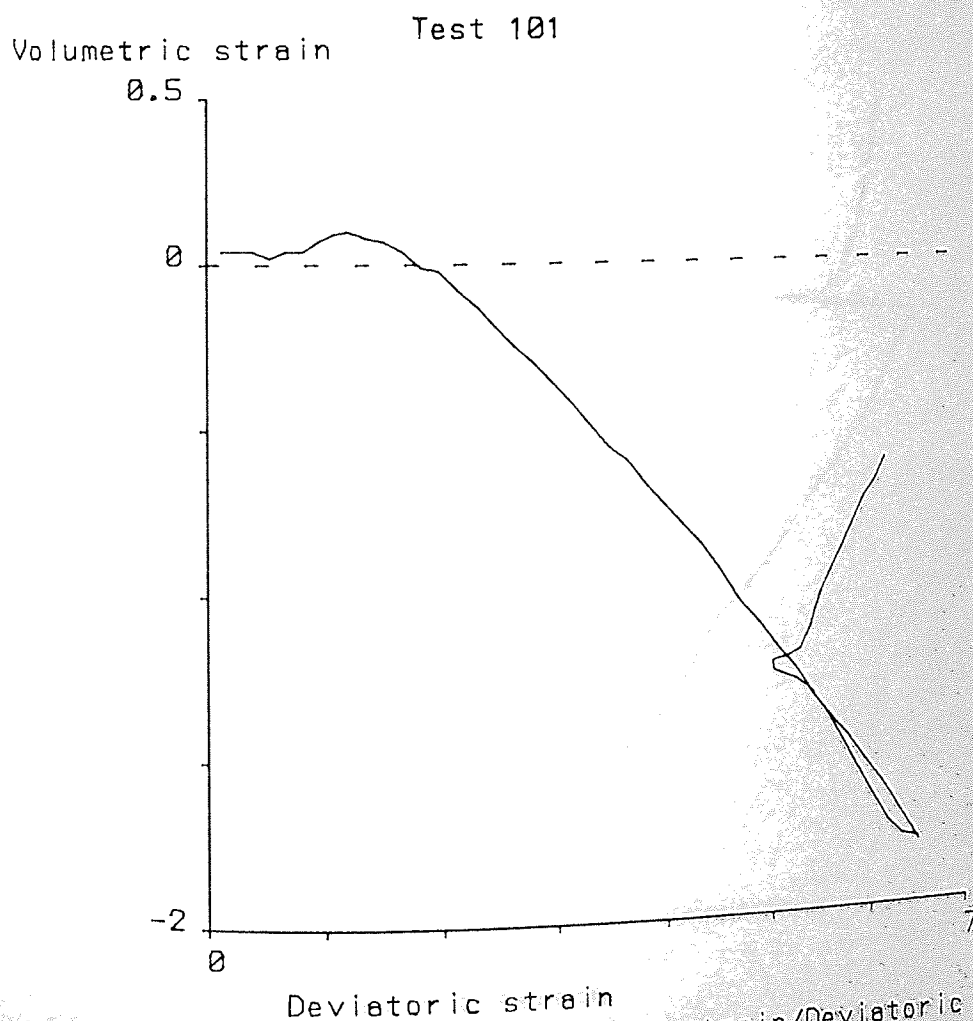
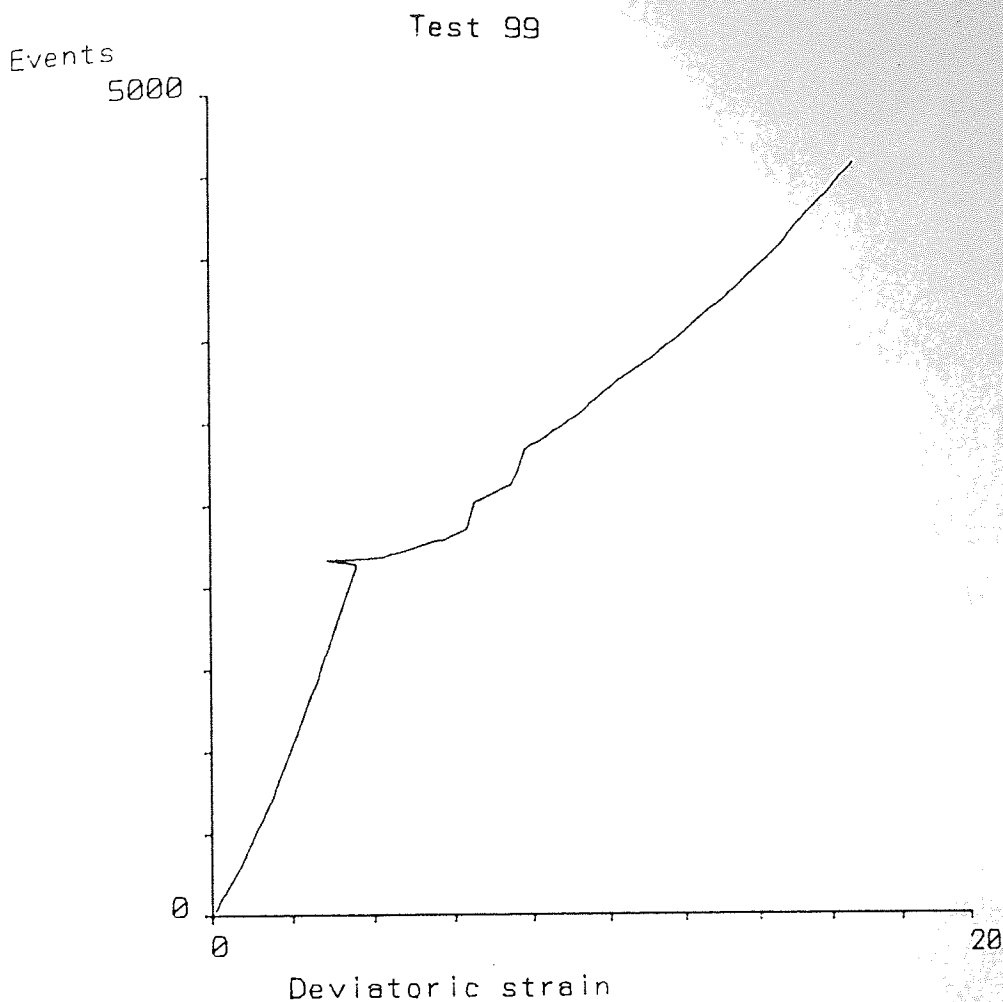

Figure 6.69 Test 101: Volumetric strain/Deviatoric strain

182
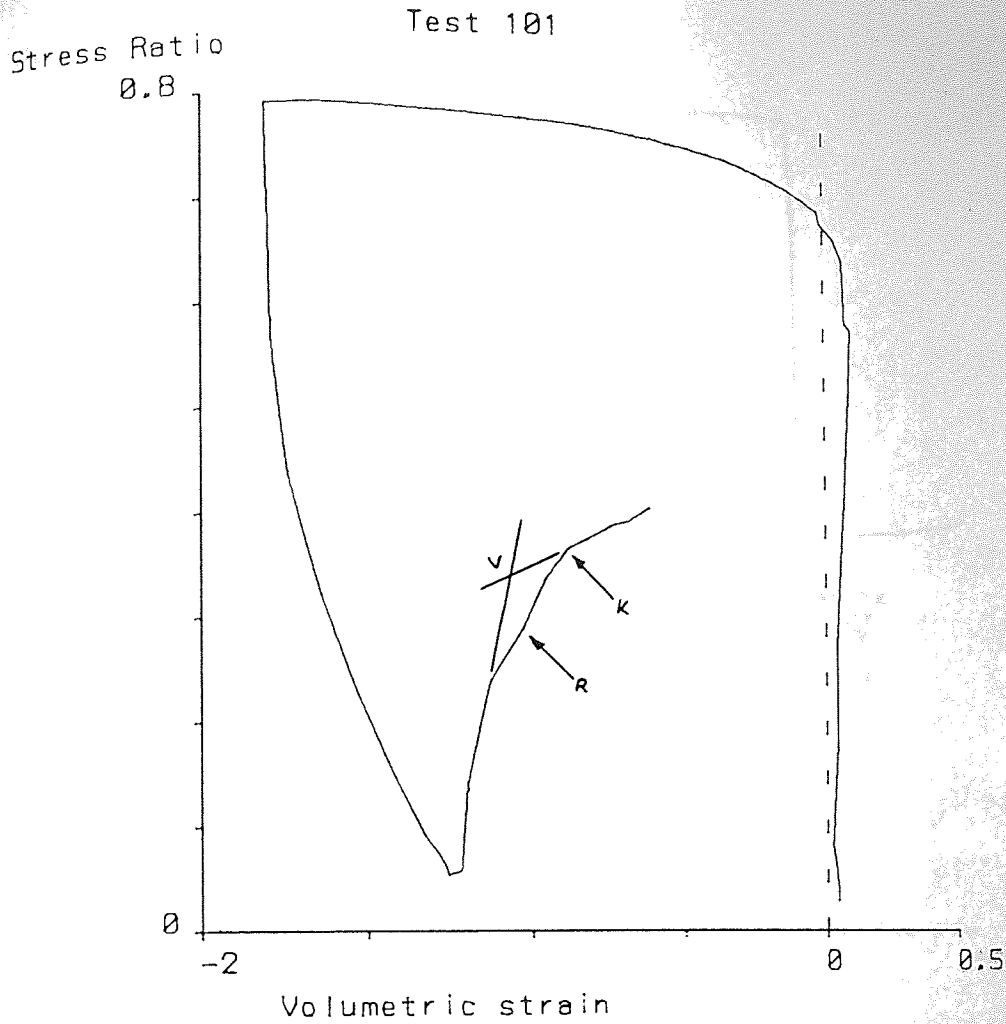
Figure 6.70 Test 101: Stress Ratio/Volumetric strain
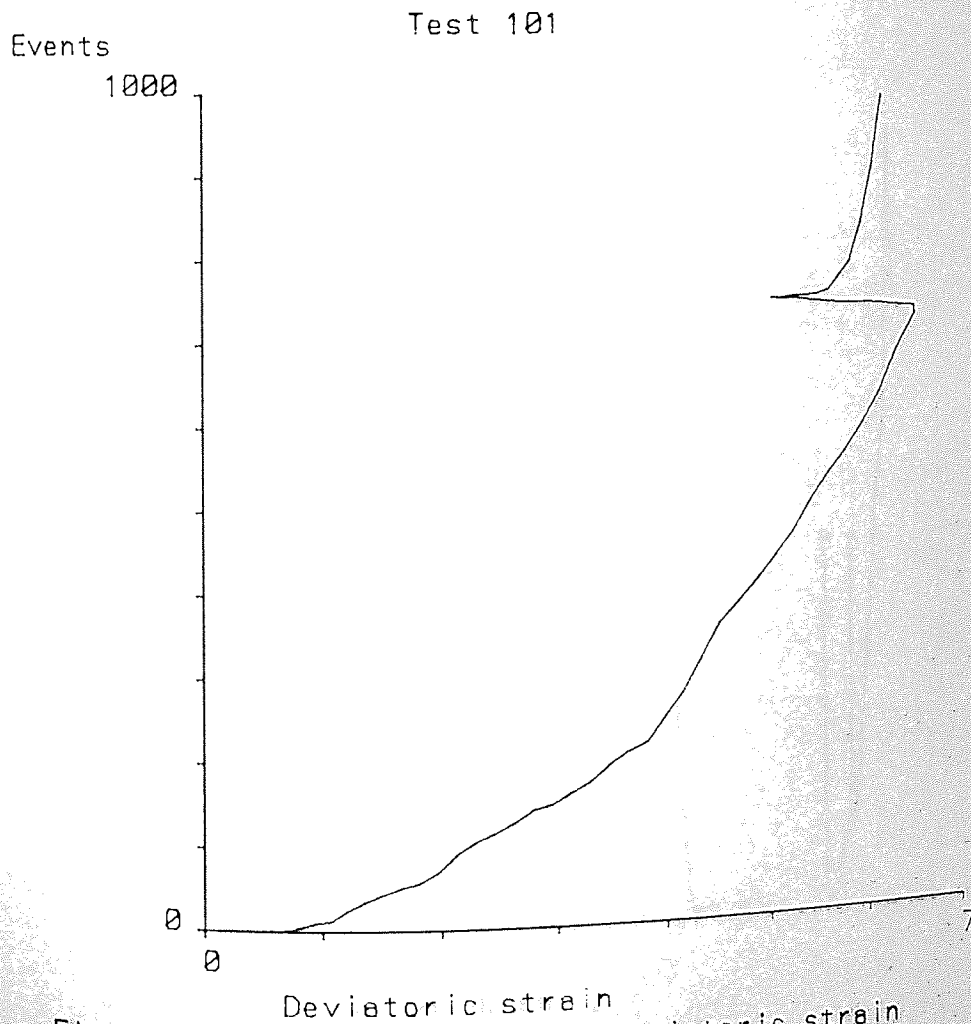
Figure 6.71 Test 101: Events/Deviatoric strain

Stress Ratio

Test 101

0.8

K
Y
R

0

0   1000
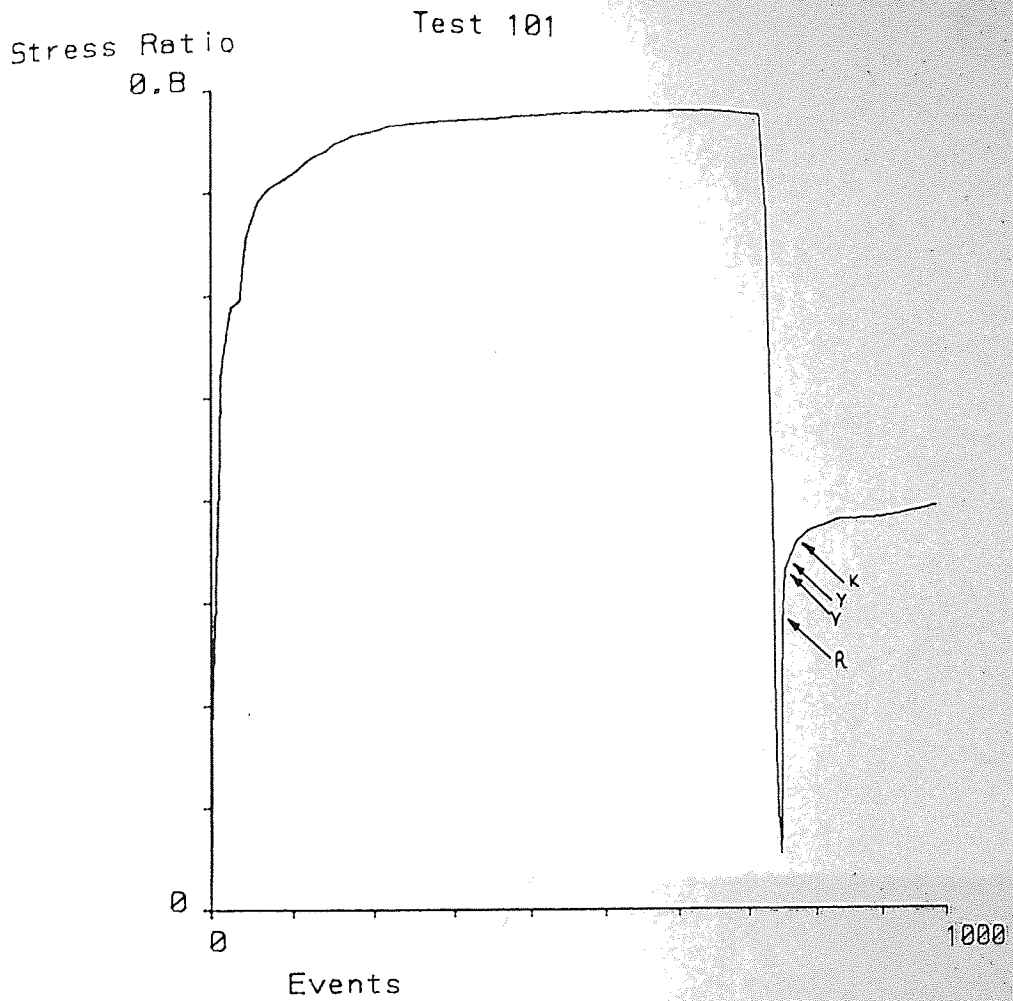
Events

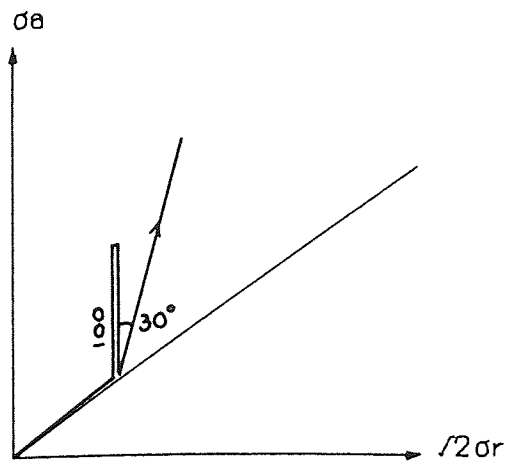**Figure 6.72 Test 101: Stress Ratio/Events**

Test 101

Event rate (average)

70

R K

0

0   140

Time (minutes)
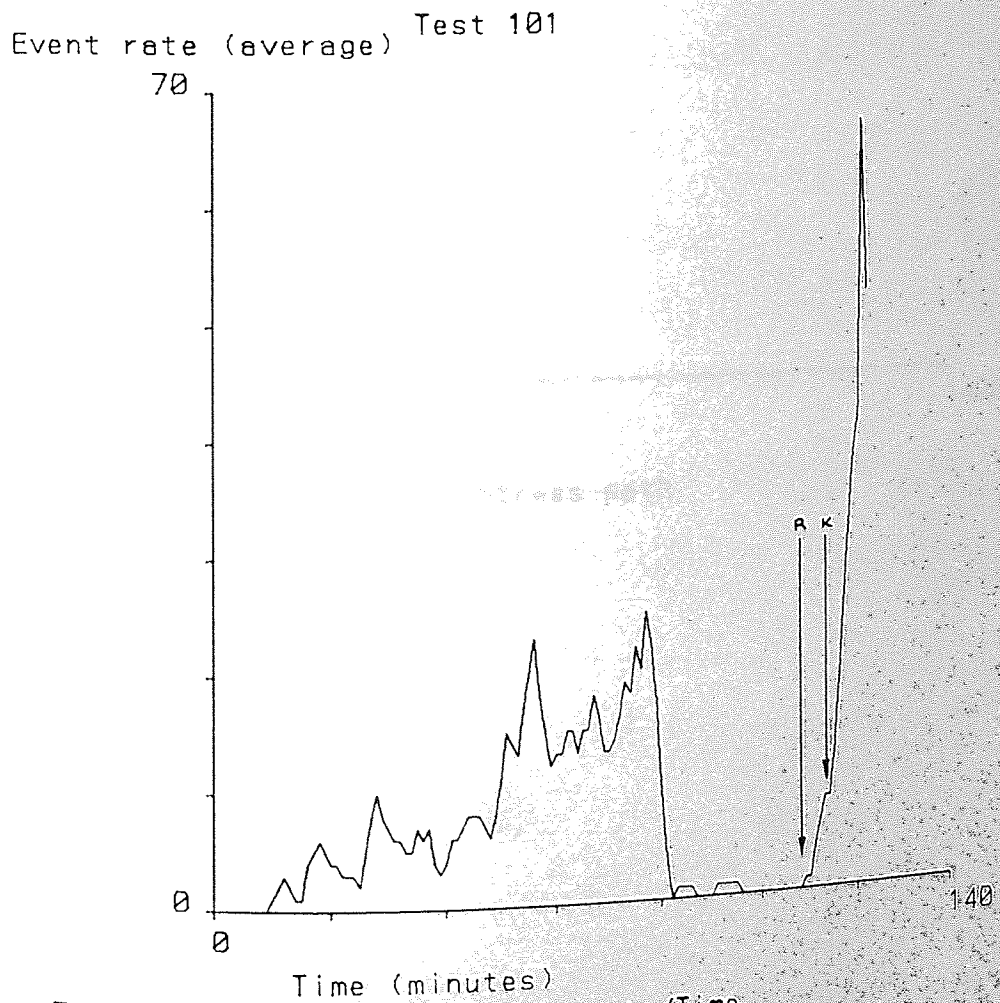
Figure 6.73 Test 101: Event rate/Time

Test 102

σa (kPa)

1400

0

0   1400

$\sqrt{2}$σr (kPa)
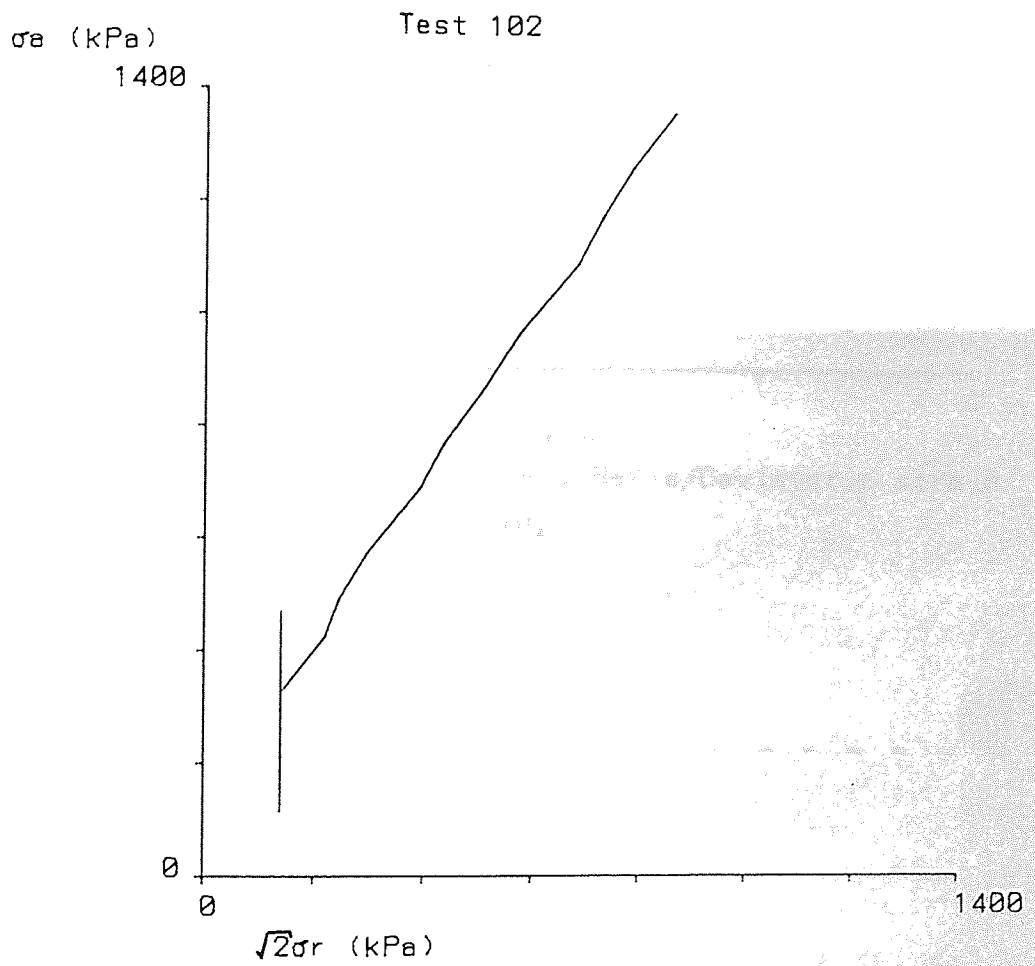
Figure 6.74 Test 102: Stress path

Test 102

Stress Ratio
0.8

0

0
Deviatoric strain
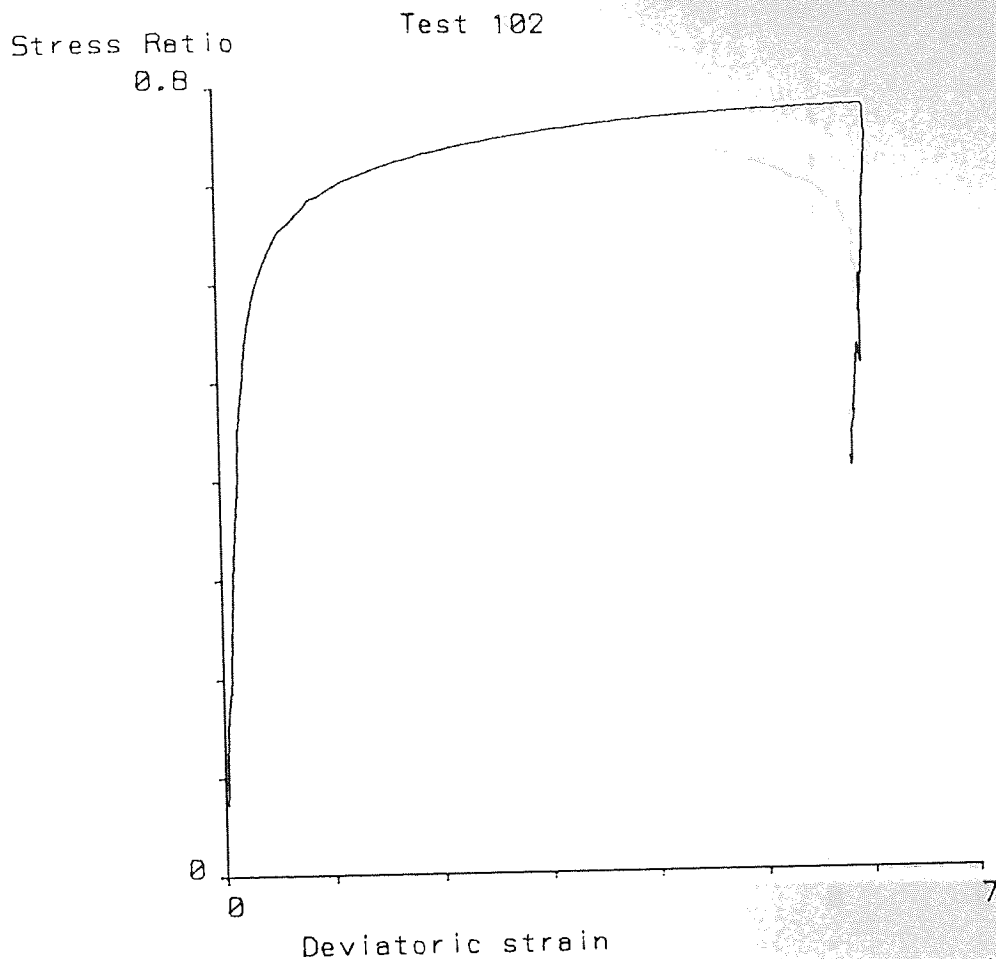
Figure 6.75 Test 102: Stress Ratio/Deviatoric strain

Test 102

Volumetric strain
0.5

0

-2

0
Deviatoric strain
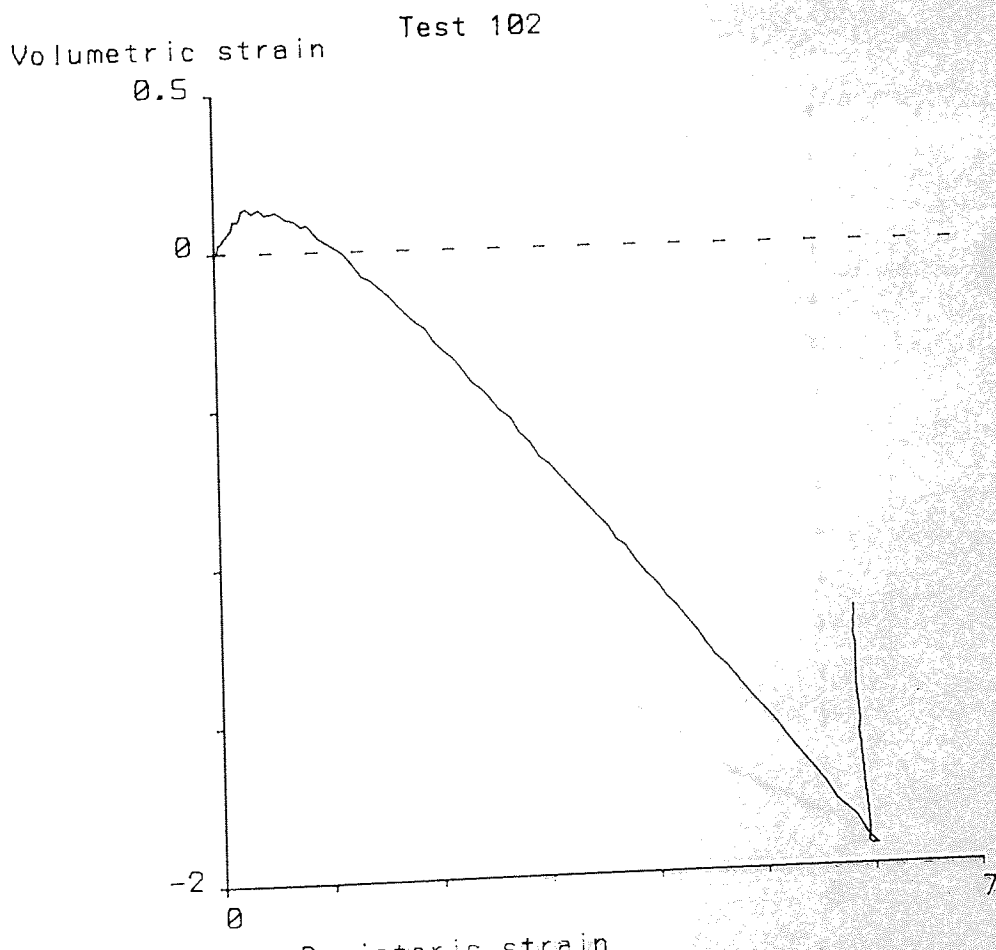
Figure 6.76 Test 102: Volumetric strain/Deviatoric strain

186

Test 102

Stress Ratio
0.8

0

-2   0   0.5
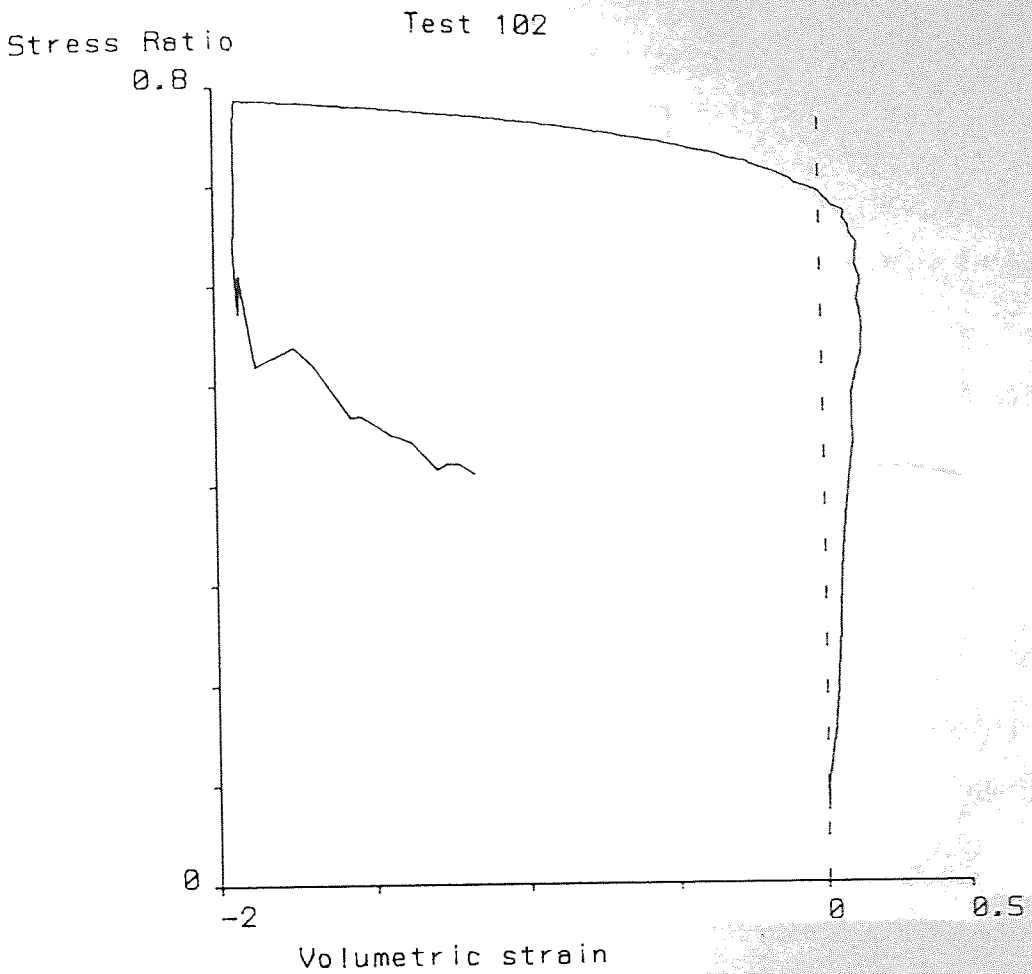
Volumetric strain

Figure 6.77 Test 102: Stress Ratio/Volumetric strain

Test 102

Events
2000

0

-2   0   0.5
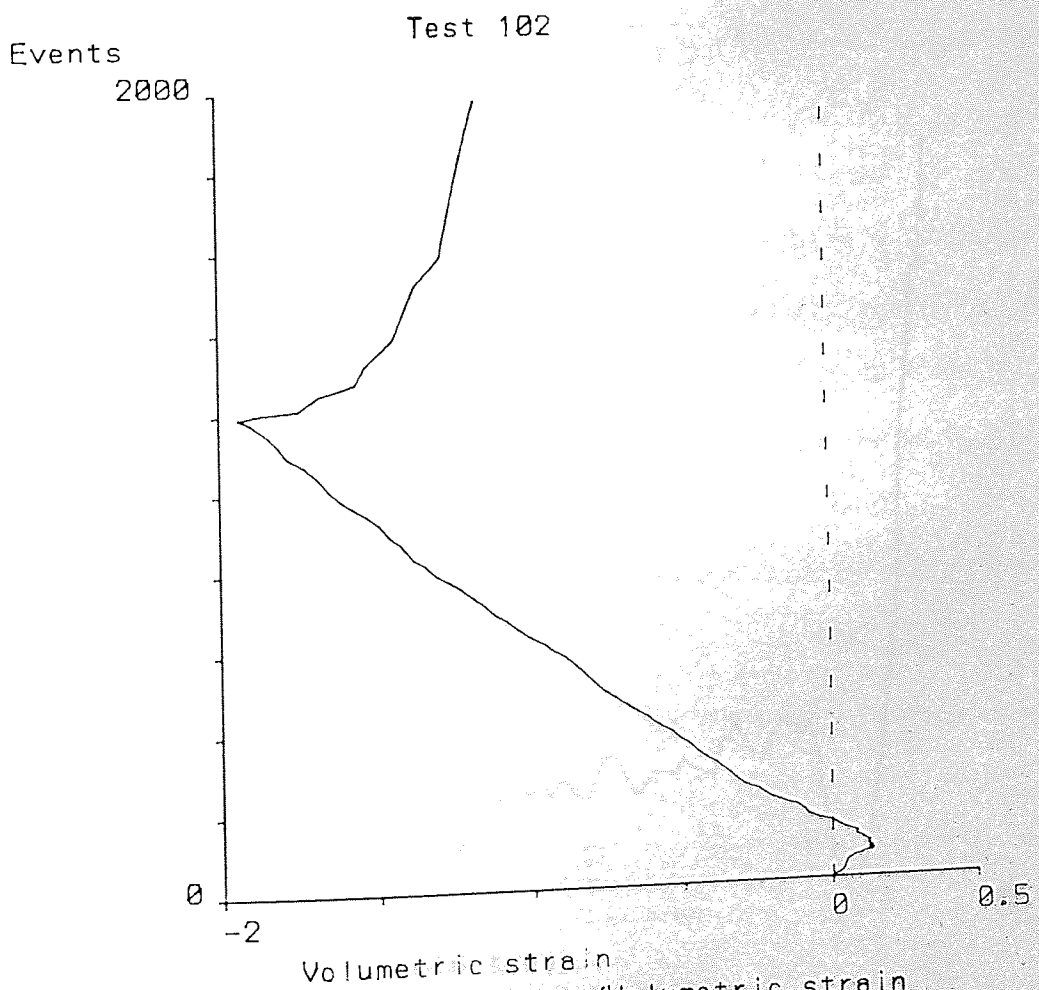
Volumetric strain

Figure 6.78 Test 102: Events/Volumetric strain

187
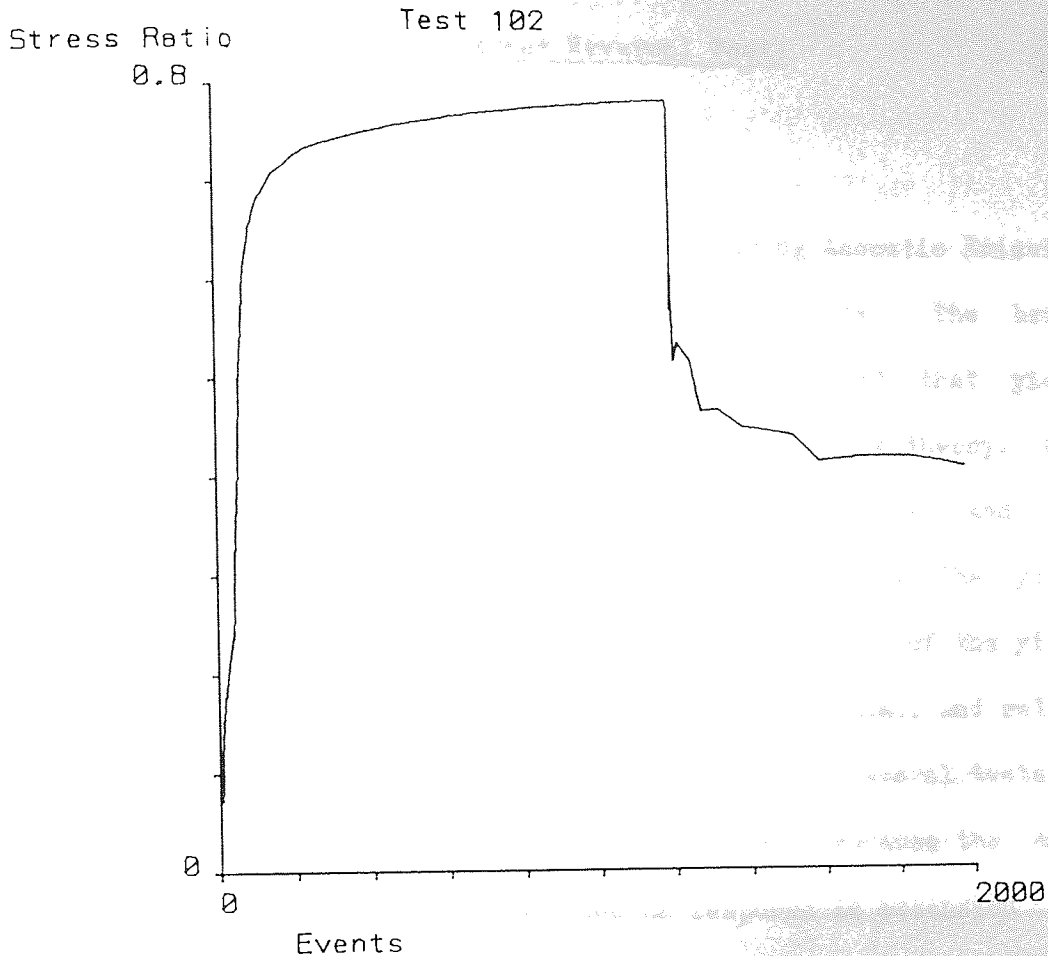
Figure 6.79 Test 102: Stress Ratio/Events
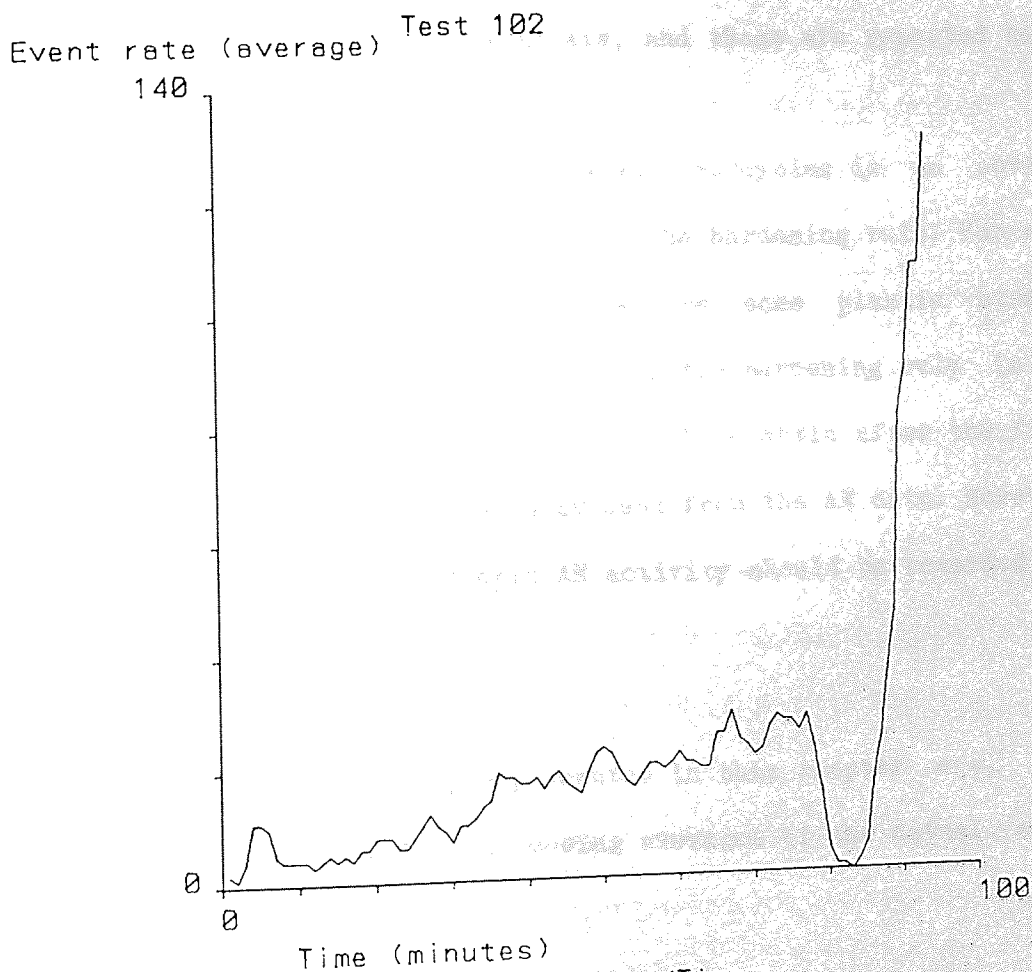
Figure 6.80 Test 102: Event rate/Time

Chapter 7

Large Stress Reversal Tests

7.1 Introduction.

Chapter 6 demonstrated the feasibility of using Acoustic Emission (AE) as a tool for identifying yield points. The brief introduction to concepts of plasticity indicated that yield surface definition is only a part of any plasticity theory. One of the additional items required is the hardening rule, and for this to be identified it is necessary to know how the yield surface changes. One simple way to find the limits of the yield surface is to load a sample into compression, unload, and reload through into extension. Over the research period several tests of this type were performed but in many of them, because the mean stress level was low, the recorded AE response in extension was almost non-existent. In fact only two tests showed sufficient information to perform any analysis, and these are reported here.

The behaviour of sand under repeated load cycles is an obvious extension for the identification of the hardening rule. For each complete cycle of load there may be some plastic strain, depending on the hardening rule. If the hardening rule is an isotropic one then all strains should be elastic after the first cycle, and this should also be evident from the AE data. However, if hardening is not isotropic AE activity should be recorded in all cycles.

The event rate/time graphs presented in this chapter are, like those in the Chapter 6, all moving averages of the actual event rate curves.

7.2 Large Stress Reversals.

Several tests were carried out in an attempt to identify the location of the yield locus following stress reversal but, for the reason given in the introduction, only two are reported here. Both tests were conducted at a constant mean stress, in order to minimise the variation in AE, because of the mean stress effect reported in Chapter 5. In Test 107 the sand was loaded into compression and then unloaded through into extension. Test 108 was the opposite to this with the sand being loaded into extension first and then unloaded through into compression. When considering these tests it was realised that reduced AE activity would occur in extension and that this would hinder the interpretation of the results. It was hoped that this reduced activity could be partly offset by testing at a higher mean stress of 300kPa which would generate more events.

The stress path followed for Test 107 is shown in Figure 7.1. Control of the stress level when unloading is seen to be good despite the rapid reduction of the stresses. The stress ratio/deviatoric strain graph is shown in Figure 7.2. Here, as in some of the tests reported in Chapter 6, the deficiency of the top platen connection is evident as the isotropic stress state is approached. The elastic unloading period is very short and small plastic strains are apparent as the sample is unloaded towards the isotropic stress. However, very close to the isotropic stress it is clear that much larger plastic strains are occurring. There is, however, no obvious yield point after stress reversal. The volumetric strain/deviatoric strain graph, Figure 7.3, shows that during the unload period contraction occurs. As the sample is

loaded through into extension volumetric contraction continues to occur until the constant volume state is reached at a deviatoric strain of about 1.5%, after which the sample expands. The stress ratio is replotted against events in Figure 7.4. The event rate/time graph, Figure 7.5, shows the large difference in event rates between compression and extension. What is clear from this figure however, is that there is a kink in the event rate some time during the extension phase. Following the hypothesis presented in the previous chapter this point is taken to be the yield point and is denoted by Y on the relevant figures.

From the stress ratio graph, Figure 7.2, it may be seen that the sample was unloaded from a stress ratio of 0.78. The maximum stress ratio, when the sample was loaded into extension, was -0.45. The yield point, Y, identified from the AE data gives the inverse yield stress ratio as -0.15. This indicates that the yield surface (or its movement) is not isotropic: if von Mises yield criterion was applicable inverse yield would be expected at a stress ratio of -0.78. Further, if the Mohr-Coloumb yield criterion (where the ratio of the principal stresses remains the same) was true, yield would be anticipated at -0.50.

The stress path followed for Test 108 is shown in Figure 7.6; it may be seen that, during the compression phase of loading, the stress path is slightly curved because of poor control. The stress ratio/deviatoric strain graph, Figure 7.7, shows that, excepting the kink near isotropic stress, the gradient is constant until some point during the compression phase. The volumetric strain/deviatoric strain graph, Figure 7.8, shows a similar, but handed, shape to that of Test 107. As was the case

for Test 107, the stress ratio/events graph (Figure 7.9) shows that the event rate in extension is much less than that in compression. Figure 7.10, the event rate/time graph, shows that there is a much more distinct event restart point, and that a substantial increase in the event rate occurs after a further small amount of deviatoric strain. The discontinuity in the event rate curve is taken to be yield, as it was for Test 107, and is marked Y on the appropriate figures.

As was found for Test 107, yield occurs at a lower stress ratio (0.11) than that which would be expected from von Mises (0.47) or Mohr-Coloumb (0.70) yield criteria. The stress ratio at which the sample was unloaded (-0.47) and the final (compressive) stress ratio (0.80) compare well with those of Test 107. Additionally it can be seen that the event rates in compression and extension parts of the tests compare well.

The tests reported in this section show that large stress reversals significantly alter the shape of the stress ratio curve; Figures 7.2 and 7.7 are combined in Figure 7.11 for the purposes of comparison. The results of these tests compare well with the results of similar tests reported in the literature, for example Khayatt (1967), and Lade and Boonyachut (1982). This type of behaviour is referred to as the Bauschinger effect, although the term 'Bauschinger effect' is more commonly applied to work-hardening in metals, and it may be modelled if a kinematic hardening rule is used. It is interesting to note that, in both tests, the slope of the volumetric strain curve at the inverse yield point is parallel to the slope of the curve immediately before unloading.

7.3 Strain Cycling.

Two tests were carried out in which a number of compression-extension cycles were performed. In both tests the samples were subject to an initial compressive primary loading and, after some deviatoric strain had occurred, were unloaded through into extension, and when a fixed amount of axial strain had occurred the samples were reloaded. This cycling was performed three times for each test. When contemplating these tests it was realised that the event rates in compression and extension could be expected to differ widely. It was suggested in Chapter 5 that this could be partly compensated for by altering the threshold voltage when the stress path entered the extension region. Unfortunately the AET5000 does not allow the threshold voltage to be adjusted once a test has started and it was therefore necessary to alter the gain setting on the AET5000. Experience has shown that, despite proper care, this adjustment can cause spurious events to be recorded, and so any events recorded near these points should be treated with caution.

Test 106 was conducted at a constant mean stress of 200 kPa and the stress path followed is shown in Figure 7.12. The large differences between the planned and actual stress path arose because of the rapid reduction in deviator stress when unloading; this is an unfortunate consequence of the manual adjustment of the cell pressure at the end of each recording interval. These mean stress variations should not, however, affect the AE response since they occur during periods of 'elastic' deformation. Figure 7.13 shows the stress ratio/deviatoric strain graph and it can be seen that after the first cycle the

193

hysteresis loop stabilises. Also it may be seen that the shape of one complete cycle is similar to that of the combined stress ratio plot for Tests 107 and 108 which is shown in Figure 7.11. Further, while the maximum compressive stress ratio reached remains approximately the same, in extension the maximum stress ratio increases with each cycle. The sample becomes stiffer with subsequent cycles as may be deduced from the unloading gradients in the various cycles. The volumetric strain/deviatoric strain graph, Figure 7.14, shows that each cycle results in a small amount of permanent volumetric contraction and that the form is very similar for the second and third cycles. The events/deviatoric strain graph is shown in Figure 7.15, the small number of events recorded at the start of the test occurring during isotropic consolidation. The isotropic stress, compression, and extension points are marked on the figure by Z, C, and E respectively so that the different cycles may be distinguished. The event rate/time graph, Figure 7.16 shows that at the end of the second cycle the event rate continues to increase; the test record does not show any reason for this irregularity. However, prior to this, it is possible to identify three changes of gradient in the event rate and these are marked Y_1, Y_2, and Y_3 on the appropriate figures. Additionally the first two stress ratio/deviatoric strain cycles are extracted and plotted in Figures 7.17 and 7.18 respectively, with the yield points marked on the relevant figures.

The shortcomings of the top platen/load cell connection are apparent with the kinks in the stress ratio curves close to the isotropic stress making it impossible to describe adequately what

194

is happening. However, once the stress path has gone beyond this point it is clear that yield is occurring; it is also apparent that with each cycle the sand becomes stiffer. The yield points identified from the AE data occur in similar positions to those found for Tests 107 and 108. Also, it may be seen that yield in extension during the second load cycle occurs at a higher stress ratio than in the first cycle, which indicates that the yield surface has expanded, or translated.

7.4 Summary.

The results from the tests reported in this chapter show that the AE method can be used to identify the inverse yield points after large stress reversals. It has not been possible to identify the actual hardening rule because of the lack of data: it is necessary to find at least three points on the yield surface for this. However, the results indicate that the yield surface, or its movement is not isotropic. The results from Test 106, with repeated load cycles, suggest that kinematic hardening may be present, but more tests need to be carried out before any firm and definite conclusions may be drawn.

The gain setting on the AET5000 was altered when the sample was in extension to compensate for the lower event rate. While an improvement in the AE response was obtained, this was at the expense of additional noise and possible false events during the adjustment period. It is apparent from the results in this chapter that the design of the top platen/load cell connection needs to be improved, as the float allowed in the current design masks any features present near the isotropic stress.
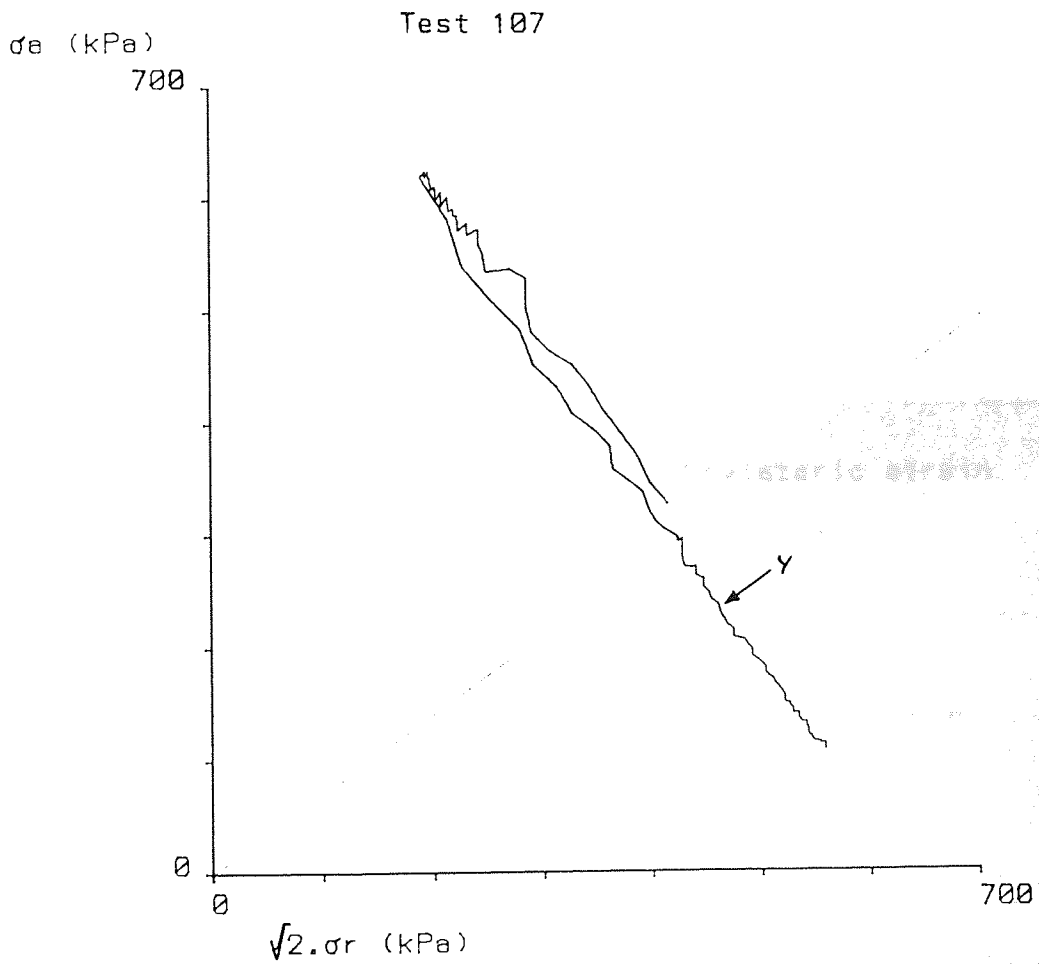
Figure 7.1 Test 107: Stress path
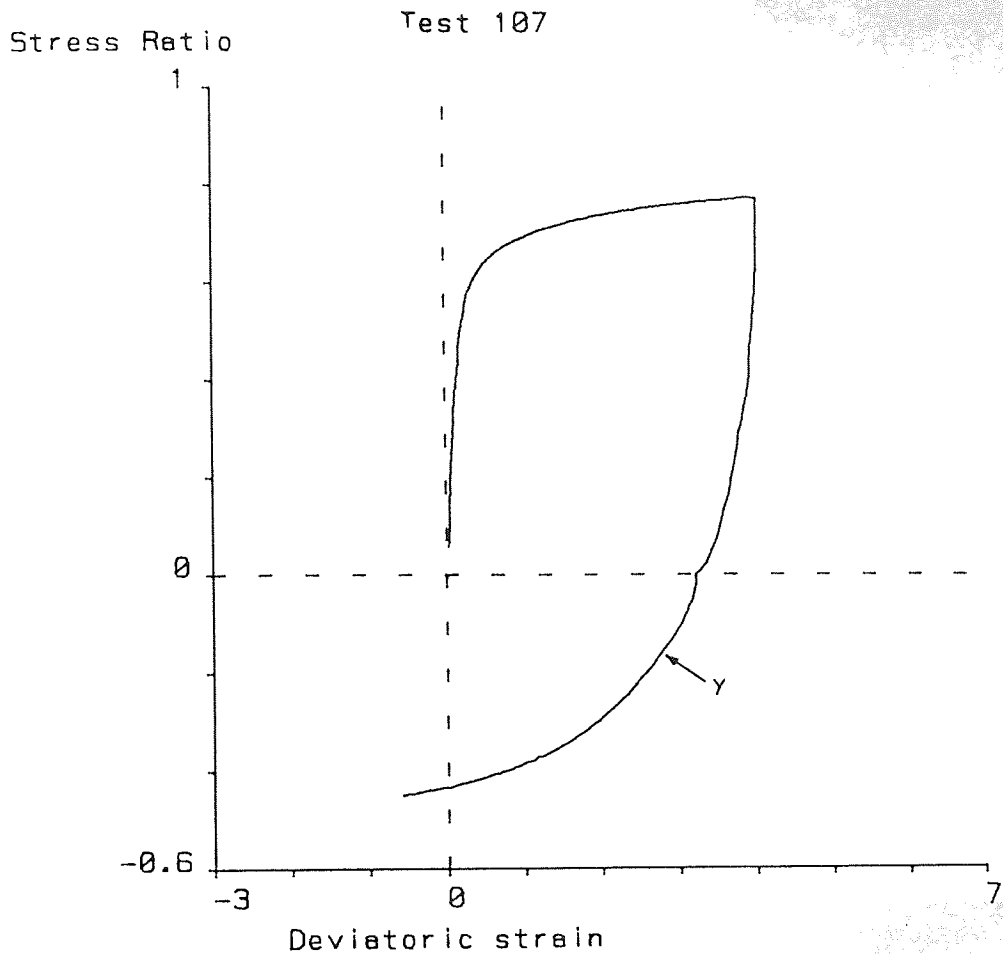
Figure 7.2 Test 107: Stress Ratio/Deviatoric strain
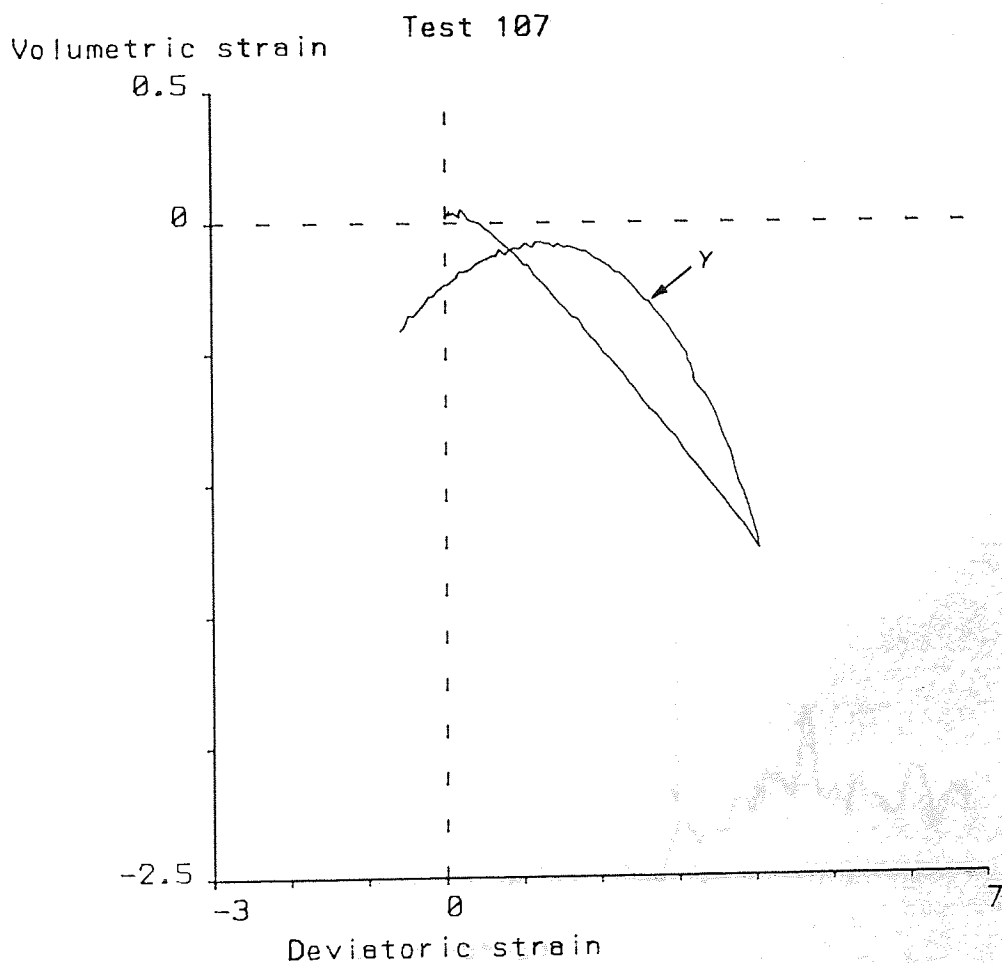
Figure 7.3 Test 107: Volumetric strain/Deviatoric strain

Test 107
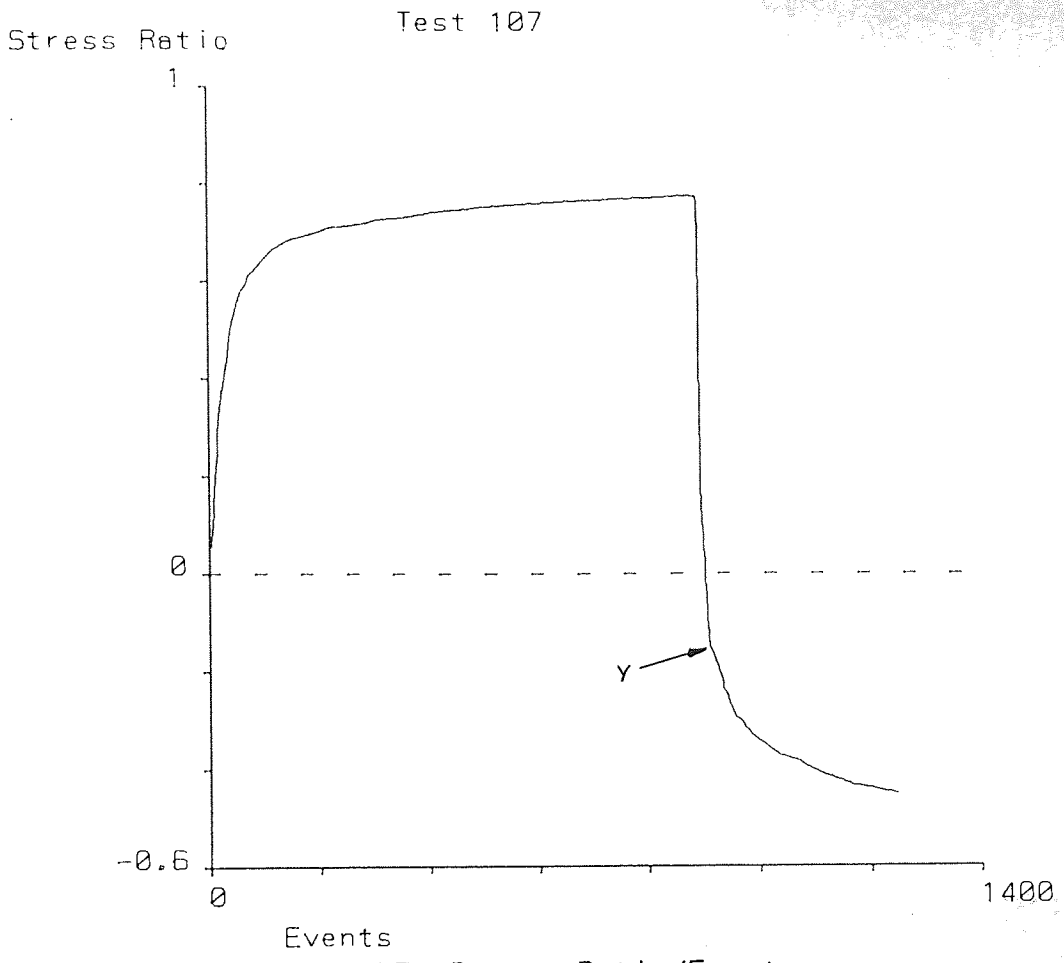
Stress Ratio

Figure 7.4 Test 107: Stress Ratio/Events
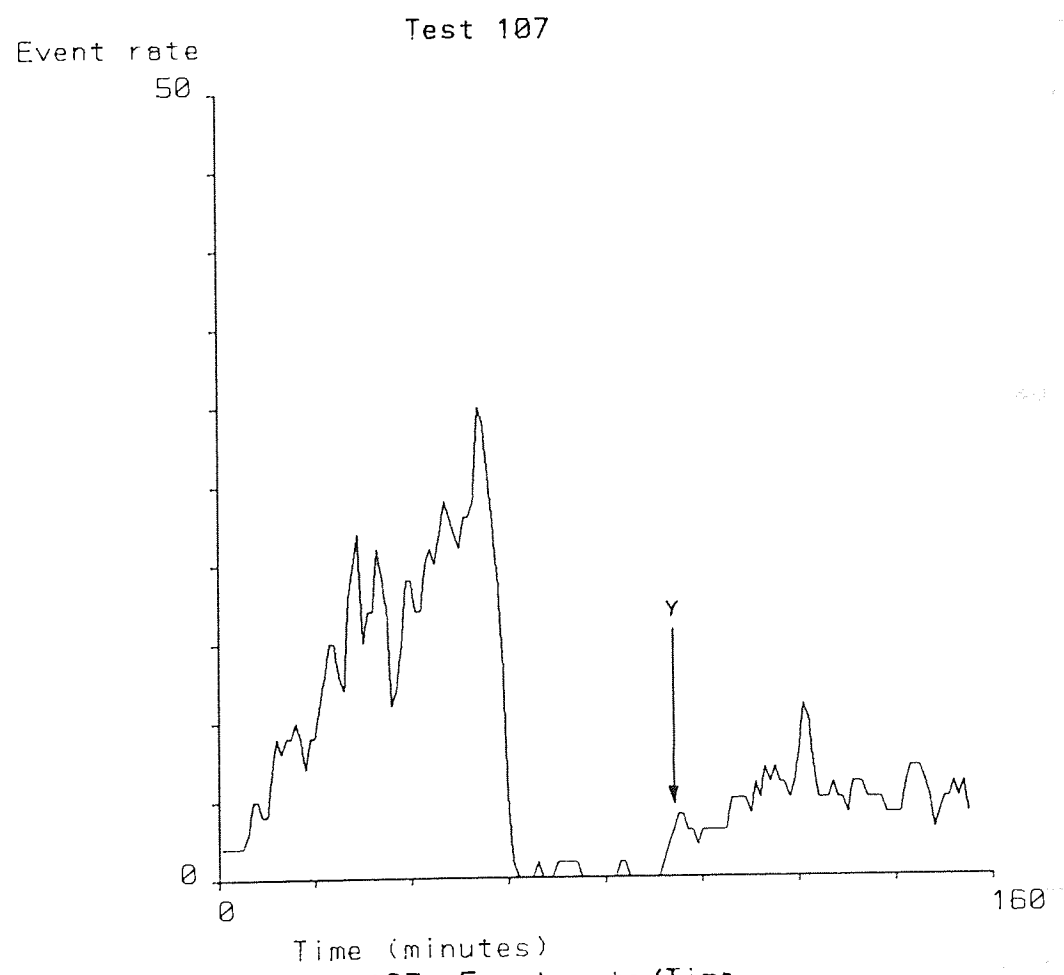
Test 107

Event rate

Figure 7.5 Test 107: Event rate/Time
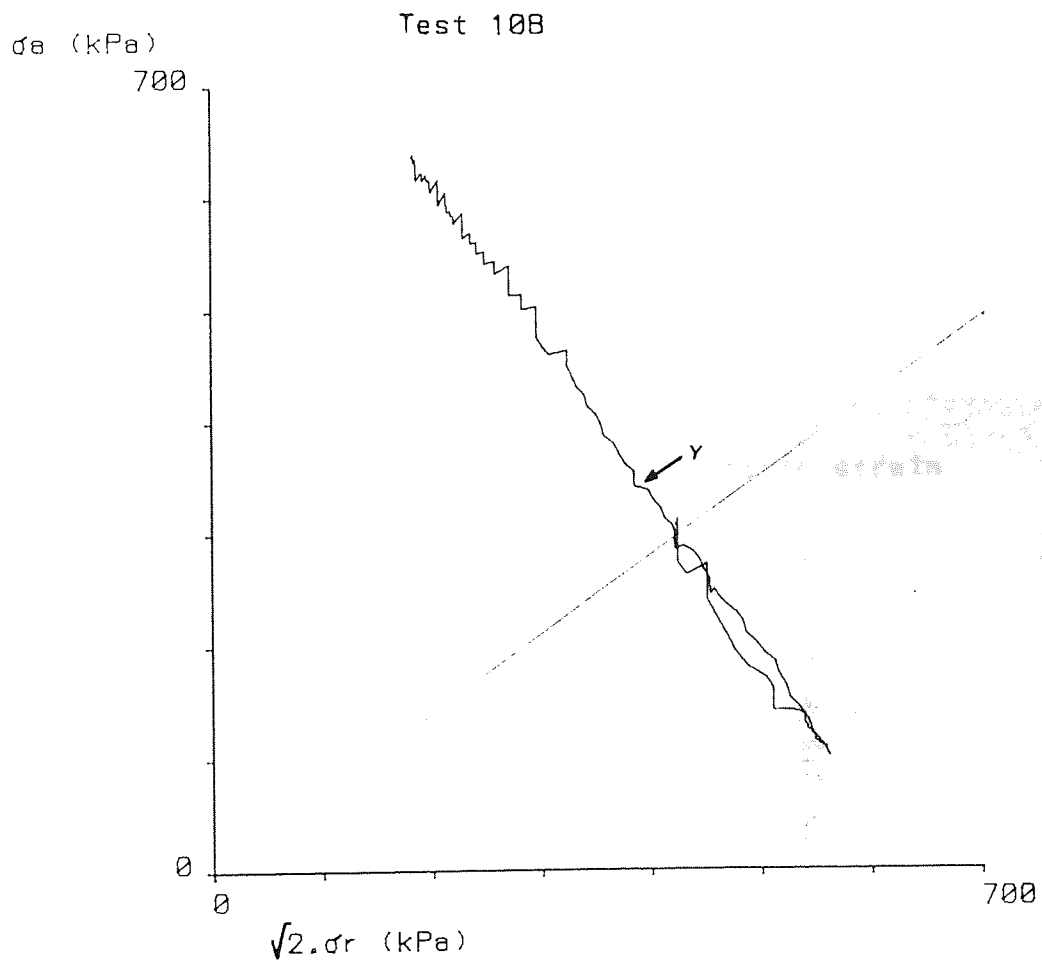
Figure 7.6 Test 10B: Stress path
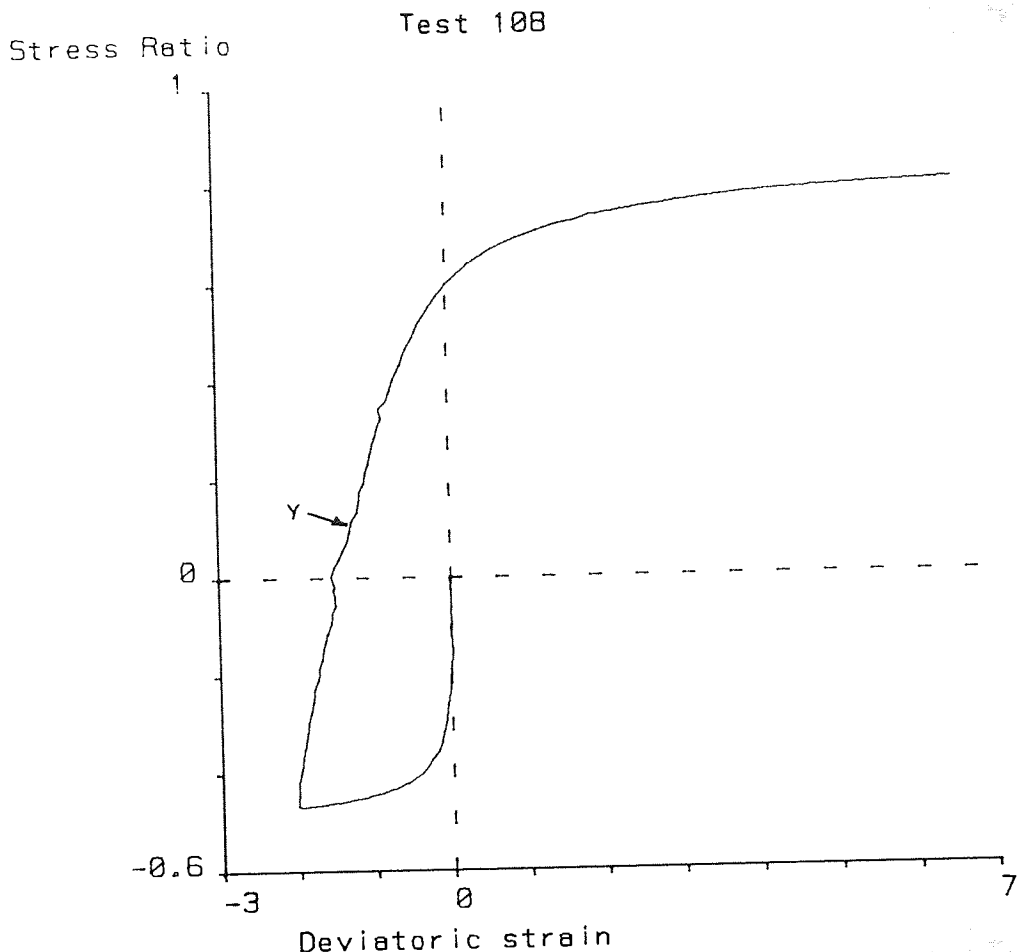
Test 108

Figure 7.7 Test 108: Stress Ratio/Deviatoric strain
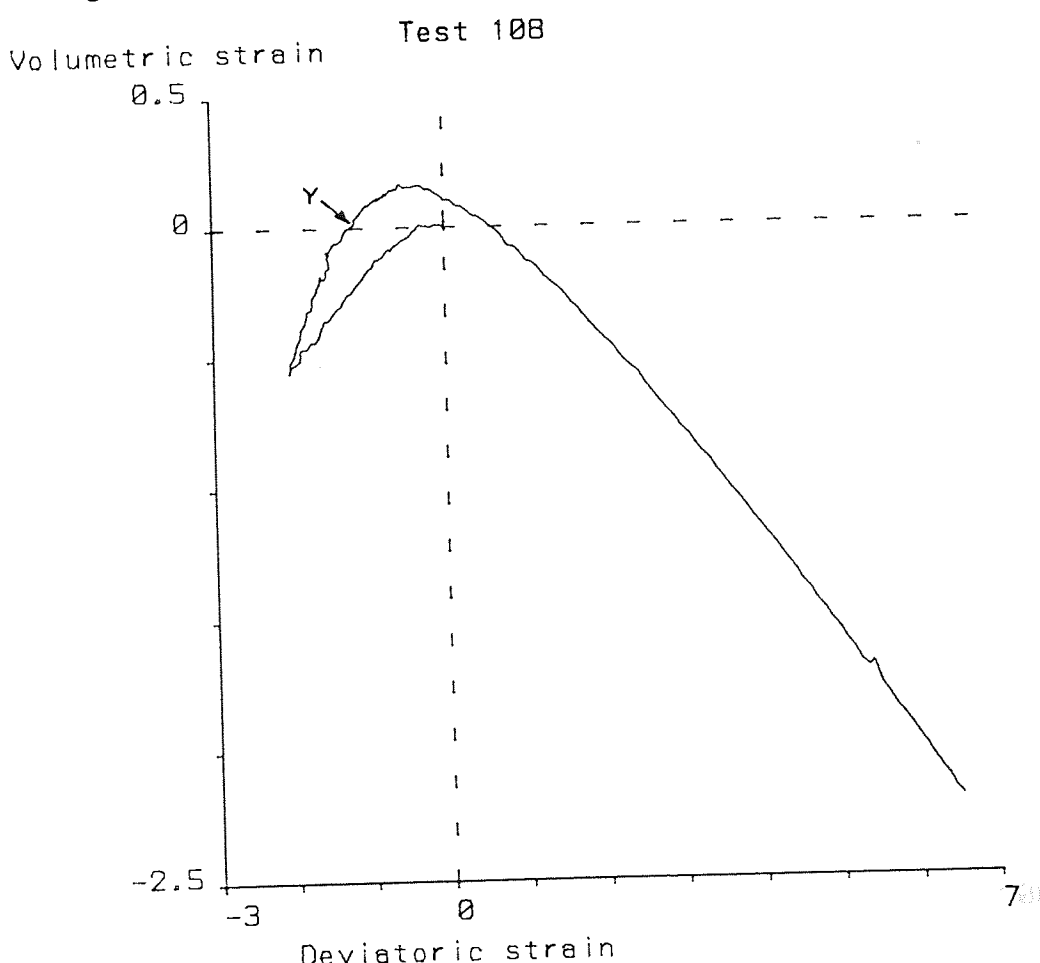
Test 108

Figure 7.8 Test 108: Volumetric strain/Deviatoric strain

Stress Ratio

Test 108

Figure 7.9 Test 108: Stress Ratio/Events
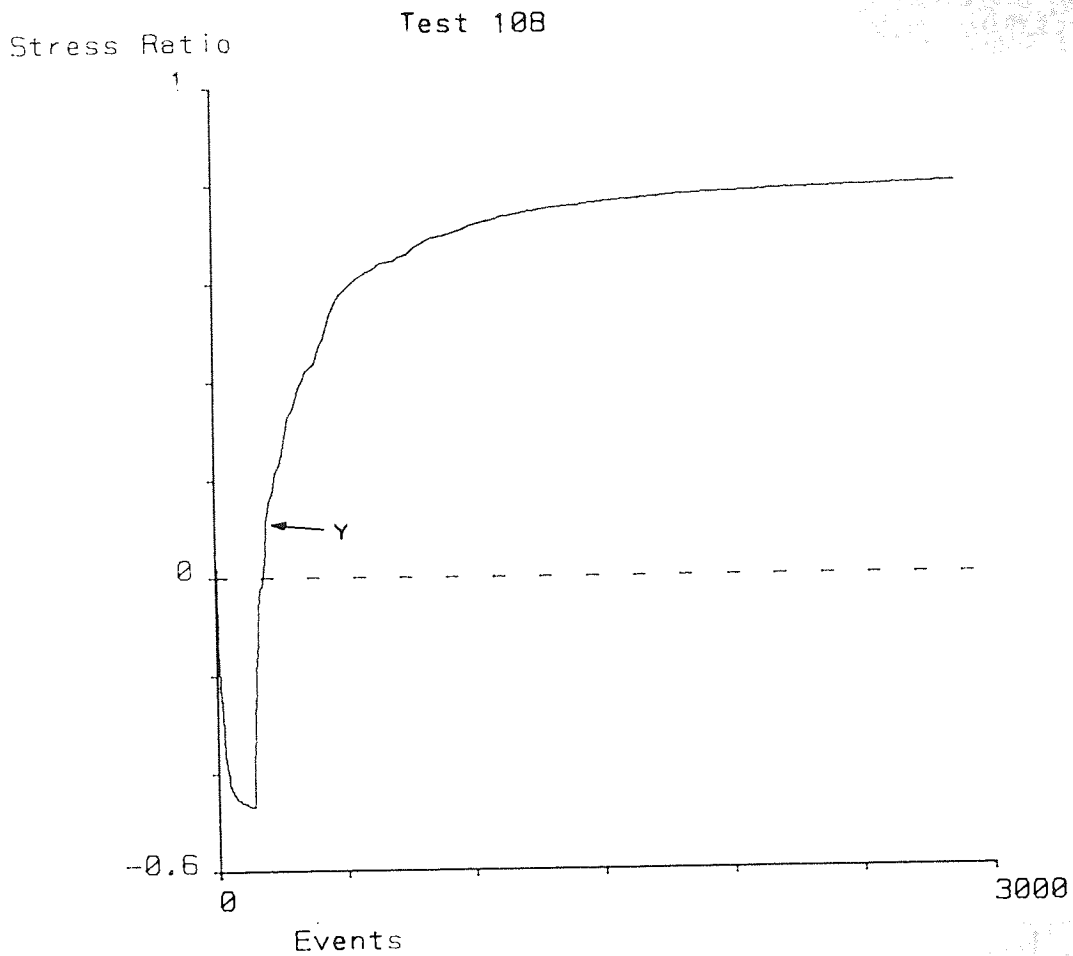
Test 108

Event rate

Time (minutes)
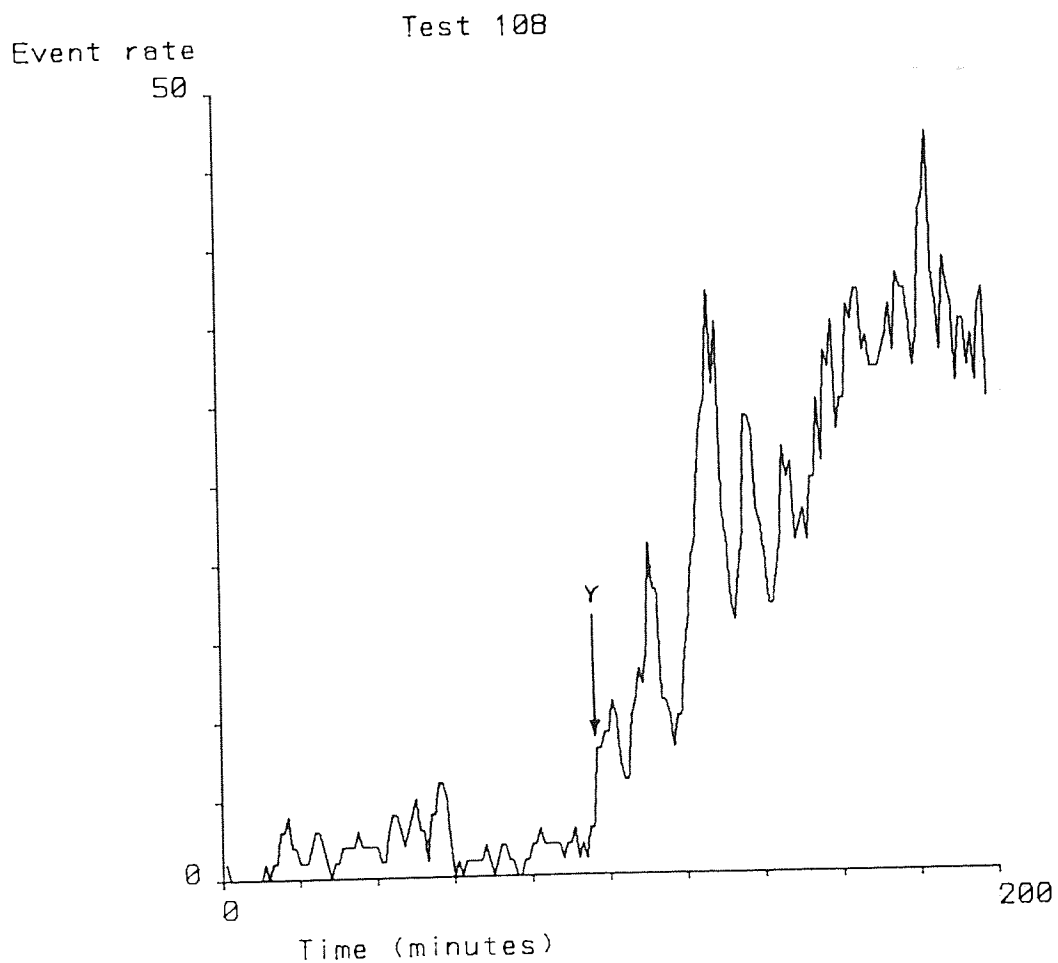
Figure 7.10 Test 108: Event rate/Time
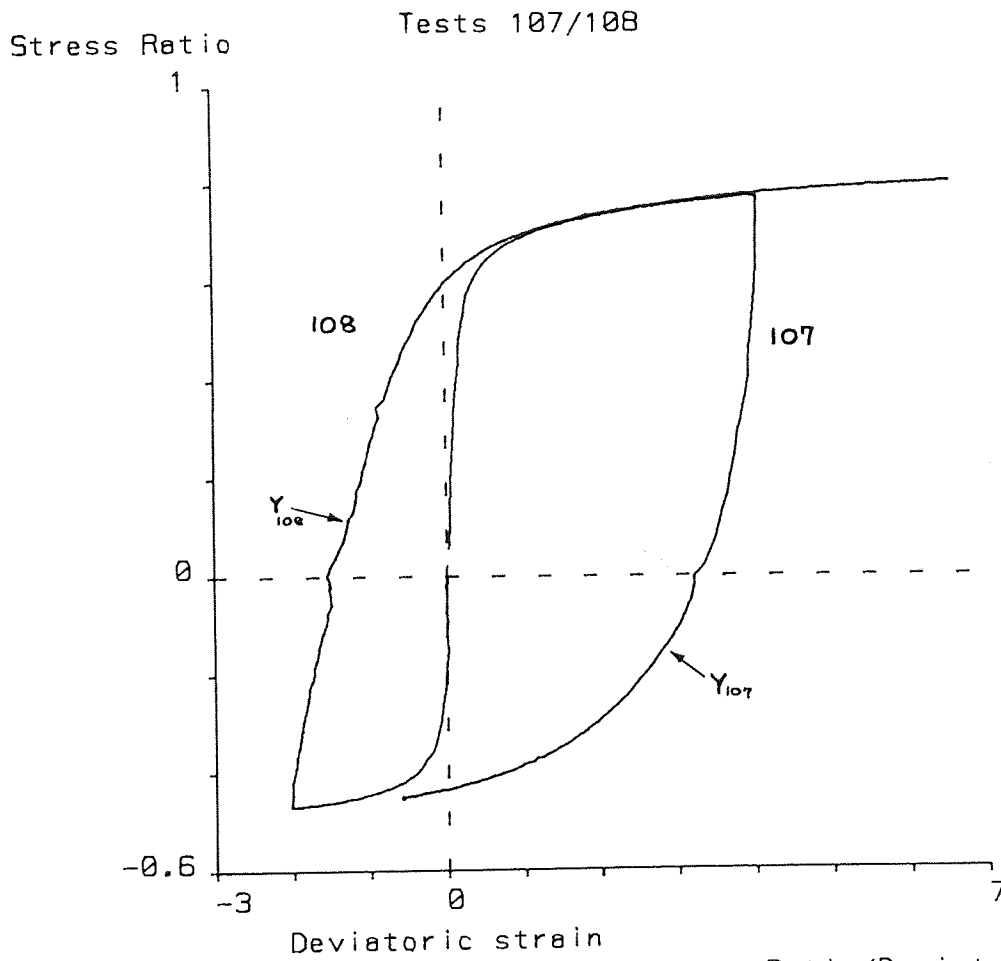
Figure 7.11 Tests 107 and 108: Stress Ratio/Deviatoric strain
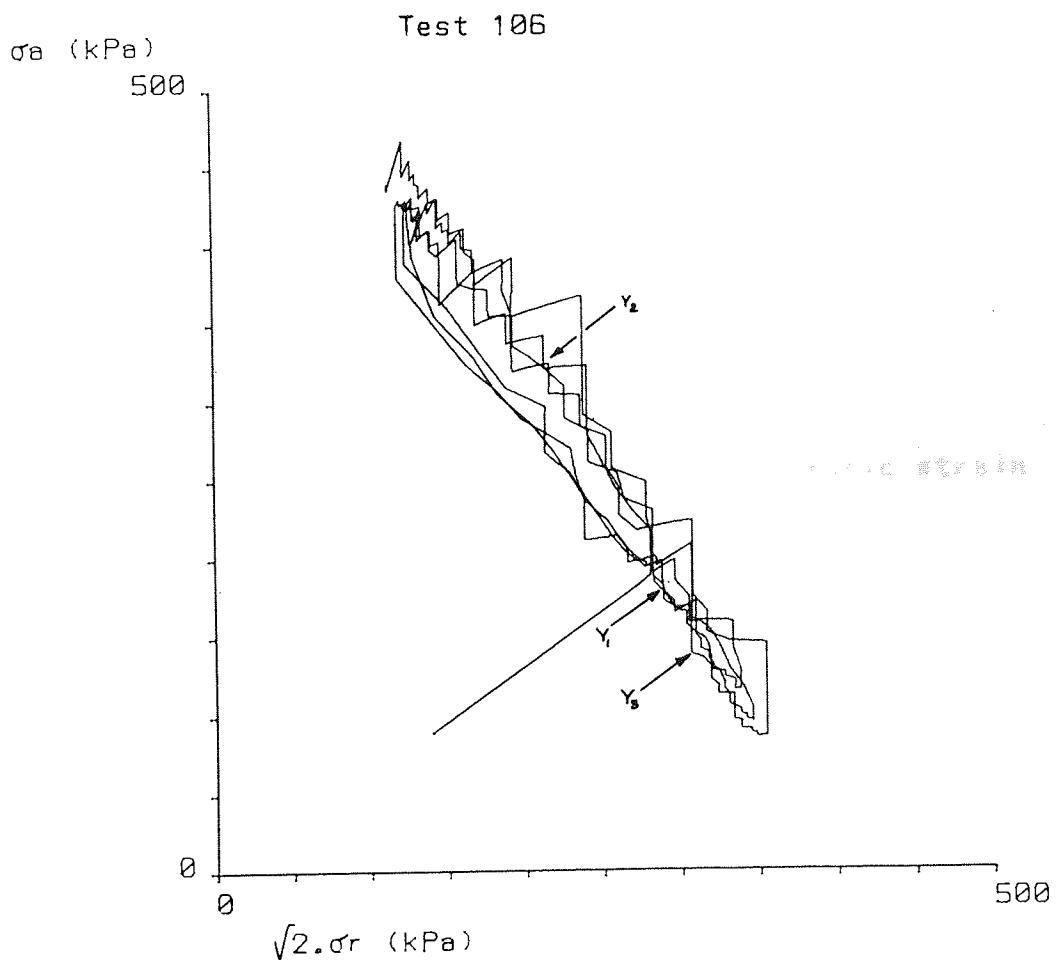
Figure 7.12 Test 106: Stress path
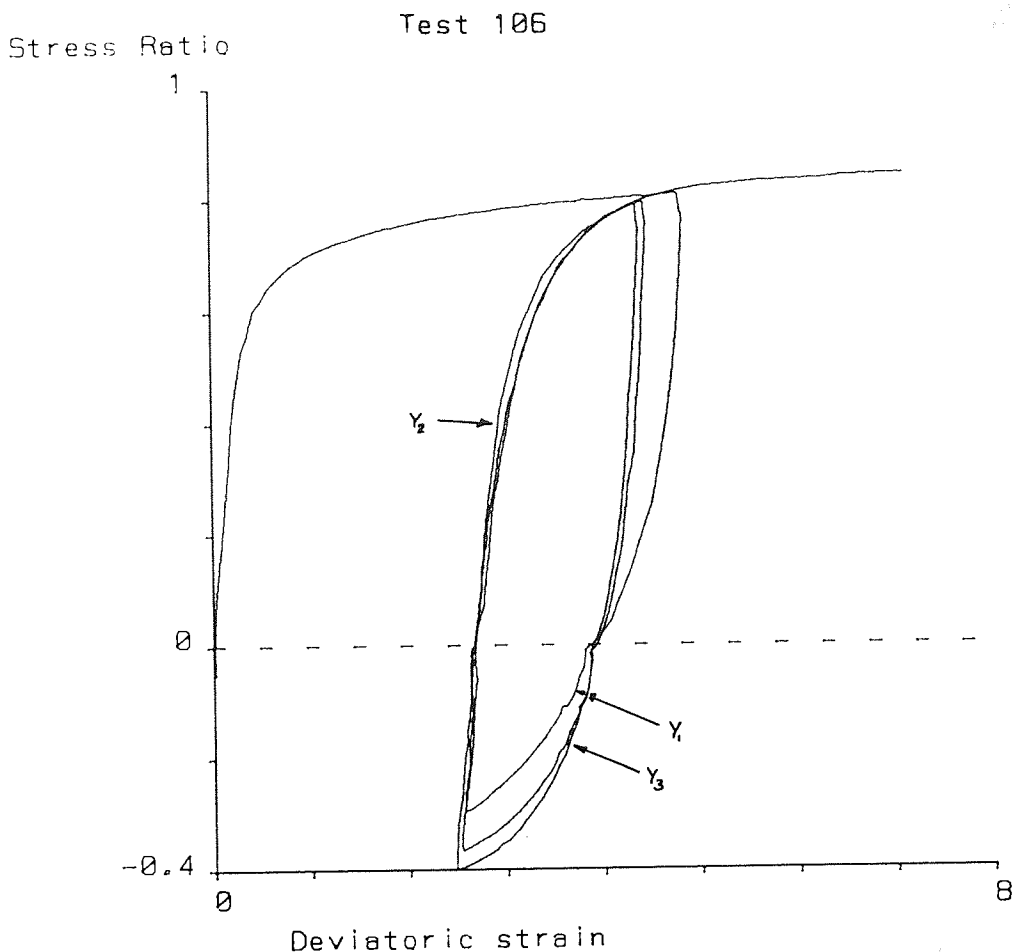
Figure 7.13 Test 106: Stress Ratio/Deviatoric strain
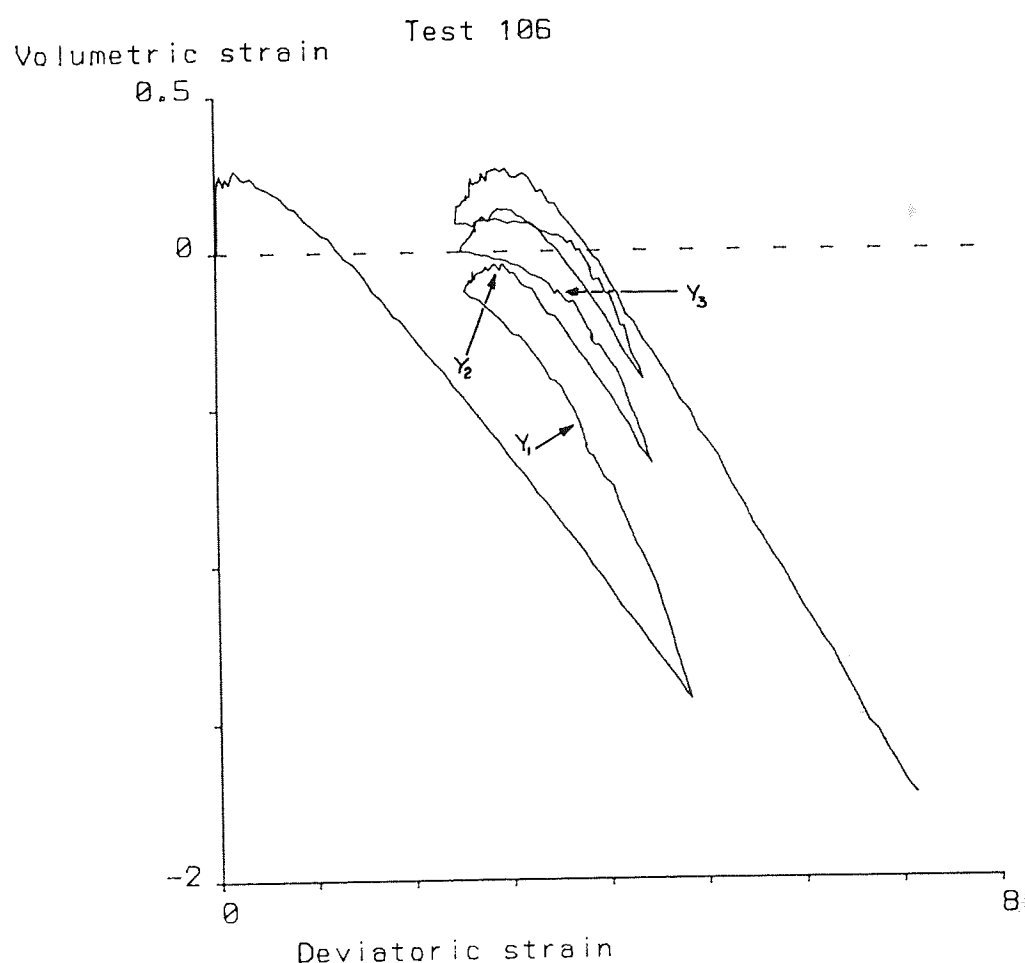
Figure 7.14 Test 106: Volumetric strain/Deviatoric strain

204

Test 106

Events
1600
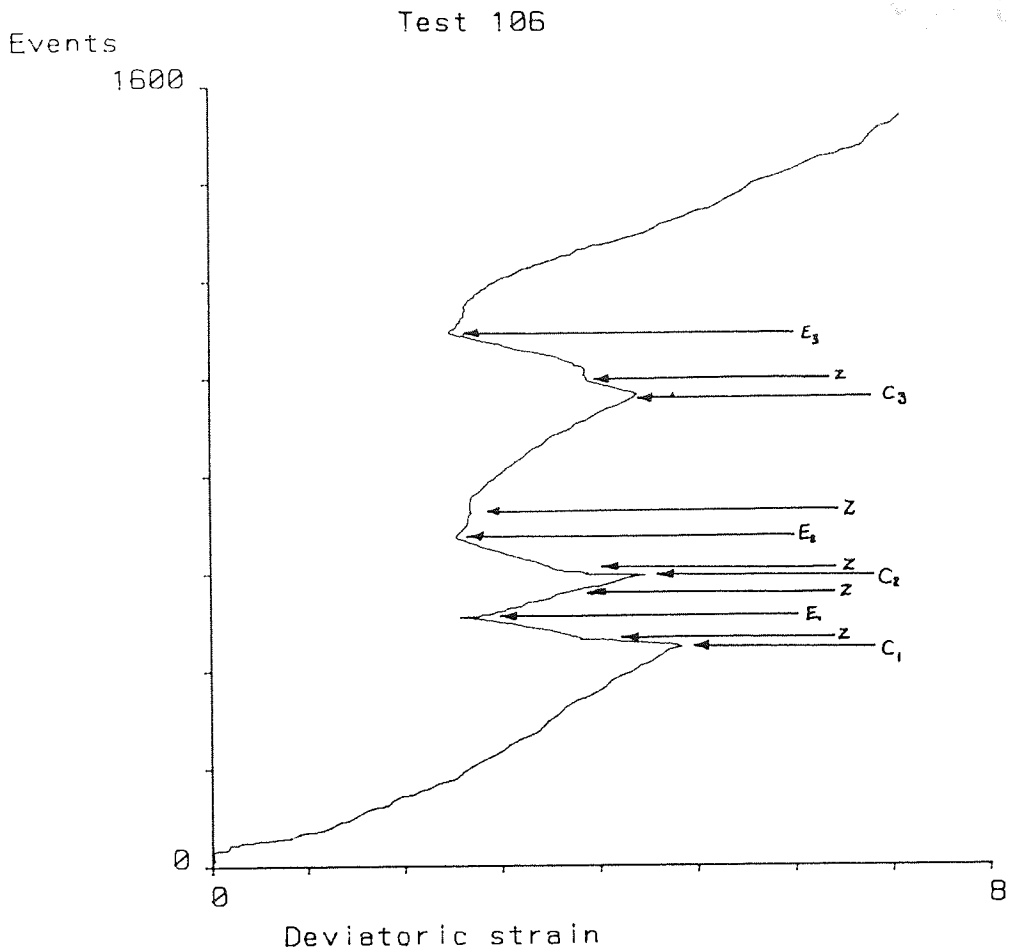
Deviatoric strain

Figure 7.15 Test 106: Events/Deviatoric strain

Test 106

Event rate
16

Time (minutes)
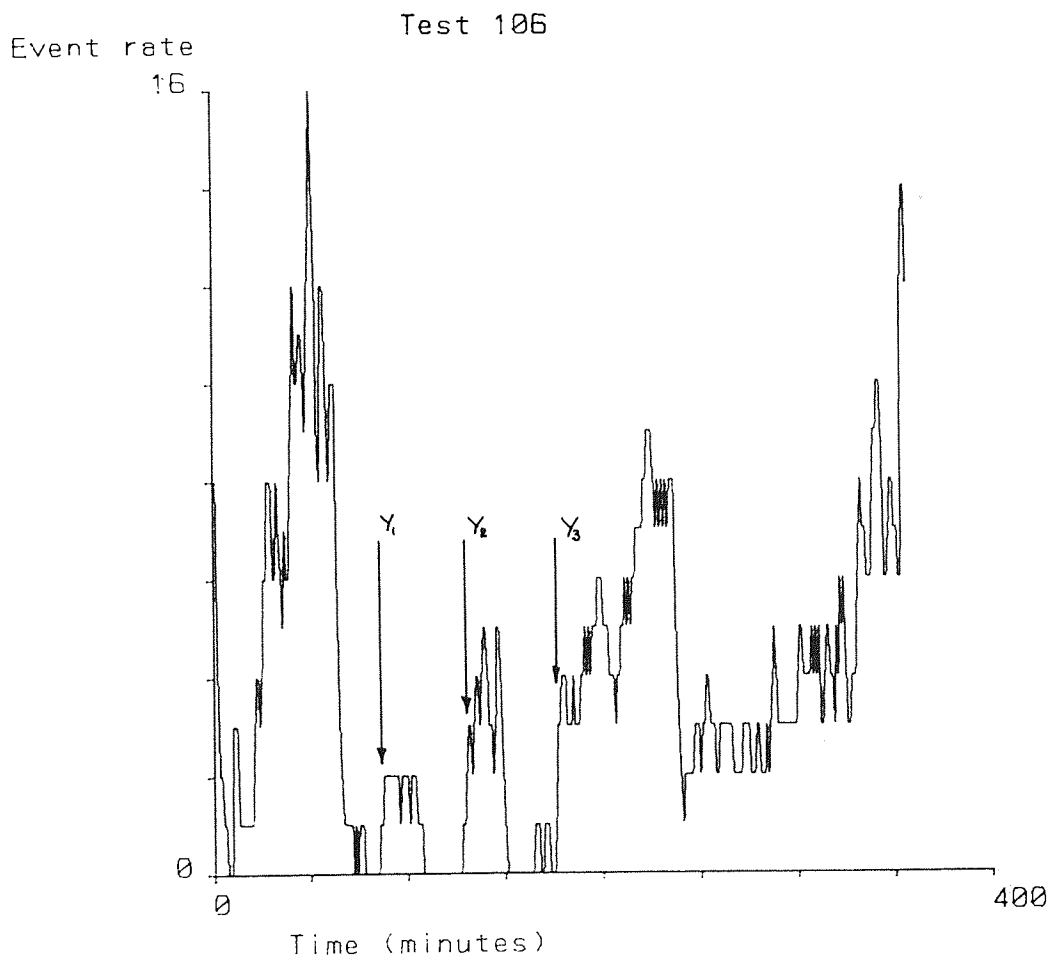
Figure 7.16 Test 106: Event rate/Time

Test 106, cycle 1

Stress Ratio
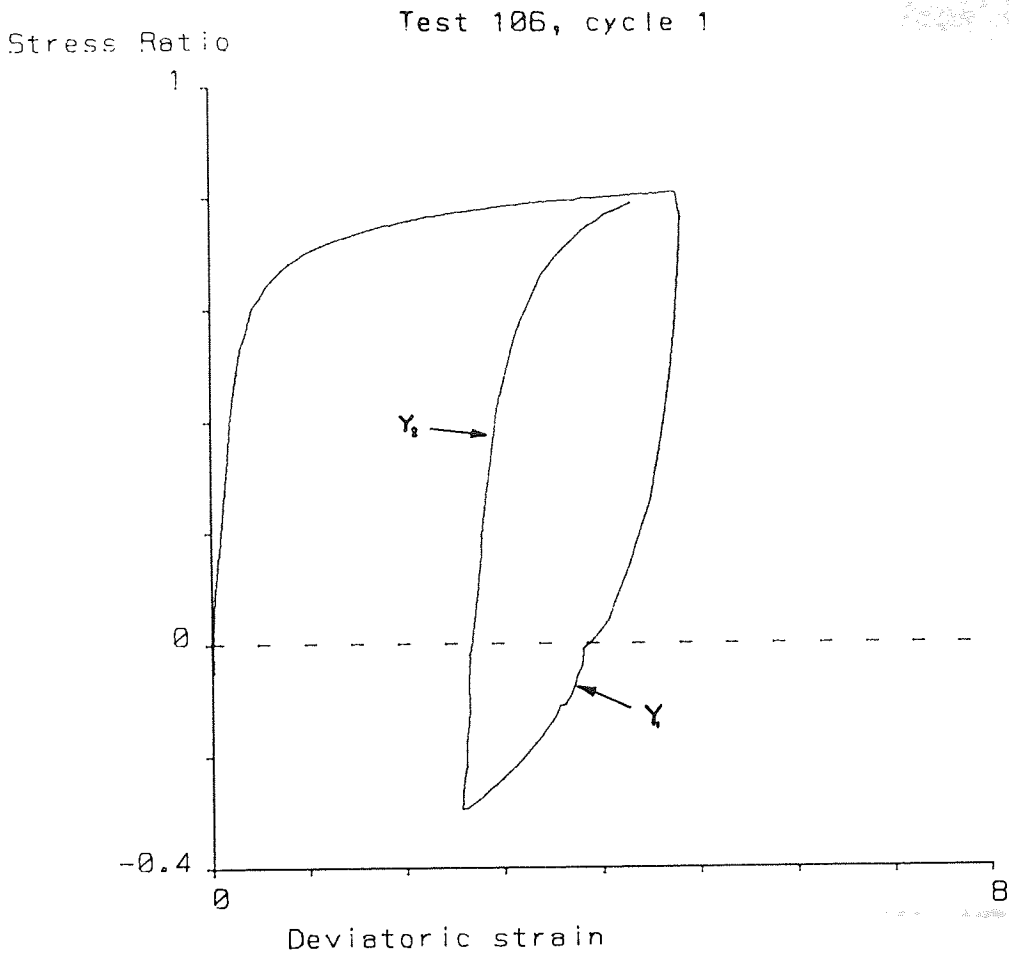
Figure 7.17 Test 106 First load cycle

Test 106, cycle 2

Stress Ratio
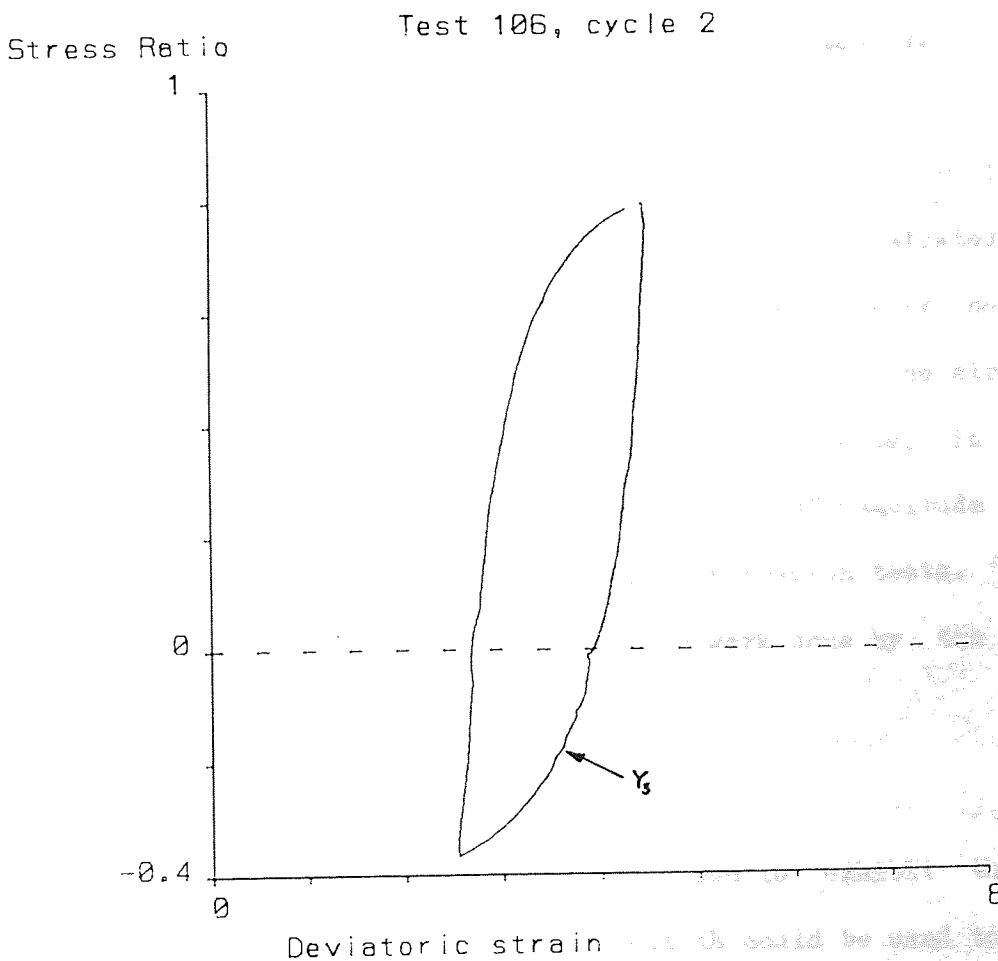
Figure 7.18 Test 106 Second load cycle

Chapter 8

Concluding Remarks.

The phenomenon of Acoustic Emission (AE) in sand has been examined. A number of test series have been performed in which different aspects of the sand's AE response have been investigated. AE has been shown to be repeatable and reliable; tests with similar stress levels have produced similar event rates even after a different stress path has been followed.

Chapter 4 showed that the AE event rate was affected by the (axial) strain rate, and was not directly proportional to it. During monotonically loaded, constant cell pressure tests the (total) AE events were found to increase, at an increasing rate, in a way which may be approximated by a power law. The AE data indicated that the sand tested became more ductile with increasing strain (in constant cell pressure tests).

The AE response of sand was shown to be both stress level and stress path dependent in Chapter 5. It was demonstrated that the stress level dependency could be compensated for by normalising the event rate with the (current) mean stress. The stress path dependence was most obvious during extension tests, in which the the number of events received was an order of magnitude less than the number recorded in comparable compression tests. This was shown to be due, primarily, to the work done by the external stresses.

In Chapter 6 the sand tested was shown to exhibit the Kaiser effect, and it was determined that AE could be used to identify

yield. It was possible to identify yield in tests involving both simple and complex stress paths. It was shown that it is the changes in event rate which are important for yield point identification, not the level of the event rate. Chapter 7 demonstrated that inverse yield points, following large stress reversals, could be identified more clearly using AE than by conventional methods of yield point identification.

In Chapter 7 it was noted that a kink occurred close to the isotropic stress state, and that this was due to inadequate design of the top platen connection. Clearly, before further large stress reversal tests are carried out, it is necessary to redesign this part of the equipment. Other research workers, using smaller specimens, have used a 'vacuum cap' arrangement where the top platen and load cell are held together by suction. It may be possible to employ this sort of technique, but the relatively large size of the specimen may prevent it.

The manual method of stress path control used for the tests in this research program was shown to be satisfactory. However, it would be beneficial to employ some form of automatic stress path control so that greater accuracy could be maintained, and more complex stress paths undertaken.

Over the research period a number of enhancements were made to the AET5000 software. In particular it became possible to calculate the AE energy of an event (see Chapter 2), and to display the characteristics of every event from a test. Unfortunately the information regarding AE energy was not

available from the manufacturer until the end of the research period, which reduced its usefulness. However, as acoustic emissions derive from the release of stored energy, and AE energy reflects both the strength and duration of an event, it would seem more relevant to use AE energy rather than AE events in any future analysis. This is supported by the correlation of AE with the work done by the external stresses.

The scope for further work using AE in soils laboratory testing is wide. Since all the tests reported in this thesis have used dense sand samples an obvious extension would be to perform a series of tests on looser specimens. This would provide a more complete description of the AE response, although the presence of the stress path and stress level effects may be anticipated. Obviously it is possible to test different types of sand but it may be more useful to direct attention towards further aspects of yield point identification.

More tests to locate the yield surface, and to identify the appropriate hardening rule could be carried out. This would, of necessity, require the modification of the top platen connection. With a revised top platen connection, and an automatic method of stress path following, large stress reversal tests, such as those reported in Chapter 7, would be much easier. This, in turn, would allow the hardening rule to be more accurately identified. Additional tests to investigate the possible isotropic yield surface could be carried out, with particular attention being given to the effect of mean stress on the AE data.

AE monitoring complements existing experimental techniques, and its non-intrusive nature is an advantage in the investigation of the behaviour of sand. AE also offers the ability to identify yield with a greater objectivity than conventional methods of yield point identification. This allows a more rigorous experimental appraisal of theoretical models which attempt to describe the behaviour of sand.

Additional details of Tests.

Notes:

The strain rate is the AXIAL strain rate, not the deviatoric strain rate.

Key for TYPE column as follows:

CCP	Constant Cell Pressure
CMS	Constant Mean Stress
CDS	Constant Deviator Stress
CAS	Constant Axial Stress
U	Undrained
PATH	Stress path (See schematic in Chapter 6)
CYCLE	Load cycle (possibly into extension)
E	Extension (Some or all of test)

Test	Porosity (%)	Strain rate (%/hour)	Threshold Voltage	Gain	Type
32	36.4	1	1.00F	4.0	CCP/CYCLE 100kPa
36	36.0	1	0.50A	2.0	CCP/CYCLE 100kPa
40	35.8	1	1.00F	4.0	CCP/CYCLE 200kPa
46	36.3	1	1.00F	4.0	CCP/CYCLE 50kPa
47	35.6	1	1.00F	4.0	CCP/E 300kPa
54	35.5	1	1.00F	4.0	CAS 300kPa
55	35.3	1	1.00F	4.0	CCP 100kPa
57	35.7	1	1.00F	4.0	U 100kPa

Test	Porosity (%)	Strain rate (%/hour)	Threshold Voltage	Gain	Type
58	35.4	1	1.00F	4.0	U 100kPa
59	35.2	1	1.00F	4.0	CMS 100kPa
60	34.9	1	0.75F	4.0	CMS 100kPa
61	34.9	1	0.50F	4.0	CMS 100kPa
63	35.5	1	1.25F	4.0	CMS 100kPa
65	35.1	1	0.50F	4.0	CMS 200kPa
66	35.2	1	0.75F	4.0	CMS 200kPa
67	35.2	1	1.00F	4.0	CMS 200kPa
69	35.1	1	1.25F	4.0	CMS 200kPa
73	35.6	1	1.00F	4.0	CMS 300kPa
74	35.7	1	1.25F	4.0	CMS 300kPa
76	35.3	1	0.50F	4.0	CMS 300kPa
77	34.9	1	0.75F	4.0	CMS 300kPa
88	35.9	3	1.00F	4.0	CCP/CYCLE 100kPA
89	36.1 No end membranes	3	1.00F	4.0	CCP 100kPa
91	– Double height	4	1.00F	4.0	CCP 100kPa
92	35.7	10	1.00F	4.0	CCP 100kPa
93	35.1	15	1.00F	4.0	CCP 100kPa
94	35.3	3	1.00F	4.0	CCP/PATH 300/100kPa

Test	Porosity (%)	Strain rate (%/hour)	Threshold Voltage	Gain	Type
95	35.8	3	1.00F	4.0	CCP/PATH 100/300kPa
96	35.6	3	1.00F	4.0	CCP/PATH 100/200kPa
97	35.1	3	1.00F	4.0	CCP/PATH 200/100kPa
98	35.2	3	1.00F	4.0	CCP/CMS 100/100kPa
99	35.3	3	1.00F	4.0	CCP/CMS 200/200kPa
100	36.3	3	1.00F	4.0	CCP/CMS 100/234kPa
101	35.2	3	1.00F	4.0	CCP/PATH 100kPa
102	35.2	3	1.00F	4.0	CCP/CDS 100kPa
103	35.8	3/2	1.00F	4.0	CCP/PATH 100kPa
106	35.6	3	1.00F	4.0/5.0	CMS/CYCLE/E 200kPa
107	35.5	3	1.00F	4.0	CMS/CYCLE/E 300kPa
108	35.0	3	1.00F	4.0	CMS/CYCLE/E 300kPa
109	35.0	1	1.00F	4.0	U/CYCLE 100kPa
110	35.1	3	1.00F	4.0	CCP 100kPa

References

ARRINGTON, M. (1975), "Acoustic Emission - An introduction for Engineers", Chartered Mechanical Engineer, April.

ARRINGTON, M. (1978), "Some industrial applications of Acoustic Emission monitoring", NDT International, June, pp117-120.

ASTM (1978), "Standard Definitions of terms relating to Acoustic Emission", ASTM E610-77, 1978 Annual book of ASTM standards, Part 11, pp603-605.

BARNES, D.J. (1985), "A study of the micro-mechanics of granular media", Ph.D. Thesis, University of Aston in Birmingham.

BEARD, F.D. (1962), "Microseismic forecasting of excavation failures", Civil Engineering (N.Y.), Vol. 32, No. 5, pp 50-51.

BEATTIE, A.G. (1976), "Energy Analysis in AE", Material Evaluation, Vol. 34, 4, pp73-78.

CADMAN, J.D., and GOODMAN, R.E. (1967), "Landslide Noise", Science, Vol. 15, pp1182-1184.

ENVIRONMENTAL PROTECTION AGENCY (1978), "Acoustic monitoring to determine the integrity of hazardous waste dams", U.S. EPA, Cincinatti.

FISCHER, C.P., and YORKE, C.A. (1964), "The detection and interpretation of microseismims in soil masses", Symposium on Soil Exploration, ASTM 351, pp121-132.

GREEN, G.E. (1969), "The strength and deformation of sand", Ph.D. Thesis, University of London.

HAHNEKAMP, H.G. (1981), "A simplified 4-channel microseismic monitoring system", Proc. 3rd Conf. on AE/MA in Geologic Structures and Materials, Pennsylvania State University, pp659-670.

HAKUNO, M., OGAWAKA, S., and HASHIZUME, T. (1968), "Analysis of noise generated by sand particles when they slide", Proc. Japanese Soc. Civil Eng., No. 164, pp51-58, (In Japanese).

HILL, R. (1950), "The mathematical theory of plasticity", Clarendon Press.

HOLUBEC, I. (1968), "Elastic behavior of cohesionless soil", Jour. Soil Mech. Found. Div., Proc. ASCE, Vol. 94, SM6, pp1215-1231.

KAISER, J. (1953), "Untersuchungen uber das auftreten Geraushen Beim Zugversuch", Ph.D. Thesis, Technische Hochschull, Munich, Germany, (In German).

KHAYATT, A.J. (1967), "Some incremental stress strain relations for sand", Ph.D. Thesis, University of Manchester.

KOERNER, R.M., LORD, A.E., and MCCABE, W.M. (1975), "Acoustic Emission studies of soil masses in the laboratory and field", Proc. 1st Conf. on AE/MA in Geologic Structures and Materials, Pennsylvania State University, pp243-256.

KOERNER, R.M., LORD, A.E., MCCABE, W.M., and CURRAN, J.W. (1976), "Acoustic Emission behavior of granular soils", Jour. Geotechnical Eng. Div., Proc. ASCE, Vol. 102, GT7, pp761-773.

KOERNER, R.M., LORD, A.E., and MCCABE, W.M. (1977), "Acoustic Emission behavior of cohesive soils", Jour. Geotechnical Eng. Div., Proc. ASCE, Vol. 103, GT8, pp837-850.

KOERNER, R.M., MCCABE, W.M., and LORD, A.E. (1981a), "Acoustic Emission behavior and monitoring of soils", Acoustic Emissions in Geotechnical Practice, ASTM STP750, V.P. Drnevich and R.E. Gray (Eds.), ASTM, pp93-141.

KOERNER, R.M., LORD, A.E., MCCABE, W.M., and MCELROY, J.J. (1981b), "AE/MA characteristics and behavior of mine tailings", Proc. 3rd Conf. on AE/MA in Geologic Structures and Materials, Pennsylvania State University, pp425-447.

KOERNER, R.M., LORD, A.E., BOYCE, G.M., and MCCABE, W.M. (1982), "Acoustic Emission determination of stress history in soil and rock", Proc. Eng. Foundation Conf., Santa Barbara.

KOERNER, R.M., LORD, A.E., and DEUTSCH, M. (1984a), "Determination of prestress in granular soils using AE", Jour. Geotechnical Eng. Div., Proc. ASCE, Vol. 110, GT3, pp346-358.

KOERNER, R.M., LORD, A.E., and DEUTSCH, M. (1984b), "Acoustic Emission Determination of preconsolidation in cohesive soils in the Laboratory", Jour. Geotechnical Eng. Div., Proc. ASCE, Vol. 110, 11, pp1537-1548.

KOLBUSZEWSKI, J. (1948), "An experimental study of maximum and minimum porosity of sands", Proc. 2nd ICSMFE, Rotterdam, Vol. 1, pp158-165.

LADE, P.V., and BOONYACHUT, S. (1982), "Large stress reversals in triaxial tests on sand", Proc. 4th Int. Conf on Numerical Methods in Geomechanics, Edmonton, pp171-182.

LADE, P.V. (1982), "Three-dimensional behaviour and parameter evaluation for an elasto-plastic soil model", Int. Symposium on Numerical Models in Geomechanics, Zurich, pp33-37.

LORD, A.E., KOERNER, R.M., and CURRAN, J.W. (1975), "Fundamental studies of Acoustic Emission in soils", Proc. 1st Conf. on AE/MA in Geologic Structures and Materials, Pennsylvania State University, pp135-148.

LORD, A.E., and KOERNER, R.M. (1979), "Estimated magnitude of acoustic emissions in soil", Technical Note, Jour. Geotechnical Eng. Div., Proc. ASCE, Vol. 105, GT10, pp1249-1253.

LORD, A.E., FISK, C.L., and KOERNER, R.M. (1982), "Utilization of steel rods as AE waveguides", Technical Note, Jour. Geotechnical Eng. Div., Proc. ASCE, Vol. 108, GT2, pp300-304.

LORD, A.E., and KOERNER, R.M. (1983), "An acoustic pressuremeter to determine in-situ soil properties", Jour. of Acoustic Emission, Vol. 2, 3, pp187-190.

MCCAULEY, M.L. (1975), "Monitoring slope stability with Acoustic Emission", Proc. 1st Conf. on AE/MA in Geologic Structures and Materials, Pennsylvania State University, pp257-269.

MITCHELL, R.J., and ROMERIL, P.M. (1984), "Acoustic Emission distress monitoring in sensitive clay", Canadian Geotechnical Jour., Vol. 21, pp176-180.

MOGI, K. (1962), "Study of elastic shocks caused by the fracture of heterogeneous materials and its relation to earthquake phenomena", Bull. Earthquake Research Inst., 40, pp125-173.

NATHAN, S.V. (1978), Discussion on "Acoustic Emission behavior of cohesive soils", Jour. Geotechnical Eng. Div., Proc. ASCE, Vol. 104, GT2, pp304-306.

NYBORD, W.L., RUDNICK, I., and SHILLING, H.K. (1950), "Experiments on acoustic absorption in sand and soil", Jour. Acoustical Soc. of America, Vol 22., No. 4, pp422-425.

OBERT L. (1975), "The microseismic method: discovery and early history", Proc. 1st Conf. on AE/MA in Geologic Structures and Materials, Pennsylvania State University, pp11-12.

POLLOCK, A. A. (1978), "Physical interpretation of AE/MA signal processing", Proc. 2nd Conf. on AE/MA in Geologic Structures and Materials, Pennsylvania State University, pp399-421.

ROMERIL, P.M. (1979), "Monitoring acoustic emissions in soils", M.Sc. Thesis, Queens University, Kingston, Ontario, Canada.

ROWE, P.W., and BARDEN, L. (1964), "The importance of free ends in triaxial testing", Proc. ASCE, Vol. 90, SM1, pp1-27.

SCHOLZ, C.H. (1968), "The Frequency-magnitude relation of microfracturing in rock and its relation to earthquakes", Bull. Seis. Soc. America, 58, 1, pp399-415.

TANIMOTO, K., and NODA, T. (1977), "A study of Acoustic Emission from sandy soils", Proc. 9th ICSMFE, Tokyo, pp315-318.

TANIMOTO, K., NISHI, U., and NODA, T. (1978), "A study of shear deformation process of sandy soils", 2nd Int. Conf. on microzonation for safer construction, San Fransisco, Vol. 2, pp971-982.

TANIMOTO, K., and NAKAMURA, J. (1981a), "Studies of Acoustic Emission in soils", Acoustic Emissions in Geotechnical Engineering Practice, ASTM STP 750, ASTM, V.P. Drnevich and R.E. Gray (Eds.), pp164-173.

TANIMOTO, K., and NAKAMURA, J. (1981b), "Use of AE technique in field investigation of soil", Proc. 3rd Conf. on AE/MA in Geologic Structures and Materials, Pennsylvania State University, pp601-612.

TANIMOTO, K., NAKAMURA, J., and FUDO, R. (1981), "Application of Acoustic Emission in in-situ test", Proc. 10th ICSMFE, Vol 2, pp573-576.

TANIMOTO, K., and NAKAMURA, J. (1982), "Study of Acoustic Emission in soils under triaxial shear", Jour. Japanese Soc. of SMFE, Vol. 22, 3, pp137-144, (In Japanese).

TANIMOTO, K., NAKAMURA, J., and ISHIKAWA, M. (1983), "The relation between Acoustic Emission and deformation of soil", Jour. Japanese Soc. of SMFE, Vol. 23, 1, pp135-143, (In Japanese).

TATSUOKA, F., and ISHIHARA, K. (1974), "Yielding of sand in triaxial compression", Jour. Japanese Soc. of SMFE, Vol. 14, 2, pp63-76.

THORNTON, C. (1974), "Deformation of sand in plane strain and axisymmetric compression", Ph.D. Thesis, University of Aston in Birmingham.

VERMEER, P.A. (1980), "Formulation and analysis of sand deformation problems", Dept. Civil Eng., Delft University.

VILLET, W.C.B., MITCHELL, J.K., and TRINGALE, P.T. (1981), "Acoustic Emissions generated during the quasi-static cone penetration of soils", Acoustic Emissions in Geotechnical Engineering Practice, ASTM STP750, ASTM, V.P. Drnevich and R.E. Gray (Eds.), pp174-193.

WADIN, J.R. (1982), "Listening to ... composite materials", Acoustic Emission Applications, Dunegan/Endevco, San Juan Capistrano, California.

WILLIAMS, R.V. (1981), "Acoustic Emission", Adam Hilger Ltd.